



**SEDIMENT CHARACTERISTICS AND HYDRODYNAMIC
CONDITIONS OF THE SWARTKOPS ESTUARY, EASTERN
CAPE PROVINCE OF SOUTH AFRICA**



Lutho Best
University of Fort Hare
Together in Excellence

**A dissertation submitted in fulfilment of the requirements for the
Degree of**

Master of Science in Geology

Department of Geology

Faculty of Science and Agriculture

University of Fort Hare


Supervisor: Prof Ken Liu

November 2021

DECLARATION

I, Lutho Best, student number: 201300380 hereby declare that I am fully aware of the University of Fort Hare's policy on plagiarism and I have taken every precaution to comply with the regulations.

I declare that this dissertation is my own work except where proper referencing and acknowledgement have been made. It has not been previously submitted for degree requirements to any other University. I, therefore, submit the dissertation for examination for the Degree of Master of Science (Geology) of the University of Fort Hare.

Signature ... 

Date: November 2021

At the Department of Geology

Faculty of Science and Agriculture

University of Fort Hare

Eastern Cape Province

South Africa



University of Fort Hare
Together in Excellence

ACKNOWLEDGEMENTS

I would like to thank God for giving me strength and perseverance to finish the project. My heartfelt gratitude goes to my supervisor Prof Ken Liu for his guidance, advice and a great support. Thank you very much for being helpful.

Special thanks to the National Research Foundation (NRF) and South African Institute for Aquatic Biodiversity (SAIAB) for bursary and funds for this project.

My sincere appreciation to Mr Machel Katwire for technical support. I would also like to thank all the staff members of the Geology Department, University of Fort Hare and all the geology postgraduate students who have assisted me throughout the study period and the research project in the University.

Lastly, my deepest appreciation goes to my parents and my family at large. Thank you so much for your support. Special thanks to my aunt and my cousin brother for unlimited love and courage. The local government commended this research and had accepted some suggestions proposed by the author for environment protection.



University of Fort Hare
Together in Excellence

ABSTRACT

This study is a part of an environmental research project aimed at providing assessment information to the grain-size distribution, mineral compositions, sedimentary structures and coastal erosion and rehabilitation methods along the Swartkops estuary, a recent developing industry area of South Africa. The methodologies used in this study comprise desk study of literature, field geological investigation and sampling, and laboratory analyses including grain-size analysis, thin section microscope study, XRD mineral composition study and SEM-EDX grain surface texture and composition analyses. The basement and surrounding areas of the Swartkops estuary consist of three formations: the Enon Formation of mainly conglomerate, the Kirkwood Formation of sandstone and mudstone, and the Sundays River Formation of dominantly mudstone with sandstone, which integrated as Uitenhage Group of Cretaceous sequence with modern estuarine sand and alluvial sediments filled in the entire basin. Grain size analysis is a useful tool to assess hydrodynamic environments. The grain size parameters showed that most of the Swartkops estuary sediments are moderately sorted with very few well and poorly sorted, coarse to fine skewed in grain size distribution. Whereas the Bluewater Bay beach sediments are mostly fine grained, well sorted, fine to coarse skewed in grain size distribution. The bivariate scatter plots are an indication of shallow marine environment by beach and coastal processes with the influence of water flow and wind influence during transportation and deposition processes. Mineralogy studies revealed that the Swartkops estuary sediments are dominantly composed of minerals such as: quartz, calcite, feldspar (orthoclase and plagioclase), aragonite, clay minerals (smectite and illite), and salts such as NaCl and MgCl₂. Skeletal carbonate minerals (shell fragments) are more than chemical precipitated carbonate minerals. Quartz is the most abundant detrital mineral observed in all the sediments and it comes from inland and transported into the estuary and the beach by fluvial streams, whereas skeletal calcite/aragonite is the most abundant biogenic carbonate derived from sea side and transported by marine currents. The study shows that grain surface textures reveal the existence of several features that reflect the depositional environments. Observed grain surface textures by microscope and SEM include V-shape pits, upturned pits caused by mechanical crashing and corrosion during transportation; crystalline precipitation of calcite, quartz, salt and clay by chemical precipitation and crystallization; dissolution pits and pores formed by dissolution, and burrow and boring by biogenetic activities. The grain surface morphologies are closely linked to different formation mechanisms and depositional environments. Well-developed sedimentary structures have been found in the beach and

estuary, including sand dune, sand ridge, straight and sinuous ripple, ripple marks, aeolian nail marks, high angle tabular cross bedding, antidune, rill mark, rhomboid mark, swash line, mud crack, gravel pavement, interfering ripples, flat topped ripple mark, linguoid mark, asymmetric sinuous ripples, dendritic pattern on sandy beach, boring and bioturbation, burrows desiccation cracks and water escape hole. Different sedimentary structures are reflective of different hydrodynamic conditions and depositional environments. Coastal erosion is a major problem for damage of road, bridge and properties in the industrial areas in Swartkops, which is also a task for this study. The author had suggested some practical mitigation-methods to local government, such as groins, revetments, shoreline hardening, planting of vegetation, and vertical walls, bulkheads, sills, which could be useful for the protection of coastal erosion.

Keywords: Swartkops estuary, grain size parameters, mineral compositions, sedimentary structures, coastal erosion and mitigation.



University of Fort Hare
Together in Excellence

TABLE OF CONTENTS

DECLARATION.....	i
ACKNOWLEDGEMENTS	ii
ABSTRACT	iii
CHAPTER 1 GENERAL BACKROUND	1
1.1 Introduction.....	1
1.2 Location of the study	3
1.3 Relation of grain size with water energy	4
1.4 Aim and objectives of the research	5
1.5 Research questions.....	6
CHAPTER 2 LITERATURE REVIEW	7
2.1 Introduction.....	7
2.2 Geology of the study area	8
2.2.1 The Enon Conglomerate Formation	9
2.2.2 The Kirkwood Formation	10
2.2.3 Sundays River Formation	11
2.3 Sediment distribution along the estuary.....	12
2.4 Hydrodynamics	13
2.5 Fluvial floods	13
2.6 Coastal erosion.....	15
2.6.1 Estuarine shoreline erosion.....	15
2.6.2 Beach erosion	17
2.7 Estuarine sediment dynamics.....	18
2.8 Beach sediment dynamics	19
CHAPTER 3 METHODOLOGY	21
3.1 Introduction.....	21
3.2 Field observation.....	21
3.3 Grain-size sieving analysis	23
3.4 Petrographic microscope.....	24
3.5 SEM and EDX analysis	26
3.6 The X-ray diffraction analysis (XRD)	27
3.7 Instruments used during the research.....	28
CHAPTER 4 GRAIN SIZE ANALYSIS	29
4.1 Introduction.....	29
4.2 Grain size measurements for sediments.....	31

4.3 Beach Sediments	36
4.3.1 Grain size statistical parameters of beach sediments.....	41
4.3.2 Discussion of the grain size analysis for beach sediments	42
4.4 Estuarine sediments	44
4.4.1 Representative estuary samples	44
4.4.2 Grain size statistical parameters of estuarine samples.....	48
4.4.3 Discussion on grain size parameters for estuarine sediments.....	51
4.5 Tidal channel sediments.....	52
4.5.1 Grain size statistical parameters for tidal channel sediments	56
4.5.2 Discussion on grain size parameters for tidal channel sediments	57
4.6 Bivariate scatter plots of grain size parameters.....	58
4.7 Summary	64
CHAPTER 5 MINERAL COMPOSITIONS	65
5.1 Technique used for mineral analysis.....	65
5.2 Mineral types, assemblage and occurrence.....	65
5.2.1 Quartz (SiO ₂)	65
5.2.2 Feldspar	67
5.2.3 Carbonate.....	70
5.2.4 Lithic fragments.....	71
5.2.5 Glauconite.....	72
5.2.6 Organic pellets.....	72
5.2.7 Sponge	73
5.2.8 Foraminifera	74
5.3 Mineral abundance.....	75
5.4 X-Ray diffraction (XRD) results.....	76
5.5 Summary	79
CHAPTER 6: GRAIN SURFACE TEXTURES	80
6.1 Introduction.....	80
6.2 V-shape pits	81
6.3 Upturned plates	81
6.4 Secondary minerals precipitation.....	83
6.5 Dissolution pits/holes.....	85
6.6 Burrow and boring holes.....	87
6.7 Summary	88
CHAPTER 7 SEDIMENTARY STRUCTURES	89

7.1 Introduction.....	89
7.2 Sediment stratification	89
7.3 Sedimentary structures formed by aeolian process	90
7.3.1 Sand dune	90
7.3.2 Sand ridge	91
7.3.3 High angle cross bedding	92
7.3.4 Antidune	93
7.3.5 Ripple marks.....	94
7.3.5.1 Straight line ripples.....	93
7.3.5.2 Sinuous line ripples.....	94
7.3.5.3 Aeolian nail marks.....	95
7.4 Sedimentary structures formed by water flow	98
7.4.1 Gravel pavement.....	98
7.4.2 Interfering ripples	99
7.4.3 Flat topped ripple mark.....	100
7.4.4 Linguoid marks.....	101
7.4.5 Asymmetric sinuous ripples	102
7.4.6 Rill marks	103
7.4.7 Rhomboid marks.....	103
7.4.8 Swash line.....	104
7.4.9 Dendritic wash mark.....	105
7.4.10 Drainage patterns on sandy beach	106
7.5 Biogenetic sedimentary structures	107
7.5.1 Boring and bioturbation.....	107
7.5.2 Burrows	107
7.6 Miscellaneous structures	108
7.6.1 Desiccation cracks (mud cracks)	108
7.6.2 Rain drops.....	109
7.7 Summary	110
CHAPTER 8: HYDRODYNAMIC ENERGY AND DEPOSITIONAL ENVIRONMENTS....	111
8.1 Introduction.....	111
8.2 Shallow marine system	111
8.3 Estuarine environments.....	112



University of Fort Hare
Together in Excellence

8.3.1 Intertidal flats.....	112
8.3.2 Saltmarshes.....	114
8.3.3 Tidal channel	115
8.3.4 Floodplain	117
8.4 Summary	119
CHAPTER 9: COASTAL EROSION AND MITIGATION.....	120
9.1 Introductory.....	120
9.2 Erosion causes.....	120
9.3 Sediment erosion.....	121
9.4 Bank erosion	121
9.5 Possible mitigation methods	122
9.5.1 Shoreline hardening.....	122
9.5.2 Groins	123
9.5.3 Revetments	124
9.5.4 Vegetation.....	125
9.5.5 Vertical walls.....	126
9.5.6 Bulkheads	127
9.5.7 Breakwater.....	128
9.6 Summary	129
CHAPTER 10 DISCUSSION AND CONCLUSION.....	130
Recommendations.....	133
REFERENCES.....	134
APPENDICES	155



University of Fort Hare
Together in Excellence

LIST OF FIGURES

Fig. 1.1 a: Geographical map showing the locations of the Swartkops and Sundays estuaries at north suburb of Port Elizabeth.	2
Fig. 1.1b: Geological map showing the Swartkops River and Uitenhage Group in north of Port Elizabeth.	3
Fig. 1.2: A satellite imagery map, showing the location of the sampling stations in Swartkops estuary and Bluewater Bay beach.	4
Fig. 2.1: Map of Algoa Bay, with the city of Port Elizabeth in the western sector. The inset map shows the position of Algoa Bay on the coast of South Africa. The general flow of the Agulhas current is indicated from north east to south west.	7
Fig. 2.2: Geological map of the Swartkops river catchment.	9
Figure 2.3: Photograph showing Cretaceous conglomerate of Enon Formation in Port Elizabeth area.	10
Figure 2.4: The map on the left shows the location of the Kirkwood Formation and the spread shown in figure 1.1b, which is one of the main source areas for Swartkops River sediments, while the photograph on the right shows interbedded porous medium to coarse-grained sandstone above maroon shales.	11
Figure 2.5: Photograph showing the Sundays River Formation dominated by mudstone with alternated siltstone and sandstone layers.	12
Fig. 2.6: The aerial photograph shows flooding in Swartkops River.	15
Fig. 2.7: Road erosion caused by wave and tide current at Port Elizabeth coast in 2012.	16
Fig. 2.8: Photograph shows erosion caused by waves and stirring up of currents along the shore on a coastal tarred road.	18
Fig.2.9: Sediment dynamics between high discharge and low discharge in the tidal river to estuarine reach.	19
Fig.3.1: The photograph shows field observation from Swartkops estuary to Bluewater beach, photograph (A) showing quartzite with quartz veins (black arrow), photograph (B) showing sand dune with vegetation, photograph (C) showing small pebbles (yellow arrow) and photograph (B) showing shell fragments.	22

Fig.3.2: The photograph showing students in the field observation and sampling along the Swartkops estuary.	23
Fig.3.3: The process and equipment for the grain size analysis.	24
Fig.3.4: Photograph showing Struers trimming machine (Accuton-50) (yellow arrow) for thin section preparation at the Geology department's thin section laboratory, University of Fort Hare.....	25
Fig.3.5: The photograph shows the microscope studies for minerals composition analysis. ...	26
Fig.3.6: Photograph shows the Scanning Electron Microscope (SEM) and the Energy Dispersive X-ray spectrometry analysis (EDX). JEOL JSM-6390 LV model Scanning Electron Microscopy.	27
Fig. 4.1: Histogram (left) and cumulative frequency curve (right) of the Sample 1, showing the grain size distribution varied from 1.5-3.5 phi which is dominant at 3 Phi (0.125 mm) and a part of at 2 phi (0.25 mm).	38
Fig. 4.2: Histogram (left) and cumulative frequency curve (right) showing grain size distribution of the Sample 2. The grain size is dominant at 3 Phi (0.125 mm) followed by small percentage of grain size of 2 Phi (0.25 mm).	39
Fig. 4.3: Histogram (left) and cumulative frequency curve (right) of Sample 14, showing grain size varied from 1.5 phi to 4.5 phi, and well sorted nature, with dominant size at 3 Phi (0.125 mm) and minor at 2 Phi (0.25 mm) and 4 phi (0.0625 mm).	40
Fig. 4.4: Histogram (left) and cumulative frequency curve (right) showing grain size distribution of Sample 15. The grain size is dominant at 3 Phi (0.125 mm) followed by small percentage of grain size of 2 Phi (0.25 mm).	41
Fig. 4.5: Histogram (left) and cumulative frequency curve (right) of the Sample 31, showing the grain size distribution varied from -1 to 5 phi. The grain size is dominant at 3 Phi (0.125mm) followed by - 1.0 Phi (2mm) and 4 Phi and other grain sizes are very limited.....	45
Fig. 4.6: Histogram (left) and cumulative frequency curve (right) showing grain size distribution of sample 32. The grain size varied from -1 to 5 phi dominant at 3 Phi (0.125 mm) followed by -1.0 (2mm) and 5 Phi (0.039 mm) and other small percentages of grain sizes. .	46
Fig. 4.7: Histogram (left) and cumulative frequency curve (right) showing grain size distribution of sample 41. The grain size distribution varied from -1 to 5 phi dominant at 3 Phi (0.125 mm) followed by - 1.0 Phi (2 mm) and other small percentages of grain sizes.	47

Fig. 4.8: Histogram (left) and cumulative frequency curve (right) of Sample 57, showing grain size varied from -1 phi to 5 phi, and with dominant size at 3 Phi (0.125 mm) and minor at 2 Phi (0.25 mm) and few -1 phi (2mm).....	48
Fig. 4.9: Histogram (left) and cumulative frequency curve (right) showing grain size distribution of sample 44. The grain size distribution varied from -1 to 5 phi. The grain size is dominant at 3 Phi (0.125) followed by – 1 Phi and other small percentages of grain sizes.	53
Fig. 4.10: Histogram (left) and cumulative frequency curve (right) showing grain size distribution of sample 45. The grain size varied from -1 to 5 phi which is dominant at 3 Phi (0.125) followed by – 1 Phi and other small percentages of grain sizes. The cumulative curve is much gentle steeped due to mixed grain size and poorly sorting.....	54
Fig. 4.11: Histogram (left) and cumulative frequency curve (right) showing grain size distribution of sample 45. The grain size varied from -1 to 5 phi wich is dominant at -1 Phi followed by 3 Phi and other small percentages of grain sizes. The cummulative curve is much gentle steeped, indicating poorly sorting and mixed grain sizes.	55
Fig. 4.12: Histogram (left) and cumulative frequency curve (right) showing grain size distribution of sample 53. The grain size varied from -1 to 5 phi, with the dominant at 3 Phi (0.125) followed by -1 Phi and other small percentages of grain sizes.	56
Fig. 4.13: Bivariate scatter plot showing standard deviation/sorting versus mean. The plot of mean versus sorting indicates that the sediments are fine to medium and very well sorted to poorly sorted.	60
Fig. 4.14: Bivariate scatter plot showing skewness versus mean. The plot between mean and skewness is useful for distinguish between depositional environments. The plot also shows that the sediments are mostly fine to medium grained.	60
Fig. 4.15: Bivariate scatter plot showing kurtosis versus skewness. The trend in the kurtosis versus skewness plot could be used to determine the type of depositional.	61
Fig. 4.16: Bivariate scatter plot showing kurtosis versus mean.The plot between mean and kurtosis indicates that most sediments are fine grained and very few medium grained.....	62
Fig. 4.17: Bivariate scatter plot showing skewness versus standard deviation/sorting. From the plot between sorting and skewness, it can be deduced that as the skewness increases, the sorting of grains also increases.	63

Fig. 4.18: Bivariate scatter plot showing kurtosis versus standard deviation/sorting. From the plot, it can be deduced that when sorting increases, the kurtosis gets narrower indicating that the samples have a positive relationship between sorting and kurtosis.	64
Fig. 5.1: Photomicrographs of various sand grains of quartz (Qtz) (blue arrows) and calcite (Cal) (yellow arrows), sample number 4 from Bluewater beach.	66
Fig. 5.2: SEM and EDX analyses for two quartz grains having the same silica (SiO ₂) chemical composition. Au peak was due to gold coating for the sample.	67
Fig.5.3: Photomicrographs showing various grains of feldspar (Fs), Quartz and Calcite (Cal). Quartz has no cleavage, while feldspar shows clear cleavage in the crystalline grain indicated by green arrow (Sample 44).	69
Fig. 5.4: SEM and EDX analyses for Albite grain (top) having silica, aluminium and sodium chemical compositions (top); and Ca-Plagioclase grain showing silica, aluminium and calcium compositions (bottom). Au peak was due to gold coating for the sample.	70
Figure. 5.5: Photomicrographs of various sand grains showing calcite (Cal), quartz (Qtz) and feldspar (Fs) grains (Sample 45).	70
Fig. 5.6: SEM and EDX analyses for low-Mg calcite grain showing calcium, oxygen and carbon of chemical compositions with minor Mg content. Au peak was due to gold coating for the sample.	71
Fig. 5.7: Photomicrographs of various sand grains showing organic pellets (OP), quartz (Qtz) and calcite (Cal), sample 31 from Swartkops estuary.	73
Fig. 5.8: Photomicrographs of shale fragments (Sh) and sponge (Sp) and various other grains, sample 57 from Swartkops estuary.	74
Fig. 5.9: Photomicrographs of various sand grains showing quartzite lithic (orange arrows), siltstone lithic (green arrow), glauconite (yellow arrow), plagioclase (grey arrow, partially replaced), foraminifera (blue arrow) and various other grains, sample 32 from Swartkops estuary.	75
Fig. 5.10: XRD patterns for all the samples, P3, P24, P43, P46, P55, P62, S20 and S8. Showing the abundance of Quartz, Calcite, Aragonite, Albite and Muscovite respectively.	78
Fig. 6.1: SEM photomicrograph showing V-shaped pits (orange and blue arrows).	81

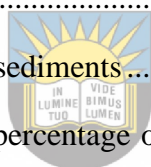
Fig. 6.2: SEM photomicrograph showing Upturned Plates on a grain surface due to collision, corrosion and precipitation (A); and (B) magnified secondary precipitated crystals within an upturned hollow.	82
Fig. 6.3: Secondary mineral contains high silica (SiO_2) content (NB: the Au peak was due to gold coating for sample and should not be taken into account).....	83
Fig. 6.4: Secondary mineral contains high calcium carbonate (CaCO_3) content (NB: the Au peak was due to gold coating for sample).....	84
Figure 6.5: Secondary minerals contain high sodium chloride (NaCl).	84
Figure 6.6: Secondary minerals contains high calcium carbonate (CaCO_3) and (NB: the Au peak was due to gold coating for sample).....	85
Fig. 6.7: SEM photomicrograph showing dissolution pits/holes on the grain surface.	86
Fig. 6.8: SEM photomicrograph showing secondary mineral precipitation on the grain surface (black arrows).	86
Fig. 6.9: SEM photomicrograph showing grain surface corrosion and dissolution pits/holes (left 3 holes and the middle hole), also secondary calcite crystals precipitated on the grain surface (middle).....	87
Fig. 6.10: Photomicrograph showing dissolution holes (shallow, irregular holes on the middle) and boring holes created by micro-organism (deeper and rounded holes on the grain surface (orange arrows).	88
Fig. 7.1: Photograph showing stabilized, partially vegetated sand dune with ripple marks on the dune stoss side in the Bluewater beach along the Swartkops estuary.....	91
Fig.7.2: Photograph showing a mega sand-ridge produced by wind and high wave at the south coast of Port Elizabeth.	92
Fig.7.3: Photograph showing high angle cross bedding with beds tilted towards the left side, which reflects the wind blow direction. High angle cross bedding ($>30^\circ$) is typical indicator of aeolian dune, while low angle cross bedding ($<25^\circ$) was formed by water currents, as well as lower velocity of wind.	93
Fig. 7.4: Photograph showing a large scaled antidune structure with low dip angle ($<15^\circ$), low amplitude and long wavelength ($\sim 5\text{m}$). Hammer is 32 cm for scale.	94

Fig. 7.5: Well developed ripples on the dune surface, the left side (lee side) of the dune is very steep.	95
Fig. 7.6: A photograph showing straight ripples with ripple crest lines parallel each other at Swartkops estuary.	96
Fig. 7.7: Photograph shows sinuous ripples with crest lines slightly vary in different directions as at Swartkops estuary. Varying in flow direction and as well as interference by late stage of wind movement caused the sinuous crest ripples.	97
Fig. 7.8: Photograph showing nail marks (arrows) which are parallel to wind blow direction from nail head to nail tail, i.e. from top to bottom in this picture.	98
Fig. 7.9: A photograph showing pebble pavement along a part of Bluewater beach, reflecting the water (tide) energy was higher at this section of beach.	99
Fig. 7.10: Photograph showing interfering ripples in the Algoa Bay, at the mouth of Swartkops estuary, which were formed by two set of ripples interfered together).	100
Fig. 7.11: Photograph showing flat topped ripples caused by later shallow water shaved the ripple crest becoming flat.	101
Fig. 7.12: Photograph showing linguoid marks in different shapes and sizes along a bank of Swartkops estuary, which were produced by strong water current on relative fine sediments.	102
Fig. 7.13: Asymmetric sinuous ripples showing current flow is on one direction (unidirectional) and the current direction is from stoss side (right) to lee side (left) on the bank of Swartkops estuary.	103
Fig. 7.14: Photograph showing rill marks on the lower beach, formed by the escape of water from saturated sands when the tide falls back to sea at Bluewater beach, Port Elizabeth.	103
Fig. 7.15: Photograph shows the uniform network of rhomboid marks at the Bluewater beach, Port Elizabeth.	104
Fig. 7.16: Photograph showing a high tide swash line (dashed line) in damp sands with shell fragments.	105
Fig. 7.17: Picture showing dendritic wash marks and mega ripples.	106
Fig. 7.18: Drainage patterns along the Bluewater beach, which form from tidal washing and scouring.	107

Fig. 7.19: A photograph showing boring holes by organisms along the Swartkops estuary.	107
Fig. 7.20: Photograph showing burrows (arrow) caused by invertebrate organisms along the beach.	108
Fig. 7.21: Mudcracks showing shallow water wet environment became dry up.	109
Fig. 7.22: Rain drops causing very shallow pits on the fine mud-silty beach surface resulting from a heavy rain event. They are rounded, very shallow pits (1-3 mm in depth) and distinguishable from biogenic boring holes.	110
Fig. 8.1: The photograph shows the tidal flat of Swartkops Estuary.	113
Fig. 8.2: The photograph shows the saltmarshes along the Swartkops estuary.	115
Fig. 8.3: Tidal channel system showing flooding having shallow water in Swartkops estuary.	116
Fig. 8.4: Tidal channel system showing runnels and ridges with some ripples marks in Bluewater beach.	117
Fig. 8.5: Picture shows vegetated floodplain along the Swartkops Estuary.	118
Fig. 9.1: Photograph shows erosion along the Durban coast, South Africa in the 23 April 2019.	121
Fig. 9.2: The photograph shows a bank erosion along the north part of Swartkops estuary.	122
Fig. 9.3: Photograph showing cement hardening for protection of the bank in the Swartkops estuary.	123
Fig.9.4: Photograph showing down drift of wood groin in the coast of Bluewater beach.	124
Fig. 9.5: Photograph showing revetment with rock boulders (left) and cement blocks (right) along the coast of Bluewater beach.	125
Fig. 9.6: Photograph showing vegetation controlling for coastal erosion.	126
Fig. 9.7: Photograph showing vertical wall for protection of wave erosion in the coast.	127
Fig. 9.8: Photograph showing bulkhead to protect bank erosion and slope failure.	128
Fig. 9.9: Photograph showing breakwaters built by rocks (left) or mud-rock mixture (right).	128

List of tables

Table 4.1 Classification of sediments and sedimentary rocks based on the grain-size.	30
Table 4.2 Formulas for calculating grain size parameters.	32
Table 4.3 Parameter values of the grain size analyses for collected samples.	33
Table 4.4: Verbal classifications of the sorting, skewness and kurtosis.	36
Table 4.5 Retained and cumulative percentage of grain size for sample 1. Aliquot mass =322.39g.	37
Table 4.6 Retained and cumulative percentage of grain size for sample 2. Aliquot mass=259.94g.	38
Table 4.7 Retained and cumulative percentage of grain size for sample 14. Aliquot mass = 397.14 g.....	39
Table 4.8 Retained and cumulative percentage of grain size for sample 15. Aliquot mass = 291.99 g.....	40
Table 4.9 Parameter values for beach sediments.....	41
Table 4.10 Retained and cumulative percentage of grain size for sample 31. Aliquot mass = 308.91g.....	45
Table 4.11 Retained and cumulative percentage of grain size for sample 32. Aliquot mass = 180.75g.....	45
Table 4.12 Retained and cumulative percentage of grain size for sample 41. Aliquot mass = 286.66 g.....	46
Table 4.13 Retained and cumulative percentage of grain size for sample 57. Aliquot mass = 273. 66 g.....	47
Table 4.14 Parameter values for estuary samples.	48
Table 4.15 Retained and cumulative percentage of grain size for sample 44. Aliquot mass = 289.67g.....	53
Table 4.16 Retained and cumulative percentage of grain size for sample 45. Aliquot mass = 204.68g.....	53
Table 4.17 Retained and cumulative percentage of grain size for sample 50. Aliquot mass = 228.08 g.....	54



University of Fort Hare
Together in Excellence

Table 4.18 Retained and cumulative percentage of grain size for sample 53. Aliquot mass = 282.60g.....	55
Table 4.19 Parameter values for tidal channel samples.	56
Table 5.1: Mineral types and their abundance (percentages).	76
Table 5.2: Percentages of minerals present in sample P3 to sample S8.	77



University of Fort Hare
Together in Excellence

LIST OF APPENDICES

APPENDIX A: GRAIN SIZE ANALYSIS	157
A.1 Sample 2	158
A.2 Sample 3.....	159
A.3 Sample 4.....	160
A.4 Sample 5	161
A.5 Sample 6....	162
A.6 Sample 7	163
A.7 Sample 8.....	164
A.8 Sample 9	165
A.9 Sample 10	166
A.10 Sample 11.....	167
A.11 Sample 12	168
A.12 Sample 13.....	169
A.13 Sample 16.....	170
A.14 Sample 17.....	171
A.15 Sample 18	172
A.16 Sample 19	173
A.17 Sample 20	174
A.18 Sample 21	175
A.19 Sample 22	176
A.20 Sample 23	178
A.21 Sample 24	179
A.22 Sample 25.....	180
A.23 Sample 27.....	181
A.24 Sample 29	182
A.25 Sample 31	183



University of Fort Hare
Together in Excellence

A.26 Sample 32	184
A.27 Sample 34	185
A.28 Sample 35	186
A.29 Sample 38	187
A.30 Sample 40	188
A.31 Sample 41	189
A.32 Sample 42.....	190
A.33 Sample 43	191
A.34 Sample 48	192
A.35 Sample 49	193
A.36 Sample 51	194
A.37 Sample 52.....	195
A.38 Sample 56	196
A.39 Sample 57	197
APPENDIX B: SEM AND EDX.....	198
B.1 Sand sample containing high calcium carbonate...	198
B.2 Sand sample containing high amount of silica	198
B.3 Sand sample containing high amount of silica	199
B.4 Sand sample containing high amount of silica	199



University of Fort Hare
Together in Excellence

CHAPTER 1 GENERAL BACKGROUND

1.1 Introduction

The Swartkops is situated at north of Port Elizabeth. Its catchment is about 120 kilometers long and 42 kilometers wide. The dominant topographical features are Elands and the Zunga Mountains in the Western part of the catchment. In the east, the mountain ranges are fringed by low lying coastal plains that are terraced around an extensive alluvial floodplain and estuary (Maclear, 1996). The Pre-Cretaceous basement, which consists of the Table Mountain Group quartzite and the shales of the Bokkeveld Group, which formed a trough where the Cretaceous and younger strata were deposited (Mackay, 1993). The Cretaceous deposits of the Uitenhage Group distributed along the Swartkops River, which is made of Enon Formation of mainly poorly sorted coarse conglomerate, Kirkwood Formation of sandstone and mudstone, and Sundays River Formation of mainly mudstone intercalated with sandstone (Maclear, 1996). The Swartkops River flows through a high urbanized industrial region of the Eastern Cape Province and forms an integral part of the Port Elizabeth municipality (Binning and Baird, 2001).



The distribution of sediments to the estuary decreases in percentages of sands from the bank to the deeper center. In the case where there is sustained tidal flow as in permanently open estuary, the distribution is reversed with muddy sediments occurring in the supratidal zone and coarser sediments flooring the tidal channel (Alanson, 1999). The Sundays River Formation is exposed along the Swartkops River and it forms a prominent escarpment (Martin, 1962). The hard rock of the east-west aligned Cape Fold Belt consisting of the fine-grained quartz of the Table Mountain sandstone (Martin, 1962).

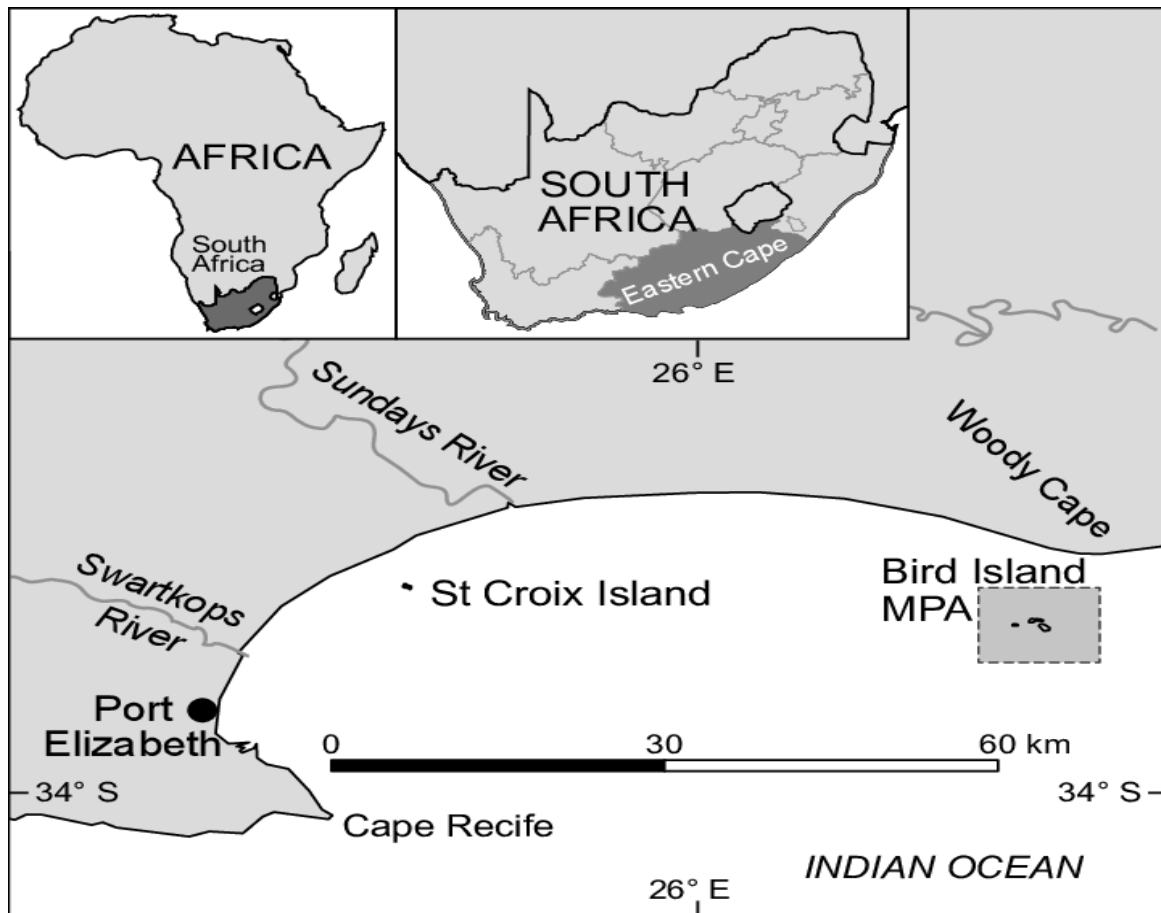


Fig. 1.1 a: Geographical map showing the locations of the Swartkops and Sundays estuaries at north suburb of Port Elizabeth (Strydom et al., 2015).

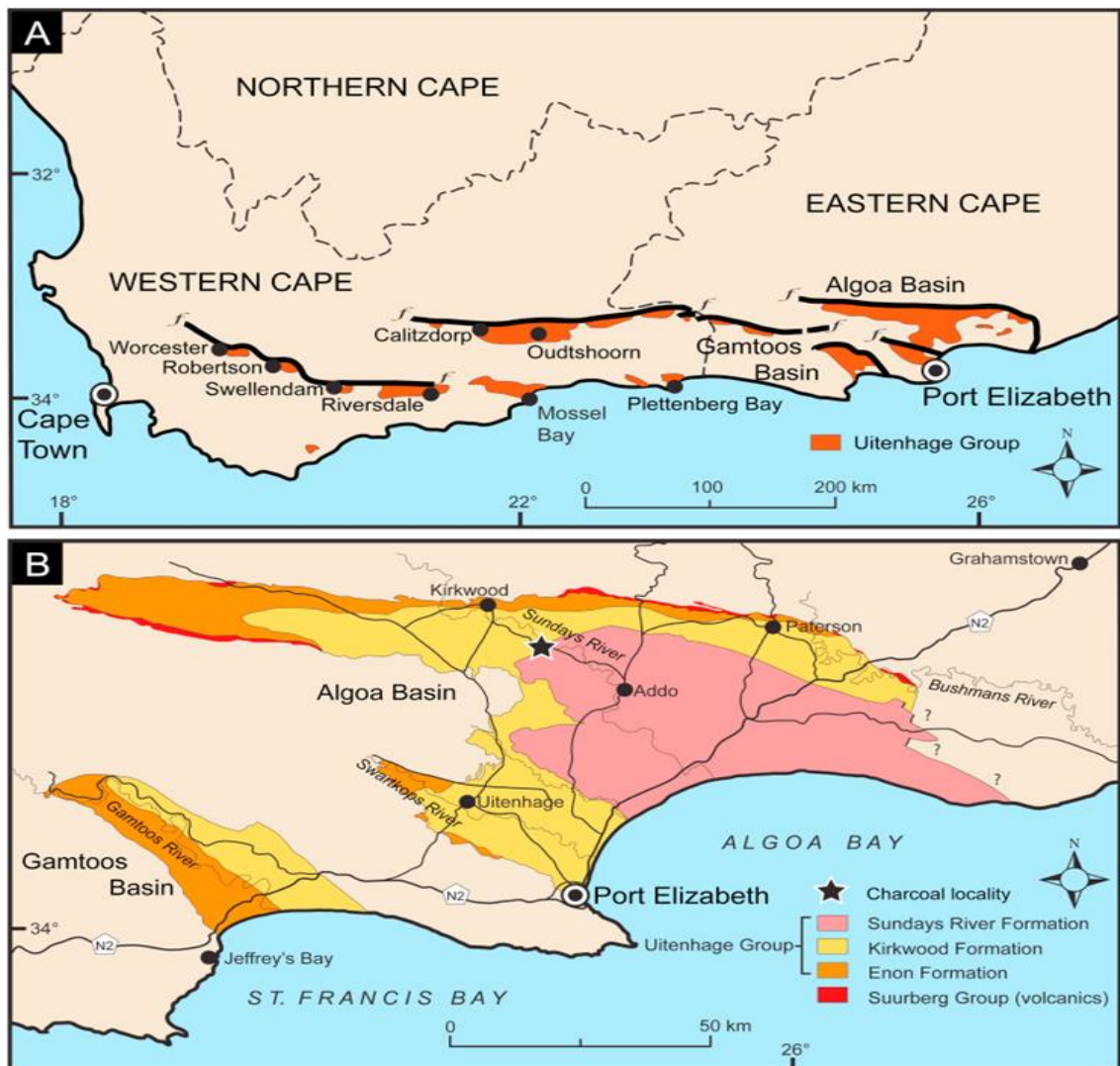


Fig. 1.1b: Geological map showing the Swartkops River and Uitenhage Group in north of Port Elizabeth (extracted from Muir *et.al.*, 2017).

1.2 Location of the study

The study area is in the Eastern Cape Province of South Africa, immediately 8 km north of Port Elizabeth and it is orientated as Northwest-Southeast and geographically located at S 33°52'30" and E 25°35'0" (Fig. 1.1b). The Western part of the study area consists of high West–Northwest striking mountains such as the Groot Winterhoek, the Elands, and the Zunga Berge. The Swartkops River, especially the upper regions, the river channel is a dominantly medium to coarse-grained sedimentary assemblage with some boulder beds. The estuary comprising supratidal mudflow sediments and, intertidal and subtidal sediment bodies of grain-flow deposits in the lower reaches is underlined by older Holocene estuarine deposits (Strydom,

1985). The estuary formed during the marine transgression in the late Pleistocene when the Swartkops River valley was filled with sediments. The Swartkops River is believed to occupy about 2 km wide floodplain of which the intermittently changes course. The system measures approximately 90 m wide in the upper reaches and it is characterized by the steep banks and winding channels. Lower reaches are significantly wider with extensive intertidal mudflats, island, saltmarshes, and sandbanks. The estimated area covered by the estuary is about 682 m (Partridge and Maud, 1987). The mouth of the estuary is located at north of Port Elizabeth and the system is extended to 16.4 km inland (Partridge and Maud, 1987). The main source of sediments in the lower reaches of the estuary is the adjacent beach and the large sandbanks characterized by the lower reaches (Fig.1.2). Sediments in the middle to upper reaches are derived from terrestrial origins, mainly by the river catchment (Slinger, 1995).

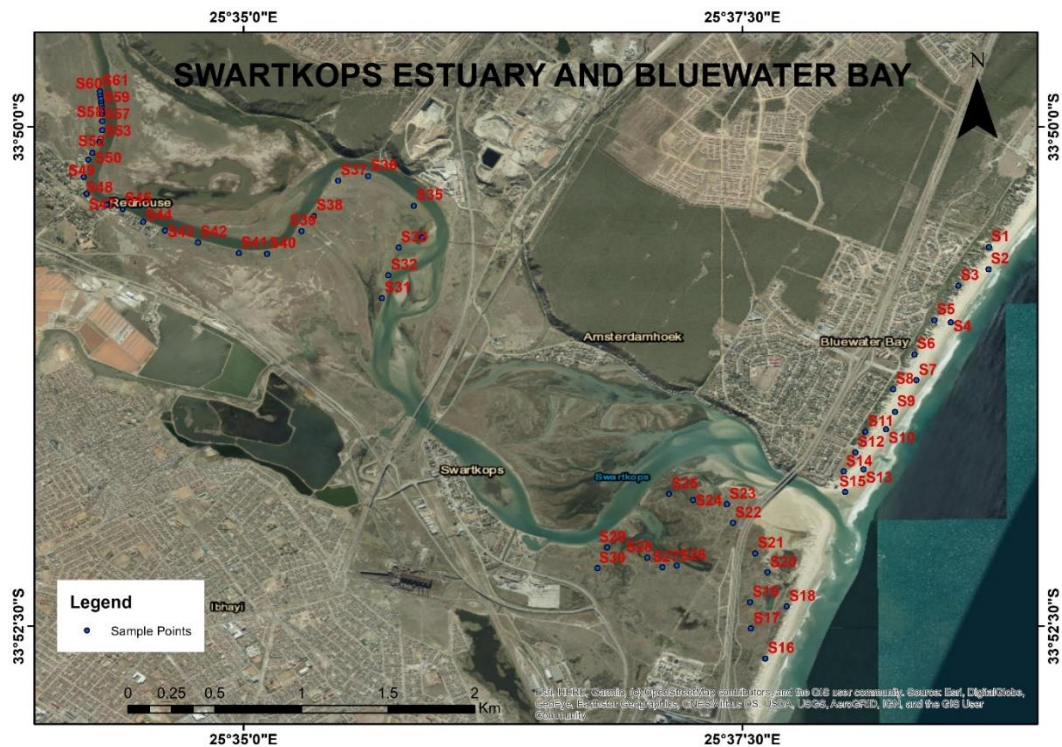


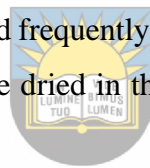
Fig. 1.2: A satellite imagery map, showing the location of the sampling stations in Swartkops estuary and Bluewater Bay beach.

1.3 Relation of grain size with water energy

It is important that the environmental effects and estuarine deposition be understood. Environmental effects can be very harmful to estuaries, for example, the heavy rain that might

cause floods and major erosions. In estuaries at large, the bank erosion is due to river flooding and wave action, speed boat wash, windblown, and the destruction of bank vegetation by people (Carter, 1987). The estuaries are composed of sediments that contain calcite, quartz, plagioclase and potassium-feldspars also other type of minerals. Other sediments in the estuaries constitute the organic materials such as small snail and shell fragments normally found in the sand sediments and the coral in the sandbank. Sedimentation produces the texture of clastic sedimentary rock by physical process and sedimentation process controls the grain shape and size.

The grain size is one of the indicators used mostly by sedimentologists for classifying unconsolidated sediments and consolidated sedimentary rocks, and further to sedimentary environments. The particle size of the materials depends on the environmental setting, hydrodynamic strength and time length during the transportation of sediments (Lopez, 2017). There are various techniques applied in grain size determination, those techniques include dry and wet sieving, the laser diffraction, sedimentation, and setting and dynamic light scattering (Lopez, 2017). One of the cheapest and frequently used techniques is the dry sieving technique where the samples or materials can be dried in the oven with a maximum temperature of 50 degrees Celsius.



University of Fort Hare
Together in Excellence

1.4 Aim and objectives of the research

The aim of the study is to character the sediments grain size, mineral compositions and the sedimentary structures, which link to the hydrodynamic environments for the formation of Swartkops estuary sediments, which is the recent developing industry area for the City of Port Elizabeth.

The specific objectives of this research are as follows:

- To analyse the sediment grain size distribution to better understand the hydrodynamic condition at the time of sediment deposition;
- To investigate mineral compositions of the sediments in the Swartkops estuary and to study the source of sediments and their depositional environment;
- To study the sedimentary structures and depositional process;
- To investigate the effects of water erosion in the estuary and coastline;
- To provide mitigation methods for protection coastal erosion.

1.5 Research questions

As stated in the objectives above, there were several task related questions we need to answer for the studies on the Swartkops estuary:

How is the sediment grain-sizes distributed in the Swartkops estuary?

What are the mineral types, abundance and the source area for these sediments?

Does grain-size variations link to hydrodynamic energy?

What are the causes for the erosion of the estuary bank and coastline?

How to protect erosion for the coastline environment?

This research project is to address the above questions, and to find effective ways to protect erosion and the environment.



CHAPTER 2 LITERATURE REVIEW

2.1 Introduction

Swartkops estuary is situated about 8 km north of Port Elizabeth, South Africa, and geographically located at longitude 25.63° E and latitude 32.87° S (Binning and Baird, 2001), (Fig. 2.1). The estuary is approximately 16.4 km long and has a permanent open tidal inlet which connects it to Algoa Bay in the Indian Ocean (Scharler and Baird, 2003). The total surface area of the estuary is about 4 km² and the average tidal prism is 3 x 10⁶ m³ with an average sediments load volume of 12 x 10⁶ m³ (Binning and Baird, 2001). During periods of low river flow, the estuary is shallow, and turbid, with an average depth of about 3 m (Scharler and Baird, 2003). The salinity gradient that exists along the longitudinal axis of the estuary throughout the year must be reversed at times due to high evaporation water levels (Binning and Baird, 2001). The estuary has extensive intertidal areas. These areas are divided between sandbanks, mud flats, and salt marshes (Winter, 1990).

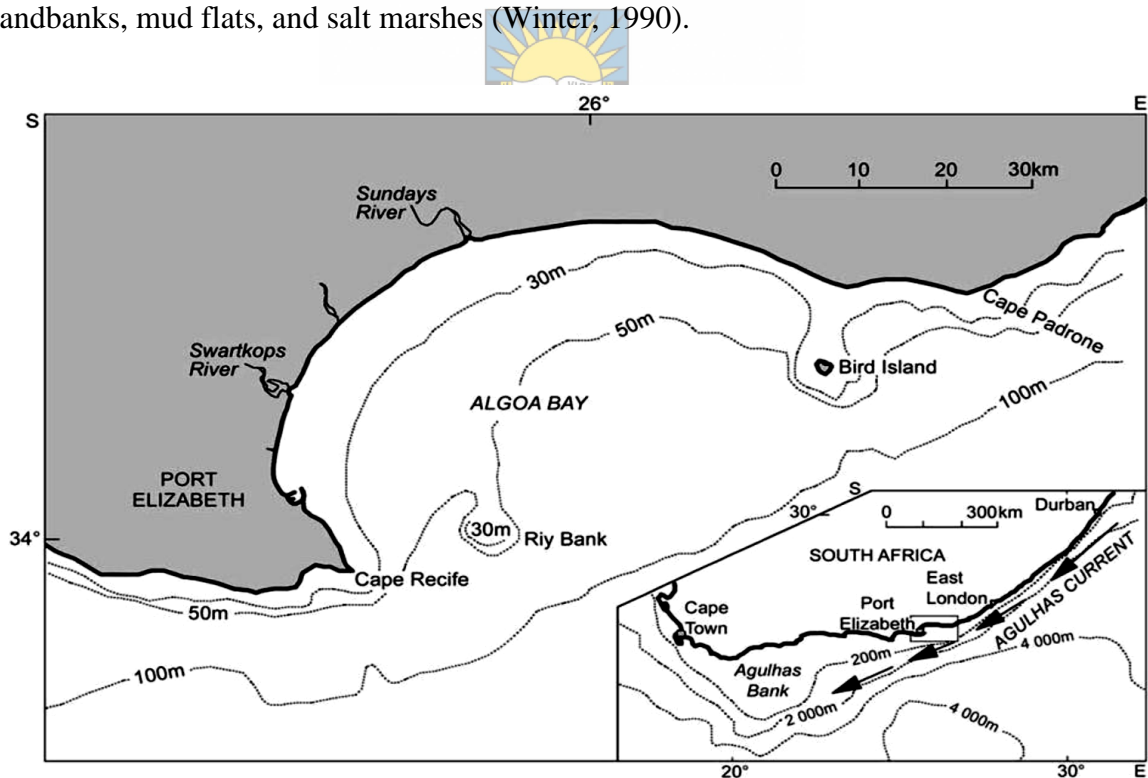


Fig. 2.1: Map of Algoa Bay, with the city of Port Elizabeth in the western sector. The inset map shows the position of Algoa Bay on the coast of South Africa. The general flow of the Agulhas current is indicated from north east to south west (Goschen and Schumann, 1988). The Swartkops River running from west to east to the Algoa Bay.

2.2 Geology of the study area

The Swartkops River originates in the West of Uitenhage, in the Groot Winterhoek Mountains catchment area (Fig 1.1b and fig.2.2). Between industrial and residential areas is the estuarine bank. In comparison to the valley's north side, which has a high slope, the south margin is moderate (Reddering, 1988). The capping of strongly cemented calcareous sandstone of the Tertiary Alexandria Formation overlies the sediments of the Uitenhage Group, resulting in a steep slope to the north of the Swartkops estuary (Reddering, 1988). Salt marshes, mudflats, and sandbanks make up the intertidal portions of the Swartkops estuary (Winter *et al.*, 1990).

The Swartkops Basin is built on a Cretaceous sandstone, shale, and mudstone foundation. Marine sedimentary layers in high-lying areas and diverse alluvial deposits in the floodplain cover the latter in a non-uniform manner. The Table Mountain sandstone and quartzite, which are Palaeozoic Silurian to early Carboniferous deposits, lie beneath the entire system. The Cretaceous System deposits in the Swartkops Basin can be classified into three formations. (Reddering and Esterhuysen, 1981), (Fig. 1.1b) namely:

- (a) (lower) Enon Formation (fluvial conglomerate)
- (b) (middle) Kirkwood Formation (fluvial sandstone, conglomerate and mudstone)
- (c) (upper) Sundays Formation (marine sandstone and shale)

The first two formations occur as outcrops in the basin, while the third formation forms the northern escarpment and major part of the hills to the south of the Swartkops River (Fig.1.1b). These units integrated as the Uitenhage Group, which has been dated as Late Jurassic to Early Cretaceous deposits (McMillan *et al.*, 1997). More younger sediments, Late Tertiary to Recent Deposits of estuarine and marine origin occurs in the valley and river streams and at the raised beaches along the coastal fringe (HKS, 1974).

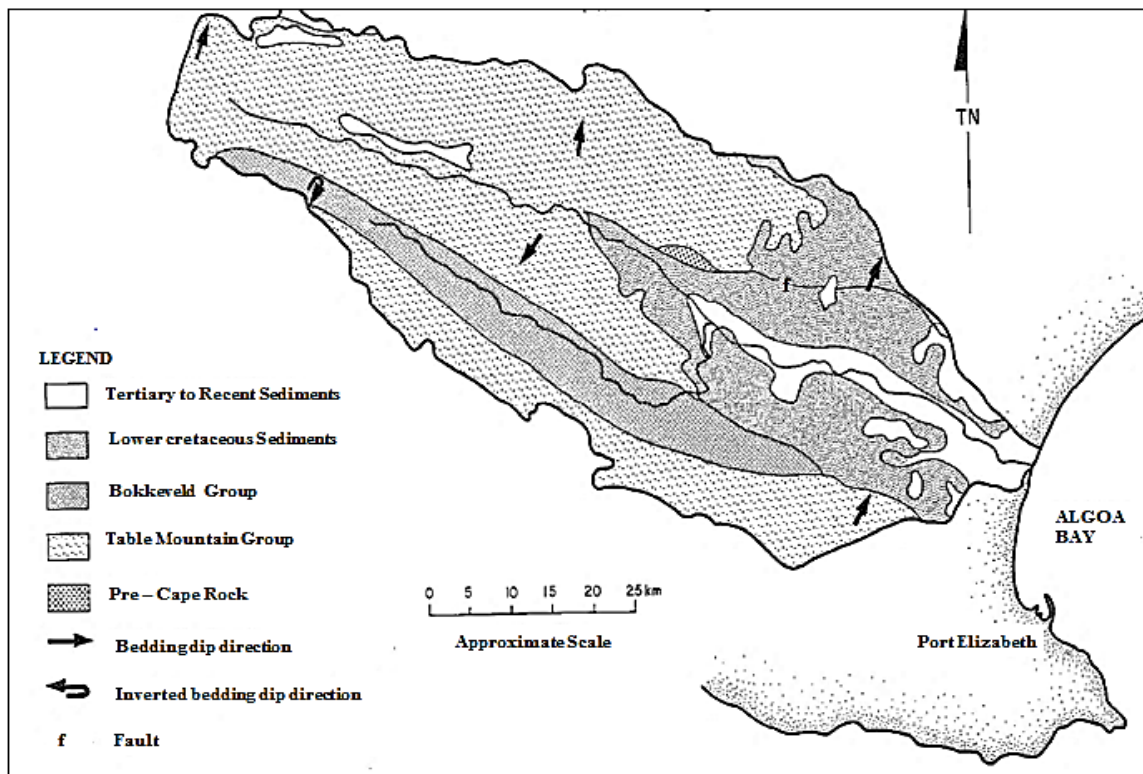


Fig. 2.2: Geological map of the Swartkops river catchment (Reddering and Esterhuysen, 1981).



2.2.1 The Enon Conglomerate Formation

The Enon Formation primarily consists of conglomerate and underlies the Kirkwood Formation and overlies the Cape Fold Belt (Fig. 1.1b and 2.3). It is a geological formation found in the Eastern Cape and Western Cape along the south coast of South Africa. The basic features of the Enon Formation contain thick bedded, poorly sorted, pebble to cobble conglomerate with sub- to well-rounded clasts, and alternated with sandstone and mudstone (Viljoen *et.al.*, 2017), (Fig. 2.3). The characteristics of sedimentary features indicate that the Enon Formation was deposited by high energy alluvial streams. Enon Formation sediments crop out along the northern margin of the basin and have been found in the Elands River valley near the Uitenhage (Frost, 1996).



Figure 2.3: Photograph showing Cretaceous conglomerate of Enon Formation in Port Elizabeth area.

University of Fort Hare
Together in Excellence

2.2.2 The Kirkwood Formation

The Kirkwood Formation is outcropped in the Eastern and Western Cape Provinces in South Africa (Fig. 1.1b). The Kirkwood Formation is made up of mostly sandstone and mudstone (Fig. 2.4). It overlies the Enon Formation and underlies the Sundays River Formation and can be divided into 3 members, that is the Swartkops Member which consists of sandstone rich unit, and lack of fossils; whilst the Colchester Member and Bethelsdorp Members contain dark grey mudstone and small amounts of sandstone (Muir *et.al.*, 2017). The thickness of Kirkwood Formation is highly variable but outreaches its maximum thickness in the Algoa Basin (Muir *et.al.*, 2017). The Kirkwood Formation in the Algoa Basin area consists of silty weathered mudrocks and small amounts of sandstone. The Kirkwood Formation in the Algoa Basin has given in the richest animal and plant fossils. The fossiliferous marine to estuarine rocks of the Colchester Member within the lower part of the Kirkwood Formation are indicative of changes in relative sea level and near to the fluvial system to marine shorelines during the Early

Cretaceous time (Bordy *et.al.*, 2015). Kirkwood Formation does not have significant age-diagnostic is normally considered as being between Late Jurassic and Early Cretaceous in age (Bordy *et.al.*, 2015).

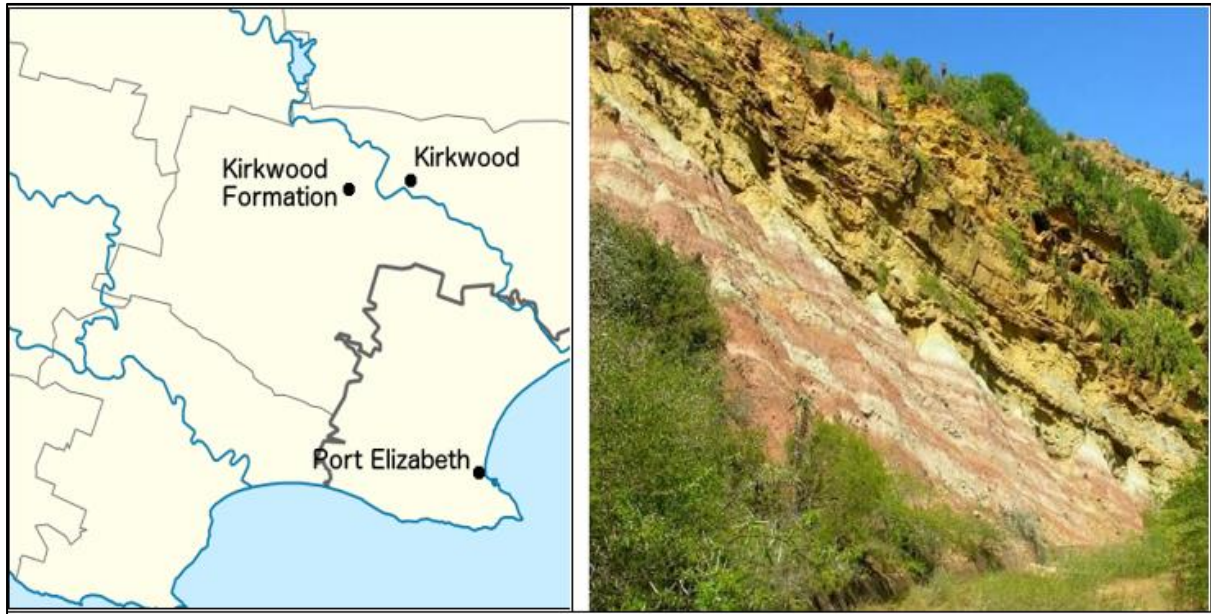


Figure 2.4: The map on the left shows the location of the Kirkwood Formation and the spread shown in figure 1.1b, which is one of the main source areas for Swartkops River sediments, while the photograph on the right shows interbedded porous medium to coarse-grained sandstone above maroon shales (Chabangu *et.al.*, 2014).

2.2.3 Sundays River Formation

The Sundays River Formation is the youngest formation found within the Uitenhage Group of the Algoa Basin (Fig. 1.1b). It overlies the Kirkwood Formation and underlies the Algoa Group. The Sundays River Formation consists of sedimentary rocks that are largely fine to medium-grained grey sandstone with shell fragments, mudstone, and siltstone (Fig.2.5). The deposit was in a shallow marine environment such as estuarine and lagoons. The outcrop of the Sundays River Formation consists of greenish-grey mudstone, and some contain gypsum and secondary limestone (Hattingh and Fourie, 2010), which indicate possible higher salinity of shallow marine to lagoon environment. The Sundays River Formation is largely covered by Tertiary to modern deposits (Hattingh and Fourie, 2010). Invertebrate fossils such as gastropods and bivalves are common in the Sundays River Formation, and they indicate Neocomian which is a Lower Cretaceous age unit (Hattingh and Fourie, 2010). The Uitenhage

Group rocks are made up of fluvial conglomerate at the bottom and younger marine mudstone at the top, reflecting a marine transgression cycle and a fining upward succession during Cenozoic times (Choiniere, 2016). The Sundays River and Kirkwood Formation rocks are best exposed through the steeper river banks of the Sundays and Bushman's Rivers in the north of Swartkops River (Choiniere, 2016).



Figure 2.5: Photograph showing the Sundays River Formation dominated by mudstone with alternated siltstone and sandstone layers.

2.3 Sediment distribution along the estuary

There are two main areas where the sediments are derived. The beach is regarded as the first that is next to the river. Marine-derived sediments typically enter the estuary through the flood-tides, although fewer residues leave the estuary during the seaward flow. When sediments are deposited in this form, they gather together on the flood tidal deltas, making the channels of the lower estuary to be in shallow water or simple to shoal. Mud deposits are present in the upper part of the estuary, and the content of mud in the sediment of Swartkops estuary is low. The large lenses point out that the estuarine deposits have been influenced over by river floods. The dominant structure is fluvial; other than that, the sediment restrains the skeletal remains of the mollusc that comes within the estuary (Reddering and Esterhysen, 1981). The cross-

bedding points out that the sediments were gathered together on tidal flood delta (Reddering and Esterhysen, 1981). The upper estuary contains more concentrated mud deposits, resulting in steep banks (Reddering and Esterhysen, 1981).

2.4 Hydrodynamics

Hydrodynamic conditions in the estuary are variable, not only in different estuary types but also in one estuary that could be different due to seasonal and climate change. The mouth of a river gets wider after the significant floods; apart from that, the water interchange is substantial after long dry periods. The sand in the mouth area is moved in and out of the Swartkops estuary mouth by strong tidal currents. The arrangement gets different and endless, which affects the tidal movement inside the estuary. It has become significant and precise that when major, the mouth can become a restriction on the floodwater movement to the sea. The flow of freshwater and the velocity tidal form the start of the likely cause of classifying the estuaries (Mark and Kowalewska-kalkwska, 2015). Current in many stratified estuaries is primarily brought around by the density and elevation dissimilarities between fresh and the salt layers (Mark and Kowalewska-kalkwska, 2015).



One effect is forcing water circulation within the estuarine, which is referred to as tidal straining. That alludes to slight differences in stratification conditions that may not get as far as to the well-mixed limit (Mark and Kowaleswska-kalkwska, 2015). In estuarine circulation, a stratified system amounts to or constitutes an extent of potential energy. In whatever way, kinetic energy is present in the movement of estuarine waters, giving less to tides, wind, and density differences (Schumann *et.al.*, 1999). The kinetic energy is interconnected to turbulent kinetic energy, lifting heavier water and adding the stratified water column to a mixed water column representing a high state of potential energy (Schumann *et.al.*, 1999). Bluewater bay beach is situated in the Algoa Bay and is exposed on the east coast of South Africa, and the easterly winds bring deep ocean waves into the bay (Ndibo, 2017). Storms, winds, and the seafloor topography are features that determine the direction and the elevation of the bay (Bremner, 1991).

2.5 Fluvial floods

The Swartkops estuary is subject to regular floods, unpredictable in duration and extent (Marais, 1982). A combination of tidal sea surges commonly causes flooding in estuaries and

is made by winds and low barometric pressures and may be exacerbated by high upstream river flow, in instances such as a tropical cyclone or extratropical cyclone. The morphology of alluvial channels and floodplain is very much overdone by high discharge (Andrew and Cooper, 1993). Consequently, floods might be regarded to produce marked geomorphological changes in large rivers that are supplied by estuaries. The impacts of the significant floods on rivers and estuaries are inadequately recorded to the extent of these rare occurrence. The role of such floods in long-term sedimentation and stratigraphic records is not known clearly (Andrew and Cooper, 1993). For an estuary structure or system, surge and ebb-tidal dominance are the essential ideas. An asymmetry in the tidal waves in which the ebb phase speed and that of a flood are different and induced by the difference in an induced asymmetry gives rise to a partiality for import or export of sediment (Townend and Pethic, 2002). The flooding has been a massive problem in the Swartkops estuary (Fig 2.6). The higher levels of the flood have been affected by the urban development on the upper valley, which has constituted the stormwater runoffs maximum level into the river. Unclean water discharge and surface water runoff need to be considered (Baird *et al.*, 1986). The overflow of the Swartkops alluvial and estuarine floodplains is happening over an average of 25 years (Carter, 1987). Intertidal areas bring about notably tidal prism which stops the mouth through scour and, also the development alongside the banks of the Swartkops River and to the other side such as the Swartkops Railway Bridge, which has affected the characteristics of flooding of the minor extent of the river (Carter, 1987). According to Reddering, the severe floods in the Swartkops estuary remove sediments down to the erosion base, which stretches from the estuary to the mouth of the Sunday's estuary (Marais, 1982). The estuaries with lots of tides have characteristics of downstream in back-barrier response to floods. There is no cohesive tidal delta, and sand barriers are eroded when floods occur (Cooper, 2001). In some cases, estuarine floods tend to show a triggering mechanism that draws a movement of sediments that accumulates and takes the involved recycling of a confirmed amount of volume of sediment at the barrier (Cooper, 2001).



Fig. 2.6 The aerial photograph shows flooding in Swartkops River.



University of Fort Hare
Together in Excellence

2.6 Coastal erosion

2.6.1 Estuarine shoreline erosion

Estuaries are a significant ecosystem, and it is quite necessary to understand the coastline changes for the importance of the resource risks. The rise of the sea level can comprise of shoreline erosion, marine submergence, inundation of low-lying coastal areas; these outcomes may be magnified by an increase in storm events (Cowart, 2009). The estuarine shoreline is regarded as a dynamic feature that experiences continued erosion. Therefore, the land is lost by short-term processes such as erosion by storms, tidal currents, and rising sea level, which is regarded as a long-term process. Once the coastal sediments are in motion, they are now reconstructed and generally based on the grain size and the weight (Rogers and Skrabal, 2001). Natural factors that influence the shoreline change and the shift in the shoreline and the changes in the habitat can result in the environmental alternation (Goodwin, 2007). Previous studies reveal that shoreline erosion is exceptionally variable from site to site, with significant ranges in erosion rates that give evidence over short distances. Studies show that the mainland marshes and low sediment bank have the highest estuarine recession rates (Corbett *et al.*, 2008). In the

Eastern Cape of South Africa, the erosion in those catchments are aggravated by the regional climate's characteristics (Fig 2.7). By the way, the maximum flood rates, drought, and reduced vegetation cover results in intensive grazing and low moisture percolation of clay soils, which constitute erosion and sedimentation (Vernon *et al.*, 1993). There are numerous cases of stabilizing the estuarine shore, such as land planning, vegetation control, the wetland toe protection, riprap revetments, the sill which is designed to protect or restore the existing or newly planted wetland vegetation, the riprap revetment, which is a sloping structure parallel to the shoreline constructed against the bank to protect it from erosion while absorbing wave energy and the bulkheads which is the vertical structure parallel to the shoreline designed to prevent overtopping, flooding or the erosion of the land.



Fig. 2.7: Road erosion caused by wave and tide current at Port Elizabeth coast in 2012.

Those are subjected to the states as geological and geotechnical characteristics of the estuary basin bed (Santos and Ferreira, 2017). In estuaries, erosion rates can be high if there is a lack of deposition sediments between storms and a little number of sediments and bay shorelines to replenish losses (Nordstrom, 1989). Erosion along the beach and estuaries and the loss of forefront properties are the results of environmental factors that act together resulting in erosion, to mitigate such acts, it is important to control the climate change on coastal processes, and the most responsible factor is global warming which causes the sea level rise (Wolanski and McLusky, 2011). Coastal erosion is again fasting up by local human interventions, leading

to a decrease in the volume of sand gravel that reaches the ocean beaches, such as the construction of dams on rivers whereby there could be a cut off of the primary source of sediment to the beaches (Wolanski and McLusky, 2011).

2.6.2 Beach erosion

Beach erosion may be caused by hydraulic action, abrasion, corrosion, and impact by wind, water, and other forces which can be natural or unnatural. Beach formation starts as eroded continental material such as sand, gravel, and even cobble material washed by streams and rivers. Dissipative beaches are typically eroded by swash bores and undertows associated with elevated water levels and storm surges (Hesp, 2011). Erosion induced by storm at a particular site can be affected by pre-storm beach profile and geological conditions (Zhang *et.al.*, 2001). Big storm waves are the direct result of erosion; nevertheless, the storm tide determines the position where storm waves attack beaches and dunes (Zhang *et.al.*, 2001). Beach erosion and dune scarping are laterally continuous alongshore and, at times, catastrophic or disastrous (Hesp, 2011). Beach erosion predictions from any cause are essential in coastal management (Short and Jackson, 2013). It forms the underlying support of setback and hazard lines, buffers zones, and retreat strategies and approximates sediment volumes needed in beach nourishment projects (Short and Jackson, 2013). Beaches can promote critical marsh and wetlands habitats, but storms can reshape them abruptly and dramatically. Beach resilience is quite limited in low energy environments where regular waves are strong enough to take back the sand that storm waves deposited (Duvat, 2009). Human-induced beach erosion can be minimal due to the coastal zone's low development level (Duvat, 2009).



Fig. 2.8: Photograph shows erosion caused by waves and stirring up of currents along the shore on a coastal tarred road.

2.7 Estuarine sediment dynamics

Estuaries can be regarded as a tidal pulsing of sediments that move upstream under low river flow, and with high tidal flow conditions and in some instances (Fig. 2.9), the downstream sediments that are pulsing downstream of sediments with high river flow and weaker tidal flows and by the way the delivery of sediments happens on the coastal zones and the catchment (Wolanski and Elliot, 2016). Marine sediments in the lower ridges dominate the Swartkops estuary, and the fluvial deposits dominate the central and upper highlands. The main channel in the Swartkops estuary of the lower reaches consists of the sandy substrate (Baird *et.al*, 1986). Estuaries are dominated by clays, silts with sands, and larger sizes deposited at the head of the estuary or even in the ocean entrances. Almost all the sediments in the estuary are called mud since the residues include organic and inorganic materials, fine-grained sediments and clay sizes and some silts; in the case of transportation, deposits are characterized by their size, composition constituents, and cohesion (Mehta and McNally, 2009). In the Swartkops estuary, the meanders, river beds, and flood plains were devised to a period of sea level. The Swartkops estuary seemed to be in a firm or steady phase, and that being the reason for minor variations, which are typical in the natural behaviour such as sandbanks in the estuary (Baird *et al.*, 1986). In the sediment movement, there is a frictional drag responsible for water movement that covers sediment beds. This frictional drag exerted by water is also responsible for the sediment grains at the water-sediment interface. The sediments' action starts when the shear stresses and the lifting forces from the turbulent currents become great to overcome frictional and gravitational forces binding the grains together on the bed (Schumann, 2003). Estuaries comprise many dynamic environments at large, so they have an objective in riverine systems merge with marine systems, and they show both floods and droughts and even the waves and tides (Reisinger *et al.*, 2017). In estuaries, the river and the tidal flows produce estuarine and sediment dynamics (McLachlan *et al.*, 2017).

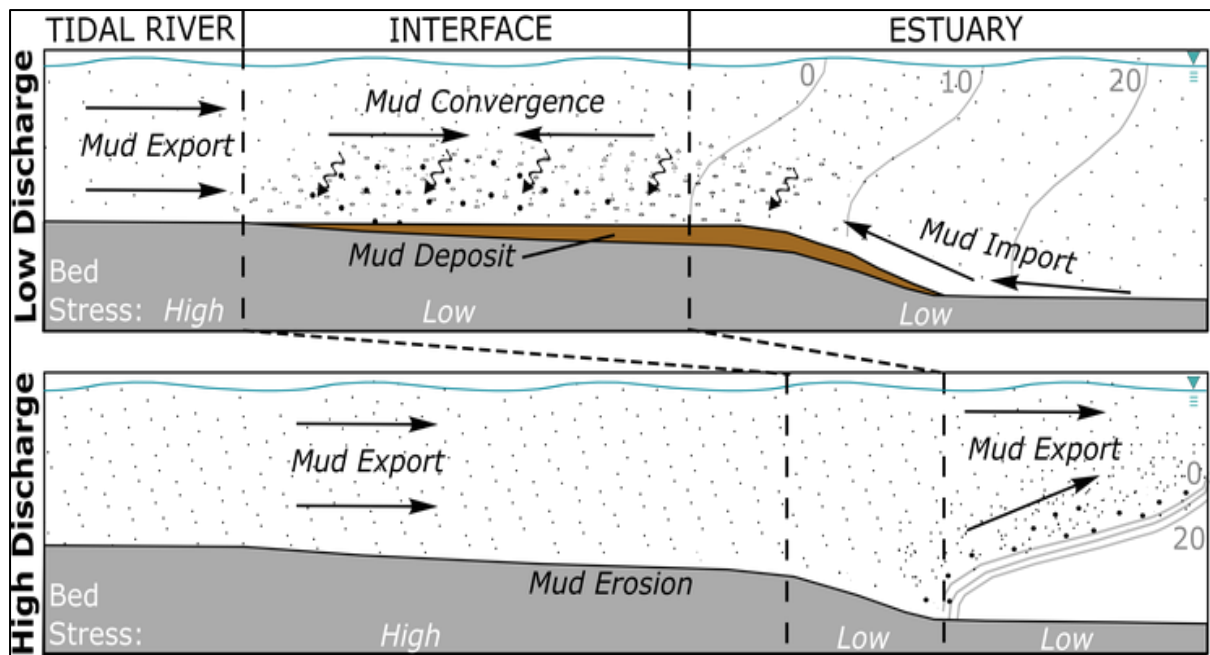


Fig.2.9: Sediment dynamics between high discharge and low discharge in the tidal river to estuarine reach (McLachlan et al., 2017).



2.8 Beach sediment dynamics

Beaches consist of sediments that can range in size from the sand up to cobbles and boulders. Adequate sand results in shallow gradient beaches, while cobbles may be stacked at a steep angle. Bluewater bay beach consists mainly of sands, and it is a wave-dominated deposited accumulation of sediment located at the shoreline and dunes. The deposition is through wave action and induced currents rather than tide induced or wind-induced currents (Van Rijn, 2010). Generally, sand coasts such as Bluewater bay are open coasts exposed to wind-generated waves. They may vary from flat, low energy, straight coastal beach plains to steep, high energy deficient, and irregular bay headlands (Van Rijn, 2010). Coastal dynamics result from three-dimensional sediment movements over time, driven by waves, currents and winds, which are influenced by the shape of the sediment mass, being the landform that defines the configuration of any given section of the coast (Eliot, 2016). Landforms may persist over time either when their features, such as beach, limit sediment transport capacity or when sediment supply rates and loss from the landform occur over a perspective timescale (Eliot, 2016). Beaches and shoreface consist mainly of quartz materials.

Heavy minerals are sometimes found as concentrated deposits within the beach and may erode and become exposed during storm events. Beaches may include materials from biogenic nature like carbonates; carbonates can be formed by direct precipitation seawater saturated with calcium carbonates. Shells and shell fragments are found on many beaches, and they are concentrated on the coast by wind and wave action. Numerous organisms can transform sediment particles into more solid material, producing protective erosion-resistant bottom layers (Van Rijn, 2010). Sandy beaches are subject to erosion, especially during winter storms and are globally retreating under sea rising sea-level. Bluewater bay beach are directly exposed to waves; greater energy is associated with the deep ocean swell (Goschen and Schuman, 2011). Beaches inside estuaries differ in form and structure, and those on the open coast (Eliot, 2016). These can physically separate erosion and recovery sediment pathways and often result in limited beach recovery after storm events unless there is a sediment source active under prevailing conditions (Eliot, 2016).



University of Fort Hare
Together in Excellence

CHAPTER 3 METHODOLOGY

3.1 Introduction

In this research, the materials and methods used involves the collection of data along the estuary and the coast which is the process of obtaining the information and the data from the field. The methodologies adopted in this work include the literature review, laboratory analysis and field work investigation. The laboratory work constitutes the petrographic, mineralogical analysis, the (SEM) scanning electronic microscopy, the (XRD) x-ray diffraction analysis and the grain size analysis.

3.2 Field observation

The fieldwork was carried out in June 2019 in Swartkops estuary, and some samples were sampled in the Bluewater Bay beach. The Swartkops estuary consists mainly of Cretaceous to Jurassic Uitenhage Group deposits, and floodplain areas are formed by quartzitic sandstone along the river banks. The estuary consists of a clast deposit of gravel and boulders. From the estuary to the Bluewater Bay, the area is mainly of sand and the dunes as the most common component along the area and also with pebbles and shells and quartz veins (Figure 3.1). Sixty-one samples were collected along the Swartkops estuary to the Bluewater Bay but in different locations (Fig. 1.2). Of those sixty-one samples, fifteen samples were collected from the Bluewater bay, and Forty-six samples were collected from Swartkops estuary. The GPS was used for the coordinates of the locations. Between the Swartkops estuary and blue water bay, there were sedimentary structures observed, such as real marks, swash zone, and ripple marks. The Swartkops, on its own, has a lot of channels, and the plain is finer with different sediment, which depends on water energy and lots of snail shells, the pebbles are lighter which were exposed for a shorter time, and the darker one which was exposed to a longer time. The Swartkops estuary has a lot of engineering projects used to protect the river bank. The Swartkops estuary has a lot of vegetation for retaining the water and full water swamps.



Fig.3.1: The photograph shows field observation from Swartkops estuary to Bluewater beach, photograph (A) showing quartzite with quartz veins (black arrow), photograph (B) showing sand dune with vegetation, photograph (C) showing small pebbles (yellow arrow) and photograph (B) showing shell fragments.



Fig.3.2: The photograph showing students in the field observation and sampling along the Swartkops estuary.

3.3 Grain-size sieving analysis



The sand samples were collected for sieve analysis for determining the particle size distribution for sand materials by allowing the sand to pass through a series of sieves of progressively smaller mesh sizes. The material that is retrieved in each sieve is weighed as a fraction of a whole mass. Therefore, the data (sand samples) collected in Swartkops estuary and blue water bay was dried up in the laboratory machine oven at the maximum temperature of 50 degrees Celsius. A pan and six sieves were used for sieving, the start was on the large sieve with a large diameter of 2.0 mm ($-\phi$) on top to a smaller sieve of the diameter of 0.0625 mm (4ϕ), and the Wentworth scale can show a pan of 0.031 mm (5ϕ). For mineral analysis, some measured mass sediments retained were used for analysing the minerals present in the sand materials. The sediments retained on each sieve were measured and recorded.



Fig.3.3: The process and equipment for the grain size analysis.

3.4 Petrographic microscope

The sediments were first dried up in the oven at a maximum temperature of 50 degrees Celsius. The sediments were then sieved before the mineral analysis so that there could be a range of grain size. Ten samples were separated in plastic bags and were achieved with the use of a progressive finer abrasive grit. The smooth samples were mounted on a 26 mm by 46 mm glass microscope slide using Struers specific resin mixed with Struers specific -40 curing agent in the ratio 5:2 by weight and they were left for 48 hours and observed under the microscope (Fig. 3.4). The magnifying microscope was used to identify the minerals that constitute the sediments

(Fig. 3.4). The minerals were then observed and recorded, and the pictures were taken and will be shown in the mineralogical composition chapter. The camera piece was used to observe the samples on the computer screen to make it simple to record the samples images. Photographs of different minerals and their petrological textures were studied to ascertain the mineral compositions and sorting of grains.



Fig.3.4: Photograph showing Struers trimming machine (Accuton-50) (yellow arrow) for thin section preparation at the Geology department's thin section laboratory, University of Fort Hare.



Fig.3.5: The photograph shows the microscope studies for minerals composition analysis.

3.5 SEM and EDX analysis

A scanning electron microscope (SEM) was used for revealing useful information about the sample, including texture, grain morphology, and recrystallization of the samples (Fig. 3.5). The SEM played a considerable part in studying the relationships between the minerals texture and shape. The samples were first coated using the carbon coating. The coating was to prevent the charging of the specimen from occurring due to the static electric field. The energy dispersive x-ray (EDX) was for the determination of the mineral chemical compositions in the samples.

Each sample was coated with gold-palladium with the use of Cressington 108carbon/A carbon coater. The scanning electron microscopy (SEM) machine Model was Jeol JSM-6390LV,

JEOL, Tokyo, Japan in a working condition of 15 KV. The quipped Energy Dispersive X-Ray micro-analyzer (EDX) Model was Jeol JSM-6390SEM, JEOL, Tokyo, Japan). The study was done at the University of Fort Hare.



Fig.3.6: Photograph shows the Scanning Electron Microscope (SEM) and the Energy Dispersive X-ray spectrometry analysis (EDX). JEOL JSM-6390 LV model Scanning Electron Microscopy.

3.6 The X-ray diffraction analysis (XRD)

The XRD analysis is a non-destructive test method used to analyze the structure of the crystalline materials. It is used to identify the crystalline phases present in a material and thereby reveal chemical composition information. It is also a measurement tool for sample purity. The eight sample sand materials were sent (about 10 grams each) to the XRD analytical and consulting in Pretoria where the samples were analyzed using the backloading preparation method. Diffractograms were obtained using the Malvern Panalytical Aeris diffractometer with PIXcel detector, and fixed slits with Fe filtered Co-K α radiation. The phases were identified using X'Pert Highscore plus software. The relative phase amounts (Weights %) were using the Rietveld method. The scanning speed is 1° 2 θ /minute.

3.7 Instruments used during the research

- Geological harmer;
- Digital camera for capturing outcrop and photos in the field;
- Global positioning system (GPS);
- Sieve set and weighing balance;
- Laboratory machine oven for drying of samples;
- Petrographic microscope;
- Scanning Electron Microscope (JEOL JSM-6390 LV model) equipped with Energy Dispersive X-ray spectrometry.



CHAPTER 4 GRAIN SIZE ANALYSIS

4.1 Introduction

Grain size analysis is an important tool for differentiating and classifying sedimentary rocks, hydrodynamic energy and sedimentary environments. Grain size analysis provides a clear picture of the sediment distribution and transport hydrodynamics in various conditions (Blott and Pye, 2001). Various mechanisms affect the grain size distribution, such as transport media, distance and local topography since grain size analysis also reflects sorting and the shape parameters (roundness and sphericity) of particles, which closely linked to the transport distance, current energy and depositional processes. The grain size of siliciclastic sediments can reflect the hydraulic energy of the environment.

The finer grains accumulate in slow-moving water and the coarser grains are carried by strong flowing currents. Grain size analysis is dependent on statistical parameters such as mean, sorting, skewness and kurtosis. The samples are presented for well sorted, moderately sorted, and poorly sorted. The beach samples are generally well sorted. The estuarine sediments are categorized as poorly sorted, moderately and few well sorted. Sorting is used for clear description for grain size distribution and it reflects the hydrodynamic condition.

Based on the grain size, unconsolidated (soft) sediments are divided into four categories which are gravel, sand, silt and clay. The particle size is measured on diameter and is transferred from millimeters to phi scale. The classification of grain size in millimeter scale and phi scale is list in the Table 4.1 below.

Table 4.1 Classification of sediments and sedimentary rocks based on the grain-size (Friedman and Sanders, 1978; modified from Blott and Pye, 2001).

Grain size		Descriptive terminology		
phi	mm/ μ m	Udden (1914) and Wentworth (1922)	Friedman and Sanders (1978)	GRADISTAT program
–11	2048 mm		Very large boulders	
–10	1024	Cobbles	Large boulders	Very large
–9	512		Medium boulders	Large
–8	256		Small boulders	Medium
–7	128		Large cobbles	Small
–6	64		Small cobbles	Very small
–5	32	Pebbles	Very coarse pebbles	Very coarse
–4	16		Coarse pebbles	Coarse
–3	8		Medium pebbles	Medium
–2	4		Fine pebbles	Fine
–1	2	Granules	Very fine pebbles	Very fine
0	1	Very coarse sand	Very coarse sand	Very coarse
1	500 μ m	Coarse sand	Coarse sand	Coarse
2	250	Medium sand	Medium sand	Medium
3	125	Fine sand	Fine sand	Fine
4	63	Very fine sand	Very fine sand	Very fine
5	31	Silt	Very coarse silt	Very coarse
6	16		Coarse silt	Coarse
7	8		Medium silt	Medium
8	4		Fine silt	Fine
9	2	Clay	Very fine silt	Very fine
			Clay	Clay

Grain size analysis has now become a wide used research method in sedimentology. Numerous authors had used this method to study different aspects of sedimentary topics, such as Folk and Ward (1957), Passega (1964), Sahu (1964), Friedman (1967), Middleton and Hampton (1976), Friedman (1977), Friedman and Sanders (1978), McLaren (1981), Blott and Pye (2001), and Boggs (2009), to mention a few.

Grains in sedimentary rocks depict a wide range of size distributions, hence the frequencies of grain size ranges determine the grain size classes (Wentworth, 1929). The unit of grain size millimetre converts to a phi (ϕ) scale using the expression as below:

$$\phi = -\log_2 D$$

Where ϕ and D represents the phi size and grain diameter in millimetre scale respectively. The obtained grain size data were presented as frequency.

4.2 Grain size measurements for sediments

Grain size analyses were done for sixty one samples. The results of the grains size for estuary and beach sediments were graphically presented as histograms and cumulative frequency curve. Figure 4.1 to 4.17 represent the typical groups of grain size distribution, and the Appendix A (Figure A1 to A61) are the remained grain size distribution graphs which were not listed in the text to save the text length. Statistic parameters were calculated for all the samples and the results are presented in Table 4.3.

The following parameters are calculated for each sample in this study, all these parameters are measured in phi (ϕ) units.

- **Median (Md)** - corresponds to the 50 percentile on a cumulative curve, where half the particles by weight are larger and half are smaller than the median. $Md = \phi_{50}$
- **Mean (Mz)** - is the average grain-size. Several formulas were used in calculating the mean in the previous literature by different authors. The most widely used graphically derived value is that given by Folk and Ward (1957). It indicates the central tendency of a grain size distribution. The calculation formula is listed as below.

$$M_z = \frac{\phi_{16} + 50\phi_{50} + 84\phi_{84}}{3}$$

- **Standard deviation (Sorting, σ_1)** - is a measuring of the grain-size variation of a sample by encompassing the largest parts of the size distribution as measured from a cumulative curve (Folk and Ward, 1957).

$$\sigma_i = \frac{\phi_{84} - \phi_{16}}{4} + \frac{\phi_{95} - \phi_5}{6.6}$$

- **Skewness (SK_i)** - measures the degree of symmetricity of grain size distribution, and describes the majority of the grain size. The more the calculated skewness values deviate from zero, the more the skewed. The formula of calculation of skewness proposed by Folk and Ward (1957) is listed as below.

$$SK_i = \frac{\phi_{16} + \phi_{84} - 2(\phi_{50})}{2(\phi_{84} - \phi_{16})} + \frac{\phi_5 + \phi_{95} - 2(\phi_{50})}{2(\phi_{95} - \phi_5)}$$

- **Kurtosis (K_G)** - is a measure of peakedness in the size distribution curve where the phi values represent the same percentages as those for sorting (Folk and Ward, 1957). Actually, kurtosis measures the sorting ratio rather than peakedness of the frequency curves. In cases where the tails are better sorted than the central parts, then it is referred to as platykurtic, and when the central part is better sorted, it is known as leptokurtic. Furthermore, if tail and the central part are both equally sorted, then it is called mesokurtic.

$$K_G = \frac{\phi_{95} - \phi_5}{2.44(\phi_{75} - \phi_{25})}$$



University of Fort Hare
Together in Excellence

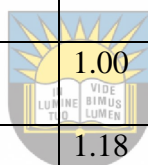
Table 4.2 Formulas for calculating grain size parameters (Source: Folk and Ward, 1957).

Mean	$M_z = \frac{\phi_{16} + \phi_{50} + \phi_{84}}{3}$	(1)
Standard deviation (Sorting)	$\sigma_i = \frac{\phi_{84} - \phi_{16}}{4} + \frac{\phi_{95} - \phi_5}{6.6}$	(2)
Skewness	$SK_i = \frac{(\phi_{84} + \phi_{16} - 2\phi_{50})}{2(\phi_{84} - \phi_{16})} + \frac{(\phi_{95} + \phi_5 - 2\phi_{50})}{2(\phi_{95} - \phi_5)}$	(3)
Kurtosis	$K_G = \frac{(\phi_{95} + \phi_5)}{2.44(\phi_{75} - \phi_{25})}$	(4)

Table 4.3 Parameter values of the grain size analyses for collected samples.

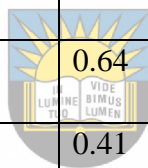
Sample No	$M_d (\phi)$	$M_z (\phi)$	σ_1	S_k	K_G
S1	2.10	2.16	0.62	0.07	0.81
S2	2.50	2.57	0.30	0.17	1.01
S3	2.49	2.58	0.34	0.30	0.98
S4	2.70	2.67	0.41	-0.08	1.05
S5	2.50	2.63	0.46	0.20	0.56
S6	2.60	2.67	0.45	0.17	0.94
S7	2.70	2.67	0.41	-0.09	0.89
S8	2.60	2.60	0.36	0.04	0.90
S9	2.60	2.63	0.32	-0.03	0.81
S10	2.70	2.67	0.38	-0.19	1.03
S11	2.50	2.53	0.47	0.01	0.70
S12	2.40	2.57	0.40	0.40	0.81
S13	2.50	2.53	0.44	0.02	1.22
S14	2.40	2.53	0.44	0.39	0.66
S15	2.20	2.43	0.49	0.47	0.60
S16	2.70	2.57	0.55	-0.50	1.17
S17	2.90	2.76	0.46	-0.41	0.90
S18	2.50	2.50	0.64	-0.06	1.17
S19	2.10	1.30	1.67	-0.51	0.90
S20	1.00	0.93	1.60	0.01	0.76

S21	2.20	2.10	1.05	-1.10	2.86
S22	2.20	2.36	0.90	0.07	3.60
S23	1.60	1.97	0.60	0.58	0.78
S24	2.30	2.30	0.66	-0.42	1.22
S25	2.50	2.43	0.53	-0.28	0.90
S26	1.00	1.30	1.40	0.26	0.91
S27	2.50	2.16	1.23	0.90	3.68
S28	1.50	1.80	0.76	-0.01	0.88
S29	1.80	1.93	0.73	0.21	0.30
S30	2.50	2.00	1.44	-0.32	1.13
S31	2.50	1.63	1.00	-1.37	1.46
S32	2.10	1.67	1.18	-0.39	0.52
S33	2.40	1.76	1.31	-0.43	3.90
S34	2.50	2.47	0.32	-0.06	1.02
S35	2.50	2.47	0.42	-0.17	1.33
S36	2.50	1.80	1.19	-0.66	0.48
S37	2.50	1.76	1.15	-0.72	1.63
S38	2.50	2.43	0.52	-0.31	1.48
S39	2.61	2.57	0.48	-0.22	0.99
S40	2.71	2.57	0.76	-0.49	1.88
S41	2.51	2.50	0.53	-0.28	2.25
S42	2.40	1.83	1.09	-0.61	2.11



University of Fort Hare
Together in Excellence

S43	2.60	2.57	0.57	-0.33	2.35
S44	2.50	1.90	1.13	-0.62	1.87
S45	2.60	2.53	0.47	-0.39	1.85
S46	2.61	2.47	0.68	-1.61	1.69
S47	2.30	2.40	0.54	0.09	2.15
S48	2.50	2.50	0.67	-0.17	1.43
S49	2.50	2.53	0.35	0.07	1.63
S50	2.40	2.43	0.71	-0.17	1.69
S51	2.50	2.30	0.78	-0.50	2.97
S52	2.60	2.50	0.74	-0.44	2.11
S53	2.50	2.43	0.64	-0.36	1.77
S54	2.70	2.53	0.41	-0.60	2.18
S55	2.60	2.53	0.44	-0.31	1.31
S56	2.50	2.50	0.47	0.10	1.22
S57	2.70	2.63	0.50	-0.12	1.16
S58	2.70	2.67	0.57	-0.13	1.34
S59	2.50	2.56	0.45	0.03	1.39
S60	2.80	2.67	0.67	-0.52	1.91
S61	2.60	2.60	0.52	-0.11	1.47



University of Fort Hare
Together in Excellence

Table 4.4: Verbal classifications of the sorting, skewness and kurtosis (after Folk, 1974).

SORTING (σ_1)	
Very well sorted	< 0.35
Well sorted	0.35 to 0.50
Moderately well sorted	0.50 to 0.71
Moderately sorted	0.71 to 1.00
Poorly sorted	1.00 to 2.00
Very poorly sorted	2.00 to 4.00
Extremely poorly sorted	> 4.00
SKEWNESS (Sk_1)	
Coarse-skewed	-1.00 to -0.30
Strongly coarse-skewed	-0.30 to -0.10
Near-symmetrical	0.10 to -0.10
Fine-skewed	0.30 to 0.10
Strongly fine-skewed	1.0 to 0.30
KURTOSIS (K_6)	
Very platykurtic	<0.67
Platykurtic	0.67 to 0.90
Mesokurtic	0.90 to 1.11
Leptokurtic	1.11 to 1.50
Very leptokurtic	1.50 to 3.00
Extremely leptokurtic	> 3.00

4.3 Beach Sediments

Beach samples are characterized by fine to medium sands in size, well sorted and unimodal in grain-size distribution. The samples mostly retained in 3 Phi size which represents as fine sands. The cumulative frequency curve (Fig. 4.1-4.4) is sharply angled and shows the grain size is very concentrated.

The Swartkops beach is dominated by well sorted sediments. According to Folk (1951), well sorted sediments suggest a mature to a super-mature stage of textural maturity of sands. The dominance of well sorted confirms that the sediments were deposited on a shallow marine environment or the beach environment where tide and wave currents sort the sediments by size (Friedman, 1961; Blott and Pye, 2001). This group includes 16 samples. For the sake of saving text space, we list only four representative samples as below.

Sample 1 (Beach sands)

Table 4.5 Retained and cumulative percentage of grain size for sample 1. Aliquot mass =322.39g.

Sieve size (φ)	Mass retained (g)	% retained	Cumulative %
-1	1.21	0.37	0.37
0	2.13	0.66	1.03
1	2.80	0.87	1.90
2	82.21	25.58	27.48
3	230.62	71.76	99.24
4	2.26	0.70	99.94
5	0.12	0.06	100
Retained total mass	321.35g		

University of Fort Hare

Together in Excellence

Aliquot mass – retained total mass

$$\text{Error} = 100\% \times \frac{\text{Aliquot mass} - \text{retained total mass}}{\text{Aliquot}} = 0.3\%$$

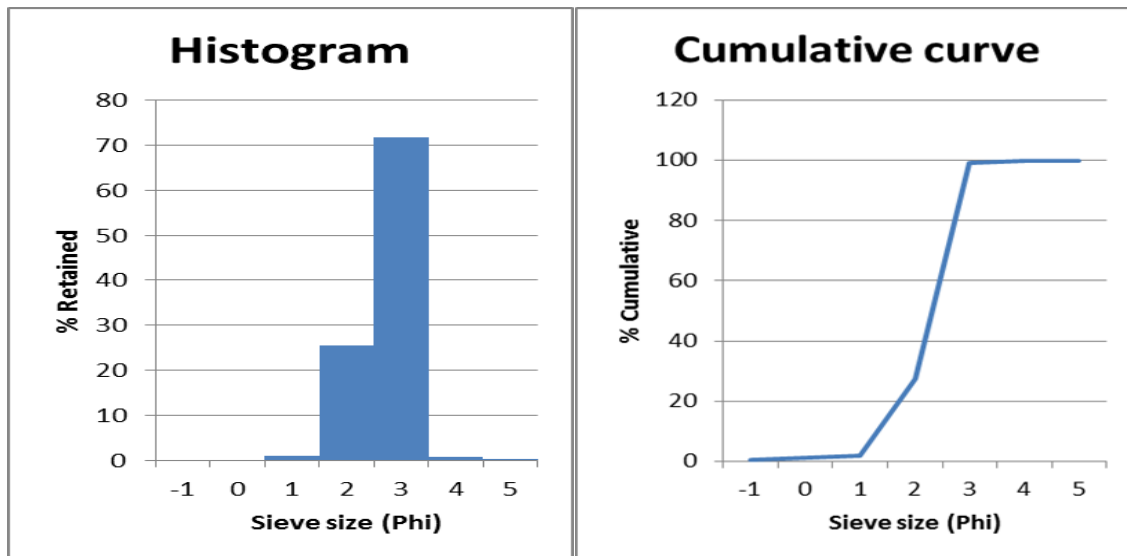


Fig. 4.1: Histogram (left) and cumulative frequency curve (right) of the Sample 1, showing the grain size distribution varied from 1.5-3.5 phi which is dominant at 3 Phi (0.125 mm) and a part of at 2 phi (0.25 mm).

Sample 2 (Beach sands)



Table 4.6 Retained and cumulative percentage of grain size for sample 2. Aliquot mass=259.94g.

Sieve size (ϕ)	Mass retained (g)	% retained	Cumulative %
-1	2.00	0.77	0.77
0	0.97	0.37	1.14
1	1.35	0.52	1.66
2	11.94	4.64	6.30
3	237.63	92.48	98.78
4	2.31	0.89	99.67
5	0.75	0.29	99.96
Retained total mass	256.95g		

Error = 1.1%

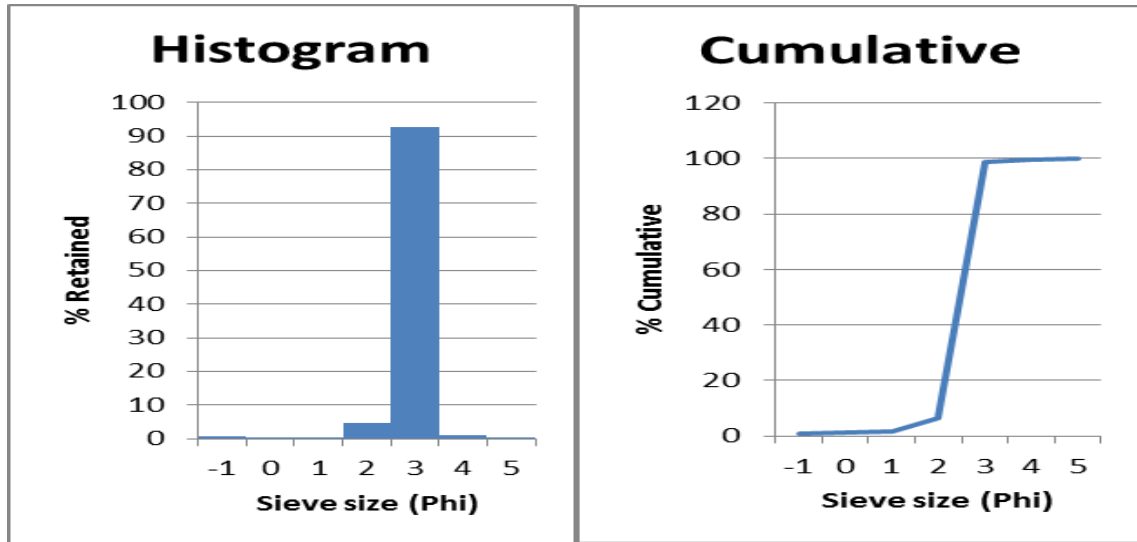


Fig. 4.2: Histogram (left) and cumulative frequency curve (right) showing grain size distribution of the Sample 2. The grain size is dominant at 3 Phi (0.125 mm) followed by small percentage of grain size of 2 Phi (0.25 mm).



Sample 14 (Beach sands)

Table 4.7 Retained and cumulative percentage of grain size for sample 14. Aliquot mass = 397.14 g.

Sieve size (ϕ)	Mass retained (g)	% retained	Cumulative %
-1	0.10	0.02	0.02
0	0.20	0.05	0.07
1	1.54	0.38	0.45
2	29.77	7.51	7.96
3	347.85	87.80	95.76
4	11.98	3.02	98.78
5	4.72	1.19	99.97
Retained total mass	396.16g		

Error = 0.2 %

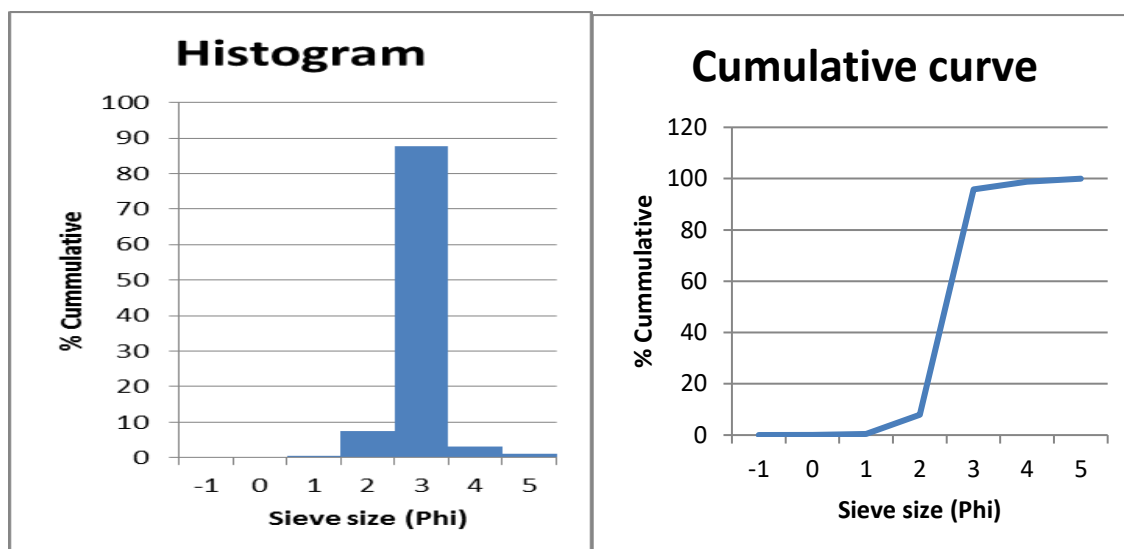


Fig. 4.3: Histogram (left) and cumulative frequency curve (right) of Sample 14, showing grain size varied from 1.5 phi to 4.5 phi, and well sorted nature, with dominant size at 3 Phi (0.125 mm) and minor at 2 Phi (0.25 mm) and 4 phi (0.0625 mm).

Sample 15 (Beach sands)

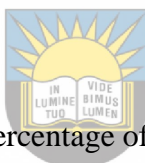


Table 4.8 Retained and cumulative percentage of grain size for sample 15. Aliquot mass = 291.99 g.

University of Fort Hare

Sieve size (ϕ)	Mass retained (g)	% retained	Cumulative %
-1	3.41	1.16	1.16
0	1.99	0.68	1.84
1	3.06	1.04	2.88
2	10.19	3.49	6.37
3	266.94	91.45	97.82
4	3.21	1.09	98.91
5	3.09	1.05	99.96
Retained total mass	291.89g		

Error = 0.03%

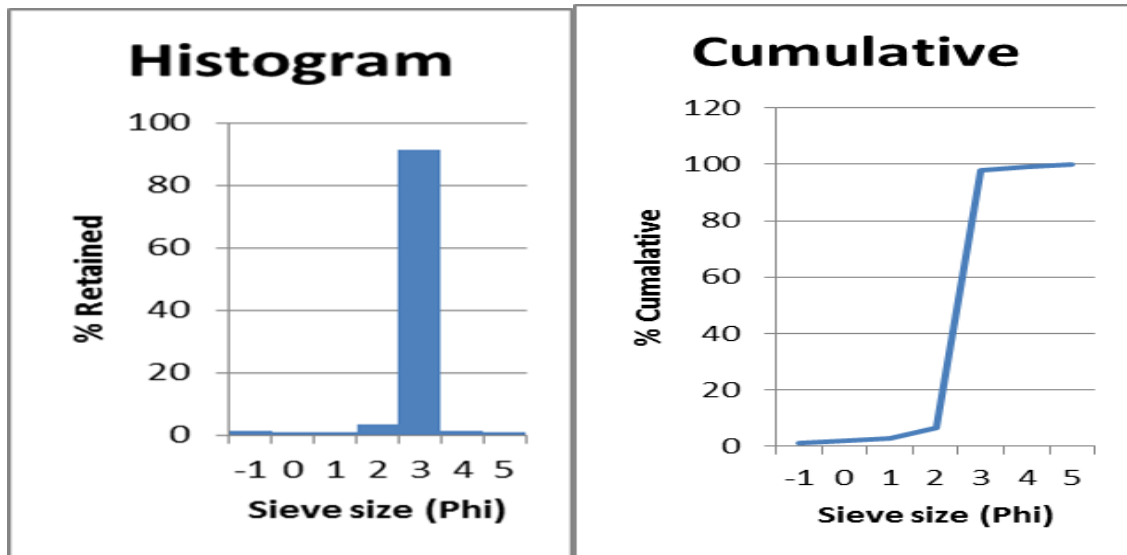


Fig. 4.4: Histogram (left) and cumulative frequency curve (right) showing grain size distribution of Sample 15. The grain size is dominant at 3 Phi (0.125 mm) followed by small percentage of grain size of 2 Phi (0.25 mm).

4.3.1 Grain size statistical parameters of beach sediments

The parameter of grain size analysis for beach sediments are listed below (Table 4.9).

Table 4.9 Parameter values for beach sediments

Sample No	M _d (Φ)	M _z (Φ)	σ ₁	S _K	K _G	Explanation for kurtosis, Skewness and sorting
S1	2.10	2.16	0.62	0.07	0.81	Moderately well sorted, near symmetrical and platykurtic
S2	2.50	2.57	0.30	0.17	1.01	Very well sorted, fine skewed and mesokurtic
S3	2.49	2.58	0.34	0.30	0.98	Very well sorted, fine skewed and mesokurtic
S4	2.70	2.67	0.41	-0.08	1.05	Well sorted, near symmetric and mesokurtic
S5	2.50	2.63	0.46	0.20	0.56	Well sorted, fine skewed and very platykurtic

S6	2.60	2.67	0.45	0.17	0.94	Well sorted, fine skewed and mesokurtic
S7	2.70	2.67	0.41	-0.09	0.89	Well sorted, near symmetric and platykurtic
S8	2.60	2.60	0.36	0.04	0.90	Well sorted, near symmetric and mesokurtic
P9	2.60	2.63	0.32	-0.03	0.81	Very well sorted, near symmetric and platykurtic
S11	2.50	2.53	0.47	0.01	0.70	Well sorted, near symmetric and platykurtic
S12	2.40	2.57	0.40	0.40	0.81	Very well sorted, fine skewed and platykurtic
S13	2.50	2.53	0.44	0.02	1.22	Well sorted, near symmetric and leptokurtic
S14	2.40	2.53	0.44	0.39	0.66	Very well sorted, fine skewed and mesokurtic
S15	2.20	2.53	0.44	0.39	0.66	Well sorted, near symmetric and mesokurtic
S17	2.90	2.76	0.46	-0.41	0.90	Well sorted, strongly coarse-skewed and mesokurtic

4.3.2 Discussion of the grain size analysis for beach sediments

Mean grain-size (Mz)

A mean is an arithmetic average of grain size that measures the average size of sediments, Mean gives an average value of a distribution of sediments. The mean grain size of the beach samples range from 2.43 to 2.67 ϕ with an average value of 2.57 ϕ , which suggests that the Swartkops beach is mostly dominated by fine grained sediments.

Median (M_d)

Median is referred to as the middle value in a set of data arranged in rank order. It is measured in terms of diameter, with half of the grains being finer and half being coarser by weight. Median can be observed from cumulative frequency curve at fifty percentile. The median of the diameter of the Swartkops samples ranges from 2.1 to 2.7 ϕ , which is consistent with the Mean value of fine sands but entered into the boundary of medium sized sands.

Sorting coefficient (σ_1)

Sediment sorting is the degree of dispersion of grain size distribution around a central value. The measurement of the degree of sorting of grain size distribution can be given by any of the statistical dispersion measurements such as standard deviation (de Mahiques, 2016). Sorting can reflect both sediment source and transportation process. Considering with aeolian transported sediments, they are usually being among the best sorted sediments and glacial sediments being among the worst sorted, whereas beach sediments are usually deposited in a relative high energy environment, therefore they are mostly well sorted (de Mahiques, 2016).

The analysed Swartkops beach samples display a standard deviation of 0.30 to 0.62 with an average value of 0.41. The average value indicates well sorted samples which are the result of long distance of transportation and wave washing.

Skewness (SK_1)



Okeyode and Jibiri (2013) stated that the skewness is the reflection of the depositional environment and implies a measure of the symmetry of the grain size distribution. They also stated that the positive values indicate skewness towards the finer grain size and negative values indicating skewness towards the coarser grain size. The skewness values of the Swartkops beach range from -0.19 to 0.4 with an average value of 0.13 suggesting that the sediments are near symmetric distributed and slightly coarse skewed in nature.

Kurtosis (K_G)

Kurtosis is the sorting of the tails in the central part of the distribution in the tails to the spread or Kurtosis reflects the degree of concentration of the grains relative to the average. Kurtosis and skewness are both parameters of the shape of the grain-size distribution.

If the tails are better sorted than the central parts, it is termed platykurtic. The kurtosis values of the Swartkops beach sands range from 0.56 to 1.22 with an average value of 0.87. The kurtosis value indicates that platykurtic nature predominates the Swartkops beach. Platykurtic distribution consists of the thinner tails than normal distribution and that results in fewer extreme positive or negative values.

4.4 Estuarine sediments

In estuaries, the nature of grain size distribution is very variable due to hydrodynamic condition that can be varied from blocked quiet water to active fluvial or marine currents which linked with river or open sea. The mean diameter is representing the granulometric characteristics of popular sediments through an average value. The measure of dispersion (sorting) is expressed as the standard deviation of sediments. Skewness and kurtosis can be translated as measurements of internal sorting and related to the amount of reworking and winnowing energy (Cadigan, 1961). The steep cumulative curve represents good sorting whereas in the case of a flat segment curve represents a poor sorting (Fig. 4.5-4.8). Sediments with normal distribution, a positive or negative skew can result if fine or coarse sediments are added respectively on either side of the limiting class sizes of the initial deposits (McLaren, 1981). The positive skewness is associated with fluvial deposits resulted from the suspended material of the fluvial currents.

4.4.1 Representative estuary samples

Poorly sorted sediments consist of grains that are of varying sizes, and they are an evidence of sediments that deposited in a low energy hydrodynamic environment, or have been deposited fairly close to the source and have not undergone much transport. The lower ridges of the estuary contains poorly sorted sediments with the dominant grain size range of 3 Phi followed by small percentages such as -1 Phi sands. Based on Wentworth scale, these grain sizes fall into fine sand and very coarse sand class. Coarse to fine sands and small quantities of silts are observed in the channel sediments of the lower ridges of the estuary and therefore these sediments results to poorly sorted coarse to fine grain sands because of the different mixed grain sizes. The centre of estuarine sediments are characterised by finer particles which are not sorted.

Sample 31 (Estuarine sample)

Table 4.10 Retained and cumulative percentage of grain size for sample 31. Aliquot mass = 308.91g.

Sieve size (ϕ)	Mass retained (g)	% retained	Cumulative %
-1	17.84	9.88	9.88
0	4.75	2.63	12.51`
1	6.97	3.86	16.37
2	13.57	7.51	23.88
3	110.87	61.41	85.29
4	19.07	10.56	95.85
5	7.46	4.13	99.98
Total mass	180.53		

Error = 0.1 %

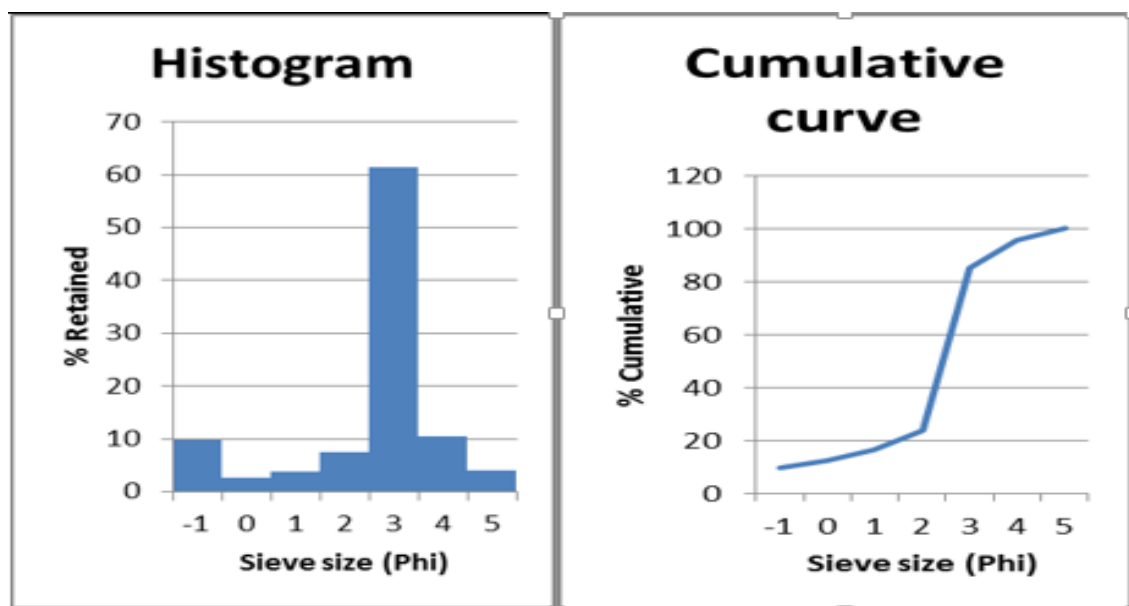


Fig. 4.5: Histogram (left) and cumulative frequency curve (right) of the Sample 31, showing the grain size distribution varied from -1 to 5 phi. The grain size is dominant at 3 Phi (0.125mm) followed by – 1.0 Phi (2mm) and 4 Phi and other grain sizes are very limited.

Sample 32 (Estuarine sands)

Table 4.11 Retained and cumulative percentage of grain size for sample 32. Aliquot mass = 180.75g.

Sieve size (ϕ)	Mass retained (g)	% retained	Cumulative %
-1	17.84	9.88	9.88
0	4.75	2.63	12.51`

1	6.97	3.86	16.37
2	13.57	7.51	23.88
3	110.87	61.41	85.29
4	19.07	10.56	95.85
5	7.46	4.13	99.98
Retained total mass	180.53g		

Error = 0.1%

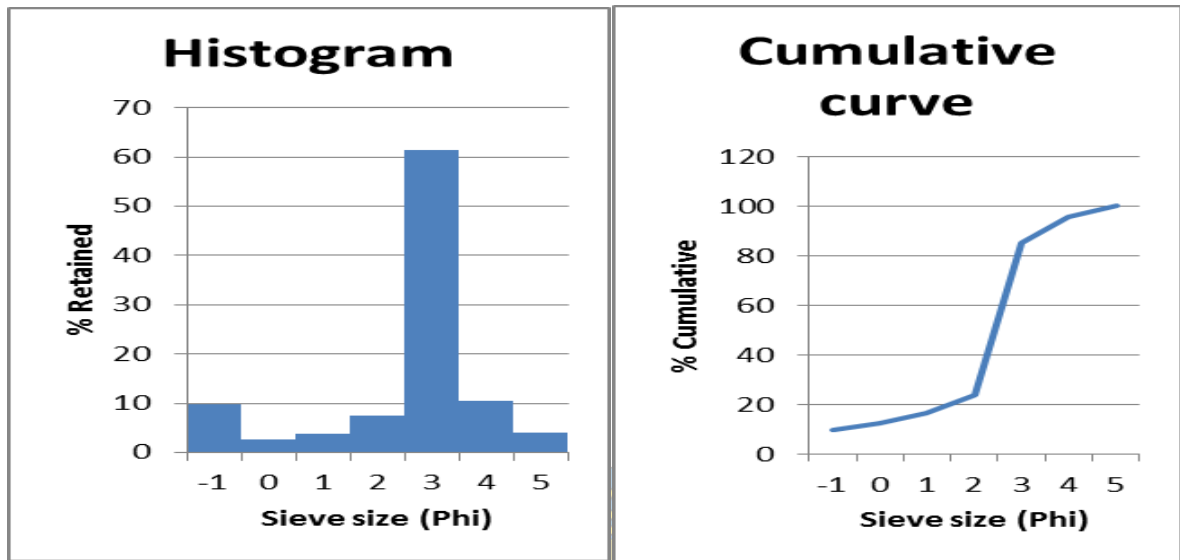


Fig. 4.6: Histogram (left) and cumulative frequency curve (right) showing grain size distribution of sample 32. The grain size varied from -1 to 5 phi dominant at 3 Phi (0.125 mm) followed by -1.0 (2mm) and 5 Phi (0.039 mm) and other small percentages of grain sizes.

Sample 41 (Estuarine sands)

Table 4.12 Retained and cumulative percentage of grain size for sample 41. Aliquot mass = 286.66 g.

Sieve size (ϕ)	Mass retained (g)	% retained	Cumulative %
-1	18.91	6.60	6.60
0	15.69	5.47	12.07
1	10.10	3.52	15.59
2	16.68	5.82	21.41
3	215.16	75.10	96.51
4	2.68	0.93	97.44
5	7.27	2.53	99.97
Retained total mass	286.49g		

Error = 0.05%

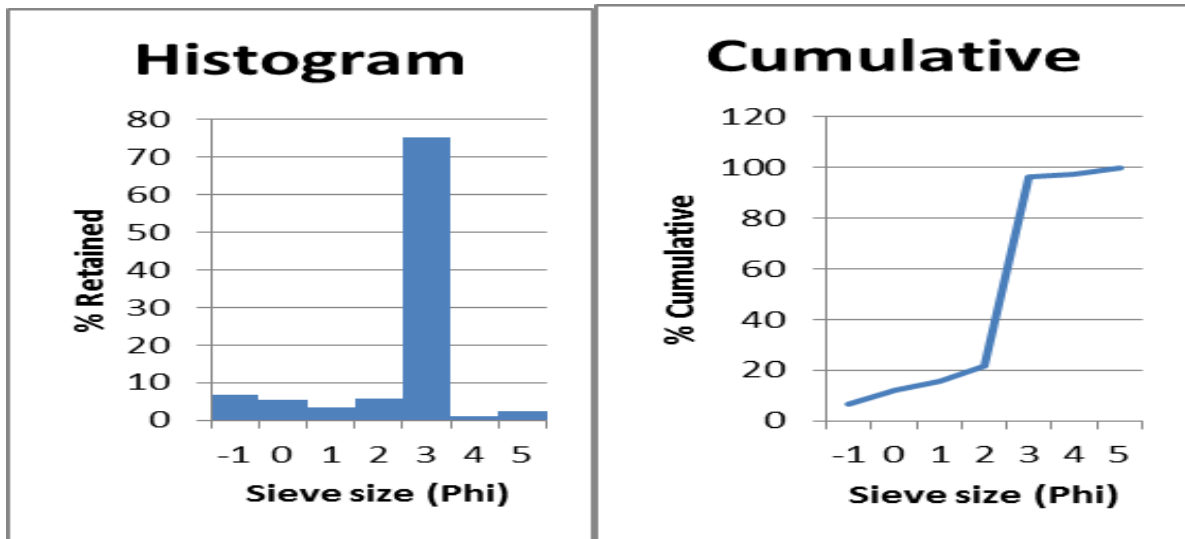


Fig. 4.7: Histogram (left) and cumulative frequency curve (right) showing grain size distribution of sample 41. The grain size distribution varied from -1 to 5 phi dominant at 3 Phi (0.125 mm) followed by – 1.0 Phi (2 mm) and other small percentages of grain sizes.

Sample 57 (Estuarine sands)



Table 4.13 Retained and cumulative percentage of grain size for sample 57. Aliquot mass = 273.66 g.

Sieve size (ϕ)	Mass retained (g)	% retained	Cumulative %
-1	7.43	2.72	2.72
0	11.06	4.06	6.78
1	9.43	3.46	10.24
2	25.16	9.23	19.47
3	199.05	73.09	92.56
4	17.71	6.50	99.06
5	2.46	0.90	99.96
Retained total mass	272.3g		

Error = 0.4%

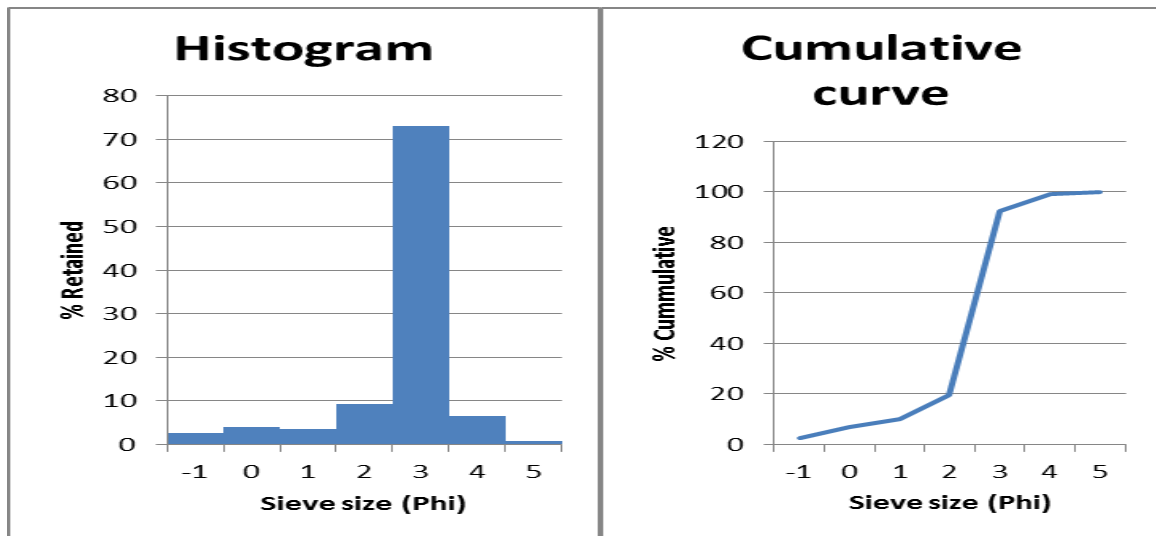


Fig. 4.8: Histogram (left) and cumulative frequency curve (right) of Sample 57, showing grain size varied from -1 phi to 5 phi, and with dominant size at 3 Phi (0.125 mm) and minor at 2 Phi (0.25 mm) and few -1 phi (2mm).

4.4.2 Grain size statistical parameters of estuarine samples

Table 4.14 Parameter values for estuary samples.

Sample No	M_d (Φ)	M_z (Φ)	σ_1	S_K	K_G	Explanation for Kurtosis, Skewness and Sorting
S16	2.70	2.57	0.55	-0.5	1.17	Moderately well sorted, strongly coarse-skewed and leptokurtic
S18	2.50	2.50	0.64	-0.06	1.17	Moderately well sorted, near symmetrical and leptokurtic
S19	2.10	1.30	1.67	-0.51	0.90	Poorly sorted, very coarse skewed and mesokurtic
S20	1.00	0.93	1.60	0.01	0.76	Poorly sorted, near symmetrical and platykurtic
S21	2.20	2.10	1.05	-1.10	2.86	Poorly sorted, coarse skewed and very leptokurtic

S22	2.20	2.36	0.90	0.07	3.60	Moderately sorted, near symmetrical and extremely leptokurtic
S23	1.60	1.97	0.60	0.58	0.78	Moderately well sorted, fine skewed and platykurtic
S24	2.30	2.30	0.66	-0.42	1.22	Moderately well sorted, strongly coarse skewed and leptokurtic
S25	2.50	2.43	0.53	-0.28	0.90	Moderately well sorted, coarse skewed and mesokurtic
S26	2.70	2.67	0.38	-0.19	1.03	Well sorted, near symmetric and platykurtic
S27	2.50	2.16	1.23	0.90	3.68	Poorly sorted, fine skewed and extremely leptokurtic
S28	1.50	1.80	0.76	-0.01	0.88	Moderately sorted, coarse skewed and platykurtic
S29	1.80	1.93	0.73	0.21	0.30	Moderately sorted, Fine skewed and very platykurtic
S30	2.50	2.00	1.44	-0.32	1.13	Poorly sorted, strongly coarse skewed and leptokurtic
S31	2.50	1.63	1.00	-1.37	1.46	Poorly sorted, coarse skewed and leptokurtic
S32	2.10	1.67	1.18	-0.39	0.52	Poorly sorted, strongly coarse skewed and very platykurtic
S33	2.40	1.76	1.31	-0.43	3.90	Poorly sorted, very coarse skewed and extremely leptokurtic
S34	2.50	2.47	0.32	-0.06	1.02	Very well sorted, near symmetrical and mesokurtic
S35	2.50	2.47	0.42	-0.17	1.33	Well sorted, strongly coarse skewed and leptokurtic

S38	2.50	2.43	0.52	-0.31	1.48	Moderately well sorted, strongly coarse skewed and very platykurtic
S40	2.71	2.57	0.76	-0.49	1.88	Moderately sorted, strongly coarse skewed and very leptokurtic
S41	2.51	2.50	0.53	-0.28	2.25	Moderately well sorted, strong coarse skewed and very leptokurtic
S42	2.40	1.83	1.09	-0.61	2.11	Moderately well sorted , strongly coarse skewed and very leptokurtic
S43	2.60	2.57	0.57	-0.33	2.35	Moderately well sorted, strongly coarse skewed and very leptokurtic
S46	2.61	2.47	0.68	-1.61	1.69	Moderately well sorted, Strongly coarse skewed and very leptokurtic
S47	2.30	2.40	0.54	0.09	2.15	Moderately well sorted, near symmetrical and very leptokurtic
S48	2.50	2.50	0.67	-0.17	1.43	Moderately well sorted, strongly coarse skewed and leptokurtic
S49	2.50	2.53	0.35	0.07	1.63	Well sorted, near symmetrical and very leptokurtic
S51	2.50	2.30	0.78	-0.50	2.97	Moderately sorted, strong coarse skewed and Very leptokurtic
S52	2.60	2.50	0.74	-0.44	2.11	Moderately sorted, Strong coarse skewed and very leptokurtic
S54	2.70	2.53	0.41	-0.60	2.18	Well sorted, strong coarse skewed and very leptokurtic
S55	2.60	2.53	0.44	-0.31	1.31	Well sorted, strong coarse skewed and leptokurtic

S56	2.50	2.50	0.47	0.10	1.22	Well sorted, near symmetrical and leptokurtic
S57	2.70	2.63	0.50	-0.12	1.16	Moderately well sorted, strongly coarse skewed and leptokurtic
S58	2.70	2.67	0.57	-0.13	1.34	Moderately well sorted, strongly coarse skewed and leptokurtic
S59	2.50	2.56	0.45	0.03	1.39	Well sorted, near symmetrical and leptokurtic
S60	2.80	2.67	0.67	-0.52	1.91	Moderately well sorted, strongly coarse skewed and very leptokurtic
S61	2.60	2.60	0.52	-0.11	1.47	Moderately well sorted, strongly coarse skewed and leptokurtic



4.4.3 Discussion on grain size parameters for estuarine sediments

University of Fort Hare
Together in Excellence

Mean grain size (Mz)

The mean values for samples collected from the Swartkops estuary range from 0.93 to 2.67 Phi (Table 4.14) with an average value of 2.25 phi. The average value of the mean grain size reveals that Swartkops estuary is dominated by fine grained sediments. This reveals that the energy of transportation medium in the estuary was lower particularly at the estuary centre (Nelson, 2015; Folk, 1974).

Median (Md)

Median can be observed from the cumulative frequency curve by finding the intercepts of the fifty percentile. The median diameters for the Swartkops estuary samples range from 1.0 to 2.8 Phi, which is fine to medium grained.

Sorting coefficient (σ_1)

For estuary sediments, the sorting could be variable from poorly to moderately sorted depending on the topography and location at the estuary. For example, the centre of estuary

shows poorly sorted sediments whereas boundary (edge) area shows moderate sorted sediments due to more active current in the shallow water environment.

From Table 4.14, the obtained values of sorting in Swartkops estuary range from 0.32 to 1.67 with an average value of 0.77. The average value indicates that they are moderately well sorted. The moderately well sorted values imply the deposition in the Swartkops estuary was under the influence of relatively stronger currents, comparing to other common estuaries. In Swartkops estuary, particularly during flooding, the water energy could be much increased to fairly high energy currents (Freidman, 1961b; Blott and Pye, 2001).

Kurtosis (K_G)

Kurtosis in the Swartkops estuary ranges from 0.3 to 3.90 with an average value of 1.60. The kurtosis value indicates that the area is leptokurtic to very leptokurtic. Okeyode and Jibiri (2013) stated that an area that is leptokurtic to very leptokurtic suggests a fluvial influence, confirming that the sands are mostly from river sourced. The abundance of very leptokurtic nature implies that the area tail and central parts are not equal.



Skewness (S_{ki})

The skewness values for the Swartkops estuary range from -1.61 to 0.9 with an average value of -0.2 that represents strongly coarse skewed and few coarse skewed. Some samples show near symmetrical. Sediments with a normal distribution that are positive or negative skewed can results if fine sediments are added on either side of the limiting class sizes of the initial deposit (McLaren, 1981). According to McLaren, the river sediments are usually positively skewed, beaches showing normal distribution with slight positive or negative skew (McLaren, 1981).

4.5 Tidal channel sediments

The histograms and cumulative frequency curves of the tidal channel sediments show bimodal distributed patterns in grain size distribution (Fig. 4.9-4.12). The distributions have two peaks on the histograms. The particles in most of the samples are retained in 3 Phi which represents finer part of the sediments, with anoter part at -1 phi which represents the coarser part of the sediments. The cumulative frequency size distribution of the samples is not so steep and therefore represent a worse sorting.

Sample 44 (Tidal channel sample)

Table 4.15 Retained and cumulative percentage of grain size for sample 44. Aliquot mass = 289.67g.

Sieve size (ϕ)	Mass retained (g)	% retained	Cumulative %
-1	76.81	26.57	26.57
0	15.37	5.31	31.88
1	9.94	3.43	35.31
2	9.23	3.19	38.50
3	159.17	55.06	93.56
4	8.90	3.07	96.63
5	9.64	3.33	99.96
Retained total mass	289.06g		

Error = 0.2 %

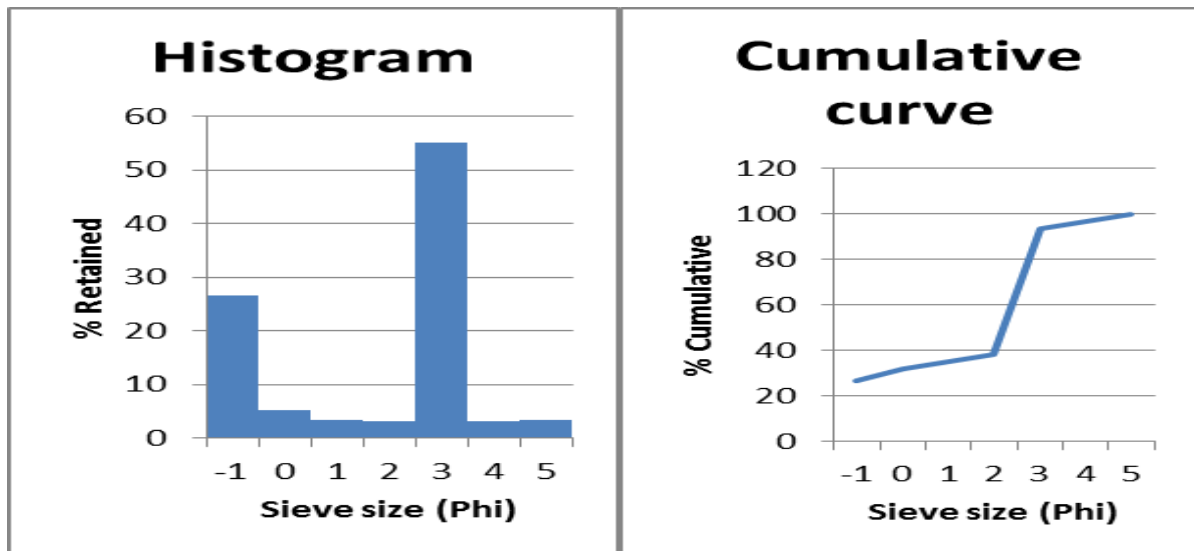


Fig. 4.9: Histogram (left) and cumulative frequency curve (right) showing grain size distribution of sample 44. The grain size distribution varied from -1 to 5 phi. The grain size is dominant at 3 Phi (0.125) followed by - 1 Phi and other small percentages of grain sizes.

Sample 45 (Tidal channel sample)

Table 4.16 Retained and cumulative percentage of grain size for sample 45. Aliquot mass = 204.68g.

Sieve size (ϕ)	Mass retained (g)	% retained	Cumulative %
-1	37.71	18.49	18.49
0	17.21	8.44	26.93
1	17.81	8.73	35.66
2	42.40	20.79	56.45

3	79.25	38.87	95.32
4	5.04	2.47	97.79
5	4.44	2.17	99.96
Retained total mass	203.86g		

Error = 0.4%

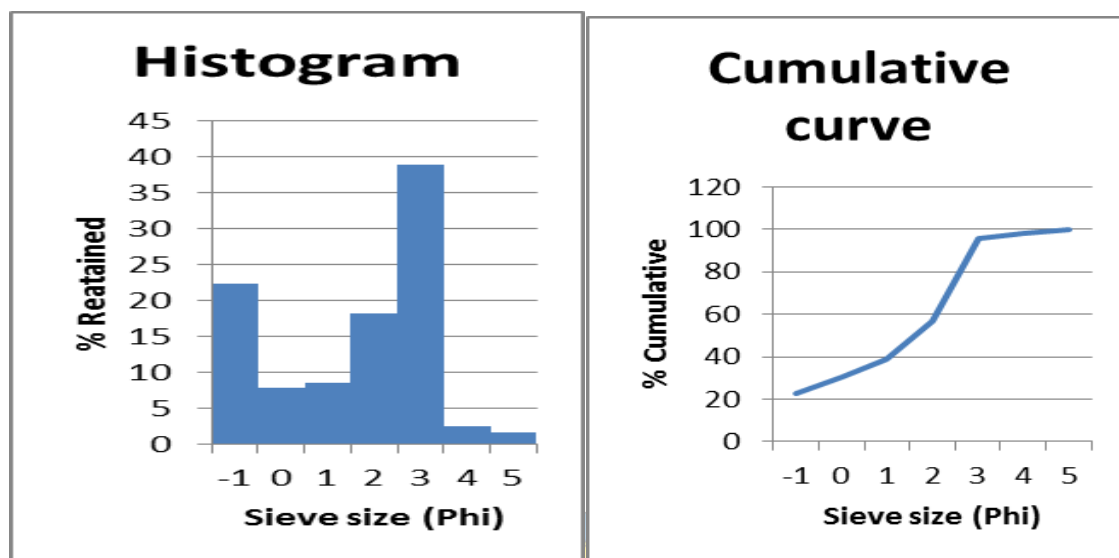


Fig. 4.10: Histogram (left) and cumulative frequency curve (right) showing grain size distribution of sample 45. The grain size varied from -1 to 5 phi which is dominant at 3 Phi (0.125) followed by - 1 Phi and other small percentages of grain sizes. The cumulative curve is much gentle steeped due to mixed grain size and poorly sorting.

Sample 50 (Tidal channel sample)

Table 4.17 Retained and cumulative percentage of grain size for sample 50. Aliquot mass = 228.08 g.

Sieve size (ϕ)	Mass retained (g)	% retained	Cumulative %
-1	111.93	49.18	49.18
0	15.27	6.70	55.88
1	9.47	4.16	60.04
2	12.06	5.29	65.33
3	58.58	25.73	91.06
4	10.06	4.42	95.48
5	10.22	4.49	99.97
Retained total mass	227.59g		

Error = 0.2 %

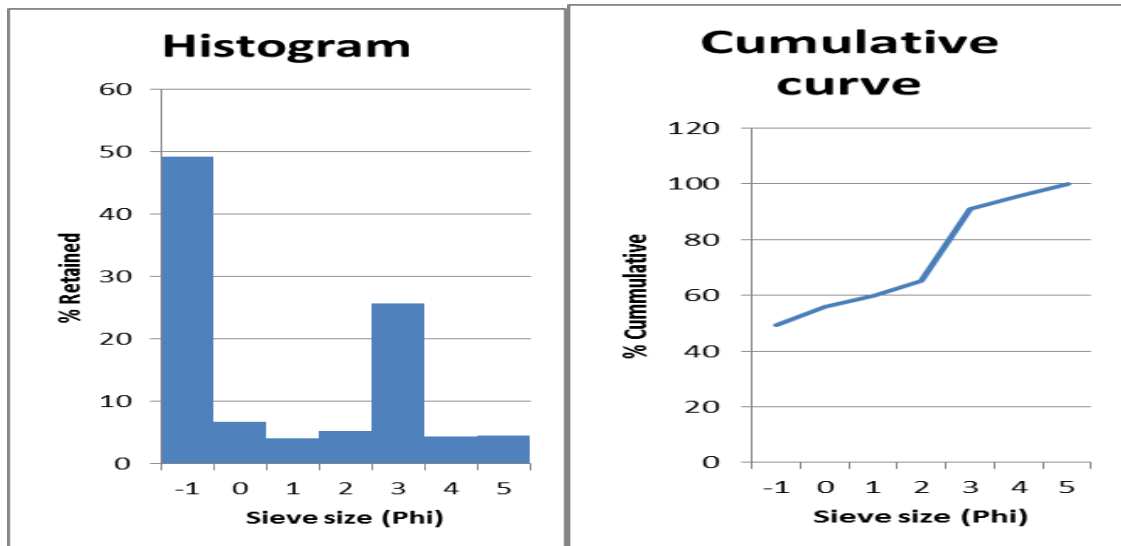


Fig. 4.11: Histogram (left) and cumulative frequency curve (right) showing grain size distribution of sample 45. The grain size varied from -1 to 5 phi which is dominant at -1 Phi followed by 3 Phi and other small percentages of grain sizes. The cumulative curve is much gentle steeped, indicating poorly sorting and mixed grain sizes.

Sample 53 (Tidal channel sample)

Table 4.18 Retained and cumulative percentage of grain size for sample 53. Aliquot mass = 282.60g.

Sieve size (ϕ)	Mass retained (g)	% retained	Cumulative %
-1	62.25	22.05	22.05
0	17.25	6.11	28.16
1	10.52	3.72	31.88
2	18.51	6.55	38.43
3	155.39	55.06	93.49
4	14.18	5.02	98.51
5	4.11	1.45	99.96
Retained total mass	282.21g		

Error = 0.1%

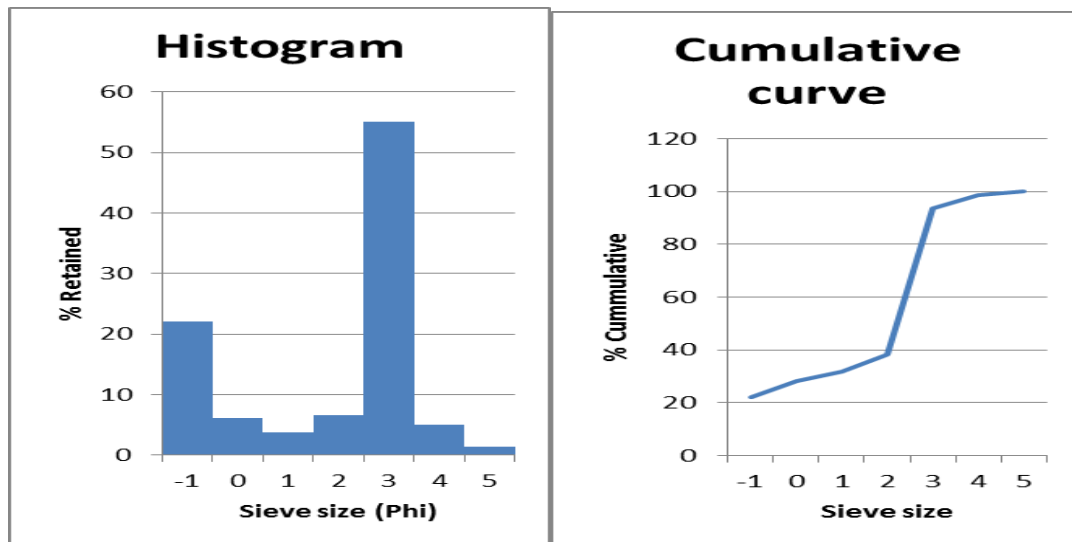


Fig. 4.12: Histogram (left) and cumulative frequency curve (right) showing grain size distribution of sample 53. The grain size varied from -1 to 5 phi, with the dominant at 3 Phi (0.125) followed by -1 Phi and other small percentages of grain sizes.

4.5.1 Grain size statistical parameters for tidal channel sediments

Table 4.19 Parameter values for tidal channel samples.

Sample No	M_d (Φ)	M_z (Φ)	σ_1	S_k	K_g	Explanation for Kurtosis, Skewness and Sorting
S10	2.70	2.67	0.38	-0.19	1.03	Moderately well sorted, near symmetrical and platykurtic
S36	2.50	1.80	1.19	-0.66	0.48	Moderately well sorted, strongly coarse skewed and very platykurtic
S37	2.50	1.76	1.15	-0.72	1.63	Moderately well sorted, strongly coarse skewed and very platykurtic
S39	2.61	2.57	0.48	-0.22	0.99	Well sorted, strongly coarse skewed and mesokurtic

S44	2.50	1.90	1.13	-0.62	1.87	Moderately well sorted , strongly coarse skewed and leptokurtic
S45	2.60	2.53	0.47	-0.39	1.85	Well sorted , coarse skewed and leptokurtic
S50	2.40	2.43	0.71	-0.17	1.69	Moderately sorted, strongly coarse skewed and very leptokurtic
S53	2.50	2.43	0.64	-0.36	1.77	Moderately well sorted, strong coarse skewed and very leptokurtic
S54	2.70	2.53	0.41	-0.60	2.18	Well sorted, strong coarse skewed and very leptokurtic

4.5.2 Discussion on grain size parameters for tidal channel sediments

Mean grain size

The mean grain size of tidal channel sediments ranges from 1.76 to 2.67 with an average value of 2.32. The average value for the size suggests the tidal channel is mostly dominated by fine grained sands. The mean values for samples collected from the Bluewater Bay beach ranges from 2.43 to 2.67 with an average value of 2.57 Phi, and the mean distribution for those collected from the Swartkops estuary range from 0.93 to 2.76 Phi with an average value of 2.25, this reveals that the samples from Swartkops estuary, tidal channel and Bluewater bay beach are dominated by fine grained sands. According to Folk and Nelson, this suggest that the energy of the transporting medium was low and constant.

Median (Md)

The diameter with half the grains by weight finer and half the grains by weight coarser is called the median. The intercept of the fifty percentile (50) is read from the cumulative frequency curve. The tidal channel samples have a median diameter of 2.40 to 2.70 Phi.

Sorting coefficient

The tidal channel samples show that the sorting range from 0.38 to 1.19 with an average of 0.73 Phi. The average value shows that the area predominates of moderately sorted sediments. The analysed beach samples show standard deviation of 0.30 to 0.62 with an average value of

0.41. The average value indicates well sorted samples which are the result of long distance of transportation. The values of sorting in Swartkops estuary range from 0.32 to 1.67 with an average value of 0.77. The average value indicates that they are moderately well sorted. The sorting of the study area indicates a high energy marine environment.

Kurtosis K_G

The kurtosis of in the tidal channel samples range from 0.48 to 2.18 with an average of 1.49 Phi. The tidal channel samples display a leptokurtic in nature. The leptokurtic nature shows a constant accumulation of finer or coarser sediments after sorting and high energy nature during deposition (Avramidis *et.al.*, 2012). The average value of the beach sediments shows an average 0.87 Phi and that indicates a platykurtic nature. The Swartkops estuary displays leptokurtic to very leptokurtic in nature.

Skewness (Ski)

The skewness values of tidal channels range from -0.17 to -0.72 with an average value of -0.43. The average value indicates that the tidal channel is near symmetrical. The tidal channel shows a very fine skewed classification. The beach sediments have an average value of 0.13 showing a near symmetric distribution. The skewness values in the Swartkops estuary ranges from -1.61 to 0.9 with an average value of -0.2 representing coarse skewed. Most of the samples dominates a positive classification with few negative skewness classifications.

4.6 Bivariate scatter plots of grain size parameters

Bivariate plots have been used widely to interpret the transportation medium, how the sediments were deposited, and their energy conditions. Bivariate plots show the reliability of differences in the fluid flow mechanism of sediment transportation and deposition (Bhattacharya *et al.*, 2016). According to Friedman (1961, 1967), the use of scatter plots measures to differentiate between river and beach sand, he further established among all statistical parameters, the standard deviation about the mean is the most effective parameter for separating sands of various origin. Many scatter plots have been shown by Moiola and Weiser (1968), whereby they distinguished between the modern beach, dune, and river sand. Their figures showed a combination of mean versus standard deviation that was considered to be more effective. The bivariate plots which are effective and used often are mean versus skewness, mean versus sorting, and mean versus kurtosis, and sorting versus skewness. The

skewness versus kurtosis plot is quite useful in determining the genesis of the sediment by quantifying the degree of normality of its size distribution (Folk, 1966).

The following plots characterize the bivariate characteristics of the Swartkops estuary and Bluewater Bay beach. Graphic mean versus standard deviation/sorting (Figure 4.13); graphic mean versus skewness (Figure 4.14); graphic mean versus kurtosis (Figure 4.15); Skewness versus kurtosis (Figure 4.16); standard deviation/sorting versus skewness (Figure 4.17); and standard deviation/sorting versus kurtosis (Figure 4.18).

Summary

Mean versus standard deviation/sorting

The plot of mean versus sorting indicates that the beach sediments are fine and the estuarine sediments are also fine to medium-grained (Fig. 4.13). The beach sediments are very well sorted to well sorted and the estuarine sediments mostly are well-sorted to sorted and few poorly sorted. The relationship between the mean and sorting (Figure 4.13) shows a negative relationship that means that the fine-grained sediments are well sorted compared to coarse-grained sediments. Mean grain size and sorting have been confirmable for being hydraulically controlled, and for that reason, all sedimentary environments which have the best-sorted sediments are of the fine sand size range (Bramha et.al., 2017).

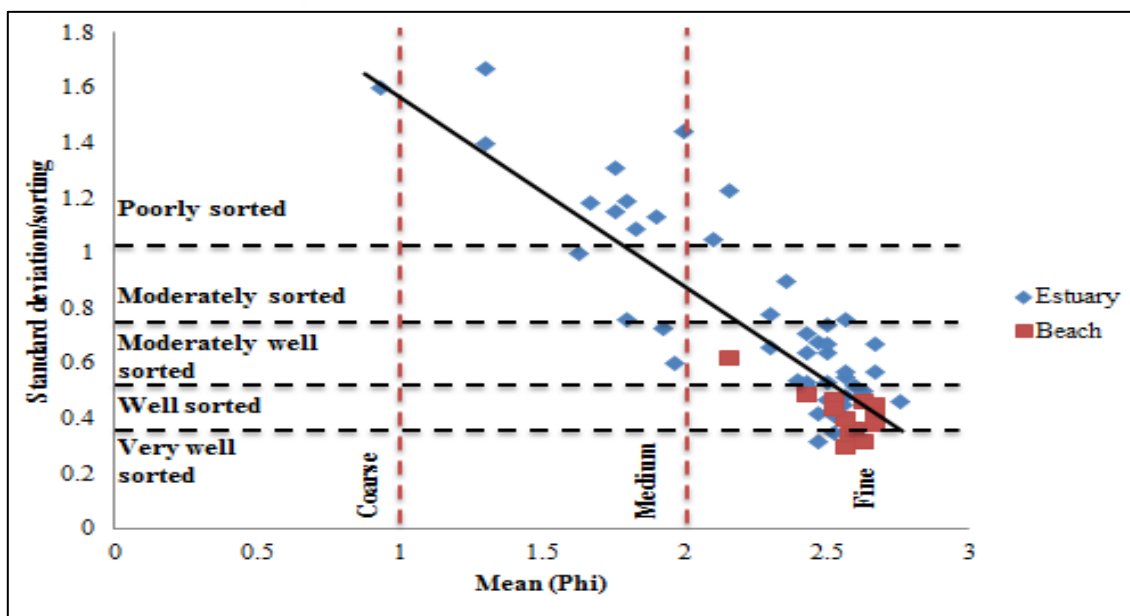


Fig. 4.13: Bivariate scatter plot showing standard deviation/sorting versus mean. The plot of mean versus sorting indicates that the sediments are fine to medium and very well sorted to poorly sorted.

Mean versus skewness

The plot of mean versus skewness (Figure 4.14) shows that most estuarine sediments are strongly coarse skewed to near symmetrical but few fine skewed. The beach sediments are coarse skewed to fine skewed. The estuarine and beach sediments also show much more coarse skewed to fine skewed. The relationship between the mean and skewness (Figure 4.14) show a slightly positive relationship that shows that the sediments are clustered possible towards the right hand in the plot, and that shows that the sediments are fluvial (Friedman, 1979).

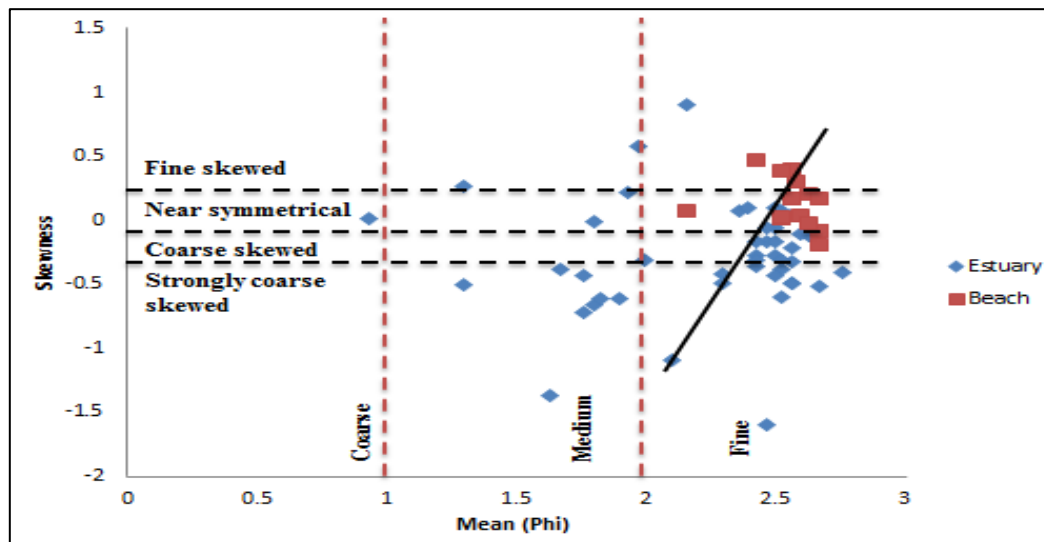


Fig. 4.14: Bivariate scatter plot showing skewness versus mean. The plot between mean and skewness is useful for distinguish between depositional environments. The plot also shows that the sediments are mostly fine to medium grained.

Skewness versus kurtosis

Kurtosis versus skewness plot is very useful in determining depositional environment such as marine or fluvial (Baiyegunhi *et.al.*, 2017). Figure 4.15 shows that sediments lie within negatively skewed and most of the samples are platykurtic to leptokurtic. The estuarine sediments are mostly mesokurtic to very leptokurtic while the beach sediments are mostly platykurtic to mesokurtic in nature. According to the skewness; the estuarine sediments are

near symmetrical to strongly coarse skewed and the beach sediments are mostly fine skewed to near symmetrical. As skewness decreases in values, kurtosis increases indicating a negative relationship. The bivariate plot shows that the sediments are mostly of the beach environment since they indicate a high energy environment.

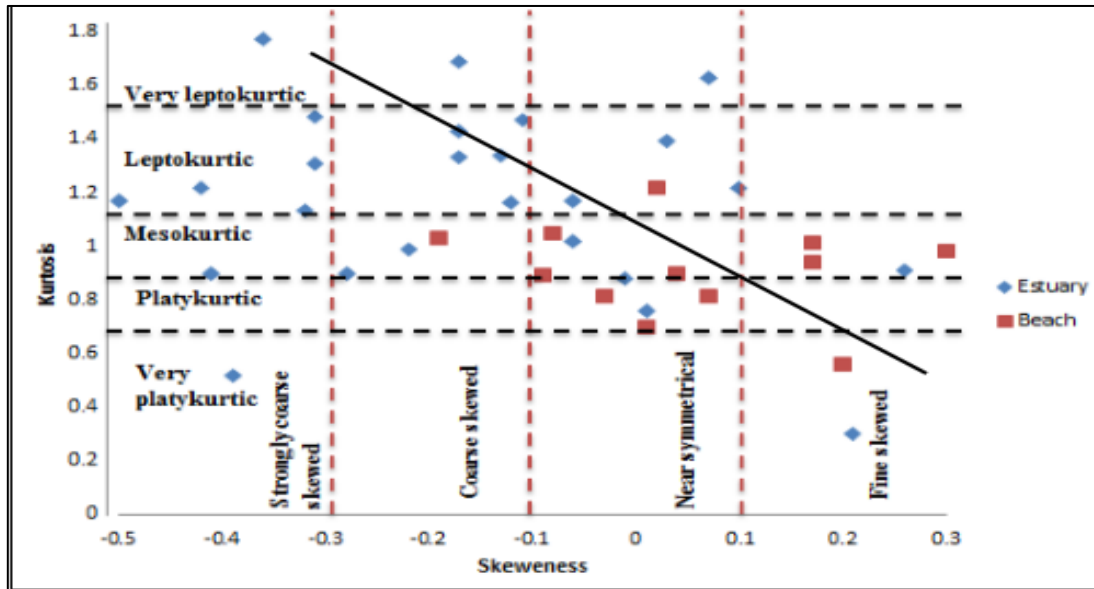


Fig. 4.15: Bivariate scatter plot showing kurtosis versus skewness. The trend in the kurtosis versus skewness plot could be used to determine the type of depositional environment. According to Friedman (1961), the values of kurtosis, whether they are high or low, indicates that the sediments were sorted in high energy environment before deposited in their current environment.

Kurtosis versus mean

The relationship between kurtosis and mean can be complicated, but the sediments show a slightly positive relationship. Figure 4.16 shows that the grain size increases as kurtosis becomes less widely distributed. This can be the result of relatively less sorting in coarse sediments. Almost all of the beach sediments are fine grained and they are very platykurtic to mesokurtic in nature. The estuarine sediments are mostly fine grained with few medium to coarse grained and these estuarine sediments are very platykurtic to very leptokurtic but most of them are leptokurtic.

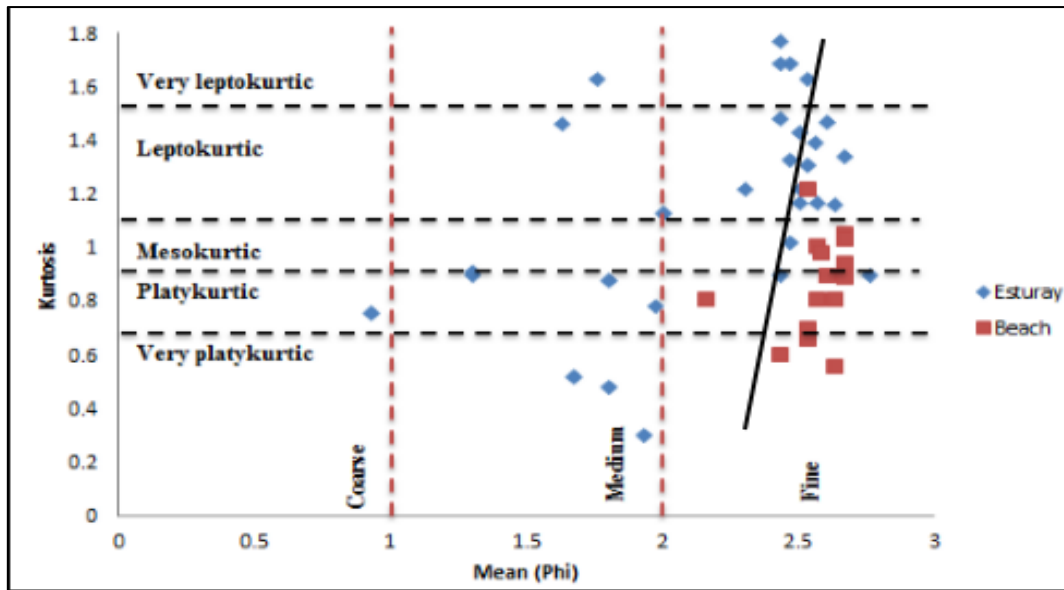


Fig. 4.16: Bivariate scatter plot showing kurtosis versus mean. The plot between mean and kurtosis indicates that most sediments are fine grained and very few medium grained.

Standard deviation/sorting versus skewness

Sorting and skewness show a negative relationship and the sediments are scattered (Figure 4.17). Okeyode and Jibiri (2012) stated that the plotting of skewness versus sorting come up with a helpful ways among beach and river sands. The plot shows that as the skewness increases the sorting of grains also increases. The bivariate plot of the sorting and skewness shows that the estuarine sediments are moderately sorted to well sorted and they are strongly coarse skewed to near symmetrical. The beach sediments are mostly well sorted with few sediments that are very well sorted and these sediments are mostly near symmetrical to fine skewed.

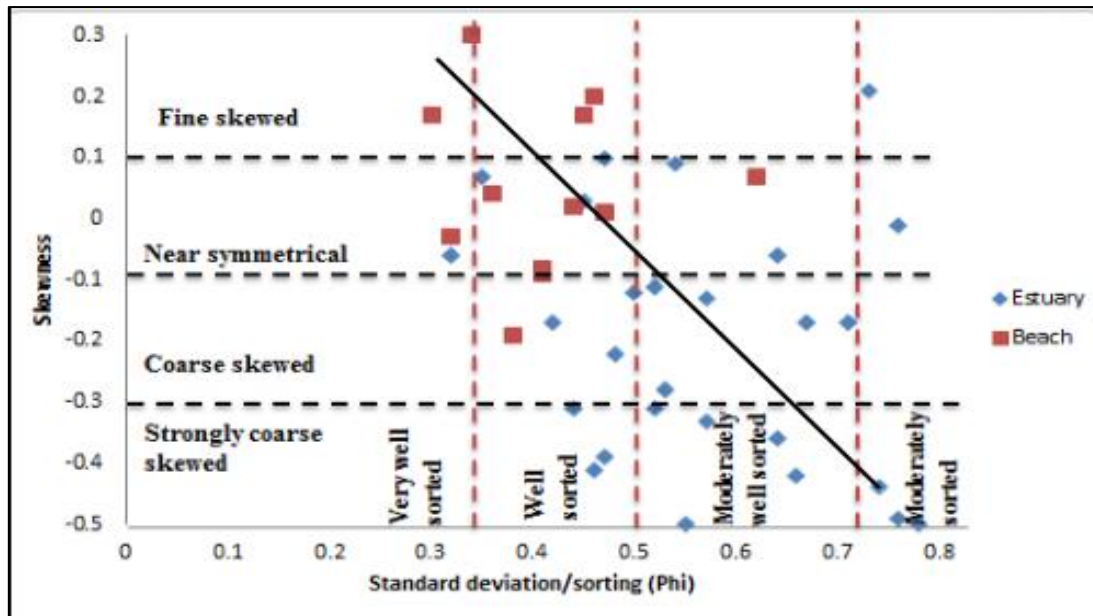


Fig. 4.17: Bivariate scatter plot showing skewness versus standard deviation/sorting. From the plot between sorting and skewness, it can be deduced that as the skewness increases, the sorting of grains also increases.

Sorting versus kurtosis



Sorting and kurtosis show a positive relationship (Figure 4.18). The bivariate plot also shows that most of the estuarine sediments are well-sorted to moderately sorted and they are leptokurtic to very leptokurtic. The beach sediments are mostly well sorted and very well sorted and they are platykurtic to mesokurtic in nature. From the plot, it is observed that the sorting increases and kurtosis gets narrower indicating that the estuarine sediments and beach sediments show positive relationship between sorting and kurtosis.

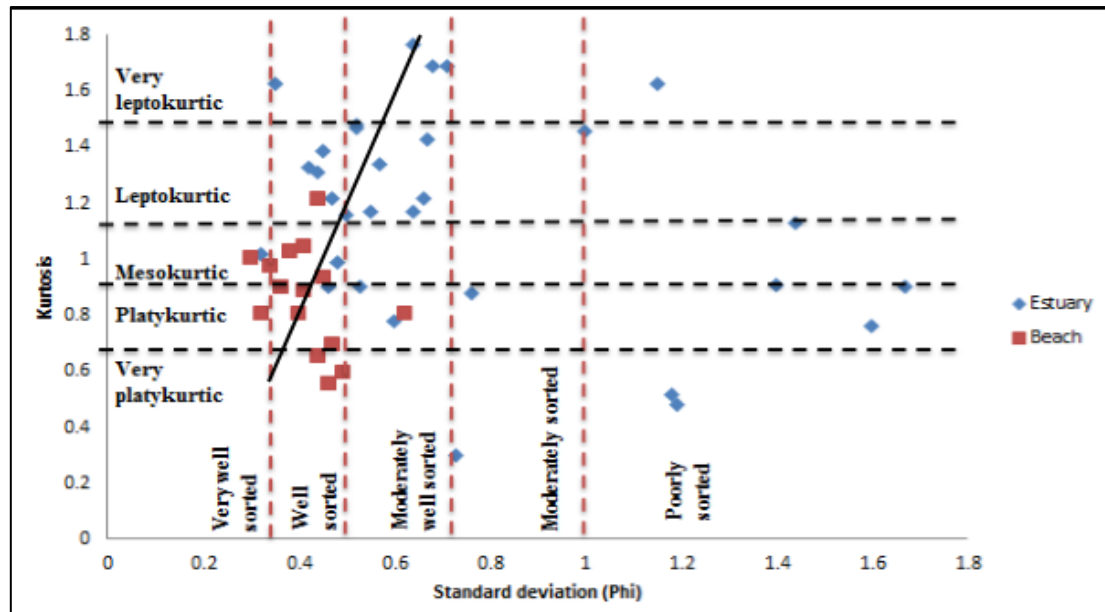


Fig. 4.18: Bivariate scatter plot showing kurtosis versus standard deviation/sorting. From the plot, it can be deduced that when sorting increases, the kurtosis gets narrower indicating that the samples have a positive relationship between sorting and kurtosis.

4.7 Summary



Most of beach sediments show a unimodal distribution, whereas the estuarine channel sediments show both unimodal and bimodal distribution. The textural characteristics of the beach sediments are fine grained whereas the estuarine tidal channel sediments indicate both the fine grain size and medium grain size particles. The beach sediments are well sorted and this indicate that the sediments were transported far from their source area. The estuarine channel sediments are moderately well sorted to well sorted which indicate that the sediments were deposited on high energy currents. Some sediments are poorly sorted and that means, their sorting is influenced by river currents, tidal waves and winds. The estuarine channel and beach sediments can be generally classified as well sorted very fine grained sands. The majority of frequency histograms for both beach and estuarine channel sediments show a unimodal distribution. This suggest that the sediments are sourced from the same provenance (Fig. 4.1-4.8). The average skewness values for the study area are strongly coarse skewed to near symmetric which maybe the absence of strong events. The average kurtosis value for the estuarine channel is leptokurtic to very leptokurtic confirming the sands are from the river. The average kurtosis value for beach sediments indicates the platykurtic nature.

CHAPTER 5 MINERAL COMPOSITIONS

5.1 Technique used for mineral analysis

This chapter is aimed at identifying and analysing mineral compositions present in the sediments. Various methods such as Scanning Electron Microscope (SEM), X-Ray Diffraction (XRD) and Petrographic Microscope analysis were used to determine mineral types, assemblage and occurrence. Mineral composition analysis also provides information about the source region and depositional environment (Maity and Maiti, 2016). XRD analysis is believed to be the most suitable for quantitative analysis compared to microscope analysis (Zhou et al., 2018). Whereas, Scanning Electron Microscope (SEM) with the aid of Energy Dispersive Spectrometry (EDS) can provide more quantitative chemical compositions of minerals, particularly for analysis of clay mineral shapes, textures and chemical compositions.

5.2 Mineral types, assemblage and occurrence

Microscope study on the mineral types found that quartz, calcite, plagioclase, orthoclase, organic carbon (pellets), and clay minerals are the main mineral types present in the beach and estuary sediments. Quartz is the most common mineral in the samples. Calcite is the second dominating mineral in all the samples. Under the petrographic microscope, the mud pellets are round, and carbonate fragments are light in colour, and occur as bio-fragments, such as shell and coral clasts. Clay minerals are mainly distributed in the estuary centre in a relative deeper water environment. It also occurs as mud-pellets such as smectite or kaolinite pellets. Organic pellets appear light brownish or dark due to organic carbon rich. The preparation methods for the thin sections were stated under methods chapter in section 3.5.

5.2.1 Quartz (SiO₂)

Quartz is the most dominant mineral in the Swartkops estuary and the Bluewater bay sediments. Quartz appears colourless when observed under the microscope, with low relief and interference colours. Quartz is highly resistant to weathering, and therefore it preserved after long distance transportation and erosion. Quartz grains vary from rounded to angular, which shows different energy levels of transportation (Figure 5.1). The micro-

texture of the quartz grains can reveal the transport and depositional processes. Quartz grains are monocrystalline or polycrystalline in nature. Monocrystalline consist of single-crystalline quartz grain, and the polycrystalline consists of numerous quartz grains (Figure 5.1) and are indicative of metamorphic rock source such as quartzite and quartz schist from surround metamorphic Cape Supergroup rocks. Monocrystalline quartz grains are more abundant than the polycrystalline quartz grain in the samples, which are sourced from vein quartz or felsic igneous rocks.

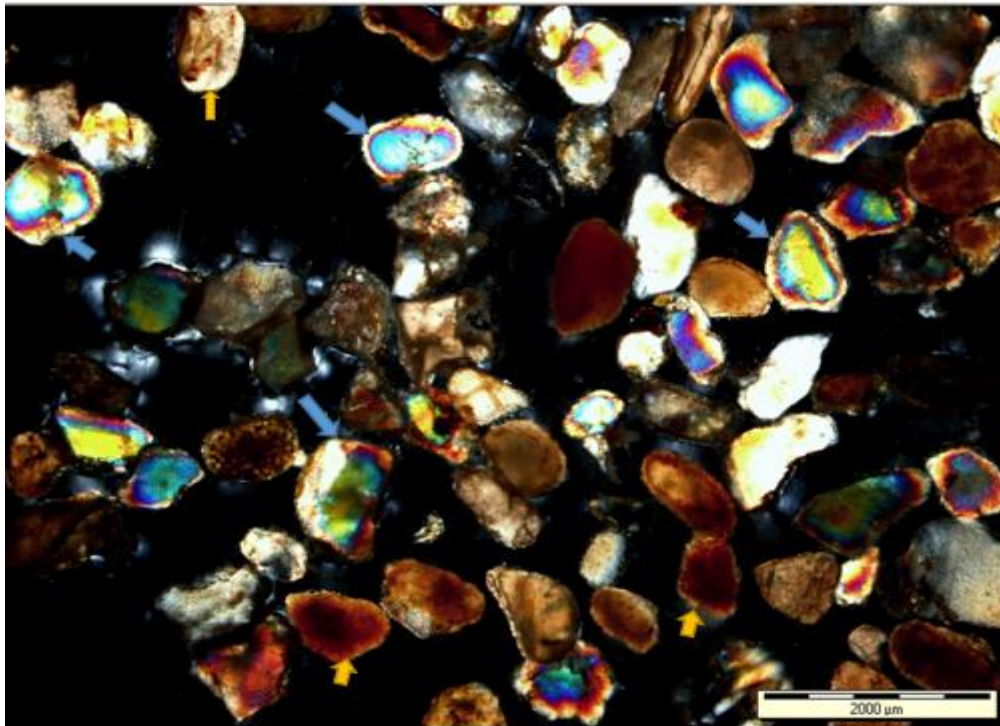


Fig. 5.1: Photomicrographs of various sand grains of quartz (Qtz) (blue arrows) and calcite (Cal) (yellow arrows), sample number 4 from Bluewater beach.

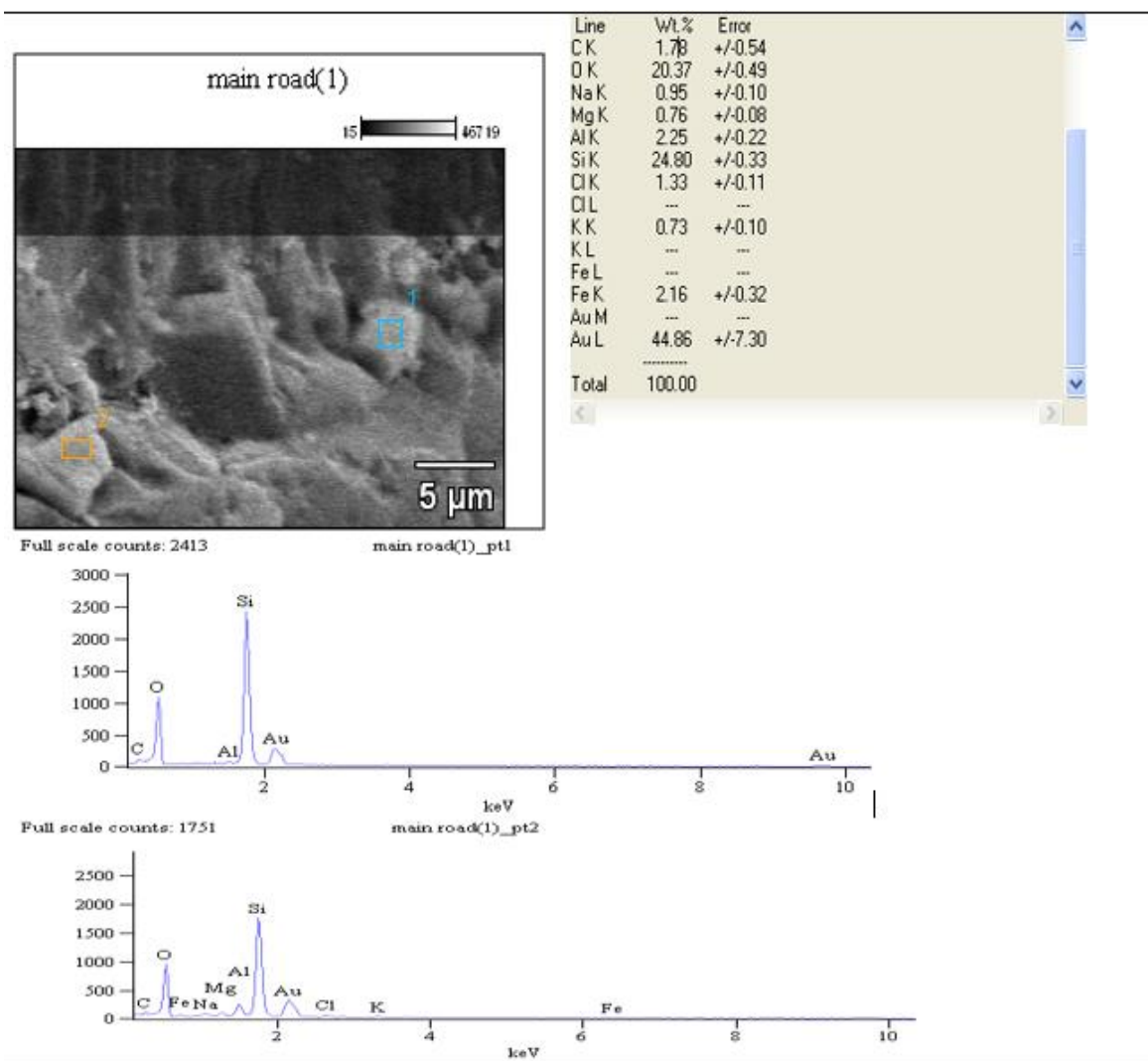


Fig. 5.2: SEM and EDX analyses for two quartz grains having the same silica (SiO_2) chemical composition. Au peak was due to gold coating for the sample.

5.2.2 Feldspar

Orthoclase (KAlSi_3O_8)

Albite ($\text{NaAlSi}_3\text{O}_8$)

Plagioclase ($\text{CaAl}_2\text{Si}_2\text{O}_8$)

Feldspars are aluminosilicate minerals that are found in igneous, metamorphic, and sedimentary rocks and include potassium, sodium, and calcium varieties, thus are classified as orthoclase (microcline), albite and plagioclase. Few albite were observed (Fig 5.4), the most abundant feldspars in the study areas are commonly orthoclase and plagioclase with an estimation percentage of 35 percent. Feldspars occur as both detrital

and authigenic forms with the former is more abundant than the later. The feldspar minerals plagioclase, microcline, and orthoclase normally show low birefringent and interference colours. Despite the fact that feldspars are the most common minerals in igneous and metamorphic rocks, they are less stable in sedimentary rocks. The majority of feldspar has been altered to clay minerals or has been total destroyed during weathering and transportation as indicated by grey arrows in figure 5.3. Microcrystalline clay minerals progress along the cleavage planes of feldspar is an indicator for feldspar alteration. Feldspar grains are medium to coarse grained and texturally sub-rounded to sub-angular (Fig 5.3) in the samples. Orthoclase is typically cloudy, with some grains showing a perthitic texture or simple twinning. In some instances, the potassium feldspar is also easily identified by its sericitization. Plagioclase is a framework silicate that belongs to the feldspar group. Plagioclase is less common in sedimentary rocks where it usually weathers to clay minerals. Plagioclase occurs as detrital grains and exhibits twinning under the microscope and shows a weak birefringence (Fig 5.9). Plagioclase is typically elongated and is identified by its polysynthetic or albite twinning of black and grey stripes, whereas microcline is distinguished by its cross twinning (Fig 5.9).

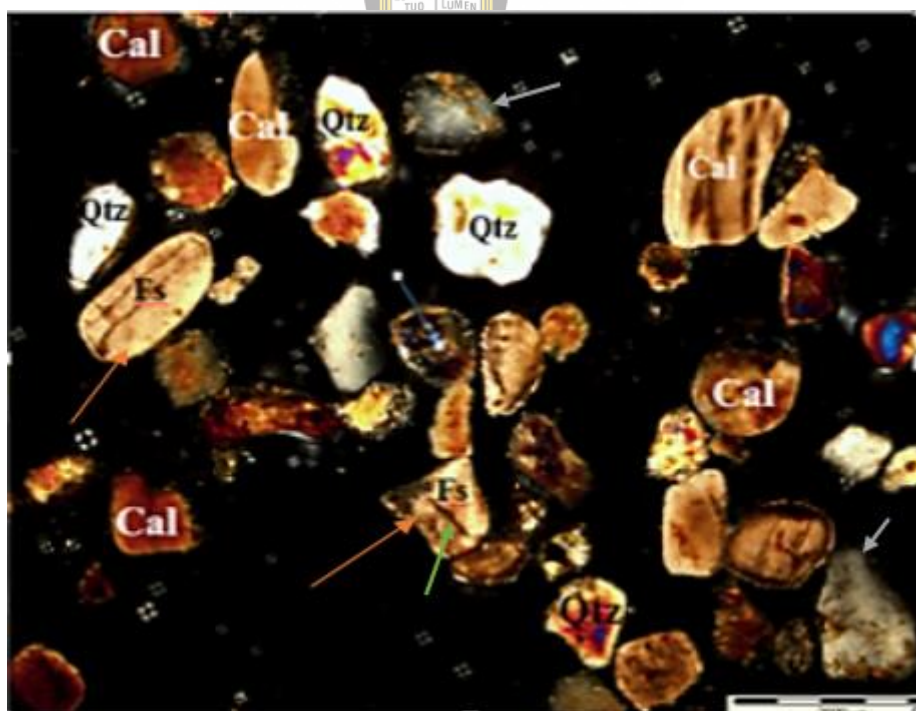


Fig.5.3: Photomicrographs showing various grains of feldspar (Fs), Quartz and Calcite (Cal). Quartz has no cleavage, while feldspar shows clear cleavage in the crystalline grain indicated by green arrow (Sample 44).

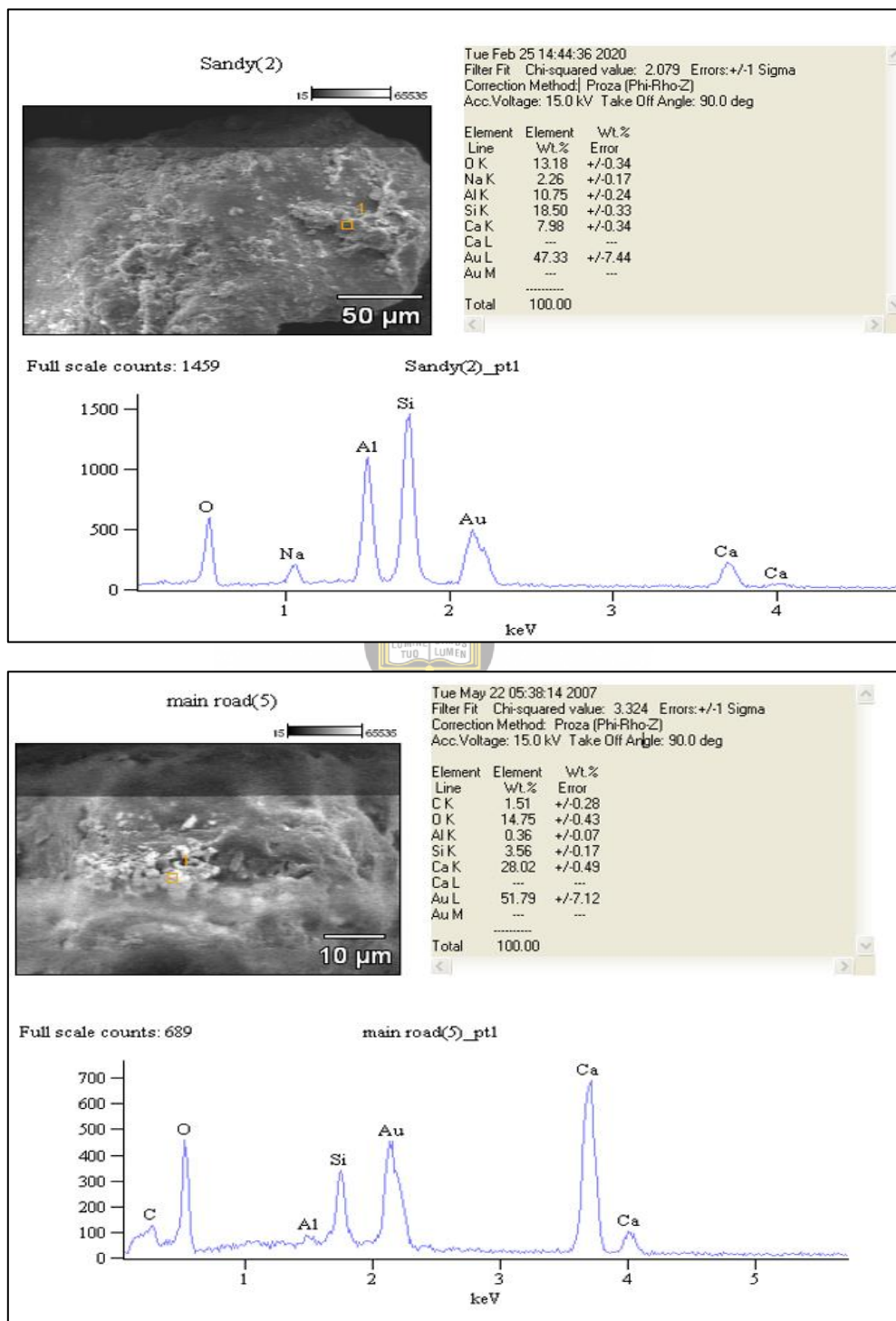


Fig. 5.4: SEM and EDX analyses for Albite grain (top) having silica, aluminium and sodium chemical compositions (top); and Ca-Plagioclase grain showing silica, aluminium and calcium compositions (bottom). Au peak was due to gold coating for the sample.

5.2.3 Carbonate

Calcite (CaCO_3)

Calcite is a carbonate mineral and stable polymorph of calcium carbonate. Their texture and mineralogy are obtained during the process of formation and diagenesis. Calcite can form up organic skeletal parts and cement of marine sediments as well. Chemical weathering is one of the methods that can break down the calcite. Groundwater can dissolve calcite under several factors, such as the temperature and pH value of fluid and ion concentration. Calcite is insoluble in cold water; acidity can cause carbon dioxide gas and dissolution. Calcite does not change colour under plain polarised light and the grains are too bright, and other grains can be brown (Figure 5.5).

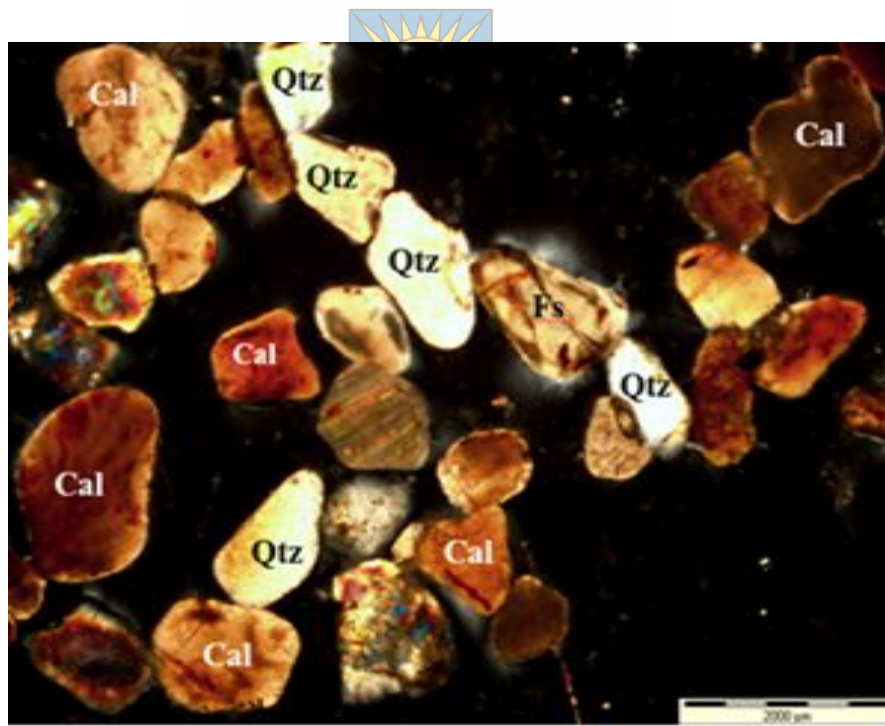


Figure. 5.5: Photomicrographs of various sand grains showing calcite (Cal), quartz (Qtz) and feldspar (Fs) grains (Sample 45).

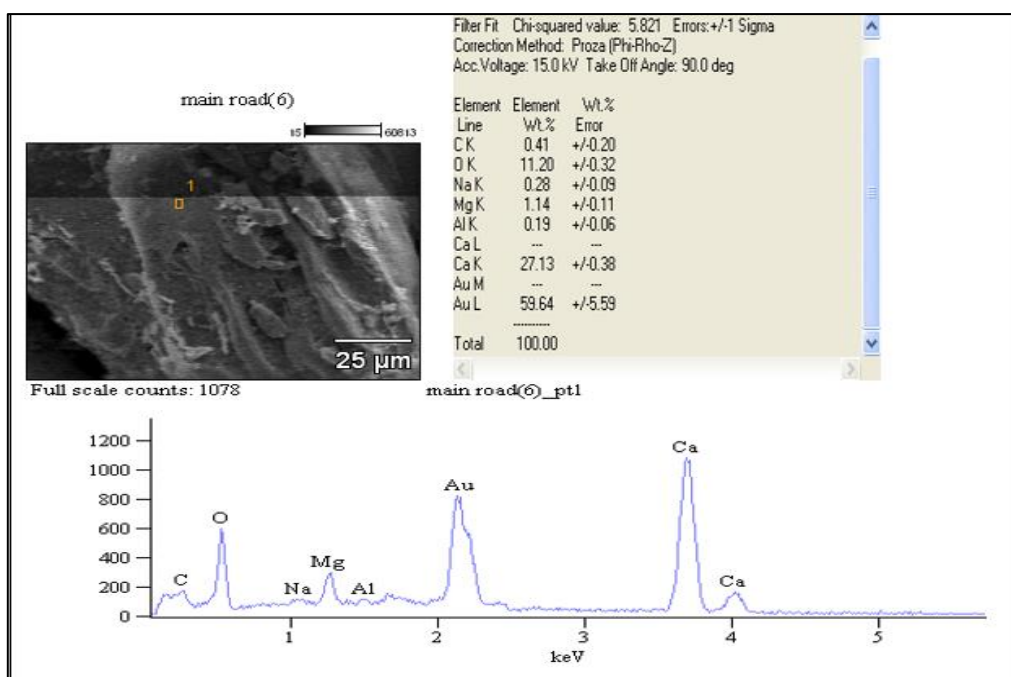


Fig. 5.6: SEM and EDX analyses for low-Mg calcite grain showing calcium, oxygen and carbon of chemical compositions with minor Mg content. Au peak was due to gold coating for the sample.



University of Fort Hare

Together in Excellence

5.2.4 Lithic fragments

Lithic fragments are a small fraction of rocks. They can be derived from a wide variety of lithotypes, and they have a source of specific texture and composition that can be recognized in thin sections. Lithic fragments can be subrounded, rounded to angular in shape. The study area samples reveal that the rock fragments observed under the microscope are from sedimentary rocks that and metamorphic rock. Quartzite and siltstone lithic were observed under the microscope. Siltstone lithic appear dark coloured with small to slightly large quartz grains (Figure 5.9). Lithic are believed to be unstable in sedimentary environments, and they are the best provenance indicators for sediments (Johnson and Bassu, 1993). Quartzite lithic appear light in colour (Figure 5.9). Shale is a fine-grained sedimentary rock and is composed of mud with a mix of clay mineral and tiny fragments of any other mineral. Shales consist of layers of sandstone or limestone. They favour the environment where silts, mud, and other sediments were deposited by slow transport of sediments. Shales are composed of quartz and feldspars and the major mineral in shales is

kaolinite. Under the microscope, shale fragments show 50 micrometres thick reddish-brown organic-rich layers that are parallel (Figure 5.8).

5.2.5 Glauconite

Glauconite is a potassium aluminium, silicate that contains ferrous and ferric iron as well as magnesium. It is a sedimentary mineral that forms as a result of authigenic alteration in a shallow sea environment. It usually comes in the form of green sand –sized pellets that are microcrystalline and have low birefringence (Figure 5.9). The presence of glauconite mineral indicates a decreasing environment, in which decomposing organic matter absorbs all available oxygen. One of the most distinguishing characteristics of the mineral is its green colour as shown in figure 5.9. Because glauconite is easily weathered, it is unlikely to withstand heavy erosion or long distance transit. As a result, glauconite is most commonly found in places close to its original environment, making it a suitable palaeo-environmental indicator.

5.2.6 Organic pellets



Organic pellets are small round, ovoid shape, or rod like shape grains (Fig 5.7). They occur in low energy environments and are common in sedimentary rocks. They form due to a process of organic and chemical deposition where they combine. Organic pellets are rich in organic carbon, and they are also made up of carbonate mud. Organic pellets found in sand sediments of the Swartkops channel are light brown to dark colours. Organic pellets lack distinct internal structure, carbonate mud and calcium can be present or their mixture.

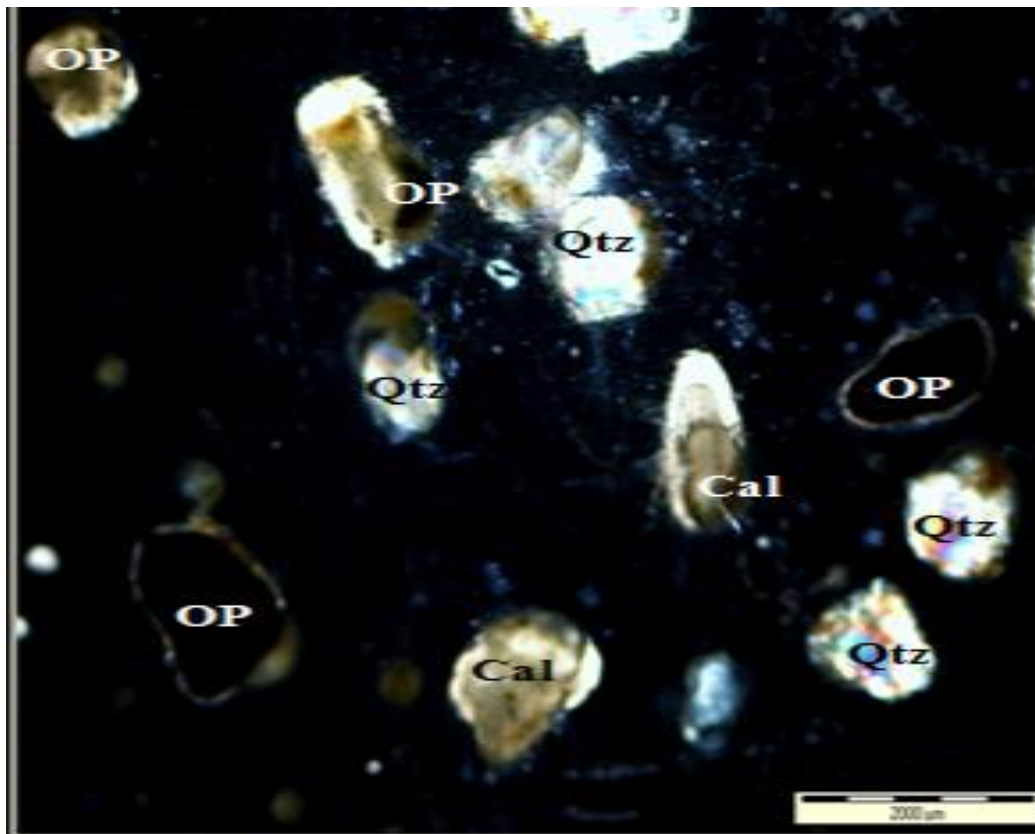


Fig. 5.7: Photomicrographs of various sand grains showing organic pellets (OP), quartz (Qtz) and calcite (Cal), sample 31 from Swartkops estuary.

University of Fort Hare
Together in Excellence

5.2.7 Sponge

Sponges are an immobile organism representing the aquatic component ecosystem with significant filter particles and a small size range filtering potential than other benthic invertebrates (Andus et.al, 2016). Figure 5.8 shows a sponge structure, the first sponge appeared in the Late Precambrian, 600 million years ago until the present. Sponges are important for water purification. They are few centimetres in size others are urn-shaped or shapeless or less than a centimetre. They differ in external appearance with bushy or fringelike projections.

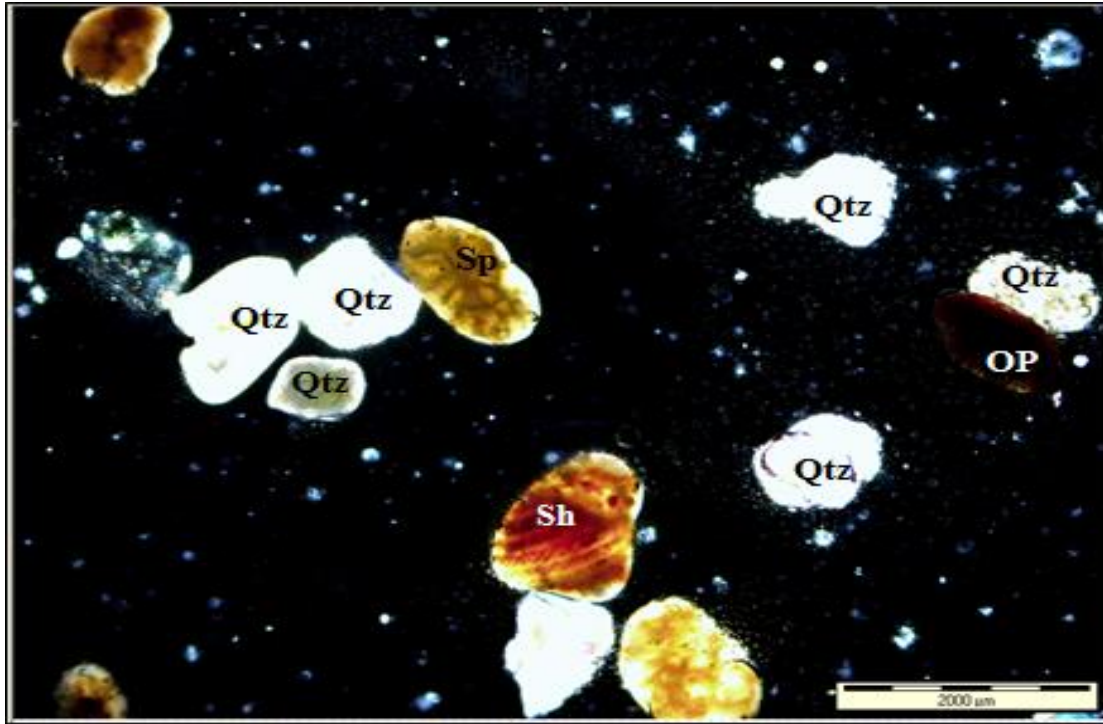


Fig. 5.8: Photomicrographs of shale fragments (Sh) and sponge (Sp) and various other grains, sample 57 from Swartkops estuary.



5.2.8 Foraminifera

University of Fort Hare

Most foraminifera are of marine origin, living on or within the sediment of the seafloor, while a lesser number float in the water at various depths. The shells of foraminifera are generally formed of calcium carbonate and can have one or more chambers (Kennett and Srinivasan, 1983). Foraminifera shells are common in all marine environments. These shells are commonly made up of calcium carbonate sediment particles (Figure 5.9).



Fig. 5.9: Photomicrographs of various sand grains showing quartzite lithic (orange arrows), siltstone lithic (green arrow), glauconite (yellow arrow), plagioclase (grey arrow, partially replaced), foraminifera (blue arrow) and various other grains, sample 32 from Swartkops estuary.


University of Fort Hare
Together in Excellence

5.3 Mineral abundance

We selected 10 samples from Swartkops estuary and 8 samples from Bluewater beach, and calculated the average abundance (percentages) for different minerals. The results are shown in the Table 5.1. The analysis was performed using a petrographic microscope for mineral identification in the Geology lab at the University of Fort Hare by visual estimation. The sediments have a high content of quartz, followed by detrital mineral K- and Ca-feldspar, lithics and clay minerals. It is obvious that quartz and lithics are more abundant in the Bluewater beach sediments compared to the Swartkops estuary sediments, whereas clay minerals and organic pellets are richer in the Swartkops estuary sediments. Other minerals have no major difference between the sediments in the two different environments of the study area. These differences are probably due to the higher

hydrodynamic environment in the beach, compared to the lower energy of an estuary environment.

Table 5.1: Mineral types and their abundance (percentages).

Samples	S18	S19	S20	S21	S22	S31	S41	S57
	Quartz	K-feldspar	Ca-feldspar	Lithics	Clay minerals	Calcite (chemical)	Calcite (organic, ie shells)	Organic pellets
Swartkops estuary (10 samples average)	60.57	3.38	2.69	4.43	14.35	4.46	5.82	4.30
Samples	S1	S2	S8	S9	S10	S11	S12	S13
	Quartz	K-feldspar	Ca-feldspar	Lithics	Clay minerals	Calcite (chemical)	Calcite (organic, i.e.shells)	Organic pellets
Bluewater beach (8 samples average)	74.93	3.45	2.71	5.87	1.55	3.38	5.66	2.45



University of Fort Hare

5.4 X-Ray diffraction (XRD) results

The XRD analysis was carried out on eight sand samples that cover the study area. The XRD was conducted at XRD Analytical and Consulting in Pretoria. Analysis of minerals by X-ray diffraction indicates qualitative results of minerals by showing the percentages of each mineral in samples. The eight samples were prepared for XRD analysis using the backloading preparation method. Diffractograms were obtained using a Malvern Panalytical Aeris diffractometer with PIXcel detector, and fixed slits with Fe filtered Co-K α radiation. The phases were identified using X'Pert Highscore plus software. XRD indicates the presents of quartz, Calcite, Aragonite, Plagioclase, and Muscovite. Quartz has the highest percentage followed by calcite. The X-ray beam is represented by the peak positions which are diffracted by the crystal lattice. Table 5.2 presents percentages of minerals present in sample P3 to Sample S8.

Quantitative results of the X-Ray diffraction (XRD) analysis (%).

Table 5.2: Percentages of minerals present in sample P3 to sample S8.

	P3		P24		P43		P46
	wt%		wt%		wt%		wt%
Quartz	87.8	Quartz	85.5	Quartz	85.1	Quartz	82.9
Calcite	3.8	Calcite	3.5	Calcite	5.5	Calcite	7.8
Aragonite	1.7	Aragonite	5.6	Aragonite	3.4	Aragonite	7.4
Plagioclase	5.6	Plagioclase	4.1	Plagioclase	4.3	Plagioclase	1.8
Muscovite	5.1	Muscovite	1.3	Muscovite	1.7	Muscovite	0.1
	P55		P62		S20		S8
	wt%		wt%		wt%		wt%
Quartz	89.3	Quartz	81.5	Quartz	83.1	Quartz	81.4
Calcite	6.6	Calcite	5.0	Calcite	6.8	Calcite	8.6
Aragonite	3.4	Aragonite	5.8	Aragonite	5.3	Aragonite	8.1
Plagioclase	0.6	Plagioclase	5.6	Plagioclase	3.7	Plagioclase	1.8
Muscovite	0.1	Muscovite	2.1	Muscovite	1.1	Muscovite	0.0



University of Fort Hare
Together in Excellence

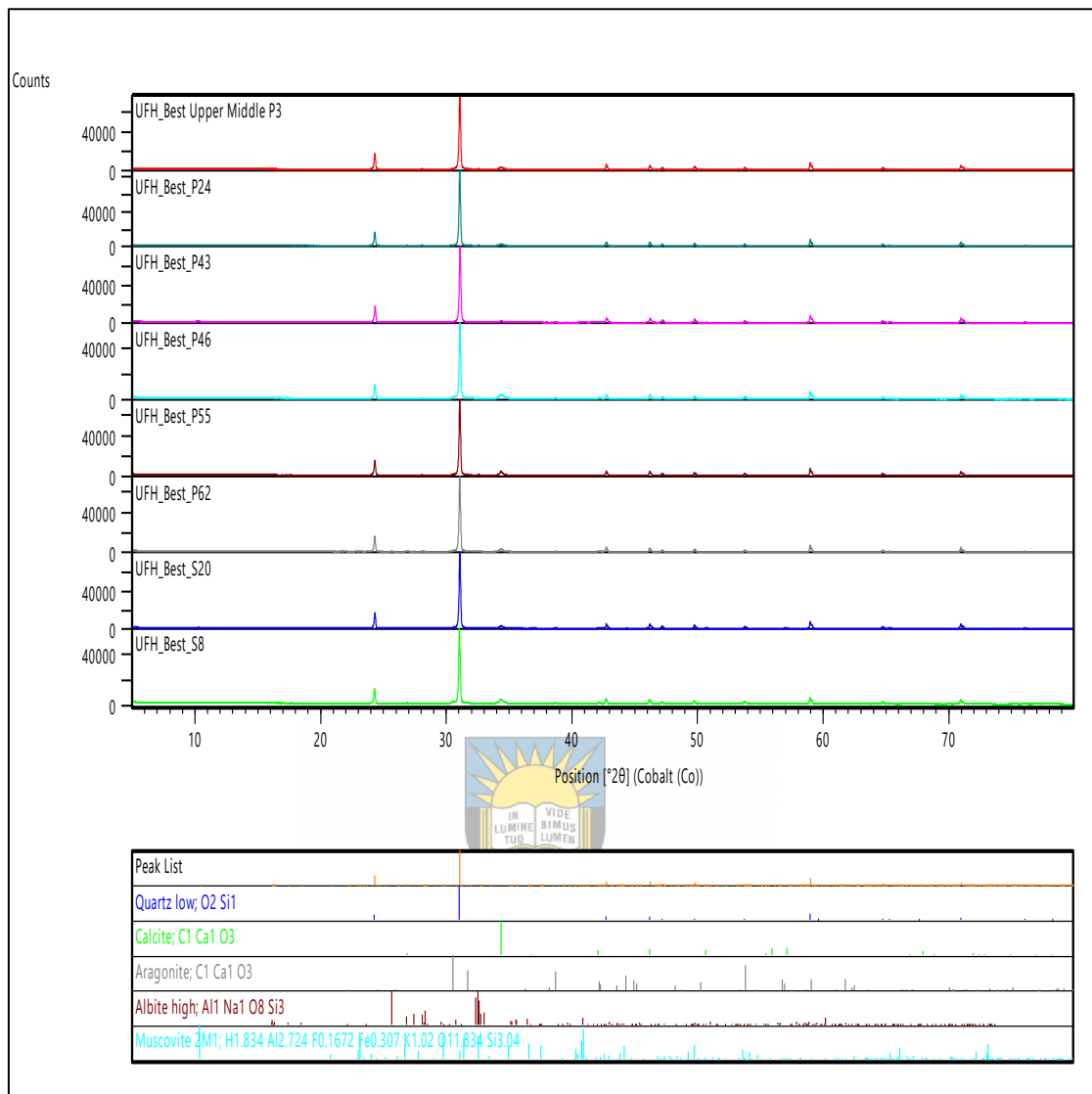


Fig. 5.10: XRD patterns for all the samples, P3, P24, P43, P46, P55, P62, S20 and S8. Showing the abundance of Quartz, Calcite, Aragonite, Albite and Muscovite respectively.

X-ray Diffraction reveals the evidence of high quartz percentage and other mineral abundance in the area of study. Quartz is the most abundant mineral and is dominant in all sediments (Fig 5.10). The plagioclase which is in the type of feldspar is present in the analysis of the X-ray diffraction. Aragonite was found in the samples, the presence of the aragonite reveals that it was a biogenic carbonate since aragonite is an unstable mineral, and is easy to transfer to calcite during diagenesis. Muscovite normally shows up in sandstone or shale deposited by fluvial streams or tide currents which results from inland

weathering. Calcite is a dominant carbonate mineral and mostly come from dead organisms such as shells and foraminifera of marine origin.

5.5 Summary

As noted under thin sections, quartz is the dominant mineral in almost all the sediment of the Swartkops estuary and the Bluewater beach. The samples of the study area comprise mainly of the grains such as quartz, calcite, feldspar and lithic fragments. Glauconite appears green in colour, it occurs in a minor amount. Plagioclase shows cleavage and twinning under the microscope. Lithic fragments appeared mainly as metamorphic quartzite and minor as mudstone clasts and both came from metamorphic rock source of Table Mountain Group of Paleozoic sequence. The sediments belong to the marine environments which have been revealed by the presence of marine organism such as shells, gastropods and algae, as well as organic pellets observed under microscope. The grains of the minerals under microscope show different shapes, some are rounded or subrounded which reflect a long distance of transportation. Whereas other grains are angular or subangular which reflect a short distance of transportation history.



University of Fort Hare
Together in Excellence

CHAPTER 6: GRAIN SURFACE TEXTURES

6.1 Introduction

Surface textures of sand grains have been studied by many geologists and have been used to reflect hydrodynamic, chemical or organic depositional environments (Greenwood, 1982; Madhavaraju *et al.*, 2009; Itamiya *et al.*, 2019) since formation of surface texture is closely linked to transportation medium and current velocity, chemical conditions and organic activities. Thus, the study of grain surface textures is a useful tool to reflecting grain transportation process and its hydrodynamic environment, as well as the climate change in the geological history (Itamiya *et al.*, 2019).

Grain surface textures can be classified as three groups based on the formation mechanisms, i.e. 1. Textures formed by physical and hydrodynamic processes; 2. Textures formed by chemical processes and variations; and 3. Textures formed by organic activities.

Group 1: Textures formed by physical or hydrodynamic process: In a high hydrodynamic water environment, grains crash or collide each other that will produce diagnostic of unique surface texture on the grain. Based on the notion that the transport agent creates distinctive surface features, we can therefore restore the original hydrodynamic environment where the texture was produced. Through the use of reflective light microscope and scanning electron microscope, we can clearly find and study the grain surface textures, such as V-shape pits and Surface cracks.

Group 2: These textures were formed due to chemical environment changes. In different chemical environment, different pH and Eh environment will affect the stability of different types of minerals, thus some minerals will become unstable and then causing dissolution, while other minerals become stable and causing precipitation and crystallization. These include the precipitation of new crystals on the grain surface or holes, and generation of dissolution pits/holes.

Group 3: These textures were created by organism or organism activities, such as micro-organism worms and algae. It could also be created by macro-organism, such as shells and fishes. Faecal pellets, burrow and boring holes are the common textures of this group.

6.2 V-shape pits

Almost all the grains show that they have V-shape pits, which were the results of grain collision during the transportation process of sediments. These V-shape pits are commonly observed on detrital sand grains such as quartz and lithics and are characteristics of beach actions. The effect of wave and tide action at coastline results in mechanical collision or abrasion for producing V-shape pits (Figure 6.1). The small cut or hollow on the quartz grain surface are good indicator for high hydrodynamic environment (Itamiya, Sugitay and Sugai, 2019), implying that the Swartkops estuary had been affected by seasonal swelling and surging waves and tide currents, which caused not only grain V-shaped pits, but also the erosion of river bank and coastline (Kinsley and Margolis, 1974; Madhavaraju *et al.*, 2009).

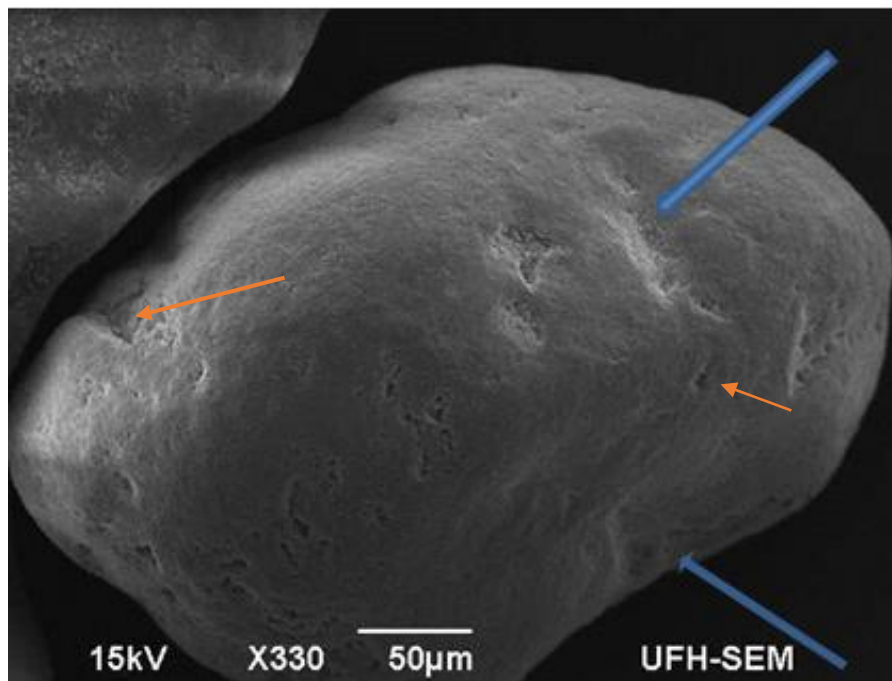


Fig. 6.1: SEM photomicrograph showing V-shaped pits (orange and blue arrows).

6.3 Upturned plates

Upturned plates are caused by mechanical crushing and chemical corrosion and secondary precipitation during transportation and early deposition (Figure 6.2). Some of the grains have upturned plates on the grain surface, and these upturned plates have an alignment roughly parallel each other. The formation process could be complicated, and passed

different stages in different environments. It is usually formed by mechanical collision at the first stage, then by chemical corrosion in a varied chemical environment in the second stage, then by chemical precipitation of crystals in the hollow at the last stage. Therefore, upturn plates are commonly found in a complicated environment, such as coastline, shallow beach and estuary, where aeolian, fluvial and marine processes reactive and overlap each other (Liu, 1997; Whalley and Krinsley, 2006). Upturned plates form in a distinctive water and energy regimes, sand particles exhibit surface collision features along fractures and cracks in an aeolian or coastline environment. Upturned pits are good indicator of high energy water or high velocity wind environment. The grains could be transported by aeolian and marine water and then deposited at near the coastline environment.

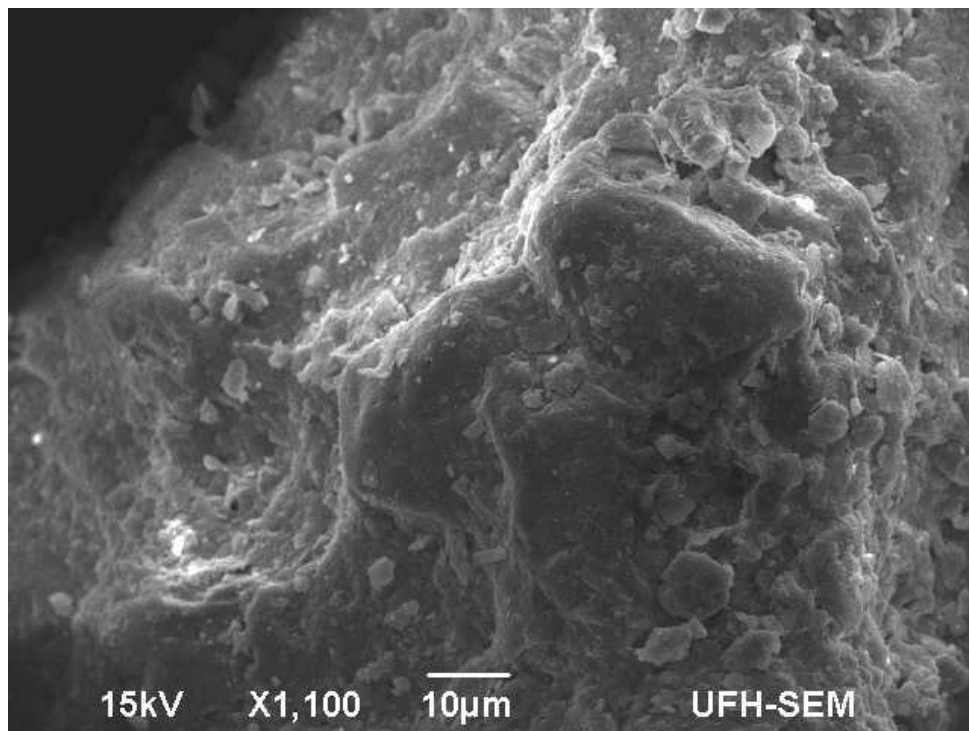


Fig. 6.2: SEM photomicrograph showing Upturned Plates on a grain surface due to collision, corrosion and precipitation and magnified secondary precipitated crystals within an upturned hollow.

6.4 Secondary minerals precipitation

The varied secondary minerals are found precipitated on the grain surface, their chemical compositions, as well as their percentages were detected using energy dispersive X-ray (EDX) detection. Secondary mineral precipitation on the grain surface are mostly made up of silica (quartz, SiO_2), calcium carbonate (calcite, CaCO_3), sodium chloride (salt, NaCl), and organic carbon, according to the XRD results. The most abundant minerals in all the samples are quartz and calcite. The calcite and salt precipitation comes from marine water, whereas silica (quartz) comes from meteoric water. The mineral composition of silica (Fig 6.3), calcium carbonate (Fig 6.4), sodium chloride (Fig 6.5) and silicate (clay) mineral (Fig 6.6) are shown in the EDX graphs below.

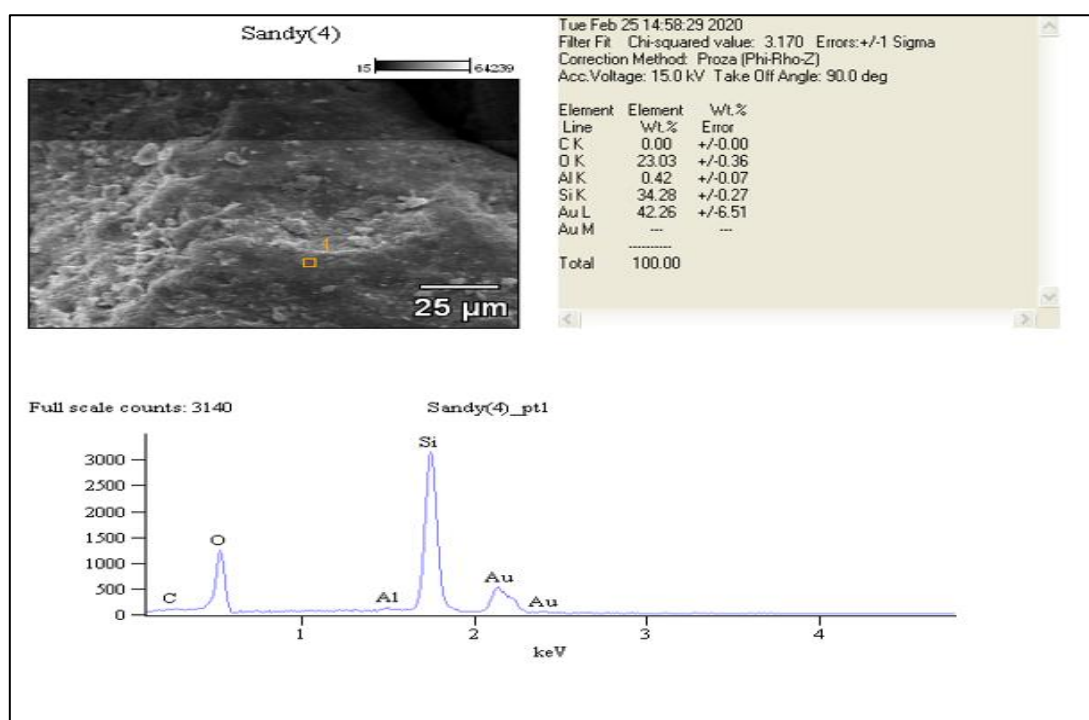


Fig. 6.3: Secondary mineral contains high silica (SiO_2) content (NB: the Au peak was due to gold coating for sample and should not be taken into account).

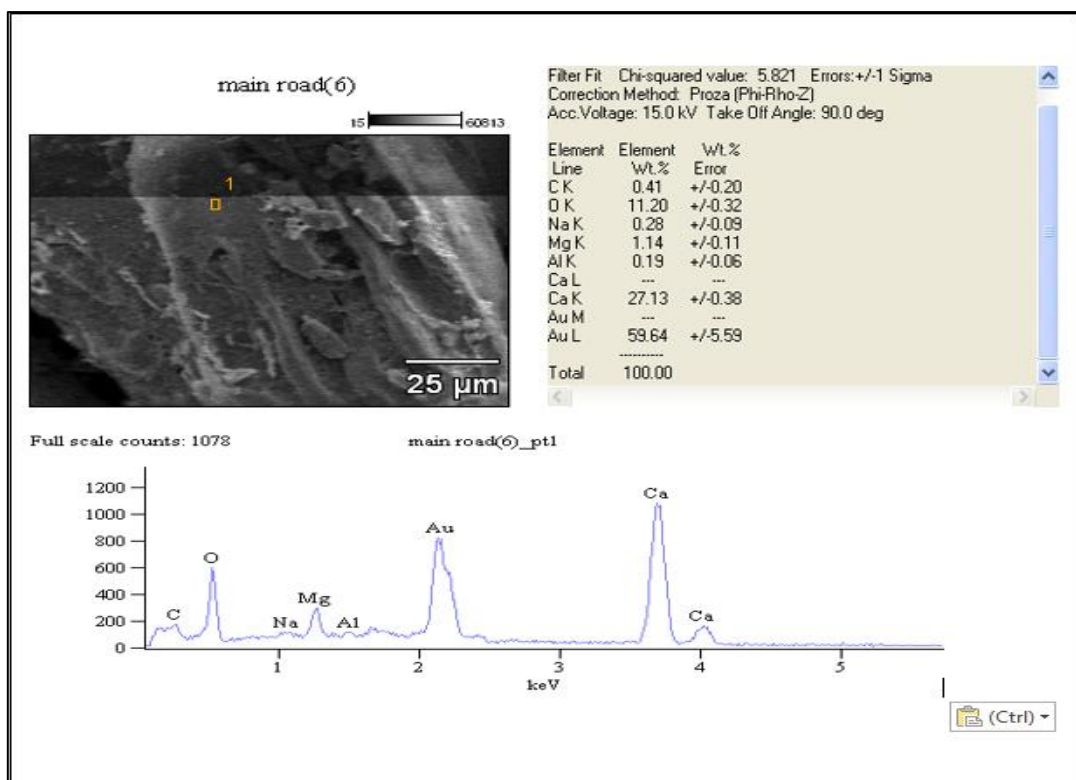


Fig. 6.4: Secondary mineral contains high calcium carbonate (CaCO_3) content (NB: the Au peak was due to gold coating for sample).

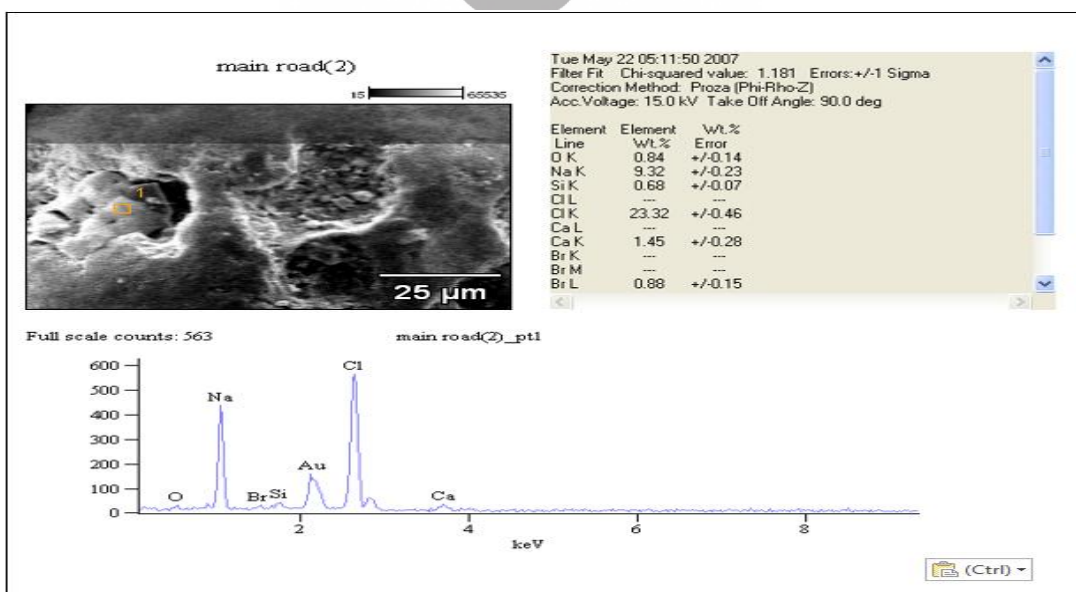


Figure 6.5: Secondary minerals contain high sodium chloride (NaCl).

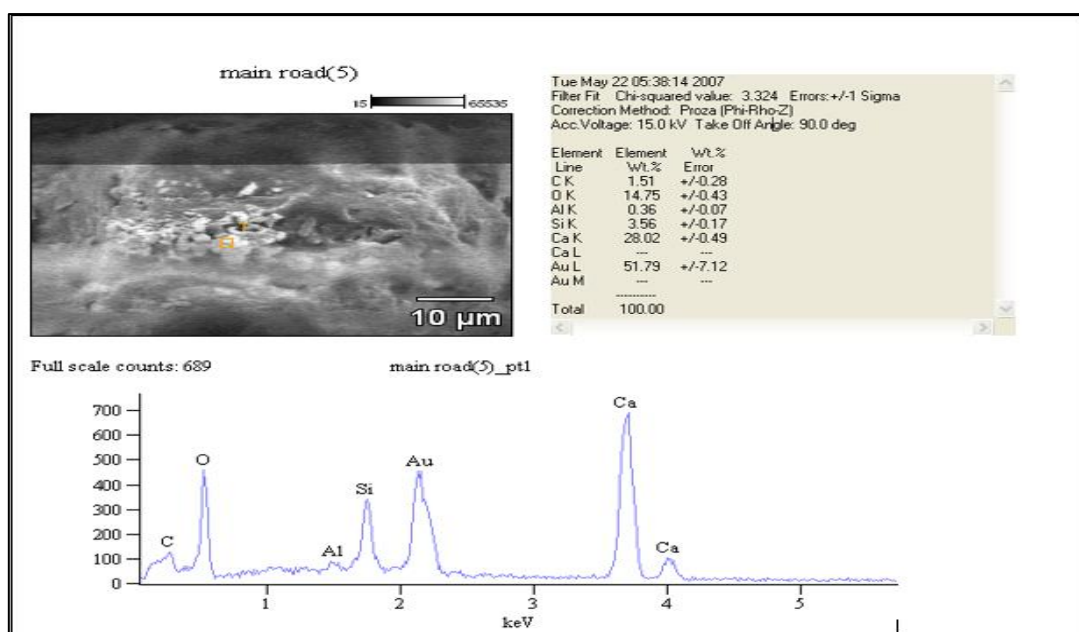


Figure 6.6: Secondary minerals contains high calcium carbonate (CaCO_3) and (NB: the Au peak was due to gold coating for sample).



6.5 Dissolution pits/holes

The formation of dissolution pits/holes on the grain surface are very common in the samples (Fig 6.7). When the environment changed, some grains become unstable, then they are easily dissolved and thus created irregular pits or holes on the grain surface. After the pits/holes created, new crystals can be precipitated in the pits/holes due to the new crystals that are stable in the new environment (Figs 6.7 and 6.8). Secondary mineral precipitation might also occur because of the weathering and leaching (Whalley and Krinsley, 2006; Kashif *et.al.*, 2019).

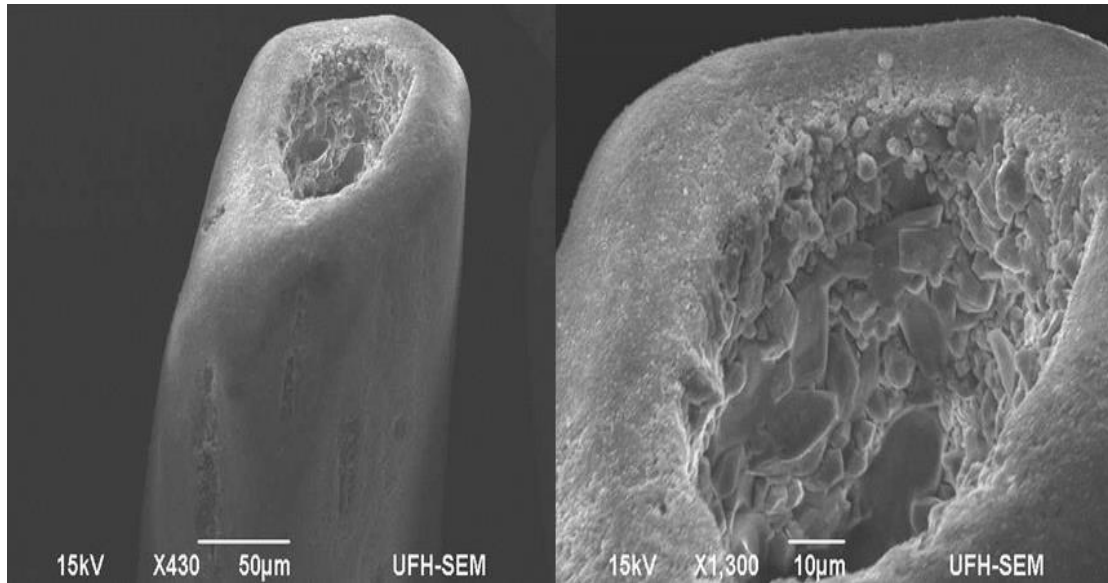


Fig. 6.7: SEM photomicrograph showing dissolution pits/holes on the grain surface.

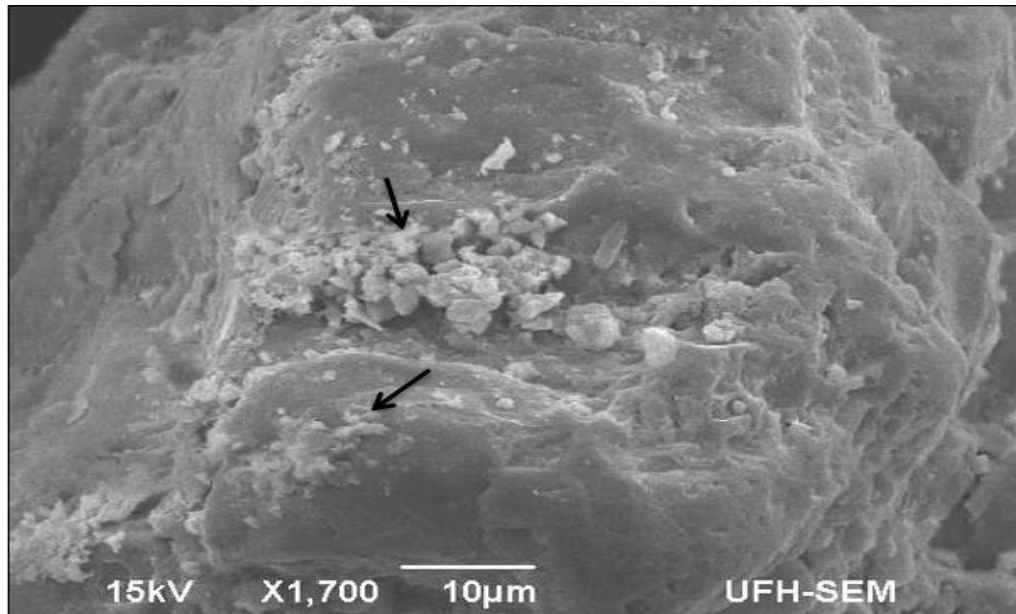


Fig. 6.8: SEM photomicrograph showing secondary mineral precipitation on the grain surface (black arrows).

Dissolution acts as an important process for replacement and recrystallization in sands and sandstones. The dissolution process can supply quartz cement and quartz overgrowths. Different minerals are stable in different pH and Eh environments, when the pH and Eh changed, some minerals become unstable and will be dissolved, while other minerals are stable and will be precipitated.

6.6 Burrow and boring holes

Burrow and boring holes have been found on the grain surface (Figs 6.9 and 6.10). These holes are similar to dissolution holes, but they are much rounded and usually deeper. Micro-organism, such as worms and algae can bore into grain surface, thus created rounded holes, which are different with the dissolution holes which are more shallow and irregular shaped.

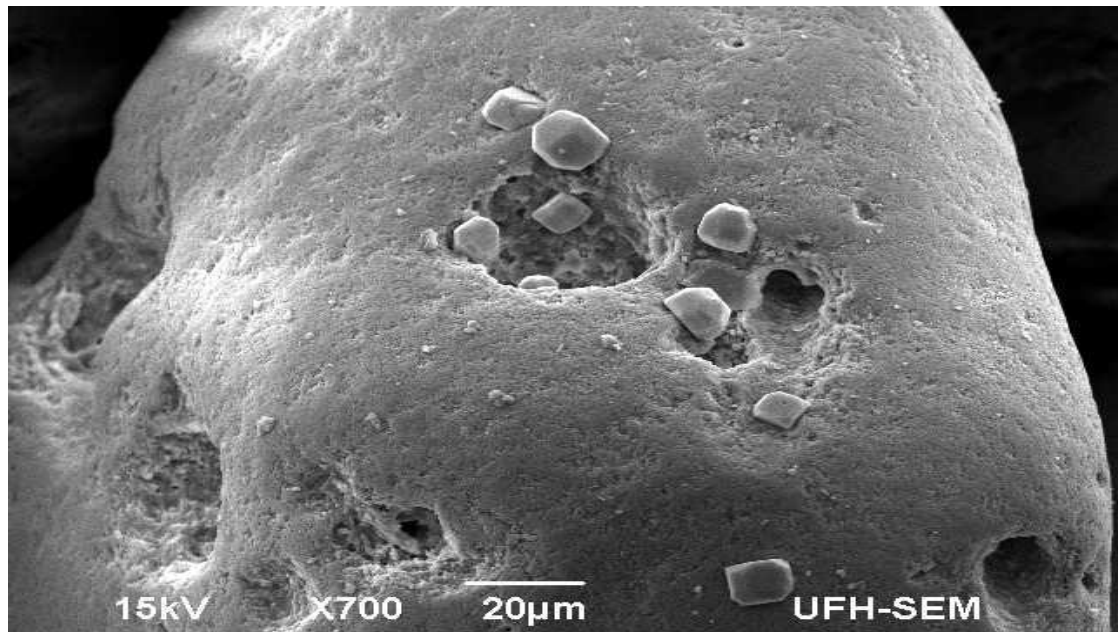


Fig. 6.9: SEM photomicrograph showing grain surface corrosion and dissolution pits/holes (left 3 holes and the middle hole), also secondary calcite crystals precipitated on the grain surface (middle). Please note the boring holes on the right, which are rounded and deeper comparing to the dissolution holes. Boring holes are created by micro-organism, such as worms and algae (the right, 2 rounded holes).

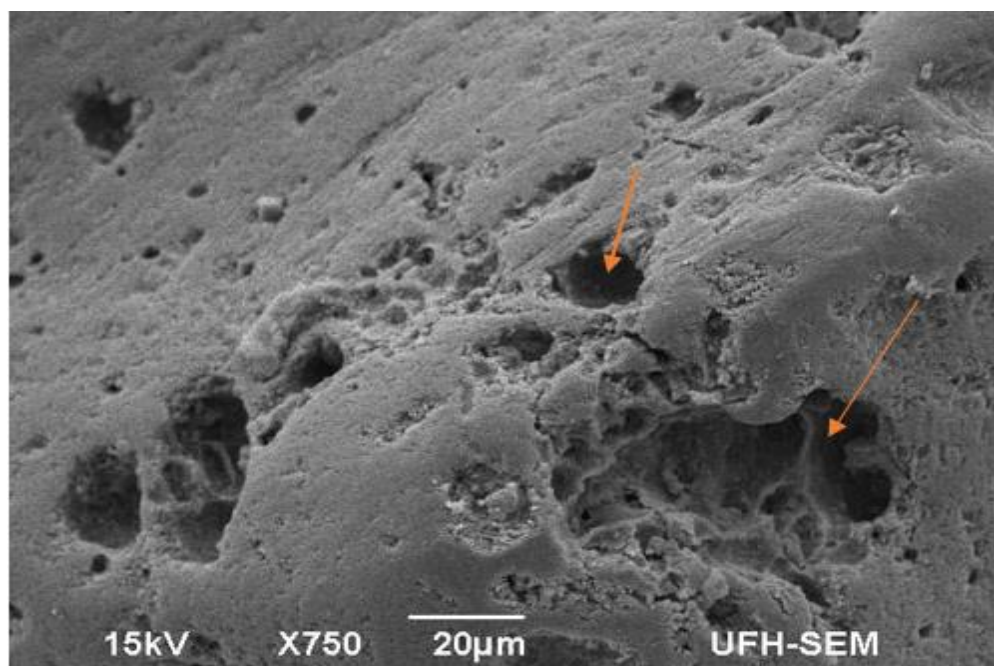


Fig. 6.10: Photomicrograph showing dissolution holes (shallow, irregular holes on the middle) and boring holes created by micro-organism (deeper and rounded holes on the grain surface (orange arrows)).



6.7 Summary

University of Fort Hare
Together in Excellence

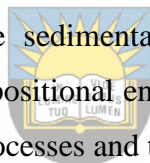
Mechanical and chemical effects on the grains, including V-shaped pits, upturned plates, dissolution pits/holes, burrow and boring holes, secondary mineral precipitations and recrystallizations. These V-shaped pits are frequently found on the surface of sand grains like quartz and are caused by shallow water movement. The upturned plates were observed and they reveal a multiple marine and aeolian processes. The burrow and boring holes reflect activities of micro-organism in the estuary and beach environment. Dissolution pits/holes reflect climate change and alternation of environments, which lead unstable minerals become dissolved while stable mineral can be precipitated. Crystalline mineral precipitation of calcite, quartz, salts and clay minerals were detected using the Energy dispersive X-ray (EDX) to detect the mineral composition. Quartz has been revealed as one of the common silica in all samples followed by calcite from the dead shells of marine organisms. SEM and EDX are useful tools to character mineral types and shapes, and as well as abundance (percentages).

CHAPTER 7 SEDIMENTARY STRUCTURES

7.1 Introduction

Sedimentary structures are the most valuable features for interpreting the depositional environment. The dunes essential characteristics are their internal structure, shape, migration and movement direction. This chapter will address the detailed description of the sedimentary structures observed in Swartkops estuary and Bluewater Bay beach. Sedimentary structures can be divided into primary and secondary structures depending on the formation process. Primary structures are formed at their original deposition while secondary structures are formed after the sediments are set down mostly by the process of diagenesis. Dunes can take a remarkable range of sizes and shapes, depending on the amount of sand available, the sand size and water/wind strength and movement directions.

Well-developed sedimentary structures have been found in the Swartkops estuary and beach area. The formation of the sedimentary structures are closely linked to the wind/hydrodynamic energy and depositional environment, therefore they are very useful tools for revealing the formation processes and the paleo-hydrodynamic environments.



University of Fort Hare

Together in Excellence

7.2 Sediment stratification

The regional geology and climate determine the characteristics of estuary sediments with hydrological and climatic conditions (Fiket *et.al.*, 2017). Stratification is one of the universal features for sediments and sedimentary rocks, such as layers or beddings and their thickness. Sedimentary structures are relatively discrete features that do not grade from one form to another (Picard *et.al.*, 1973; Pichard and High, 1973). Therefore, they are good indicator for special hydrodynamic mechanism and formation process. Sediments are deposited as different bedforms, and as a result, they form horizontal, continuous or discontinuous stratifications (Pichard and High, 1973). Stratification in estuaries is mostly driven by or controlled by fluvial or marine currents (Li *et.al.*, 2018). Marine beaches are formed by the action of waves and the tides, but the fluvial channels are deposited sediments by uni-direction river flow, and thus resulting formation of different bedforms (McKee, 1953). In most estuaries, significant changes in sediment stratification happen at several geographical and temperature scales. The stratification

changes can have a substantial impact on the hydrodynamic processes controlling sediment transportation and deposition (Scully and Friedrichs, 2003), therefore stratification is essential in interpreting geologic events and can reveal practical results for deposits of different sized sediments in different layers.

7.3 Sedimentary structures formed by aeolian process

7.3.1 Sand dune

Dune is a large landform piled up by large amount of mass windblown sands. Dunes are common in the inland desert environment, but also in the coast area. They are built by the flow of aeolian processes, aided by high tide and wave if in the coast. Coastline dune textures depend on the sand grain types and sizes. In modern tropical and subtropical area, sands are composed of mainly detrital (quartz) grains, with skeletal and non-skeletal grains such as ooids, pellets and organic shell fragments (Ahr, 2011). Dunes are composed of moderately to well-sorted sands (63-1000 micrometres) with a mean grain size ranges from 160-300 micrometres (Lancaster, 2005). Dune sands are composed mostly of quartz, lithics and various quantities of shell fragments in the Blue Lagoon beach. Dunes have three primary modes of deposition: the migrating of winds ripples, the fallout from the suspensive grains, and the avalanched grains deposited by the grain fall (Lancaster, 2005). Sediment supply for dune formation originates from inland, and also from continental shelves in the coast dunes (Maun, 2009). Because of the extensive range in grain size, the sand samples are skewed more finer than the coarser particles (Maun, 2009). The dune sand texture is vital for identifying its mobility by wind, water percolation rate, the movement through the soil, and the dune's morphology (Gradus, 2012). Grain size distribution determines the morphology of the dune (Gradus, 2012). Two types of dunes are identified in the Swartkops estuary area, a stabilized vegetated sand dune and a mobile un-vegetated sand dune (Fig. 7.1); the former was formed in Pliocene-Pleistocene in age, and the later is Holocene in age and is still in the formation/change process.

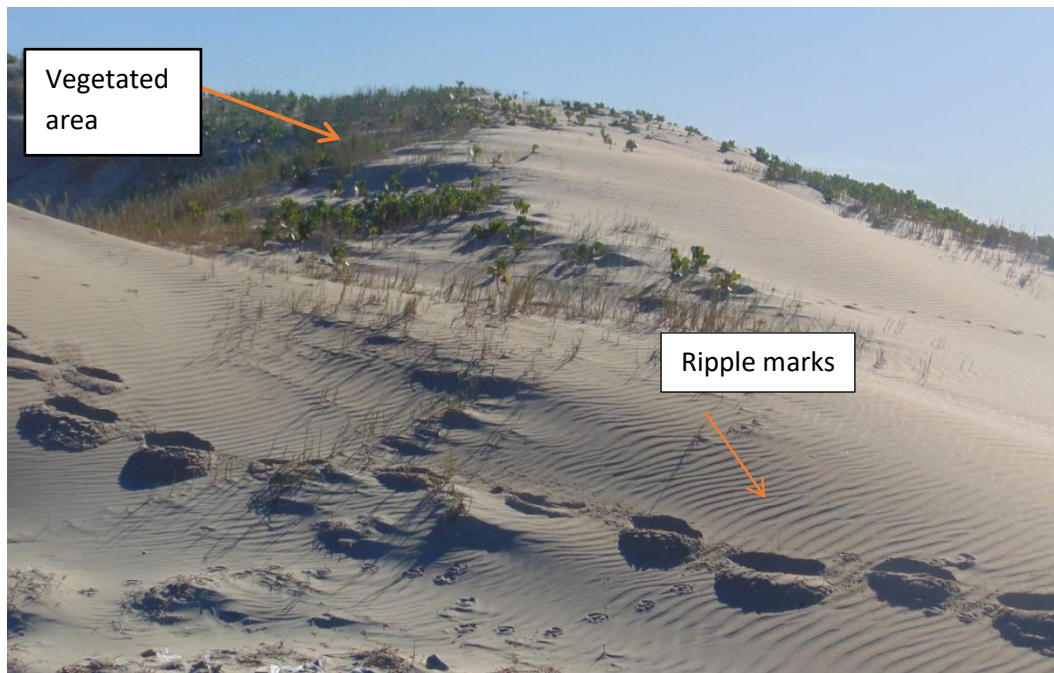


Fig. 7.1: Photograph showing stabilized, partially vegetated sand dune with ripple marks on the dune stoss side in the Bluewater beach along the Swartkops estuary.



7.3.2 Sand ridge

Sand ridge are elongated sand bodies that are larger and geographically more stable in comparison to the modern dunes, being orientated at an oblique to the strongest wind direction (Desjardins *et. al.*, 2012). Sand ridge is made up of dunes and compound dunes of different forms and sizes which migrate both on the stoss and lee side of the ridge (Fig.7.2). Four conditions are required for the formation of a sand ridge, and these are initial irregularities, sufficient sand supply, a wind/current capable of moving, and enough time for the sand to be moulded into a ridge (Desjardins *et al.*, 2012).



Fig.7.2: Photograph showing a mega sand-ridge produced by wind and high wave at the south coast of Port Elizabeth.

7.3.3 High angle cross bedding



University of Fort Hare
Together in Excellence

Cross bedding form as a results of running water and the water flows creates the bedforms such as ripples. The steep faces tilt down-current which indicates flow direction and roughly parallel to the direction of sediment transport (Fig.7.3). The direction and dip angle of a cross-beddings are usually consistent. Cross bedding can help us to interpret the wind/water flow direction, and the depositional environment. From the sediment composition and the dip angle of cross bedding, we can ascertain whether it is formed by wind or water process. High angle cross bedding (dip $>30^{\circ}$) is usually deposited by wind, whereas low angle cross beddings (dip $<25^{\circ}$) are formed by both, wind and water current. Fig 7.3 shows a high angle cross bedding which was typical for aeolian formation, and the wind blow direction is from right to left.



Fig.7.3: Photograph showing high angle cross bedding with beds tilted towards the left side, which reflects the wind blow direction. High angle cross bedding ($>30^\circ$) is typical indicator of aeolian dune, while low angle cross bedding ($<25^\circ$) was formed by water currents, as well as lower velocity of wind.



7.3.4 Antidune

University of Fort Hare

Antidune cross-bedding occurs in an upper flow regime, the flow Froude number (Fr) is greater than 1, that means that the water/wind velocity is high and the hydrodynamic energy is strong. Since the strong water/wind movement, it cuts the wave crest height down and extends the wavelength longer. Thus, antidune always shows low amplitude in height, and a long wave cycle in length. Actually, antidune can reach up to 5 m in wavelength in the field with a very low ($<15^\circ$) dip angle (Fig 7.4).

Therefore, antidune is a good indicator for fast flow water/wind environment. It always formed in a high energy, upper flow regime of hydrodynamic environment.



Fig. 7.4: Photograph showing a large scaled antidune structure with low dip angle ($<15^\circ$), low amplitude and long wavelength ($\sim 5\text{m}$). Hammer is 32 cm for scale.

University of Fort Hare
Together in Excellence

7.3.5 Ripple marks

Ripples, on the other hand, are created by more subtle forces, such as sand grains that hop around rather than blowing in the wind—hop length determines ripple spacing. The grain size under erosive conditions has the greatest influence on the development of well-developed ripples. Grain sorting happens in locations where the wind or water movement is moderate but consistent, leaving coarser grains behind due to their weight. Those grains can accumulate and form mega-ripples. But only for a short time, as weather conditions change. The well-developed rippled (figure 7.5) was taken along the Bluewater beach, showing a wave dominated environment.



Fig. 7.5: Well developed ripples on the dune surface, the left side (lee side) of the dune is very steep.

7.3.5.1 Straight line ripples

The asymmetric ripples are formed when current (tide or fluvial current) flows in a single direction, whereas symmetry ripples formed by wave in a marine environment. In the case of asymmetric ripple, the water flow direction is from stoss side to lee side; whereas in the case of symmetric ripple, we can't determine the flow direction, but we can determine its flow orientation, which is vertical to the ripple crest line from both side, i.e. it could from any side vertical to the crest line. Thus it is an orientation, not a direction. Straight ripples show a straight line arrangement of the ripple crests, indicating a stable wave/current movement and stable hydrodynamic environment. Baas (1994) highlighted that straight ripples are non-equilibrium bedform at all velocity flows. Straight ripples could be forked by current flowing in a shallow marine environment (Fig. 7.6).



Fig. 7.6: A photograph showing straight ripples with ripple crest lines parallel each other at Swartkops estuary.

7.3.5.2 Sinuous line ripples



Curvy cross-laminae are created by sinuous ripples. As illustrated in figure 7.7, they have a pattern of curving up and down of crest lines. Trough cross lamination is created by sinuous ripples. Under this type of ripple, all laminae generated at an angle to the flow as well as downstream. The wind direction and velocity were not stable, and could have a small variation during the formation. These ripples show a ripple crest that is short and changed lightly in direction. Sinuous ripples produce curvy cross-laminae and dips generally in an angle to the flow.



Fig. 7.7: Photograph shows sinuous ripples with crest lines slightly vary in different directions as at Swartkops estuary. Varying in flow direction and as well as interference by late stage of wind movement caused the sinuous crest ripples.

7.3.5.3 Aeolian nail marks



Wind blow not only produces ripples, but also remains aeolian nail marks on the dune surface. Aeolian nail structures are formed when sands blow by wind meets obstacles, such as pebbles, shell fragments or coarse sands. Then the sands movement will be stacked at the obstacle, and remains a shadow tail below the obstacle and formed a nail shaped mark/structure parallel to wind direction. The obstacle is the nail head, and the tail is the nail small side. Which gradually dies out from the head. Therefore, the direction from nail head to the tail, reflected the wind below direction (Figure 7.8).



Fig. 7.8: Photograph showing nail marks (arrows) which are parallel to wind blow direction from nail head to nail tail, i.e. from top to bottom in this picture.


University of Fort Hare
Together in Excellence

7.4 Sedimentary structures formed by water flow

7.4.1 Gravel pavement

Pebble bed can be found along the Bluewater beach (Fig 7.9). The sizes of pebbles vary from 2-3 cm to 7-8 cm in diameter, most commonly 4-6 cm in size. The shape of pebbles are also variable from rounded to subangular, with mostly subrounded in shapes. These characteristics reflect the transported distance and time of the pebbles; the pebbles transported longer time or distance, they become more round. The size of pebbles are linked to water energy, the more big pebble size, the stronger the water energy (Paszkowski and Shone, 1994). Pebble compositions are mostly quartzite, with small amount of sandstone, chert and shell fragments (Paszkowski and Shone, 1994), which reflect the sources were come from Cape Supergroup (quartzite) and Karoo Supergroup (sandstone), as well as from sea side (shells and chert) (Blair and McPherson, 1999).



Fig. 7.9: A photograph showing pebble pavement along a part of Bluewater beach, reflecting the water (tide) energy was higher at this section of beach. Whereas other section of the beach is covered by sands, reflected a reduced water energy environment comparing to the gravel/pebble beach at the Swartkops estuary area.



University of Fort Hare
Together in Excellence

7.4.2 Interfering ripples

Two sets of ripples meet at high angles to generate interference ripples (Figure 7.10). The dominant current direction is represented by the more continuous ripples, while the subordinate current is represented by the smaller connecting ridges. If the two sets of current are equal in energy, then it remains only separate troughs and ridges on the floor, It is usually the first reached current produced a set of ripples, then at later time, second current from different direction swiped the area and altered the first set ripples, resulting in interfering ripples. In any habitat with two competing currents, such as ephemeral streams or shallow marine environments, interference ripples can form (Gough, 2021).



Fig. 7.10: Photograph showing interfering ripples in the Algoa Bay, at the mouth of Swartkops estuary, which were formed by two set of ripples interfered together.

7.4.3 Flat topped ripple mark



The flat topped ripple mark indicates a very shallow water environment, such as the intertidal environment. The flat-topped ripple markings observed had been exposed to the beach and the estuary. Various kinds of flat-topped ripple marks can be observed such as simple, parallel, linear forms. At shallow water environment, after the first set of ripple was produced, the later stage current shaved the top (the crest) of the first set of ripples, thus all the first set ripples become flat in the ripple crest (top). Flat top ripples are formed only in a very shallow water environment, i.e. not deeper than the crest, thus water can cut the crest becoming flat (Fig 7.11).



Fig. 7.11: Photograph showing flat topped ripples caused by later shallow water shaved the ripple crest becoming flat.

7.4.4 Linguoid marks

Linguoid marks have curved lee slope surfaces, like catenary and sinuous ripples, resulting in irregular shape and sized laminae. Linguoid marks create a downstream angle as well as an angle to the flow. Linguoid mark has discrete crest, i.e. each linguoid mark has own crest, and the crest is isolated and parallel to water movement direction, not vertical to the water movement direction like ordinary ripple marks. Lunate ripples, also known as crescent ripples, are similar to linguoid ripples but with curved stoss sides instead of the lee slope. The rest of the features are the same. As languid ripple form, curve cross laminae are formed mainly in trough shaped low areas between adjacent ripple forms. These ripples have curved slopes surface that generate the dip at an angle to the flow as well as downstream.



Fig. 7.12: Photograph showing linguoid marks in different shapes and sizes along a bank of Swartkops estuary, which were produced by strong water current on relative fine sediments.

7.4.5 Asymmetric sinuous ripples

The presence of asymmetric ripples indicates that there is only one main current direction. The current erodes and deposits sand/silt grains along water channel. It can be formed in fluvial environment, and also in marine environment. Since the ripple is not symmetric, the stoss side is always longer than the lee side. Thus the water flow direction is also from toss to lee side direction (Fig 7.13).



Fig. 7.13: Asymmetric sinuous ripples showing current flow is on one direction (unidirectional) and the current direction is from stoss side (right) to lee side (left) on the bank of Swartkops estuary.

7.4.6 Rill marks

Rill marks are erosional sculptures; they commonly occur in the intertidal zones due to running tiny rivulets along the low beach surface. As the tide rises, water enters the beach sands; when the tide was retreating, numerous tiny rivulets run down along the low beach from sands and producing shallow flow-lines (Fig 7.14). Rill marks is a good indicator for very shallow water environment, at a range of water depth of few centimetres.



Fig. 7.14: Photograph showing rill marks on the lower beach, formed by the escape of water from saturated sands when the tide falls back to sea at Bluewater beach, Port Elizabeth.

7.4.7 Rhomboid marks

Rhomboid marks are useful environmental indicators. These marks are roughly rhombohedra-shaped and are elongated in the direction of water flow as shown (Figure 7.15). The current flow direction over the beach surface can be examined from the shape of the rhomboid marks and, these rhomboids are bowed in the direction of current flow and are pointed down-current. In most cases, the rhomboid marks are formed by the back

wash of tidal flow along the gentle beach (Hoyt and Henry 1963). The cause for the formation of rhomboid rill patterns is the deflecting and channelling effect of tiny uniformly distributed irregularities on a smooth, even sand surface swept by the rear part of the backwash (Otvos, 1964).



Fig. 7.15: Photograph shows the uniform network of rhomboid marks at the Bluewater beach, Port Elizabeth.

University of Fort Hare
Together in Excellence

7.4.8 Swash line

The Swash line is the highest line of wave or tide running up along the beach (Fig 7.16). Swash zone is the intertidal zone from low limit of wave/tide to high limit of wave/tide. Swash line is characterized by the turbulent layer of water that washes up on the beach after an incoming wave/tide has broken. Swash movement on the beach provides the principal mechanism for exchange between subaqueous and subaerial zones of the beach and the change in the shoreline (Masselink and Hughes, 1998). The sediment transport mechanism in the swash zone (from low tide to high tide) has less attention than those of the surface zone. That is because of the difficulty in giving out the high-quality field measurements of sediment transport and partly due to the processes complexity (Elfrink and Baldock, 2002). The swash zone is characterized by flows that are so strong and unsteady, high turbulence levels, high sediment transport rates, and rapid morphological

changes, and these represent the most dynamic region of the near shore zone (Puleo and Masselink, 2006).



Fig.7.16: Photograph showing a high tide swash line in damp sands with shell fragments.

7.4.9 Dendritic wash mark

Dendritic wash marks are erosional structures formed along fluvial or tidal channels (Figure 7.17) at Swartkops estuary. They are formed by water erosion during strong flood stage and they could be exposed and destroyed by next flooding. The ultimate origin of all erosional structures is stream scouring. Mega ripples (Figure 7.17)), on other hand, occur in tidal or fluvial channel by higher energy water deposition (Haldar, 2020). Mega ripples can indicate transport direction by gradual lower their height and flatting (Figure 7.17).

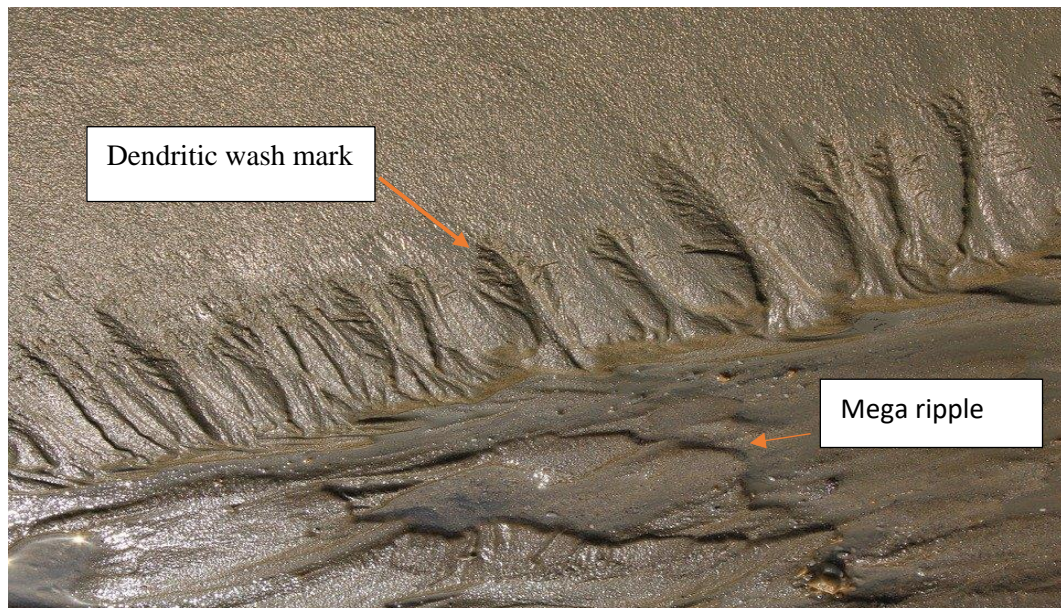


Fig. 7.17: Picture showing dendritic wash marks and mega ripples.

7.4.10 Drainage patterns on sandy beach

Drainage patterns can be termed as back flow erosion marks. These marks can result from tidal channel to the beach surface erosion. Beach drainage patterns are an example of shoreline erosion. Micro tributaries reach the main rivulets at right angles to the drainage pattern in the drainage morphology. An example of drainage patterns was discovered in the Bluewater beach (Figure 7.18).



Fig. 7.18: Drainage patterns along the Bluewater beach, which form from tidal washing and scouring.

7.5 Biogenetic sedimentary structures

7.5.1 Boring and bioturbation

Bioturbation is an alteration and disturbance of a site along the estuary or the beach by living organism, the turning and mixing of sediments by the organism. Bioturbation structures are produced by living organism's interaction and the soft sediments that manifest into a wide range of forms like footprints, burrow, trails, mound, or organic pellets as shown (Figure 7.19).



Fig. 7.19: A photograph showing boring holes by organisms along the Swartkops estuary.

7.5.2 Burrows

Burrows are very common in shallow marine environment, and created by diversity of invertebrate and vertebrate species, ranging from insects and worms, fish, amphibians, reptiles, and mammals. The burrows and bioturbation activities have a profound impact on physical and biogeochemical properties and processes. Burrowing crustaceans alter the physical environment of all sedimentary habitats, including sand flats, salt marshes, mangrove swamp, and coastal lagoons. When burrowing animals have a high sediment turnover rate, they are susceptible to erosion and contribute significant volumes of

sediment particles to bedload transport and resuspension. Burrow hole is more large in size than a boring hole, and it could be multiple layers if cutting in a vertical section (Fig. 7.20).



Fig. 7.20: Photograph showing burrows (arrow) caused by invertebrate organisms along the beach. Burrows are irregular in shape; they could be multiple layers in the vertical section.



7.6 Miscellaneous structures

University of Fort Hare
Together in Excellence

7.6.1 Desiccation cracks (mud cracks)

Mud cracks formed as muddy sediments that dries and contracts (Fig. 7.21). They form largely because of solar radiation. When wet muddy sediments dry out, the removal of water and result in a loss of volume and shrink of sediments. At last, mud cracks will be gradually formed. Formation of mud cracks reveals a very shallow water environment, where wet environment that is drying up.



Fig. 7.21: Mudcracks showing shallow water wet environment became dry up.

7.6.2 Rain drops

Raindrop imprints are a less puzzling structure that can be found on beaches. The surface of fine sediments (silts and mud) is marked by the effects of rain drops after heavy rain event. When the rain soaks into mud, it leaves behind a rounded imprint (pit). Rain imprints are always rounded in shape, and the pits are very shallow (1-3 mm in depth) and near the same size in a group. It can be distinguished with organic borings which are deeper holes and more variable in sizes (Fig. 7.22).



Fig. 7.22: Rain drops causing very shallow pits on the fine mud-silty beach surface resulting from a heavy rain event. They are rounded, very shallow pits (1-3 mm in depth) and distinguishable from biogenic boring holes.

7.7 Summary

Different types of sedimentary structures have been found in the Swartkops estuary and Bluewater beach. The structures generated by aeolian processes include Sand dune, Sand ridge, and High angle cross bedding, Antidune, Straight line ripples, Sinuous line ripples and Aeolian nail marks. The structures produced by wave and tide include Gravel pavement, Interfering ripples, Flat topped ripples, Linguoid marks, Asymmetric sinuous ripples, Rill marks, Swash line, Rill marks, Rhomboid marks, Dendritic wash marks. The structures produced by organisms are Boring, Burrow and Bioturbation; and the Miscellaneous structures include Desiccation cracks and Rain drop prints.

Sedimentary structures are useful tools and good indicators for hydrodynamic energy and sedimentary environment. The ripple marks in the Swartkops estuary and the Bluewater beach are common types of aeolian dunes and shallow marine environment. The beach and estuarine sediments show an agitation water by wave and tide currents, while dune environments show high dune ridges, high dip angle cross-beddings and special antidune structures, representing formation in a strong wind system environment. For wave and tide sediments, most of sedimentary structures are different types of ripple marks and biogenetic structures such as boring, burrow and bioturbation structures formed in shallow marine or estuary environments. In different section of the coastline, the wave/tide energy was different, therefore, gravel pavement, sand beach and muddy flat can be co-existed in an integrated system.

CHAPTER 8: HYDRODYNAMIC ENERGY AND DEPOSITIONAL ENVIRONMENTS

8.1 Introduction

The chemical, physical, and biological processes that occur during the deposition of a specific kind of sediments and the lithification of the resulting rock types are referred to as the depositional environment (Shanmugam, 2006). Environmental analysis is based on environmental-relevant rock and sediment characteristics. Each depositional environment has specific properties that provide essential information about a particular area's geologic features and formation history. Sediments on the earth's surface convey information about the past environment (Balasubramanian and Kalasaiah, 2013). Estuaries are important in linking continent and sea, and are closely related to human activity and living environment, therefore study of estuary is of important significance for economic development and for human living environment. The Swartkops estuarine sediments are very variable in size and shapes, which are linked to variable sub-environments in the coast of the estuary.



8.2 Shallow marine system

University of Fort Hare

Together in Excellence

Swartkops and Bluewater beach are part of a shallow marine system that shows variable energy condition and variable sized sediments. The sedimentary features in the area provide evidence of variable low to high-energy environments, such as mega ripples caused by an excessive storm. The shallow marine deposits in the Swartkops estuary and Bluewater beach areas are dominated by trough and tabular crossbedding, erosional surface, ripple marks, and gravel pavements (Figure 7.3-7.22). These characteristics suggest that the area of study experienced significant marine transgression, and that these structures represent a general transition from fluvial to marine shoreline deposits (Figure 8.1). Estuarine environments face a lot of change in sediment grain sizes and cumulate rates, including the change in freshwater runoff and the raise in sea level. The effects of tides are the ones that dominate the patterns of sedimentation in the Swartkops estuary. The tide shapes the estuary's interior into a series of tidal flats and channels (Clifton, 1982). The centre of the Swartkops estuary, where sediments consist of mud material, whereas in the tidal channels, sediments are coarser, and ripples and mega-ripples can be found. The runoff channels depend on the grain size of the sediments. There is a complex dynamic

interaction between the four groups of sand shoals, channels, mudflat, and marshlands since they are controlled by the motion of freshwater and saline water (de Vriend, 2019). The constructive waves alter beach morphology by causing the movement of sediments up the beach and resulting in steeping the beach profile. Beach morphology is important because the more significant the morphological variability, the more likely the wind velocity retards, and flow variation occurs across the backshore.

8.3 Estuarine environments

8.3.1 Intertidal flats

Intertidal flats are areas where tides or rivers have deposited sediments. Mudflats are wetlands that form in intertidal zones as shown in Figure 8.2. The intertidal flats are found in areas such as estuaries, bays, and lagoon. Swartkops estuary has extensive intertidal flats covering 1.6 km², and the estuary is predominantly sandy and wide intertidal and supratidal areas in the lower estuary. In contrast, it is muddier in the upper estuary and has steep banks (Baird *et al.*, 1988). The mudflats that form in the intertidal area are in the form of mud, resulting from the deposition of estuarine silts and clays. Intertidal flats are flat in shape and contain no features, sandy and muddy areas exposed between tidal levels. They are frequently cut by creeks meandering and partly vegetated on their inner margins to coastal marshes or swamps (Evans, 1982). The intertidal areas with low and high tide marks contain vegetation that lacks mud banks' root to coarse sand flats (Schutte *et al.*, 2019). Evans further discussed that the intertidal flats maybe 10-20 km wide, extended for hundreds of kilometres along the shoreline, and vertical ranges from approximately 17 meters (Evans, 1982).

Evans further suggested that the term "intertidal flats" should be restricted to areas exposed between high and low watermarks of astronomically induced tides and not include those that are flooded by marine waters during abnormal meteorological conditions, for which the suitable applicable be supratidal flat (Evans, 1982). The intertidal flats physical structure ranges from coarse sand beaches on wave-exposed coasts to suitable fine sediments mudflat in estuaries and another inlet marine. Tidal flats in intertidal areas are formed more favorably in a sufficient supply of fine-grained sediments. When the sediment supply of the sediment is cut off, the tidal flats become subjected to shoreline erosion that can damage the zonation set by tides action. Intertidal areas are very dynamic

systems. They are influenced by local energy levels, especially in high-energy sand flat areas that reveal a microstructure controlled by repeated erosion and deposition during the reworking of sediments (Elliot *et al.*, 1998). Estuaries and coastal systems have experienced very significant losses of intertidal flats and marine environments due to diking, irrigation withdrawals, dam construction, and so these effects disrupted the natural flow of water, blocked sediment transport to the river deltas, and that resulted in the loss of intertidal flats (Yang and Wang, 2015). Intertidal flats are important in estuarine circulation, sediment dynamics, water quality, salinity stratification, and intrusion (Yang and Wang, 2015).



Fig. 8.1: The photograph shows the tidal flat of Swartkops Estuary.

8.3.2 Saltmarshes

Saltmarshes are tidal marsh or coastal marsh and coastal ecosystems in the upper coastal intertidal areas between lands and open saltwater flooded by tides. The Swartkops estuary has the third-largest salt marshes along the South African coastline and exhibits various estuarine flora (Colloty *et al.*, 2000). They form mudflats that are raised to the level of an average of high tide. In an estuary, the presence of saltmarshes reduces the tidal amplitudes by creating a frictional drag on surface water and permits water storage on marsh surfaces (Reed *et al.*, 1999). Saltmarshes are depositional areas, and they are likely to store pollutants. Saltmarshes maintain elevation with rising sea levels by trapping the mud and the sand (FitzGerald *et al.*, 2020). Sediments enter the marshes in two ways: through the creek systems and across the marsh front at high stages of the tide (Adnitt *et al.*, 2007). Swartkops estuarine saltmarshes and the Bluewater bay rely on the energy provided by tides and waves that can transport coastal sediments and changing the shape of the landform. The processes of sediment erosion and deposition are managed by the relationship between particle size and the current strength (Adnitt *et al.*, 2007). Vegetation in saltmarshes is one of the transported components for trapping sediments and for wave attenuation. Saltmarshes develop well in favourable conditions where waves and currents are not too strong, and that is essential for mud to settle and seedling to establish (De Groot and Van Duin, 2013). When time passes, the sediments in saltmarshes go through auto compaction, and that is where sediment density increases and increases in flexibility against edge erosion (De Groot and Van Duin, 2013). Sediment destabilization by animals can result in the erosion of saltmarshes. Saltmarshes provide coastal protection because of the stability they present, and they minimize the duration of storm surges. Saltmarshes are very important in flood defence.

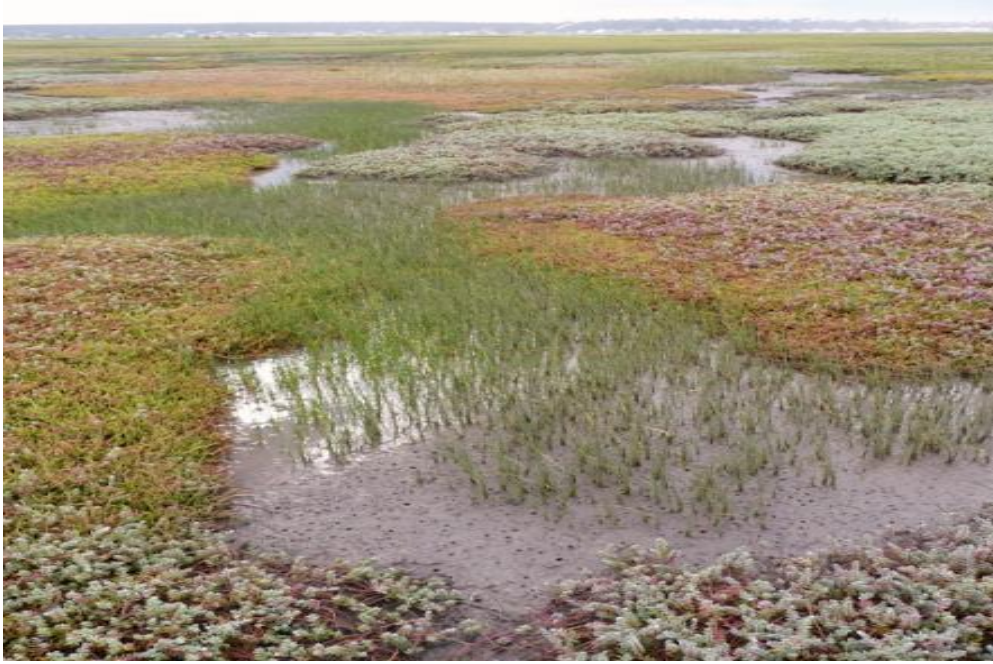


Fig. 8.2: The photograph shows the saltmarshes along the Swartkops estuary.

8.3.3 Tidal channel



Tidal channels are the portion of the stream affected by the ebb and flow of ocean tides. The Swartkops have tidal channels that are vertical and having shallow water, rhombic shapes (Figure 8.3). Along the Bluewater bay beach, the tidal channels have soft sediments with special ripple marks with a flat top, and the channel is deposited with modern conglomerate with quartzite rocks (Fig. 8.4). Different sedimentary facies in tidal channels depend on the depth of a channel and whether or not the flow of tidal waters enters through the channel is free or restricted (Gastaldo and Huc, 1992). Tidal channels of less than 10 m widths in the inside area may be at least 5 m in depth, and ordinary tidal channels may range from up to 7.5 m (Gastaldo and Huc, 1992). Tidal channels have geomorphic features that can be classified into two ways: erosive features that are scours and pools, and depositional features consist of dunes, point bars, and bars (Madricardo *et.al.*, 2020). According to the deposits, tidal environments have channels, and therefore tidal channels are like meandering fluvial systems with a predominance of channel margins and overbank areas (Dalrymple and Choi, 2007).

Many modern tidal environments indicate observations of channel bar systems geomorphology (Dalrymple and Choi, 2007). They have high energy in tidal movement,

and sediments such as coarser-grained to gravel deposits are frequent on the channel floor. Sediments subjected to tidal hydrodynamics are assigned and grouped or classified into specific sedimentary facies, and that is important for recording strong tidal constituents that affect a coastal area (Longhitano *et al.*, 2012). Tidal currents are essential in controlling sediment transport. Sand is found in channels in tide-dominated estuaries; however, silt and clay indicate the tidal flats and deposits of saltmarshes (Lanzoni and Seminara, 2002). Tidal channels are typically meandering, and those results of non-linear interactions between morphology and flow dynamics (Dronkers, 2020). Flood and ebb flow usually follow different estuaries paths that lead to multi-channel systems of flood and ebb dominated channels (Dronkers, 2020).



Fig. 8.3: Tidal channel system showing flooding having shallow water in Swartkops estuary.



Fig. 8.4: Tidal channel system showing runnels and ridges with some ripples marks in Bluewater beach.

University of Fort Hare
Together in Excellence

8.3.4 Floodplain

Floodplain is an area of land close to the stream or an estuary that stretches from the banks to its channels to the base of the enclosing valley walls, which shows flooding during the period of discharge. The Swartkops floodplain is finer with different sediments which depend on water energy. The Swartkops estuary has an extensive floodplain and is partially stratified and with a relatively tidal prism (Allanson, 2001). The Swartkops estuary floodplain in the lower and middle reaches is covered by vegetation, the upper ridges of the Swartkops estuary, the flood supports vegetation that is different from those found in other places in the floodplain (Baird *et al.*, 1986). The Swartkops estuary is identified by flood tide dominant currents for marine and sand deposition (Baird *et al.*, 1986). The development of floodplain constitutes two processes that are erosion and aggradation.

Floodplain erosion describes the process in which the earth disappears gradually by flood movement.

The floodplain deposits can be represented as sediment types that range from clay to gravel size particles, including terrigenous and organic deposits (Aslan, 1978). Fluvial processes and their development form floodplain and nature is necessary to stream power and character of sediments (Nanson and Croke, 1992). Flood plain most important deposits are developed by a process that functions in and near the river channel. These deposits are referred to as accretion deposits that develop in the channel and the vertical accretion deposits. Depositional processes are differentiated according to the energy environment and supply of sediments. The floodplain can represent the eroded and sorted sediments accumulation in sediment sinks which can undergo biogenic for timespan (Lewin, 1978). Floodplain is important; two folds characterize their importance; the floodplain deposits are economically important reservoirs of oil and natural gases; second, the floodplain gives clear, detailed records of past and present processes and continental environments (Aslan, 1978).



Fig. 8.5: Picture shows vegetated floodplain along the Swartkops Estuary.

8.4 Summary

Although certain lagoonal and estuarine habitats are dominated by quiet-water conditions, marginal marine is defined by high-energy waves and currents. The Swartkops estuary has a shallow marine environment and that has been proven for having significant amount of mature clastic sediments along with marine algae as well as skeletal material from animals like shells and corals. Delta, beach, and barrier island, estuarine, lagoonal and tidal flat are the depositional settings in marginal marine environments. The four types of sand shoals, channels, mudflats, and wetlands have a complicated dynamic relationship. Intertidal flats, saltmarshes, tidal channel, floodplain, ebb tidal delta and estuarine silt have been regarded as estuarine depositional sub-environments. The change of deposition rate in estuarine environments is usually higher due to changes in freshwater and sea water fluctuation. The energy level of the estuarine environments can vary significantly, from relatively shallow areas affected by waves and tides to deeper areas only influenced by severe storms.



University of Fort Hare
Together in Excellence

CHAPTER 9: COASTAL EROSION AND MITIGATION

9.1 Introduction

This chapter presents practical applications on coastal and estuarine models in planning for erosion protection against hazardous hydrological forces such as high tides, river floods, and storm surges. Coastal and estuarine floods during dangerous storms can result in coastal and estuarine erosion. Morphodynamic and hydrodynamic modeling processes are important for planners and decision-makers to evaluate the environmental impacts of hazardous hydrological forces controlled by sediment transport, tide, waves, and river floods (Ding *et al.*, 2013). Nordstrom (1989) highlighted that shore protection structures are an essential solution for developed bay beaches than ocean beaches. Strategies can be developed to intensify values that complement and supplement those given out by beaches; therefore, those strategies ought to be designed precisely for bayside location (Nordstrom, 1989).

9.2 Erosion causes

Estuarine erosion is usually caused by moving water, such as waves or currents. In addition to this information taller waves have the power to move sand and other sediments, both offshore, into deeper water along the shoreline (Skrabal and Rogers, 2001). When deposits are in motion, they are redistributed according to weight and grain size (Skrabal and Rogers, 2001). Erosion, even if it is by wind or water, involves three actions: movement, soil detachment, and deposition (Ritter, 2012). Erosion can be a slow process than can happen unnoticed and later occur at an alarming rate. Beaches can experience erosion when there is a reduction in sediment supply from eroding cliffs, reduction of sand supply from inland dunes, increased wave attack, and reduction of fluvial sediments supply to the coast (Baird and Lewis, 2015). Coastal erosion, especially on the sandy coast, can result from many factors such as man-induced activities and interference with coastal structures such as littoral transport that is the most common cause of coastal erosion (Karsten, 2020). Loss of sand at coastal protrusions that is the loss of material from protruding area to one or two sides is a natural cause of coastal erosion, and it normally occurs in sandstone foreland or headland where the currents wash away the fine eroded material and the coarse material is transported alongshore (Karsten, 2020).



University of Fort Hare
Together in Excellence

9.3 Sediment erosion

In the estuarine environment, erosion occurs by eroding shoreline and bottom sediments and beaches (Fig. 9.1). Sediment erosion occurs by the action of waves, tidal currents, deflation, and littoral currents (Elgama, 2016). Comparing the induced tidal currents and the grain size is quite useful in the determination of erosion, erosion direction, and the risk of erosion (Heise *et al.*, 2010). Small changes in fine sediments content, particularly in sands, can have a strong effect on the erosion and sorting of the sediments in the seabed (Garwood *et al.*, 2013). The erosion rate is controlled by the sheer bed strength and the variation depth; therefore, under steady flows, soft, partially consolidated beds; they erode differently than dense, settled beds (Van Leussen and Dronkers, 1988). The general agreement that bottom shear stresses exerted by waves and currents are the dominant forces causing the erosion and that sites specific sediment characteristics that include particle size distribution, density particle, water content, and biological disturbance control resistance of erosion (Sanford and Maa, 2001).



Fig. 9.1 Photograph shows erosion along the Durban coast, South Africa in the 23 April 2019.

9.4 Bank erosion

The Swartkops estuary constitutes a wave-dominated semi-diurnal tide with a vertical range of 1.8 m, with dunes-topped sandy barriers. Significant tides in Swartkops estuary to Bluewater Bay beach are causing erosion, and high tides are causing bank erosion (Fig.

9.2). Factors such as ocean waves, sea level, vegetative state of the dunes, and flood duration are essential. Bank erosion usually takes place in the upper ridges of the estuaries and in rivers. Bank erosion is usually associated with meanders' evolution, as one bank is silting and the opposite bank is eroding. There is no reliable/ distinct formula to estimate the banks' stability (Wolanski and Elliot, 2016). The eroded sediment moves along the topographic gradient towards the channel or in a downstream direction, and banks are characterised by bare sediments, live vegetation, or snags (Roy *et al.*, 2003). Bank erosion supplies coarse sediments to channels; coarse sediments supplied from upstream and stored as a channel makes a substrate important for macro-invertebrates (Florsheim *et al.*, 2008).



Fig. 9.2: The photograph shows a bank erosion along the north part of Swartkops estuary.

9.5 Possible mitigation methods

9.5.1 Shoreline hardening

Shoreline hardening involves the insertion of artificial structures such as large stones or boulders, concrete or steel walls. The Swartkops estuary has a lot of engineering projects for the protection of riverbanks (Figure 9.3). The main function of the shoreline hardening is to protect the landward of the structure. In the case of the environment, structures such as steel walls can result in the interruption of the longshore sand movement. Therefore, the hardening of the shoreline of the eroding beach can result in the beach's loss or disappearance. The best way to minimize the impact and maximize the beach's long period

is to locate the structures as far landward as possible (Skrabal and Rogers, 2001). Protection and safety have been dominant historically and refer to rigid armouring structures such as revetments to protect the existing upland estuarine boundary and preserve dry land (Peterson *et al.*, 2019). The primary environmental concern with engineered hardened shorelines is preventing natural up-slope transgression of saltmarsh and other productive shoreline habitats as sea level rises.



Fig. 9.3: Photograph showing cement hardening for protection of the bank in the Swartkops estuary.

9.5.2 Groins

Groins usually are built perpendicular to the shore (Figure 9.4), and it's a strong structure built from the bank or ocean shore that limits the movement of sediments and cut on water flow. Groins are built from different materials such as stone rubble, wood, sand, and other various materials. Groins are shorter structures built on straight stretches of the beach away from inlets sand intend to trap moving sand in longshore currents (Bush *et al.*, 2001). It should be noticed that when the groin is working correctly, additional or more stones or wood should be piled up on one side of the groin than the other, but the problem with the groin that also needs to be addressed is that they trap sand that is flowing to the adjacent beach (Bush *et al.*, 2001). Therefore, after a groin is built, the increased rate of erosion results on the adjacent beaches, which should be considered (Bush *et al.*, 2001). The groin's length is quite vital for the protection of the beach and can be based on beach width. The

general length is 100 m and the distance between the two groins adjacent usually is two to four times the groin's length, and the flat sandy coast is preferable for three to four times the groin length (Ye, 2017).



Fig.9.4: Photograph showing down drift of wood groin in the coast of Bluewater beach.

University of Fort Hare
Together in Excellence

9.5.3 Revetments

Revetments are stones or concrete structures built adjacent to the shoreline and planned to protect the underlying soil from erosion (Ciarmiello and Di Natale, 2016). The more extensive stone layers are placed on the front-water with smaller layers placed below it, and the latter prevents basal soil washing. Therefore, the main erosion protection is undertaken by the upper stone layers (Ciarmiello and Di Natale, 2016). Revetments can be built to similar heights as sea walls, but revetments have gentle slopes and much larger structural footprints (Figure 9.5). Beach widths are reduced seaward of shore parallel structures such as revetments because of the placement loss that is followed by the occurring effects of coastal processes such as erosion (Dugan *et al.*, 2011). Revetments can be permeable and impermeable; the permeable revetments are built from rock or concrete and timber; the reason is that they reduce the erosive power of waves by making their energy disappear as they are intact with the shore. The impermeable revetments are

sloping defences made of stone or concrete, acting as a fixed-line defence and barrier for high tides and storm surges. Revetments are relatively low maintenance, but the erosion at the structure's base can cause structural failure and disrupt the natural dune process.



Fig. 9.5: Photograph showing revetment with rock boulders (left) and cement blocks (right) along the coast of Bluewater beach.



9.5.4 Vegetation

Planting vegetation is important for coastal erosion because it promotes shoreline stabilization, trapping incoherent sediments, and can reduce wave current energy (Ciarmiello and Di Natale, 2016). Generally, vegetation planting allows reasonable erosion control to be accomplished in low energy environments such as estuarine tidal zone. Shoreline vegetation can be from open and sheltered habitats as bulkheads change a habit and preventing shoreline movement in response to changing sea levels (Dugan *et al.*, 2011). Coastal dunes act as a safeguard against coastal hazards such as wind, wave overtopping, and tidal inundation. For that reason, the costal vegetation is important for the protection of the beach (Figure 9.6). Storm tides and waves change the shore profile, and these can cause periodic erosion that can be followed by natural recovery. Wetland vegetation, especially along the estuaries, plays an important role in protecting water quality by trapping sediments and taking nutrients and prevents erosion by stabilizing the shoreline by absorbing wave energy, trapping sediments, slowing stormwater runoff, and moderating storm the effects of storm floods.



Fig. 9.6: Photograph showing vegetation controlling for coastal erosion.

9.5.5 Vertical walls



The vertical walls are there to retain the soil behind it during storm waves. Vertical walls can be called by various names, such as sea walls, bulkheads, or retaining walls. The vertical walls are designated not by the presence of waves but for maintaining the soil's weight and additional groundwater trapped landward of the structure (Skrabal and Rogers, 2001). These structures are generally massive concrete structures placed along the stretch of the shoreline at the beaches. The walls must be implanted or inserted deep enough to stop the structure's toe from being pushed waterward when eroded by waves as shown in figure 9.7. Since the vertical walls are made to hold up the soil's weight rather than to resist the waves, then even small losses of backfill can lead to collapse (Skrabal and Rogers, 2001). The vertical wall can cause unpleasant environmental impacts. Structures must be strong on account of the high wave loading and, for that reason, are needed to be strong massive structures or better suited to low- to medium wave environments where the wave loading is moderate (Shand and Blacka, 2017).



Fig. 9.7: Photograph showing vertical wall for protection of wave erosion in the coast.

9.5.6 Bulkheads

Bulkheads are vertical, shore-anchored obstacles built along the shoreline to prevent erosion. Bulkheads can be made of wood, concrete, vinyl, or steel, and they can be freestanding or supported by a series of tiebacks (Fig 9.8). Bulkheads, when properly designed and built, can significantly limit or even eliminate shoreline retreat at a site (Benoit and Roberts, 2007). The scour caused by reflected waves will raise the water level at the bulkhead's base. As a result, riprap such as stone or other riprap is frequently used at the toe to absorb some of the wave force. When a bulkhead is built along the shoreline, the region landward of the bulkhead is usually filled in, and the marsh or beach is converted to uplands (Benoit and Roberts, 2007).



Fig. 9.8: Photograph showing bulkhead to protect bank erosion and slope failure.

9.5.7 Breakwater

Breakwaters consist of a single structure or a series of units placed offshore of the project site to reduce wave action on the shoreline. When correctly built and constructed, rock is commonly utilized in construction and has shown to be quite durable. Some breakwaters run parallel to the shoreline and are built of rock, stone or concrete. They limit long-shore drift, which prevents sediment movement and erosion along the shoreline. Breakwaters are simple to maintain. Shore and bank are well-protected with the structure (Fig. 9.9).

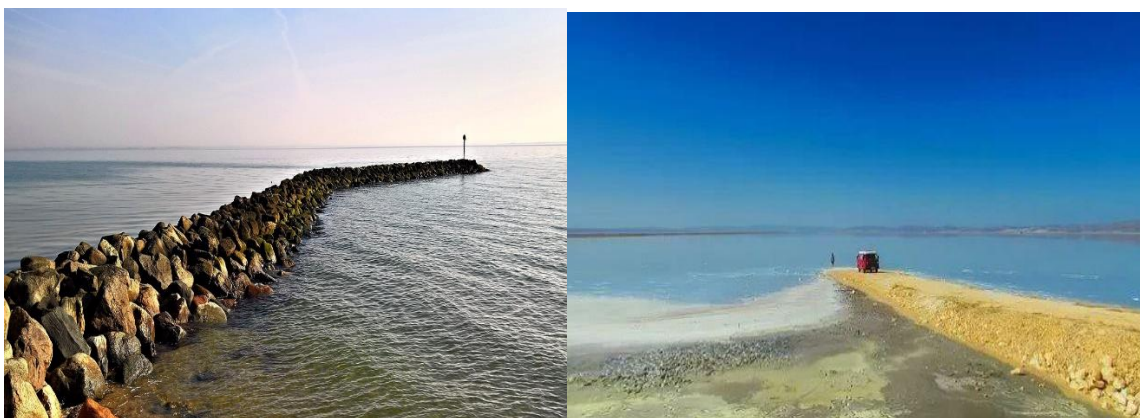


Fig 9.9: Photograph showing breakwaters built by rocks (left) or mud-rock mixture (right).

9.6 Summery

Globally, rising sea levels have had a significant impact on the coastal erosion. Abrasion is very prevalent in the regions where there are strong winds, fast currents and high waves. Loose sands, soft rocks and weak beds are all factors affecting erosion. Since wave, tide and river current are all interactative in the coastal zone in beach and estuary, morphology change and erosion are the routine phenomena in the coast environment.

In the case of Swartkops estuary, flooding and erosion could cause serious influence on the landscape stability, property safety and industrial development. Therefore, mitigating the coastal erosion is a major task for economic development in South Africa. In this study, we proposed some mitigation methods to local gorvenment, such as Shoreline hardening, Groin, Revetment, Vegetation, Vertical well, Bulkhead, Sills and Breakwater are the potential way to prevent erosion. Local government encourages this research and had used some of methods in the environment protection.



University of Fort Hare
Together in Excellence

CHAPTER 10 DISCUSSION AND CONCLUSION

The study has provided new insights and detailed information for the Swartkops estuary and coastal erosion protection. Through this study, the following discussion and conclusion were drawn:-

Through literature review, field trips and the study on the collected samples, we have improved the knowledge and understanding of the Swartkops estuary. According to the Wentworth scale, the sediment sample collected in the estuary indicates a fairly consistent grain size, fine to medium of arenaceous sands. Grain size analyses were very useful for determining the depositional environment and hydrodynamic conditions as well as the transporting mechanism and current energy conditions. The grain size distribution is ranged from -1 to 5 phi, with predominant size at 3 Phi (0.125 mm) that are regarded as well sorted. The Bluewater beach sediments in the estuary shows that the sediments are fine grained with an average size of 2.57 phi, the sorting that has an average of 0.41 indicating well sorted, the skewness of an average of 0.13 showing the strongly coarse skewed for these samples, and the kurtosis of an average 0.87 indicating the platykurtic nature. The Swartkops channel grain size-parameters shows that most sediment are dominated by fine-grained sediments with an average value of 2.25, moderately well sorted (0.77), leptokurtic to very leptokurtic (1.60), and the skewness of an average of -0.2 that shows a strongly coarse skewed. The fine grained sediments reveal that the energy of transporting medium was low and constant (Nelson, 2015; Folk, 1974). Grain size parameters for channel sediments shows an average mean of 2.32 suggesting that the tidal channel is dominated by fine grained sands, the sorting coefficient with an average of 0.73 showing that the area is dominated by moderately sorted sediments. The kurtosis has an average of 1.49 indicating leptokurtic in nature, and the skewness average of -0.43 indicating that the tidal channel of grain size distribution is near symmetrical.

The bivariate scatter plots of grain size parameters have been widely used to interpret the deposition mechanism, energy conditions and transportation medium. The histograms and cumulative frequency reveal a unimodal grain size distribution for most of the beach and estuarine sediments, but there are few bimodal grain size distributions in the estuarine

sediments. The cumulative frequency diagrams show well sorted beach sediments, compared the estuarine sediments with some poorly sorted samples. The bivariate plots show that the mean versus sorting have a negative relationship indicating that the fine-grained sediments are well sorted compared to coarse-grained sediments. The bivariate plot between mean versus skewness shows a slightly positive relationship which implies a fluvial environment in affection. The skewness versus kurtosis shows that sediments in the Swartkops channel and the Bluewater beach lie within negatively skewed, which shows that most sediments are from the beach environment. The relationship between kurtosis and the mean shows a slightly positive relationship results from less sorting in coarse sediments. The relationship between sorting and skewness shows a negative relationship which can help to distinguish between the beach and river sands (Okeyode and Jibiri, 2012). The bivariate plot of sorting versus kurtosis shows a positive relationship which means that the sorting increases, the kurtosis gets wider. Thus bivariate plots can be used to distinguish fluvial and marine originated sediments in the study area.

The Swartkops estuary and the Bluewater beach constitute of similar mineral compositions. Quartz, calcite, feldspar and lithic fragments are the most abundant minerals in the study area. Quartz is the most dominant mineral in all the samples observed under microscope thin sections. The lithic fragments are classified as quarzitic, shale, sandstone and siltstone, with carbonate minerals coming from marine organisms, such as shells and corals. Glauconite, foraminifera, sponge and organic pellets are present in a small amount, they were obtained from marine source.

The scanning electron microscope reveals the sediments' properties and their textures, showing different types of micro-textures that include V-shaped pits resulting from mechanical crushing during transportation; upturn plates due to collision and corrosion; dissolution pits resulting from chemical solution; secondary mineral precipitation of silica, calcite, salt and clay due to precipitation and recrystallization; boring and burrow resulting from organism activities. These micro-textures are good indicators of water energy and sedimentary environment.

Numerous well-developed sedimentary structures have been found in the Swartkops estuary and the Bluewater beach. The structures generated by aeolian processes include Sand dune, Sand ridge, High angle cross bedding, Antidune, Straight line ripples, Sinuous line ripples and Aeolian nail marks. The structures produced by wave and tide include

Gravel pavement, Interfering ripples, Flat topped ripples, Linguoid marks, Asymmetric sinuous ripples, Rill marks, Swash line, Rill marks, Rhomboid marks, Dendritic wash marks. The structures produced by organisms are Boring, Burrow and Bioturbation; and the Miscellaneous structures include Desiccation cracks and Rain drop prints. Most of the structures were formed in the lower flow regime, such as different types of ripples and cross-beddings. Some of structures were formed in the upper flow regime, such as antidune cross bedding and gravel pavement. Some of structures are the first time reported by the author, such as high angle cross-bedding, antidune, aeolian nail marks, rill marks and rhomboid marks. These sedimentary structures are essential for interpreting hydrodynamic energy and depositional environments. The results of biological, physical and chemical processes during deposition prove the stratigraphic record.

Hydrodynamics and the depositional environment of the estuaries and beaches describe the chemical, physical, and biological processes associated with the deposition of certain sediments. Estuarine environments constitute intertidal flats, salt marshes, tidal channels, floodplains, and ebb-tidal delta. The Bluewater beach consists of pebbles that are well rounded, and these pebbles indicates a shallow marine environment in an upper-flow regime of hydrodynamic condition.

Estuarine erosion is primarily caused by the movement of water, such as wave and tide currents. Erosion can start slow unnoticed and later occur at an alarming rate. The migration of a conspicuous sandbank in the main river channel near Swartkops village is controlled by ebb river flood currents (Esterhysen and Rust, 1987). Fluvial floods and estuarine currents have steadily eroded the southern channel bank (cut-bank) of the meander stream situated downstream of the Swartkops village (Esterhysen and Rust, 1987). Erosion of the cut bank and deposition on the point bars in gradual lateral and downstream shift of the channel. Coastlines are affected by storms, floods, and other natural events that cause erosion which can be the storm surge at high tide with strong waves that can create the most damaging conditions. The sea-level rise is the severity of the problems that cause erosion and damage of properties. Beach nourishment is an important strategy to deal with coastal erosion, such as placing the buffer against the erosion. The engineering projects play a vital role in stabilising the river bank and coastline. Mitigation projects to protect erosion include shoreline hardening, groins, revetments, vegetation planting, vertical wells, bulkheads and breakwaters.

Recommendations

To develop additional ways to rehabilitate coastal erosion and find other causes of coastal erosion, more research on the environmental geology and sedimentology of the Swartkops estuary is needed.



University of Fort Hare
Together in Excellence

REFERENCES

- Abdel-Fattah, Z.A., 2019.** Morpho-sedimentary characteristics and generated primary sedimentary structures on the modern microtidal sandy coast of eastern Nile Delta, Egypt. *Journal of African Earth Sciences*, 150, pp.355-378.
- Adnitt, C., Brew. D., Cottle. R., Hardwick, M., John, S., Leggett, D., McNulty, S., Meakins, N., and Stainland, R., 2007.** Joint Defra / Environment Agency Flood and Coastal Erosion Risk Management R&D Programme. Saltmarsh management manual. R&D Technical Report SC030220 Product Code: SCHO0307BMKH-E-P.
- Ahr, W.M., 2011.** Geology of Carbonate Reservoirs: The Identification, Description and characterisation of hydrocarbon reservoirs in carbonate rocks. John Wiley and Sons.
- Alanson, B., 1999.** Estuaries of South Africa. Cambridge University, version 2008, vol 2, 666pp.
- Allanson, B., and Baird, D., 2008.** Estuaries of South Africa, A broad-ranging review of the current status of South Africa's estuarine research and management. pp.5-27.
- Allanson, B.R., 2001.** Some factors governing the water quality of microtidal estuaries in South Africa. *Water SA*, 27(3), pp.373-386.
- Andrew, J and Cooper, G., 1993.** Sedimentation in the cliff-bound, microtidal Mtamvuna Estuary, South Africa, *Marine Geology*, Volume 112, Issues 1–4, pp. 237-256.
- Andus, S., Tubić, B., Ilić. M., Đuknić, J., Gačić, Z., and Paunović, M., 2016.** Freshwater sponges–skeletal structure analysis using Light Microscopy and Scanning Electron Microscopy. *Water Research and Management* 6, pp.15-17.
- Aslan, A., 1978.** Floodplain sediments. In: Middleton G.V., Church M.J., Coniglio M., Hardie L.A., Longstaffe F.J. (eds) *Encyclopedia of Sediments and Sedimentary Rocks*. Encyclopedia of Earth Sciences Series. Springer, Dordrecht.
- Assallay, A.M., Rogers, C.D.F., Smalley, I.J. and Jefferson, I.F., 1998.** Silt: 2–62 μm , 9–4 ϕ . *Earth-Science Reviews*, 45(1-2), 61-88.

Avramidis P., Samiotis A., Kalimani E., Papoulis D., Lampropoulou P., Bekiari V., 2012. Sediment characteristics and water physicochemical parameters of the Lysimachia Lake, Western Greece, *Environ Earth Sci.*, 70 (1): 383-392.

Azhikodan, G., and Yokoyama, K., 2018. Sediment transport and fluid mud layer formation in the macro-tidal Chikugo river estuary during a fortnightly tidal cycle. *Estuarine, Coastal and Shelf Science*, 202, 232-245.

Baas, J.H., 1994. A flume study on the development and equilibrium morphology of current ripples in very fine sand. *Sedimentology*, 41(2), 185-209.

Baird, D., Hanekom, N.M. and Grindley, J.R., 1986. Report No. 23: Swartkops (CSE 3). In: *Estuaries of the Cape. Part 2. Synopses of available information on individual systems.* (Eds.) Heydorn, A.E.F. and Grindley, J.R. CSIR Research report No, 422: 82 pp.

Baird, D., Marais, J.F.K. and Martin, A.P., 1988. The Swartkops estuary. Unpublished report.

Balasubramanian, A., and Kalasaiah, M., 2013. Depositional Environments. 10.13140/RG.2.2.29422.61767.



Baiyegunhi, Christopher, Liu, Kuiwu and Gwavava, Oswald. "Grain size statistics and depositional pattern of the Ecca Group sandstones, Karoo Supergroup in the Eastern Cape Province, South Africa" *Open Geosciences*, vol. 9, no. 1, 2017, pp. 554-576. <https://doi.org/10.1515/geo-2017-0042>

Beck, J.S., 2005. Sediment transport dynamics in South African estuaries. Doctoral dissertation, Stellenbosch: University of Stellenbosch. 226pp.

Bell, R., Green, M., Hume, T. and Gorman, R., 2000. What regulates sedimentation in estuaries. *Water Atmos*, 8(4), 13-16.

Bhattacharya, R.K., Chatterjee, N.D. and Dolui, G., 2016. Grain size characterization of in stream sand deposition in controlled environment in river Kangsabati, West Bengal. *Modeling Earth Systems and Environment*, 2 (3), 118pp.

Benoit, J. and Roberts, S., 2007. The national academies report on mitigating shore erosion along sheltered coasts. In *Coastal Sediments' 07*, 1601-1608.

Binning, K. and Baird, D., 2001. Survey of heavy metals in the sediments of the Swartkops River Estuary, Port Elizabeth South Africa. *Water S.A.*, 27: 461-466.

Bird, E., and Lewis, N., 2015. Causes of beach erosion. In *Beach Renourishment* (pp. 7-28). Springer, Cham.

Blair, T.C., and McPherson, J., 1999. Grain-size and textural classification of coarse sedimentary particles, *Journal of Sedimentary Research*, VL - 69, pp. 6-19. DOI - 10.2110/jsr.69.6.

Blott, S. J., and Pye, K., 2001. GRADSTAT: A grain size distribution and statistics, Package for the analysis of unconsolidated sediments. *Earth surfaces processes and landforms*, 26: 1237-1248.

Bourgeois, J., 1982. Tanguet. In: *Beaches and Coastal Geology*. Encyclopedia of Earth Sciences Series. Springer, New York, NY. https://doi.org/10.1007/0-387-30843-1_453.

Bovi, R.C., Silva, L.F.S.D., Zenero, M.D.O., Carvalho, C.C.D. and Cooper, M., 2017. Sediment morphology, distribution, and recent transport dynamics in a reforested fragment. *Revista Brasileira de Ciência do Solo*, 41.

Braat, L., Leuven, J.R., Lokhorst, I.R. and Kleinhans, M.G., 2019. Effects of estuarine mudflat formation on tidal prism and large-scale morphology in experiments. *Earth Surface Processes and Landforms*, 44(2), pp.417-432.

Braat, L., van Kessel, T., Leuven Jasper, R.F.W., and Kleinhans, M.G., 2017. Effects of mud supply on large-scale estuary morphology and development over centuries to millennia, *Earth Science Dynamics*, vol 5, pp. 617-652. <https://doi.org/10.5194/esurf-5-617-2017>.

Bremner J. M., 1991. The bathymetry of Algoa Bay. In: *Algoa Bay-Marine Geoscientific Investigations*, Bremner JM, Du Plessis A, Glass JGK, Day RW (ed). Bulletin of the Geological Survey South Africa 100, Pretoria, Government Printer, 3-18.

Brenninkmeyer, B.M., 1982. Rill marks. In: *Beaches and Coastal Geology*. Encyclopedia of Earth Sciences Series. Springer, New York, NY. https://doi.org/10.1007/0-387-30843-1_372.

Brooks, G.R., Doyle, L.J., Davis, R.A., DeWitt, N.T. and Suthard, B.C., 2003. Patterns and controls of surface sediment distribution: west-central Florida inner shelf. *Marine Geology*, 200(1-4), 307-324.

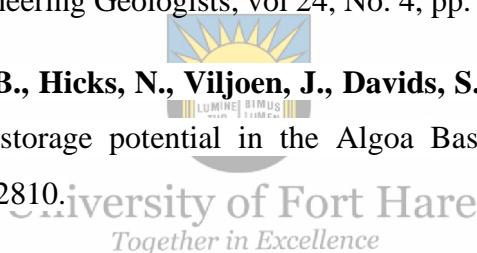
Bush, D.M., Pilkey, O.H., and Neal, W.J., 2001. Coastal Topography, Human Impact on*, Editor(s): John H. Steele, *Encyclopedia of Ocean Sciences* (Second Edition), Academic Press, pp. 581-590, <https://doi.org/10.1016/B978-012374473-9.00078-3>.

Cadée, G.C., 2001. Sediment dynamics by bioturbating organisms. In *Ecological comparisons of sedimentary shores* (pp. 127-148). Springer, Berlin, Heidelberg.

Cadigan, R.A., 1961. Geological interpretation of grain size distribution measurements of Colorado Plateau Sedimentary Rocks, *The Journal of Geology*, Vol. 69, No. 2, (pp. 121-144). <https://doi.org/10.1086/626724>.

Carter, G. Neal., 1987. Geology of Port Elizabeth Republic of south Africa. *Bulletin of the association of Engineering Geologists*, vol 24, No. 4, pp. 441-467.

Chabangu, N., Beck, B., Hicks, N., Viljoen, J., Davids, S. and Cloete, M., 2014. The investigation of CO₂ storage potential in the Algoa Basin in South Africa. *Energy Procedia*, 63, pp.2800-2810.



China, Q. and Polina, L., 2018. Sediment Particle Size Analysis: Report on Grain Size Experiment.

Choiniere, J., 2016. 35th International geological congress, PRE 9: Early Cretaceous Basins along the Southern Cape Coast, Cape Town, South Africa.

Ciarmiello, M., Di Natale, M., 2016. Coastal Erosion Control. In: Kennish M.J. (eds) *Encyclopaedia of Estuaries*. *Encyclopedia of Earth Sciences Series*. Springer, Dordrecht. https://doi.org/10.1007/978-94-017-8801-4_386

Clifton, E.H., 1982. “Estuarine Deposits”, *Sandstone Depositional Environments*, Peter A. Scholle, Darwin Spearing.

Clifton, H.E., 2005. Coastal Sedimentary Facies. In: Schwartz M.L. (eds) *Encyclopedia of Coastal Science*. *Encyclopedia of Earth Science Series*. Springer, Dordrecht. https://doi.org/10.1007/1-4020-3880-1_84.

Colloty, G.C. and Adams, J.B., 2000. The use of a botanical importance rating to assess changes in the flora of the Swartkops Estuary over time. *Water SA*, 26(2), pp.171-180.

Cooper, J.A.G., 2001. Geomorphological variability among microtidal estuaries from the wave-dominated South African coast, *Geomorphology*, Volume 40, Issues 1–2, pp. 99-122.

Corbett, D.R., Walsh, J.P., Riggs, S.R., Ames, D.V. and Culver, S.J., 2008. Shoreline change within the Albemarle-Pamlico estuarine System, North Carolina.

Costa, P.J.M., 2016. Sediment Transport. In: Kennish M.J. (eds) *Encyclopedia of Estuaries*. Encyclopedia of Earth Sciences Series. Springer, Dordrecht.

https://doi.org/10.1007/978-94-017-8801-4_187

Cowart, L., 2009. Analysing Estuarine Shoreline Change in Coastal North Carolina, Department of geological science, A Thesis presented to the Faculty of the Department of Geological Sciences East Carolina University.

Coyne, A., Gorse, L., Curti, C., Schafer, J., Grosbois, C., Morelli, G., Ducassou, E., Blanc, G., Maillet, G.M. and Mojtahid, M., 2016. Spatial distribution of trace elements in the surface sediments of a major European estuary (Loire Estuary, France): Source identification and evaluation of anthropogenic contribution. *Journal of Sea Research*, 118, pp.77-91.

Dalrymple, R.W. and Choi, K., 2007. Morphologic and facies trends through the fluvial–marine transition in tide-dominated depositional systems: a schematic framework for environmental and sequence-stratigraphic interpretation. *Earth-Science Reviews*, 81(3-4), pp.135-174.

Das, G.K., 2016. Sediment Grain Size. In: Kennish M.J. (eds) *Encyclopaedia of Estuaries*. Encyclopaedia of Earth Sciences Series. Springer, Dordrecht. https://doi.org/10.1007/978-94-017-8801-4_148.

Das, G.K., 2017. Bioturbation structures. In *Tidal Sedimentation of the Sunderban's Thakuran Basin* (pp. 123-140). Springer, Cham.

De Groot, A.V. and Van Duin, W.E., 2013. Best practices for creating new salt marshes in a saline estuarine setting, a literature study (No. C145/12). IMARES.

de Mahiques, M.M., (2016). Sediment Sorting. In: Kennish M.J. (eds) Encyclopaedia of Estuaries. Encyclopaedia of Earth Sciences Series. Springer, Dordrecht. https://doi.org/10.1007/978-94-017-8801-4_348.

De Vriend. H., 2019. Estuarine morphological modelling. Available from http://www.coastalwiki.org/wiki/Estuarine_morphological_modelling.

Desjardins, P.R., Buatois, A.L., and Mangano, G.M., 2012. Chapter 18 - Tidal Flats and Subtidal Sand Bodies, Editor(s): Dirk Knaust, Richard G. Bromley, Developments in Sedimentology, Elsevier, Volume 64, pp. 529- 561. <https://doi.org/10.1016/B978-0-444-53813-0.00018-6>.

Ding, Y., Kuiry, S.N., Elgohry, M., Jia, Y., Altinakar, M.S., and Ken-Chia, Y., 2013. Impact assessment of sea-level rise and hazardous storms on coasts and estuaries using integrated processes model, Ocean Engineering, Volume 71, pp. 74-95, <https://doi.org/10.1016/j.oceaneng.2013.01.015>.

Douglas, E.J., Lohrer, A.M. and Pilditch, C.A., 2019. Biodiversity breakpoints along stress gradients in estuaries and associated shifts in ecosystem interactions. Scientific reports, 9(1), pp.1-11.

Dronkers, J. and van Leussen, W. eds., 2012. Physical processes in estuaries. Springer Science & Business Media.

Dronkers, J., 1986. Tidal asymmetry and estuarine morphology. Netherlands Journal of Sea Research, 20(2-3), pp.117-131.

Dronkers, J., and van den Berg. J., 2019. Coastal and marine sediments. Available from http://www.coastalwiki.org/wiki/Coastal_and_marine_sediments.

Drury, M.R., and Urai, J.L., 1990. Deformation-related recrystallization processes, Tectonophysics, Volume 172, Issues 3–4, pp.235-253, [https://doi.org/10.1016/0040-1951\(90\)90033-5](https://doi.org/10.1016/0040-1951(90)90033-5).

Dugan, J.E., Airoidi, L., Chapman, M.G., Walker, S.J., Schlacher, T., Wolanski, E. and McLusky, D., 2011. 8.02-Estuarine and coastal structures: environmental effects, a focus on shore and nearshore structures. *Treatise on estuarine and coastal science*, 8, pp.17-41.

Duvat, V., 2009. Beach erosion management in Small Island Developing States: Indian Ocean case studies. Department of Geography, Institute of Littoral and Environment, La Rochelle University, France, *WIT Transactions on Ecology and the Environment*, Vol 126, pp.149-160. Doi: 10.2495/CP090141.

Dyer, K.R., 1995. Sediment transport processes in estuaries. In *Developments in Sedimentology* (Vol. 53, pp. 423-449). Elsevier.

East, H., 2004. Estuary Sedimentation: a review of estuarine sedimentation in the Waikato region.

Elfrink, B. and Baldock, T., 2002. Hydrodynamics and sediment transport in the swash zone: a review and perspectives. *Coastal Engineering*, 45(3-4), pp.149-167.

Elgama, A.A., 2016. Sediment Erosion. In: Kennish M.J. (eds) *Encyclopedia of Estuaries. Encyclopedia of Earth Sciences Series*. Springer, Dordrecht.

Eliot, M., 2016. Coastal sediments, beaches and other soft shores. *Coast adapt information manual*, 8.

Elliott, M., Nedwell, S., Jones, N.V., Read, S.J., Cutts, N.D. and Hemingway, K.L., 1998. Intertidal sand and mudflats & subtidal mobile sandbanks (volume II). An overview of dynamic and sensitivity characteristics for conservation management of marine SACs. Scottish Association for Marine Science (UK Marine SACs Project), p.151.

Esterhuysen, K., and Rust, L.E., 1987. Channel migration in the lower Swartkops estuary. *South African Journal of Science*. Vol.83, pp. 521-525.

Evans, G., 1982. Intertidal flats. In: *Beaches and Coastal Geology. Encyclopaedia of Earth Science*. Springer, Boston, MA. https://doi.org/10.1007/0-387-30843-1_241

Ferreira, M.G.A., and Santos, S.N.C., 2017. Sedimentation and erosion in harbour estuaries, Open access peer-reviewed chapter. DOI:10.5772/intechopen.74049.

Fiket, Z., Pikelj, k., Ivanić, M., Barišić, D., Vdović, N., Dautović, J., Gobac, Z., Mikac, N., Bermanec, V., Sondi, I., and Kniewald, G., 2017.Origin and composition of sediments in a highly stratified karstic estuary: An example of the Zrmanja River estuary (eastern Adriatic),*Regional Studies in Marine Science*, Volume 16, pp. 67-68.
<https://doi.org/10.1016/j.rsma.2017.08.001>.

FitzGerald, D.M., Hughes, Z.J., Georgiou, I.Y., Black, S. and Novak, A., 2020.Enhanced, Climate-Driven Sedimentation on Salt Marshes. *Geophysical Research Letters*, 47(10), p.e2019GL086737.

Florsheim, J.L., Mount, J.F. and Chin, A., 2008. Bank erosion as a desirable attribute of rivers. *BioScience*, 58(6), pp.519-529.

Folk, R.L., 1966. A Review of Grain-size Parameters. *The Journal of International Association of Sedimentologists*. University of Texas, Austin, Texas (U.S.A.), 6(2).

Folk, R.L. and Ward W.C., 1957. Brazos River bar: a study in the significance of grain size parameters *J. Sediment. Petrol.*, 27: 3-26.

Folk, R.L., 1974. Petrology of sedimentary rocks: Hemphill Publishing Company, Austin TX, 182.



Fontes R.F.C., Miranda L.B., Andutta F., 2016. Estuarine Circulation. In: Kennish M.J. (eds) *Encyclopedia of Estuaries*. *Encyclopedia of Earth Sciences Series*. Springer, Dordrecht. https://doi.org/10.1007/978-94-017-8801-4_176.

Fourriere, A., Claudin, P., and Andreotti, B., 2009. Bedforms in a turbulent stream: formation of ripples by primary linear instability and of dunes by nonlinear pattern coarsening. *Journal of fluid mechanics*. vol. 649, pp. 287–328.

Friedman, G. M., 1961b. Distinction between dune, beach and river sands from textural characteristics. *Jour. Sed. Petrology*, 31, pp. 514-529.

Friedman, G.M, and Sanders, J.E., 1978. Principles of Sedimentology. Wiley, New York, 792 pp.

Friedman, G.M., 1967. Dynamic processes and statistical parameters compared for size frequency distribution of beach river sands. *Journal of Sedimentary Petrology*, 37, pp. 327-354.

Friedman, G.M., 1979. Differences in size distribution of populations of particles among sands of various origins, *Sedimentology*, 26: 859-862.

Frost, S., 1996. Early Cretaceous alluvial palaeosols (Kirkwood Formation, Algoa Basin, South Africa) and their palaeoenvironmental and palaeoclimatological significance (Doctoral dissertation, Rhodes University).

Garwood, J.C., Hill, P.S. and Law, B.A., 2013. Biofilms and size sorting of fine sediment during erosion in intertidal sands. *Estuaries and coasts*, 36(5), pp.1024-1036.

Gastaldo, R.A. and Huc, A.Y., 1992. Sediment facies, depositional environments, and distribution of phytoclasts in the Recent Mahakam River delta, Kalimantan, Indonesia. *Palaaios*, 7(6), pp.574-590.

Geyer, W.R. and Ralston, D.K., 2015. Estuarine frontogenesis. *Journal of Physical Oceanography*, 45(2), pp.546-561.



Goodwin, L., 2007. Evaluating the Impacts of Environmental Parameters on Shoreline Erosion and Related Aspects: Assessing the Current Status of Vegetation, Sediments, and Biota (Doctoral dissertation, Graduate School of the College of Charleston).

Goschen, W.S. and Schumann, E.H., 2011. The physical oceanographic processes of Algoa Bay, with emphasis on the western coastal region. *South African Environmental Observation Network (SAEON) and the Institute of Maritime Technology (IMT). IMT document number: PO106-10000-730002*, pp.1-84.

Goschen, W.S., and Schumann, E.H. 1988. Ocean current and temperature structure in Algoa Bay and beyond in November 1986. *South African Journal Marine Science*, 7:101-116.

Gough, A., 2021. Sedimentary structures, *Encyclopaedia of Geology (Second Edition)*, Academic Press, pp. 787-808.

Gradus, Y. ed., 2012. Desert development: Man and technology in sparselands. Vol. 4. Springer Science & Business Media.

Grasso, F. and Le Hir, P., 2019. Influence of morphological changes on suspended sediment dynamics in a macrotidal estuary: diachronic analysis in the Seine Estuary (France) from 1960 to 2010. *Ocean Dynamics*, 69(1), pp.83-100.

Greenwood B., 1982. Sand, surface texture. In: Beaches and Coastal Geology. Encyclopedia of Earth Sciences Series. Springer, New York, NY. https://doi.org/10.1007/0-387-30843-1_387.

Haldar, S.K., 2020. Introduction to mineralogy and petrology. Elsevier.

Hardaway, C.S., Milligan, D.A., Varnell, L., 2016. Estuarine Beaches. In: Kennish M.J. (eds) Encyclopedia of Estuaries. Encyclopedia of Earth Sciences Series. Springer, Dordrecht.

Hattingh, J. and Fourie, C., 2010. Eskom Thyspunt Transmission Line Integration Project EIA: Geo-Technical Specialist Report. Creo Design (PTY) LTD.

Heise, B., Harff, J., Ren, J. and Liang, K., 2010. Patterns of potential sediment erosion in the Pearl River Estuary. *Journal of Marine Systems*, 82, pp.S62-S82.

Hesp, P., 2011. Dune Coasts, Treatise on Estuarine and Coastal Science, VL - 3, pp. 193-221. DO - 10.1016/B978-0-12-374711-2.00310-7.

Hicks, D.M. and Hume, T.M., 1996. Morphology and size of ebb tidal deltas at natural inlets on open-sea and pocket-bay coasts, North Island, New Zealand. *Journal of coastal research*, pp.47-63.

HKS-Hill, Kaplan, Scott and Partners. 1974. Environmental study, Swartkops River basin. Port Elizabeth City Engineer, Port Elizabeth. Technical Data Report published by the Port Elizabeth City Engineer. Hydrology, hydraulics. Part 2, 51-24.

Hopley, D., 2011. Encyclopedia of modern coral reefs: structure, form and process. Springer.

Hoyt, J.H. and Henry, V.J., 1963. Rhomboid ripple mark, indicator of current direction and environment. *Journal of Sedimentary Research*, 33(3), pp.604-608.

Hughes, M., 2016. Climate change impacts on beaches and estuary sediments. *Coast Adapt Impact Sheet 1*, National Climate Change Adaptation Research Facility, Gold Coast.

Hunt, S. and Jones, H.F., 2019. Sediment grain size measurements are affected by site-specific sediment characteristics and analysis methods: implications for environmental monitoring. *New Zealand Journal of Marine and Freshwater Research*, 53(2), pp.244-257.

Itamiya, H., Sugita, R., and Sugai, T., 2019. Analysis of the surface microtextures and morphologies of beach quartz grains in Japan and implications for provenance research. *Prog Earth Planet Sci* 6, 43. <https://doi.org/10.1186/s40645-019-0287-9>.

Joan L. Florsheim, Jeffrey F. Mount, Anne Chin, 2008. Bank Erosion as a Desirable Attribute of Rivers, *Bioscience*, Volume 58, Issue 6, pp.519–529.

Johnsson, M.J. and Basu, A., 1993. The system controlling the composition of clastic sediments. *Special Papers-Geological society of america*, pp.1-1.

Karsten, M., 2020. Natural causes of coastal erosion.

Kashif, M., Cao, Y., Yuan, G., Asif, M., Javed, K., Mendez, J.N., Khan, D., and Miruo, L., 2019. Pore size distribution, their geometry and connectivity in deeply buried Paleogene Es1 sandstone reservoir, Nanpu Sag, East China. *Pet. Sci.* **16**, 981–1000.

Kennett, J.P. and Srinivasan, M.S. (1983). Neogene planktonic foraminifera: a phylogenetic atlas. Hutchinson Ross.

Kennish, M.J., 1986. Ecology of estuaries. v. 1: Physical and chemical aspects.-v. 2: Biological aspects.

Knight, J. and Burningham, H., 2014. A paraglacial coastal gravel structure: Connell's Bank, NW Ireland. *Journal of Coastal Research*, (70), pp.121-126.

Kowalewska-Kalkowska H., Marks R., 2015. Estuary, Estuarine Hydrodynamics. In: Harff J., Meschede M., Petersen S., Thiede J. (eds) Encyclopedia of Marine Geosciences. Springer, Dordrecht. https://doi.org/10.1007/978-94-007-6644-0_164-1.

Kuang, C., Liang, H., Gu, J., Su, T., Zhao, X., Song, H., Ma, Y. and Dong, Z., 2017. Morphological process of a restored estuary downstream of a tidal barrier. Ocean & Coastal Management, 138, pp.111-123.

Lan, X., Zhang, Z., Li, R., Wang, Z., Chen, X. and Tian, Z., 2012. Distribution of clay minerals in surface sediments off Yangtze River estuary.

Lancaster, N., 2005. Sedimentary processes | Aeolian Processes, Editor(s): Richard C. Selley, L. Robin M. Cocks, Ian R. Plimer, Encyclopedia of Geology, Elsevier, pp. 612-62.

Lanzoni, S. and Seminara, G., 2002. Long-term evolution and morphodynamic equilibrium of tidal channels. Journal of Geophysical Research: Oceans, 107(C1), pp.1-1.

Largier, J.L., 1993. Estuarine fronts: how important are they? Estuaries, 16(1), pp.1-11.

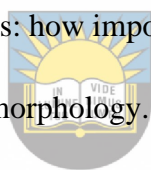
Lewin, J., 1978. Floodplain geomorphology. Progress in Physical Geography, 2(3), pp.408-437.

Li, M., Wei, T., Wang, Z., and Chen, J., 2018. Non-flood season neap tides in the Yangtze estuary offshore: Flow mixing processes and its potential impacts on adjacent wetlands, Physics and Chemistry of the Earth, Parts A/B/C, Volume 103, pp. 127- 139.

Lisle, T.E., 1989. Sediment transport and resulting deposition in spawning gravels, north coastal California. Water Resources Research. 25: 1303-1319.

Liu, K.W, 1997. Cainozoic aeolian sediments and their diagenesis at Isipingo beach, Natal south coast, South Africa. In: B.J. Liu and W.H. Li (-eds), Basin Analysis and Global Sedimentology. VSP Inc. Publ, The Netherlands (Proceedings of the 30th International Geological Congress, Vol. 8), 121-140.

Longhitano, S.G., Mellere, D., Steel, R.J. and Ainsworth, R.B., 2012. Tidal depositional systems in the rock record: a review and new insights. Sedimentary Geology, 279, pp.2-22.



University of Fort Hare

Together in Excellence

Lopez, G.I., 2017. Grain size analysis. Encyclopedia of Earth Science Series Encyclopedia of Geoarchaeology Allan S. Gilbert (Volume Ed.) pp. 341-348.

Mackay, H.M., 1993. The Impact of the urban runoff on the water quality of the Swartkops River Estuary: Implication for water quality management .WRC report kV 45/93, Pretoria.

Macleary, A.G.L., 1996. The Geohydrology of the Swartkops River Basin in the Uitenhage region Eastern Cape, South Africa. (MSc) Department of Geological Science, University of Cape Town, pp.55-95.

Madricardo, F., Montereale-Gavazzi, G., Sigovini, M., Kruss, A., Toso, C. and Foglini, F., 2020. Seafloor morphology and habitats of tidal channels in the Venice Lagoon, Italy tidal channel habitats. In Seafloor Geomorphology as Benthic Habitat (pp. 187-198). Elsevier.

Madhavaraju, J., Barragán, J.C.G., Hussain, S.M., and Mohan, S.P. 2009. Microtextures on quartz grains in the beach sediments of Puerto Peñasco and Bahía Kino, Gulf of California, Sonora, Mexico. *Rev. Mex. Sci. Geol*, 26(2): 1-15.

Magar, V., 2016. Estuarine sediment composition, Encyclopedia of Earth Sciences Series. pp. 285-289. DOI - 10.1007/978-94-017-8801-4-374.

Maity, S.K., and Maiti, R., 2016. Understanding the sediment sources from mineral composition at the lower reach of Rupnarayan River, West Bengal, India – XRD-based analysis, *GeoResJ*, volume 9-12, pp. 91-103, 10.1016/j.grj.2016.09.004.

Marais, J.F.K., 1982. The effects of river flooding on the fish populations of two Eastern Cape estuaries. *African Zoology*, 17(3), pp.96-104.

Margolis, S., and Krinsley, D.H., 1974. Processes of formation and environmental occurrence of microfeatures on detrital quartz grains: *American Journal of Science*, 274: 449–464.

Martin, A.R.H., 1962. Evidence relating to the Quaternary history of the wilderness of lakes. *Transactions of Geological Society of South Africa*, 55pp.

Masselink, G. and Hughes, M., 1998. Field investigation of sediment transport in the swash zone. *Continental Shelf Research*, 18(10), pp.1179-1199.

Masselink, G. and Puleo, J.A., 2006. Swash-zone morphodynamics. *Continental Shelf Research*, 26(5), pp.661-680.

Maun, M. A., 2009. The biology of coastal sand dunes. Oxford University Press.

Maynard, C., Mcmanus, J., Crawford, R., and Paterson, D., 2011. A comparison of short-term sediment deposition between natural and transplanted saltmarsh after saltmarsh restoration in the Eden Estuary (Scotland). *VL – 4*, pp.103-113.

McKee, E.D., 1953. Report on studies of stratification in modern sediments and in laboratory experiments. US] Office of Naval Research.

McLachlan, R.L., Ogston, A.S. and Allison, M.A., 2017. Implications of tidally-varying bed stress and intermittent estuarine stratification on fine-sediment dynamics through the Mekong's tidal river to estuarine reach. *Continental Shelf Research*, 147, pp.27-37.

McLaren, P., 1981. An interpretation of trends in grain size measures, *Journal of Sedimentary petrology*, VOL. 51, NO. 2, pp.0611-0624. 0022-4472/81/0051-0611/\$03.0.

McManus, J., 1998. Temporal and spatial variations in estuarine sedimentation. *Estuaries*, 21(4), pp.622-634.

McMillan, I.K., Brink, G.J., Broad, D.S. and Maier, J.J., 1997. Late Mesozoic sedimentary basins of south coast of South Africa. In: *African Basins, Sedimentary Basins of the world*, 3 (Ed. R.C. Selly), 319-376.

Megahan, W.F., 1999. Sediment, sedimentation. In: *Environmental Geology. Encyclopedia of Earth Science*. Springer, Dordrecht. https://doi.org/10.1007/1-4020-4494-1_296.

Mehta, A.J., 1991. "Review notes on cohesive sediment erosion." *Coastal Sediments '91*, N. C. Kraus, K. J. Gingerich, and D. L. Kriebel, eds., ASCE, 40-53.

Mehta, A.J., and McNally, W.H., 2009. Coastal zones and estuaries – Sediment Transport in Estuaries, ©Encyclopaedia of Life Support Systems (EOLSS). pp. 1-9.

Moiola, R.J and Weiser, D. (1968). Textural parameters: an evaluation. *Journal of Sedimentary Petrology*, 38: 45- 53.

Muir, R.A., Bordy, E.M., Reddering, J.S.V, and Viljoen; J.H.A., 2017. Lithostratigraphy of the Kirkwood Formation (Uitenhage Group), including the Bethelsdorp, Colchester and Swartkops Members, South Africa. *South African Journal of Geology*; 120 (2): 281–293.

Nanson, G.C. and Croke, J.C., 1992. A genetic classification of floodplains. *Geomorphology*, 4(6), pp.459-486.

Nayak, G.N., 2014. Estuary as a sedimentary depositional environment – A review, *Gondwana Geological Society*, VL- ISSN: 0970-261X, pp.121-132.

Ndibo, S.G., 2017. Grain Size Distribution and Mineral Composition of the Channel and Floodplain Sediments of the Swartkops Estuary, Port Elizabeth, South Africa (Doctoral dissertation, University of Fort Hare).

Nelson, S.A., 2015. Sediment and Sedimentary Rocks. *Physical Geology*. Tulane University. 1-10.

Nichols, M.M. and Boon, J.D., 1994. Sediment transport processes in coastal lagoons. In *Elsevier oceanography series* (Vol. 60, pp. 157-219). Elsevier.

Nordstrom, K.F., 1989. Erosion control strategies for bay and estuarine beaches. *Coastal Management*, 17(1), pp.25-35.

Nordstrom, K.F., 1989. Erosion control strategies for bay and estuarine beaches, *Coastal Management*, 17:1, 25-35, DOI: [10.1080/08920758909362072](https://doi.org/10.1080/08920758909362072).

Okeyode, I.C. and Jibiri, N.N., 2013. Grain size analysis of the sediments from Ogun River, South Western Nigeria. *Earth Science Research*, 2(1), p.43.

Otvos, E.G., 1964. Observations on rhomboid beach marks. *Journal of Sedimentary Research*, 34(3), pp.683-687.

Oyedotun, T.D.T., 2016. Sediment characterisation in an Estuary-beach system. *J Coast Zone Manag*, 19(433), p.2.

Partridge, T.C and Maud, R.R., 1987. Geomorphic evolution of South Africa since the Mesozoic. *South African journal of Geology*, 178-208.

Passchier, C., and Trouw, R., 2005. Microtectonics, New York: Springer.

Paszkowski, T. and Shone, R.W., 1994. A modern South African braided-river gravel deposit: a possible analogue for the Archaean Ventersdorp contact reef. *International Geology Review*, 36(8), pp.753-770.

Peterson, N.E., Landry, C.E., Alexander, C.R., Samples, K. and Bledsoe, B.P., 2019. Socioeconomic and environmental predictors of estuarine shoreline hard armoring. *Scientific reports*, 9(1), pp.1-10.

Picard, M.D and High, L.R., 1973. Sedimentary Structures of Ephemeral stream, *Developments in Sedimentology*, Volume 17, pp.189-201.

Pillay, S., Lindsay, P., Mason, T.R., and Wright, C.I., 1996. Suspended particulate matter and dynamics of the Mfolozi estuary, Kwazulu-Natal: Implications for environmental management. *Environmental Geology*, 28(1), pp.40-51.

Prasad, K.R., Arun, T.J. and Limisha, A.T., 2020. Variability in the Granulometric Characteristic of a Tropical River-Estuary-Near Shore Ecosystem from its Source to Sink, Southwest Coast of India. *International Journal of Applied Environmental Sciences*, 15(2), pp.179-197.

Psuty, N.P., Duffy, M., Pace, J.F., Skidde, D.E. and Silveira, T.M., 2010. Northeast coastal and barrier network geomorphological monitoring protocol: Part I—ocean shoreline position. *Natural Resource Report NPS/NCBN/NRR-2010/185*. National Park Service, Fort Collins, Colorado, 146p.

Pye, K., and Croft, D., 2007. Forensic analysis of soil and sediment traces by scanning electron microscopy and energy-dispersive X-ray analysis: An experimental investigation, *Forensic Science International*, Volume 165, Issue 1, pp. 52-63.

Ralston, D.K., Geyer, W.R., Traykovski, P.A. and Nidzieko, N.J., 2013. Effects of estuarine and fluvial processes on sediment transport over deltaic tidal flats. *Continental Shelf Research*, 60, pp.S40-S57.

Reddering, J.S.V. and Esterhuysen, K., 1981. The sedimentary ecology of the Swartkops estuary. *Rosie Report No. 1*. Geology Department, UPE. 89 pp.

Reddering, J.S.V., 1988. Coastal and catchment basin controls on estuary morphology: south-eastern Cape coast. *S. Afr. J. Sci.*, 84: 154-157.

Reed, D.J., Spencer, T., Murray, A.L., French, J.R. and Leonard, L., 1999. Marsh surface sediment deposition and the role of tidal creeks: Implications for created and managed coastal marshes. *Journal of Coastal Conservation*, 5(1), pp.81-90.

Reisinger, A., Gibeaut, J.C., and Tissot, P.E., 2017. Estuarine Suspended Sediment Dynamics: Observations Derived from over a Decade of Satellite Data. *Front. Mar. Sci.* 4:233. Doi: 10.3389/fmars.2017.00233.

Reynolds, W.J., 1988. Ebb-tidal delta dynamics for a tide-dominated barrier island. In *Hydrodynamics and Sediment Dynamics of Tidal Inlets* (pp. 348-363). Springer, New York, NY.

Ritter, J., 2012. Soil erosion-Causes and effects. Factsheet. Ministry of Agriculture. Food and Rural Affairs, Ontario.

Rogers, S., and Skrabal, T., 2001. North Carolina. Division of Coastal Management, North Carolina Sea Grant College Program and North Carolina State University. College of Design, *The Soundfront Series* (No. 1). North Carolina Sea Grant, NC State University.

Roy, A.H., Rosemond, A.D., Paul, M.J., Leigh, D., and Wallace, J.B., 2003. Stream macro-invertebrates response to catchment urbanisation (Georgia, U.S.A). *Freshwater biology* 48: 329-346.

Sanford, L.P. and Maa, J.P.Y., 2001. A unified erosion formulation for fine sediments. *Marine Geology*, 179(1-2), pp.9-23.

Schubel, J.R., 1982. Estuarine sedimentation. *Beaches and Coastal Geology: Encyclopedia of Earth Science*. Boston, MA: Springer, p.324.

Scharler U.M., and Baird. D., 2003. The influence of catchment management on salinity, nutrient stoichiometry and phytoplankton biomass of Eastern Cape estuaries, South Africa. *Estuarine, Coastal and Shelf Science*, 56 (3/4): 735-748.

Schumann, E, Largier, J, and Slinger J., 1999. Estuarine hydrodynamics. In: Allanson BR, Baird D (eds) Estuaries of South Africa. Cambridge University Press, Cambridge, UK, pp. 27–52.

Schumann, E.H., 2003. Towards the management of marine sedimentation in South African estuaries with special reference to the Eastern Cape. *Water Research Commission, 1109*(1), p.03.

Schumann, E.H., 2015. Keurbooms Estuary floods and sedimentation. *South African Journal of Science*, 111(11-12), pp.1-9.

Schumann, E.H., Largier, J.L. and Slinger, J.H., 1999. Estuarine hydrodynamics. *Estuaries of South Africa*, 3, pp.27-52.

Schutte, C.A., Ahmerkamp, S., Wu, C.S., Seidel, M., De Beer, D., Cook, P.L.M. and Joye, S.B., 2019. Biogeochemical dynamics of coastal tidal flats. In *Coastal wetlands* (pp. 407-440). Elsevier.

Scully, M., and Friedrichs, C., 2003. The influence of asymmetries in overlying stratification on near-bed turbulence and sediment suspension in a partially mixed estuary. *Ocean Dynamics*. Volume 53, page 208-219. <https://doi.org/10.1007/s10236-003-0034-y>

Shand, T., and Blacka, M., 2017. Design Guidance Report: Guidance for coastal protection works in Pacific island countries.

Shanmugam, G., 2006. The tsunamite problem. *Journal of Sedimentary research*, 76(5), pp.718-730.

Short, A., and Jackson, D., 2013. Beach Morphodynamics, *Treatise on Geomorphology*, VL - 10, Page 106-129. 10.1016/B978-0-12-374739-6.00275-X.

Short, A.D., 2012. Coastal processes and beaches. *Nature education knowledge*, 3(10), p.15.

Skilbeck, C.G., Heap, A.D. and Woodroffe, C.D., 2017. Geology and sedimentary history of modern estuaries. In *Applications of paleoenvironmental techniques in estuarine studies* (pp. 45-74). Springer, Dordrecht.

Slinger, J.H., 1995. The evolution of thermohaline structure in a closed estuary. South African Journal of Aquatic Science 16 (1/2) 60-77.

Sly, P.G., 1989. Sediment dispersion: part 1, fine sediments and significance of the silt/clay ratio. In Sediment/Water Interactions (pp. 99-110). Springer, Dordrecht.

Smalley, I.J., Kumar, R., Dhand, K.H., Jefferson, I.F. and Evans, R.D., 2005. The formation of silt material for terrestrial sediments: particularly loess and dust. Sedimentary Geology, 179(3-4), pp.321-328.

Stembridge J.E., 1982. Present-day shoreline changes, worldwide. In: Beaches and Coastal Geology. Encyclopedia of Earth Sciences Series. Springer, New York, NY. https://doi.org/10.1007/0-387-30843-1_342.

Strydom, N.A., 1985. Fish larval dynamics in the mouth region of the Gamtoos estuary. MSc thesis, University of Port Elizabeth, pp104.

Strydom, N.A., Kisten, Y., Patrick, P., and Perissinotto, R., 2015. Dynamics of recruitment of larval and juvenile Cape stumpnose *Rhabdosargus holubi* (Teleostei: Sparidae) into the Swartkops and Sundays estuaries, South Africa. African Journal of Marine Science, 37(1), pp.1-10.

Suganraj, K., 2013, ‘‘Grain size statistical parameters of coastal sediments at Kameswaram Nagapattinam District, east coast of Tamilnadu, India,’’ *Inter. Jour. of Recent Scintific Resea.* vol. 4, (2), 102-106.

Townend, I. and Pethick, J., 2002. Estuarine flooding and managed retreat. Philosophical Transactions of the Royal Society of London. Series A: Mathematical, Physical and Engineering Sciences, 360(1796), pp.1477-1495.

Valentine, E.M., 2016. Sediments in the marine environments, a broad sandy beach with greyness, outfalls and a jetty near Hartlepool, County Durham.

Valle-Levinson A., 2011. Classification of Estuarine Circulation, Editor(s): Eric Wolanski, <https://doi.org/10.1016/B978-0-12-374711-2.00106-6>. Donald McLusky, Treatise on Estuarine and Coastal Science, Academic Press, volume 1, pp.75-86.

Van Leussen, W. and Dronkers, J., 1988. Physical processes in estuaries: An introduction. In *Physical processes in estuaries* (pp. 1-18). Springer, Berlin, Heidelberg.

Van Rijn, L.C., 2010. Coastal erosion control based on the concept of sediment cells. *Conscience project Final Report*. Available at: URL: [http://www. leovanrijn-sediment. com/papers/Coastalerosion2012. pdf](http://www.leovanrijn-sediment.com/papers/Coastalerosion2012.pdf) (accessed 1 May 2016).

Vernon, C.J., Burns, M.E.R., and Wiseman, K.A., 1993. Report No.42: Nahoon (CSE 44), Qinira (CSE 45) and Gqunube (CSE 46). Estuaries of the Cape. Part 2. Synopses of available information on individual systems. (Eds.) Morant, P.D. CSIR Research Report No, 441: 48 pp.

Viljoen, J.H.A, Reddering, J.S.V, Bordy, E.M, and Muir, R.A., 2017; Lithostratigraphy of the Enon Formation (Uitenhage Group), South Africa. *South African Journal of Geology*; 120 (2): 273–280.

Vriend, N.M., Hunt, M.L., and Clayton, R.W., 2012. Sedimentary structure of large sand dunes: examples from Dumont and Eureka dunes, California, *Geophysical Journal International*, Volume 190, pp.981–992. doi:10.1111/j.1365-246X.2012.05514.x.

Wang, C., Chen, M., Qi, H., Intasen, W. and Kanchanapant, A., 2020. Grain-Size Distribution of Surface Sediments in the Chanthaburi Coast, Thailand and Implications for the Sedimentary Dynamic Environment. *Journal of Marine Science and Engineering*, 8(4), p.242.

Wang, H., Chen, Z., Wang, K., Liu, H., Tang, Z. and Huang, Y., 2016. Characteristics of heavy minerals and grain size of surface sediments on the continental shelf of Prydz Bay: implications for sediment provenance. *Antarctic Science*, 28(2), p.103.

Wang, X.H. and Andutta, F.P., 2013. Sediment transport dynamics in ports, estuaries and other coastal environments. *Sediment Transport Processes and Their Modelling Applications*, p.13.

Watling, R.J. and Watling, H.R., 1982. Metal surveys in South African estuaries I. Swartkops River. *Water SA*, 8(1), pp.26-35.

Wentworth, C.K., 1922. A scale of grade and class terms for clastic sediments. *Journal of Geology*, 30: 377-392.

Whalley, B., and Krinsley, D., 2006. A scanning electron microscope study of quartz grains from glacial environments, *Sedimentology*, VL - 21, page 87-105, 10.1111/j.1365-3091.1974.tb01783.x.

Winter, P.E.D., 1990. The estuarine-marine exchange of dissolved and particulate material at the Swartkops River estuary, Algoa Bay, South Africa. PhD thesis, University of Port Elizabeth.

Wolanski, E., and Elliott, M., 2016. Estuarine sediment dynamics, In book: *Estuarine ecohydrology*, pp.77-125.

Wolanski, E., and McLusky, D., 2011. Treatise on estuarine and coastal science, estuarine and coastal geology and geomorphology, V. 3, pp.1-285.

Yang, Z. and Wang, T., 2015. Responses of estuarine circulation and salinity to the loss of intertidal flats—A modelling study. *Continental Shelf Research*, 111, pp.159-173.

Ye, Y.C., 2017. *Marine Geo-hazards in China*. Elsevier.

Zhang, W., Yu, L., Hutchinson, S.M., 2001. Diagenesis of magnetic minerals in the intertidal sediments of the Yangtze Estuary, China, and its environmental significance. *Science of the Total Environment*, Volume 266, Issues 1–3, pp.169-175.

Zhou, X., Liu, D., Bu, H., Deng, L., Liu, H., Yuan, P., Du, P., and Song, H., 2018. XRD-based quantitative analysis of clay minerals using reference intensity ratios, mineral intensity factors, Rietveld, and full pattern summation methods: A critical review, *Solid Earth Sciences*, Volume 3, Issue 1, pp.16-29.

APPENDICES

APPENDIX A: GRAIN SIZE ANALYS

A.1 Sample 2 (Beach sand)

Table A.1 Retained and cumulative percentage of grain size for sample 2. Aliquot mass = 416.34 g.

Sieve size (ϕ)	Mass retained (g)	% retained	Cumulative %
2	1.40	0.33	0.33
3	396.13	95.25	95.58
4	16.06	3.86	99.44
5	2.38	0.57	100.01
Retained total mass	415.97g		

Error = 0.8 %

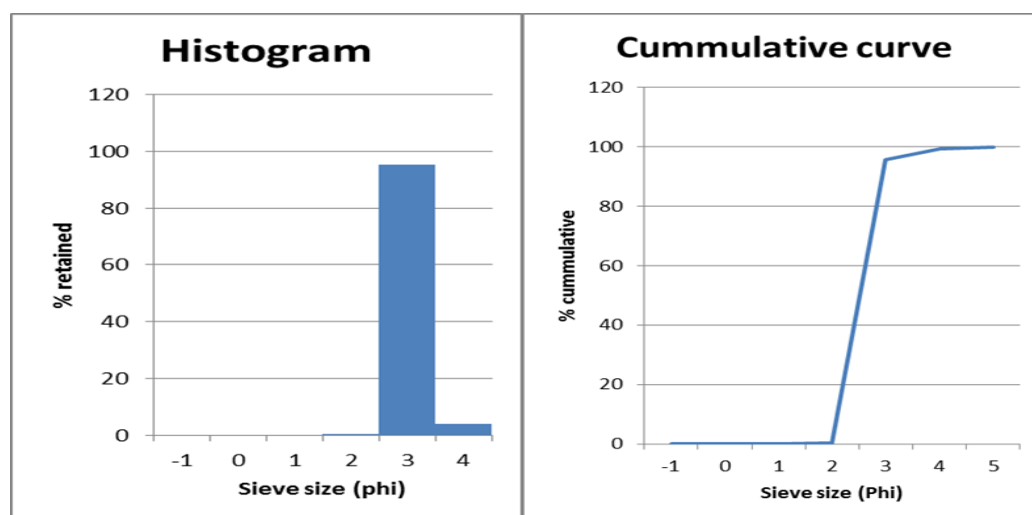


Fig. A.1: Histogram (left) and cumulative frequency curve (right) of sample 2, showing the grain size distribution varied from 3.5-4.5 phi which is dominant at 3 Phi (0.125 mm).

A.2 Sample 3 (Beach sand)

Table A.2 Retained and cumulative percentage of grain size for sample 3. Aliquot mass = 623.92 g.

Sieve size (ϕ)	Mass retained (g)	% retained	Cumulative %
1	0.47	0.07	0.07
2	3.16	0.5	0.57
3	603.15	96.80	97.37
4	13.53	2.17	99.54
5	2.76	0.44	99.98
Retained total mass	623.07g		

Error = 0.1%

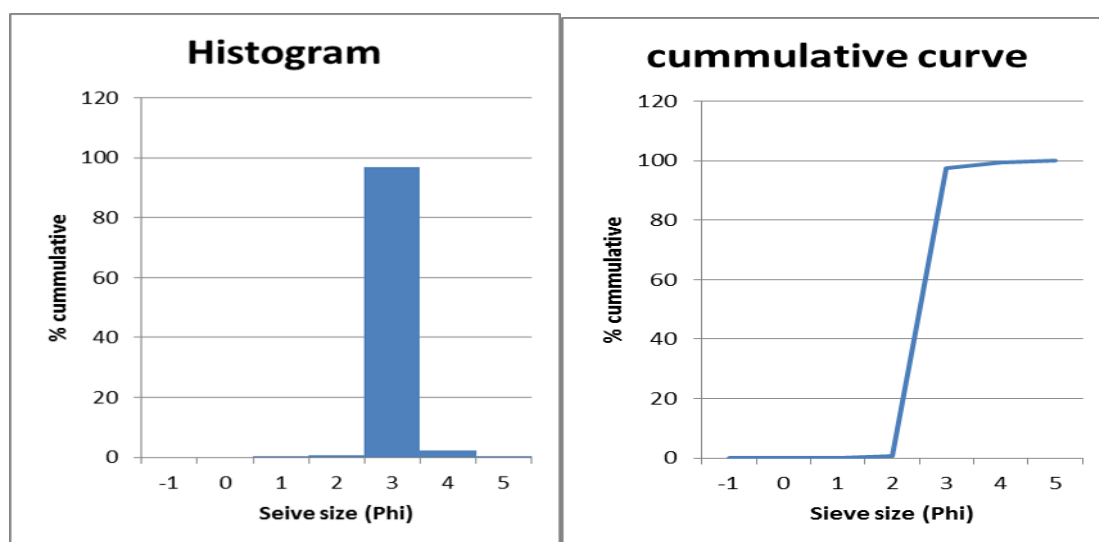


Fig. A.2: Histogram (left) and cumulative frequency curve (right) of the sample 3, showing the grain size distribution varied from 3.5- 4.5 phi wich is dominant at 3 Phi (0,125 mm) with minor size at 4 phi(0.0625).

A.3 Sample 4 (Beach sand)

Table A.3 Retained and cumulative percentage of grain size for sample 4. Aliquot mass = 493.04 g.

Sieve size (ϕ)	Mass retained (g)	% retained	Cumulative %
1	0.04	0.008	0.008
2	7.25	1.47	1.47
3	475.64	96.65	98.12
4	8.50	1.72	99.84
5	0.69	0.14	99.98
Retained total mass	492.12g		

Error = 0.1 %

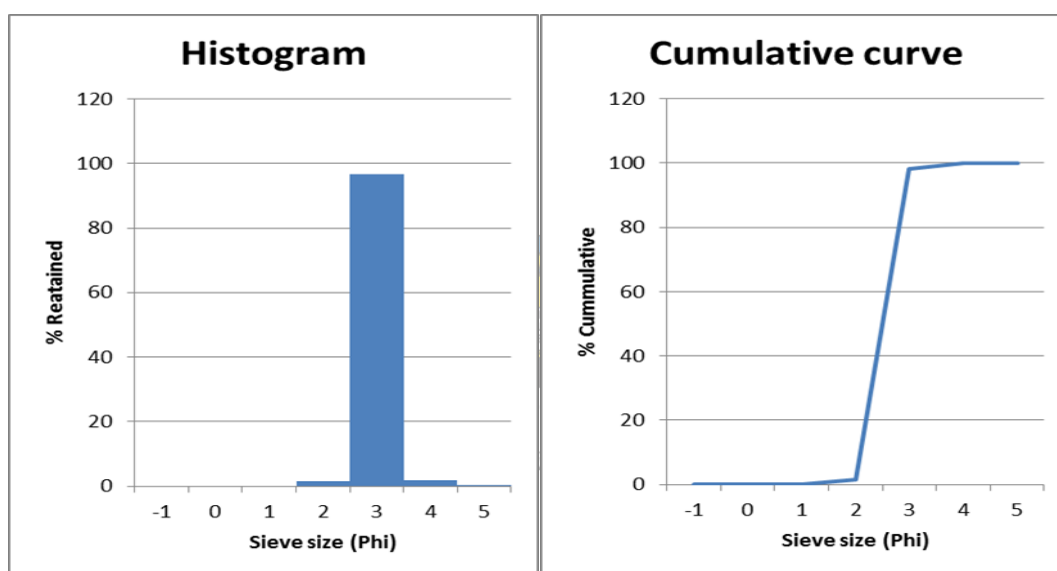


Fig. A.3: Histogram (left) and cumulative frequency curve (right) of sample 4, showing grain size distribution size varied from 1.5 to 4.5 phi, and well sorted nature, with dominant size at 3 Phi (0.125 mm) and minor sizes at 2 Phi (0.25 mm) and 4 Phi (0.0625 mm).

A.4 Sample 5 (Beach sand)

Table A.4 Retained and cumulative percentage of grain size for sample 5. Aliquot mass =315.51 g

Sieve size (ϕ)	Mass retained (g)	% retained	Cumulative %
-1	1.41	0.36	0.36
0	0.58	0.18	0.54
1	0.73	0.23	0.77
2	5.18	1.64	2.41
3	302.59	96.14	98.55
4	3.68	1.16	99.71
5	0.81	0.25	99.96
Retained total mass	314.71g		

Error = 0.2 %

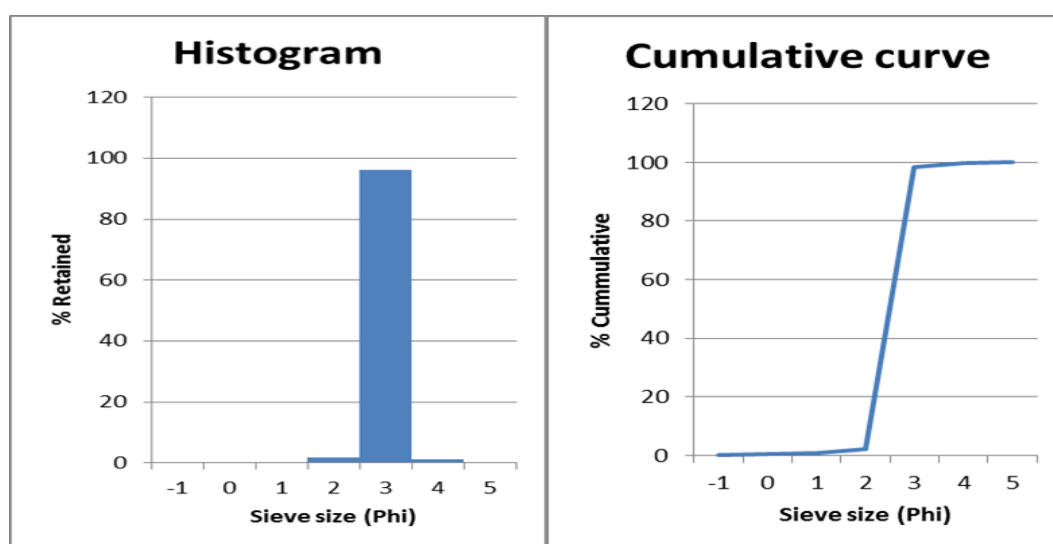


Fig. A.4: Grain size-frequency histogram (left) showing well sorting in sample 5 and cumulative frequency (right) showing the distribution of sediments, the sediment grain size is dominant at 3 Phi (0.125 mm).

A.5 Sample 6 (Beach sand)

Table A.5 Retained and cumulative percentage of grain size for sample 6. Aliquot mass = 264.55 g

Sieve size (ϕ)	Mass retained (g)	% retained	Cumulative %
1	0.07	0.02	0.02
2	2.09	0.80	0.82
3	250.46	96.21	97.03
4	7.53	2.89	99.92
5	0.17	0.06	99.98
Retained total mass	260.32g		

Error = 1.5 %

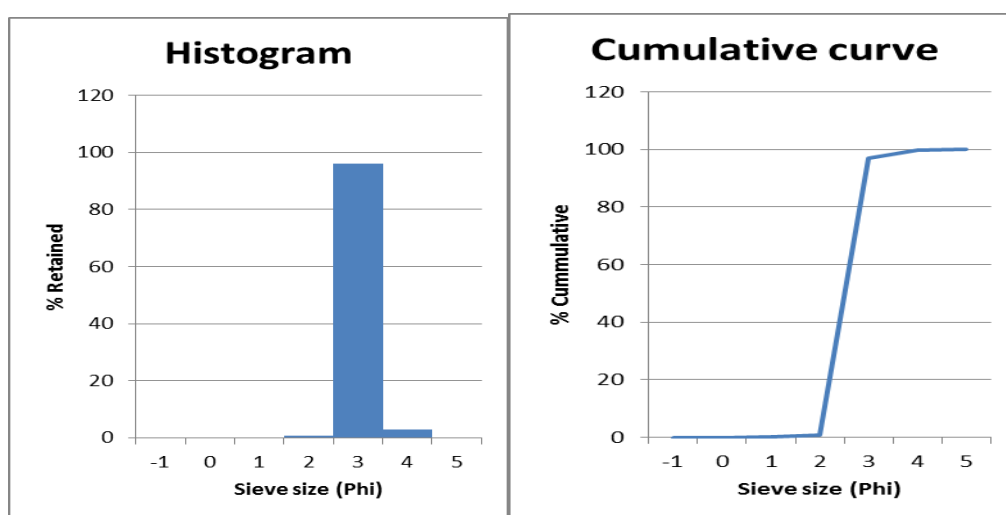


Fig. A.5: Histogram (left) and cumulative frequency curve (right) of sample 6, showing grain size distribution size varied from 1.5 to 4.5 phi, and well sorted nature, with dominant size at 3 Phi (0.125 mm) and minor sizes at 2 Phi (0.25 mm) and 4 Phi (0.0625 mm).

A.6 Sample 7 (Beach sand)

Table A.6 Retained and cumulative percent of grain size for sample 7. Aliquot mass = 255.94 g.

Sieve size (ϕ)	Mass retained (g)	% retained	Cumulative %
0	0.70	0.27	0.27
1	1.07	0.41	0.68
2	4.78	1.87	2.55
3	240.36	94.19	96.74
4	7.13	2.79	99.53
5	1.12	0.43	99.96
Retained total mass	255.16g		

Error = 0.3 %

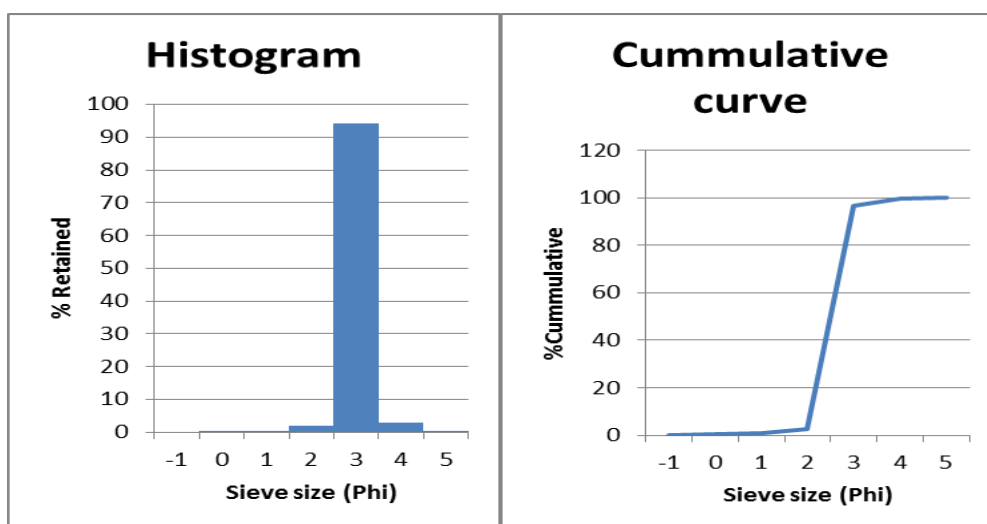


Fig. A.5: Histogram (left) and cumulative frequency curve (right) of sample 7, showing grain size distribution size varied from 1.5 to 4.5 phi, and well sorted nature, with dominant size at 3 Phi (0.125 mm) and minor sizes at 2 Phi (0.25 mm) and 4 Phi (0.0625 mm).

A.7 Sample 8 (Beach sand)

Table A.7 Retained and cumulative percentage of grain size for sample 8. Aliquot mass =492.42 g.

Sieve size (ϕ)	Mass retained (g)	% retained	Cumulative %
1	0.07	0.01	0.01
2	2.09	0.42	0.43
3	482.3	98.10	98.53
4	6.36	1.29	99.82
5	0.81	0.16	99.98
Retained total mass	491.63g		

Error = 0.1 %

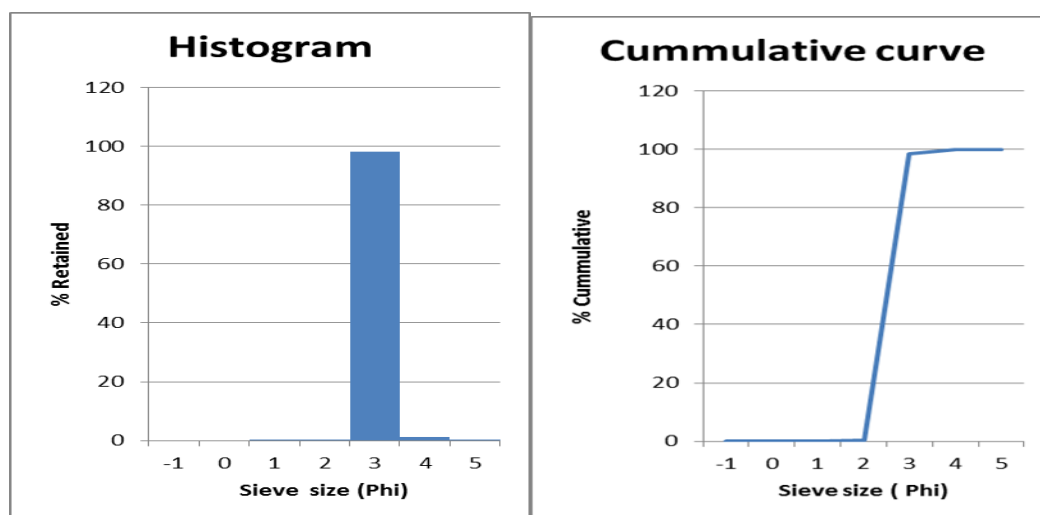


Fig. A.7: Histogram (left) and cumulative frequency curve (right) of the sample 8, showing the grain size distribution varied from 3.5- 4.5 phi wich is dominant at 3 Phi (0,125 mm) with minor size at 4 phi (0.0625).

A.8 Sample 9 (Beach sand)

Table A.8 Retained and cumulative percentage of grain size for sample 9. Aliquot mass = 514.57 g.

Sieve size (ϕ)	Mass retained (g)	% retained	Cumulative %
1	0.10	0.01	0.01
2	2.31	0.44	0.45
3	503.26	97.86	98.31
4	7.72	1.50	99.81
5	0.87	0.16	99.97
Retained total mass	514.26g		

Error = 0.06 %

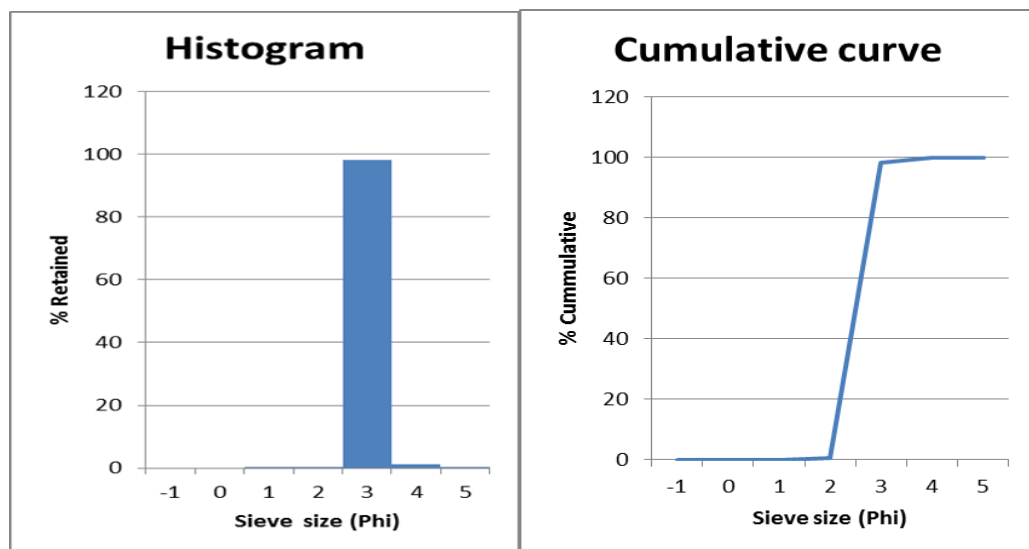


Fig. A.8: Histogram (left) and cumulative frequency curve (right) of the sample 9, showing the grain size distribution varied from 3.5- 4.5 phi wich is dominant at 3 Phi (0,125 mm) with minor size at 4 phi (0.0625).

A.9 Sample 10 (Beach sand)

Table A.10 Retained and cumulative percentage of grain size for sample 10. Aliquot mass = 322.32 g.

Sieve size (ϕ)	Mass retained (g)	% retained	Cumulative %
1	0.16	0.04	0.04
2	5.38	1.64	1.71
3	305.64	95.00	96.71
4	9.11	2.83	99.54
5	1.41	0.43	99.97
Retained total mass	321.7g		

Error = 0.1%

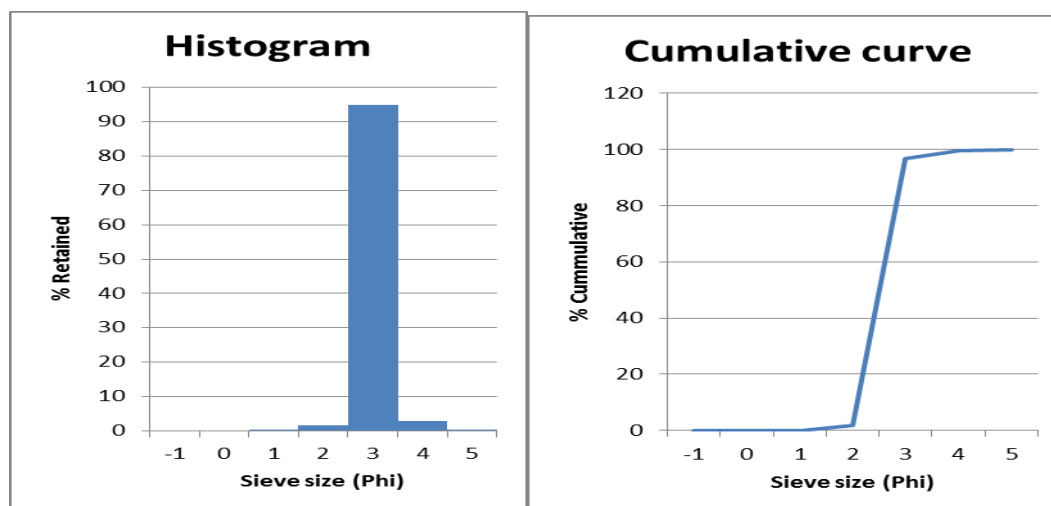


Fig. A.9: Histogram (left) and cumulative frequency curve (right) of sample 10, showing grain size distribution size varied from 1.5 to 4.5 phi, and well sorted nature, with dominant size at 3 Phi (0.125 mm) and minor sizes at 2 Phi (0.25 mm) and 4 Phi (0.0625 mm).

A.10 Sample 11 (Beach sand)

Table A.10 Retained and cumulative percentage of grain size for sample 11. Aliquot mass = 431.46 g.

Sieve size	Mass retained (g)	% retained	Cumulative %
2	1.02	0.23	0.23
3	408.88	94.98	95.21
4	14.99	3.48	98.69
5	5.60	1.30	99.99
Retained total mass	430.49g		

Error = 0.2%

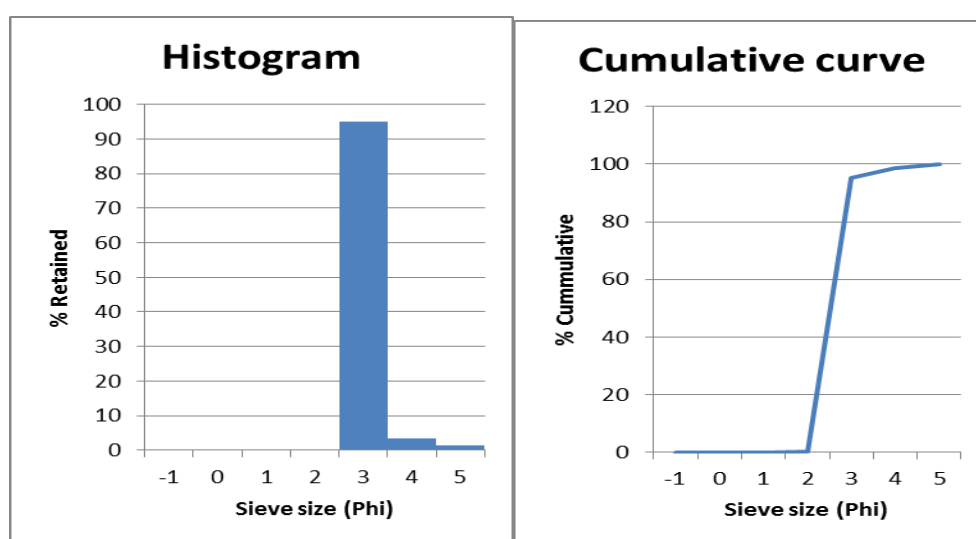


Fig. A.10: Histogram (left) and cumulative frequency curve (right) of sample 11, showing grain size distribution size varied from 3.5 to 4.5 phi, with dominant size at 3 Phi (0.125 mm) and minor sizes at 4 Phi (0.0625 mm).

A.11 Sample 12 (Beach sand)

Table A.11 Retained and cumulative percentage of grain size for sample 12. Aliquot mass = 312.64 g.

Sieve size (ϕ)	Mass retained (g)	% retained	Cumulative %
-1	1.14	0.36	0.36
0	0.18	0.05	0.41
1	0.11	0.03	0.44
2	1.11	0.35	0.79
3	296.97	95.36	96.15
4	11.98	3.84	99.99
5	1.01	0.32	100.31
Retained total mass	311.39g		

Error = 0.3 %

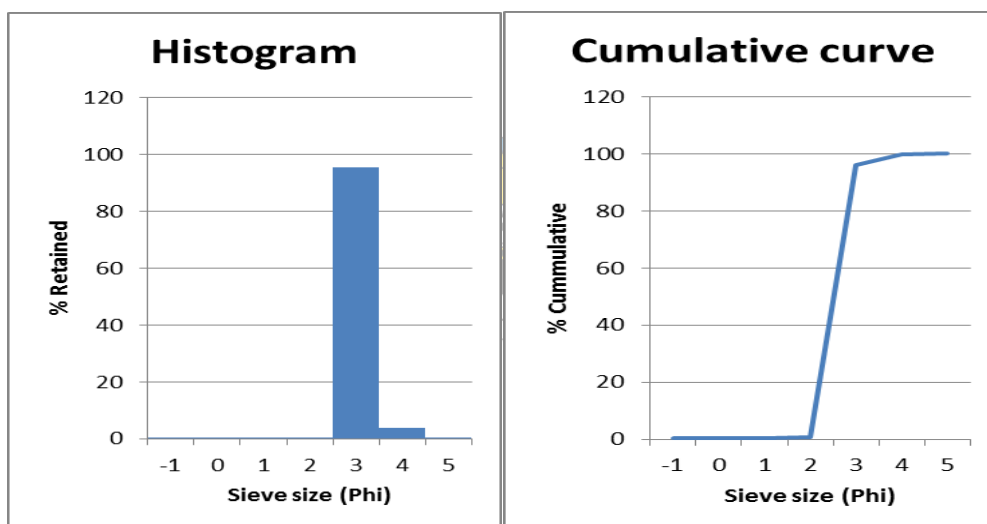


Fig. A.11: Histogram (left) and cumulative frequency curve (right) of sample 12, showing grain size distribution size varied from 3.5 to 4.5 phi, with dominant size at 3 Phi (0.125 mm) and minor sizes at 4 Phi (0.0625 mm).

A.12 Sample 13 (Beach sand)

Table A.12 Retained and cumulative percentage of grain size for sample 13. Aliquot mass = 159.50 g.

Sieve size (ϕ)	Mass retained (g)	% retained	Cumulative %
1	0.63	0.39	0.39
2	6.05	3.83	4.22
3	144.33	91.40	95.62
4	6.80	4.30	99.92
5	0.09	0.05	99.97
Retained total mass	157.9g		

Error = 1.0%

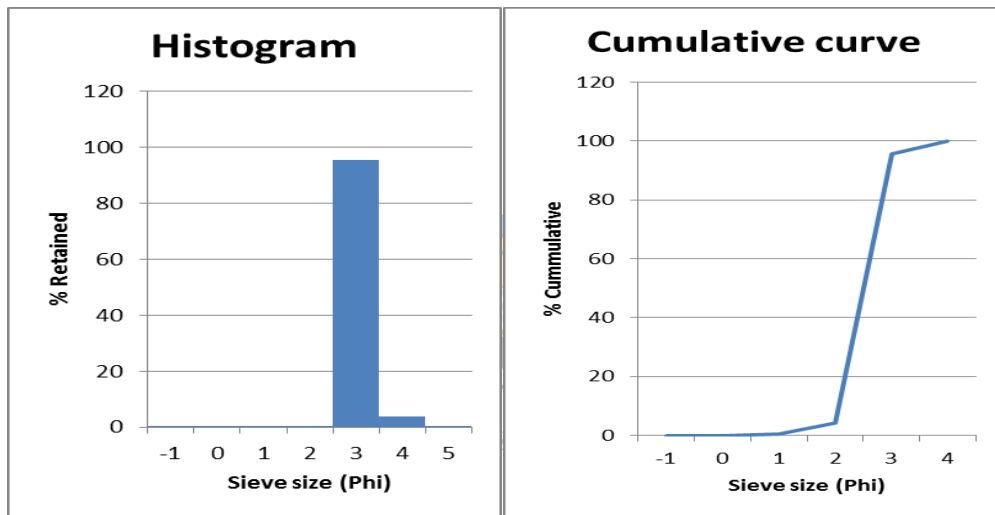


Fig. A.12: Histogram (left) and cumulative frequency curve (right) of sample 13, showing grain size distribution size varied from 3.5 to 4.5 phi, with dominant size at 3 Phi (0.125 mm) and minor sizes at 4 Phi (0.0625 mm).

A.13 Sample 16 (Estuarine sands)

Table A.13 Retained and cumulative percentage of grain size for sample 16. Aliquot mass = 515.32 g.

Sieve size (ϕ)	Mass retained (g)	% retained	Cumulative %
1	2.05	0.39	0.39
2	29.58	5.75	6.14
3	473.50	92.10	98.24
4	8.56	1.66	99.9
5	0.39	0.07	99.97
Retained total mass	514.08g		

Error = 0.2%

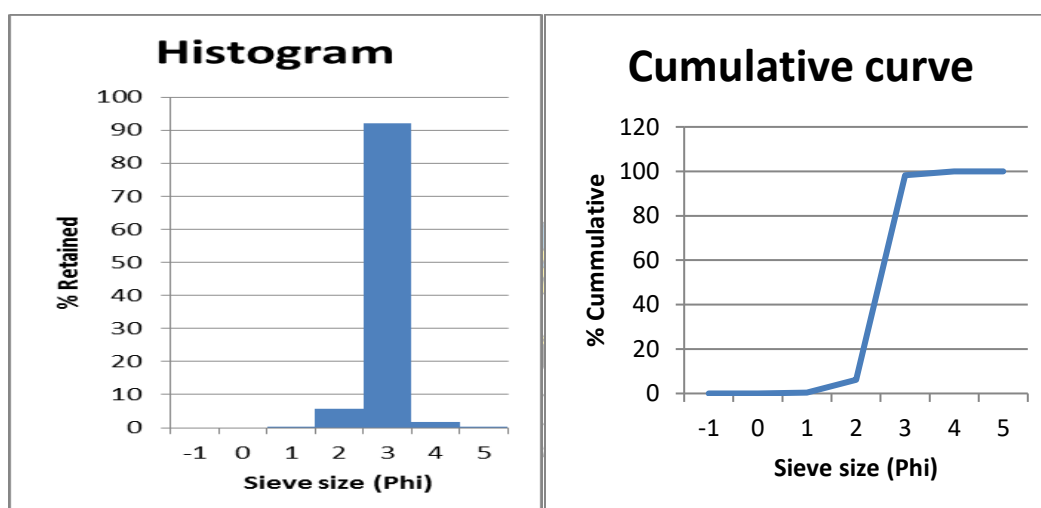


Fig. A.13: Histogram (left) and cumulative frequency curve (right) of Sample 16, showing grain size varied from 1.5 phi to 4.5 phi, and well sorted nature, with dominant size at 3 Phi (0.125 mm) and minor at 2 Phi (0.25 mm) and 4 phi (0.0625 mm).

A.14 Sample 17 (Estuarine sands)

Table A.14 Retained and cumulative percentage of grain size for sample 17. Aliquot mass = 330.03 g.

Sieve size	Sample mass	% retained	Cumulative %
0	0.20	0.06	0.06
1	1.00	0.30	0.36
2	14.49	4.39	4.75
3	303.72	92.13	96.88
4	9.83	2.98	99.86
5	0.41	0.12	99.98
Retained total mass	329.65g		

Error = 0.1%

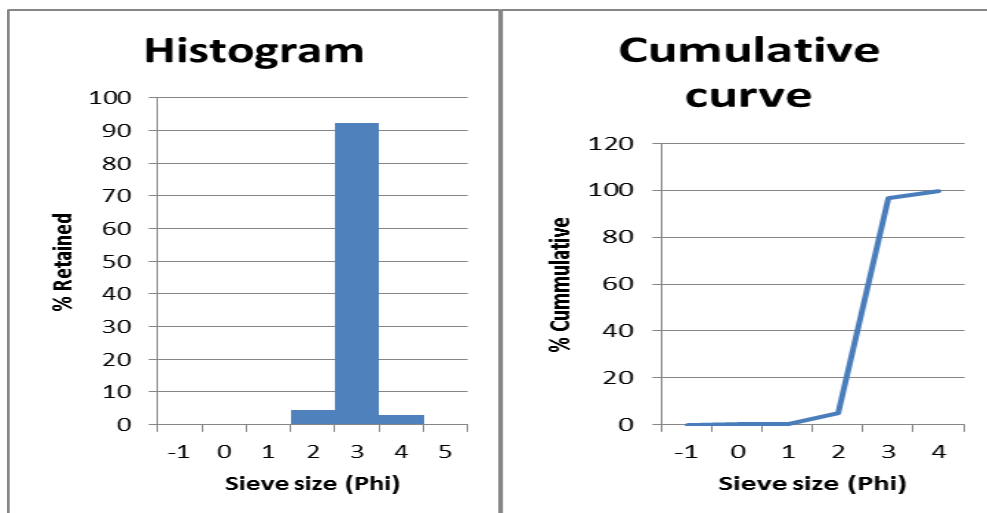


Fig. A.14: Histogram (left) and cumulative frequency curve (right) of sample 17, showing grain size varied from 1.5 phi to 4.5 phi, and well sorted nature, with dominant size at 3 Phi (0.125 mm) and minor at 2 Phi (0.25 mm) and 4 phi (0.0625 mm).

A.15 Sample 18 (Estuarine sand)

Table A.15 Retained and cumulative percentage of grain size for sample 18. Aliquot mass = 187.35 g.

Sieve size (ϕ)	Mass retained (g)	% retained	Cumulative %
-1	1.40	0.75	0.75
0	1.32	0.70	1.45
1	2.45	1.31	2.76
2	12.65	6.78	9.54
3	161.96	86.82	96.36
4	6.54	3.50	99.86
5	0.22	0.11	99.97
Retained total mass	186.54g		

Error = 0.4%

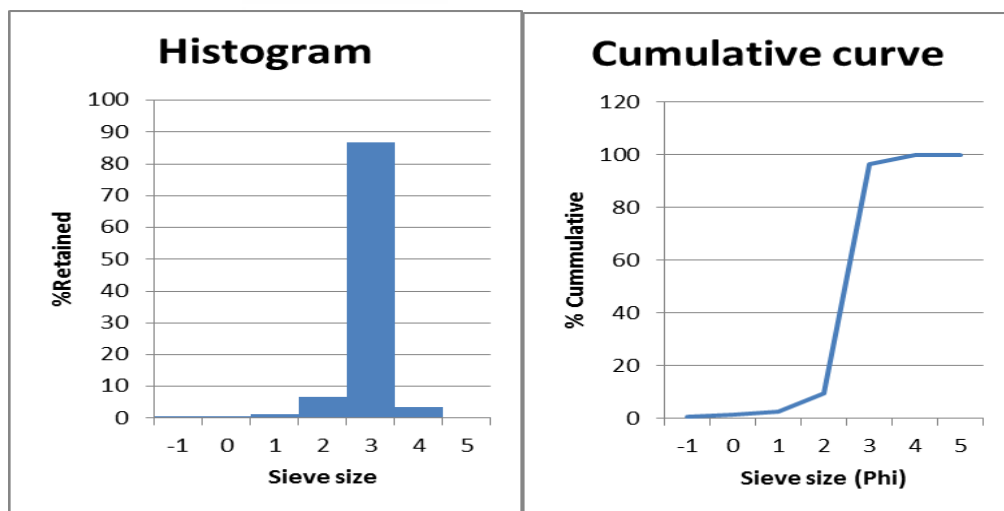


Fig. A.15: Histogram (left) and cumulative frequency curve (right) of sample 18, showing grain size varied from 1.5 phi to 4.5 phi, and well sorted nature, with dominant size at 3 Phi (0.125 mm) and minor at 2 Phi (0.25 mm) and 4 phi (0.0625 mm).

A.16 Sample 19

Table A.16 Retained and cumulative percentage of grain size for sample 19.

Aliquot mass = 383.05 g.

Sieve size (ϕ)	Mass retained (g)	% retained	Cumulative %
-1	0.13	0.03	0.03
0	1.60	0.41	0.44
1	1.90	0.49	0.93
2	8.30	2.16	3.09
3	366.91	95.81	98.9
4	3.28	0.85	99.75
5	0.80	0.20	99.95
Retained total mass	382.92g		

Error = 0.03 %

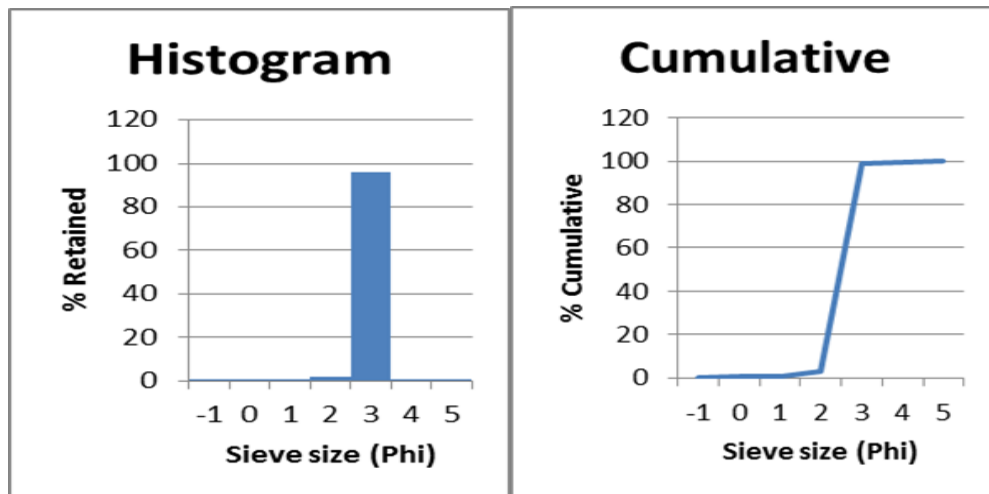


Fig. A.16: Histogram (left) and cumulative frequency curve (right) showing grain size distribution of the Sample 19. The grain size is dominant at 3 Phi (0.125 mm) followed by small percentage of grain size of 2 Phi (0.25 mm).

A.17 Sample 20 (Estuarine sand)

Table A.17 Retained and cumulative percentage of grain size for sample 20.

Aliquot mass = 286.07 g.

Sieve size (ϕ)	Mass retained (g)	% retained	Cumulative %
-1	2.20	0.76	0.76
0	1.80	0.62	1.38
1	1.85	0.64	2.02
2	5.28	1.84	3.86
3	269.80	94.41	98.27
4	3.62	1.26	99.53
5	1.22	0.42	99.95
Retained total mass	285.77g		

Error = 0.1%

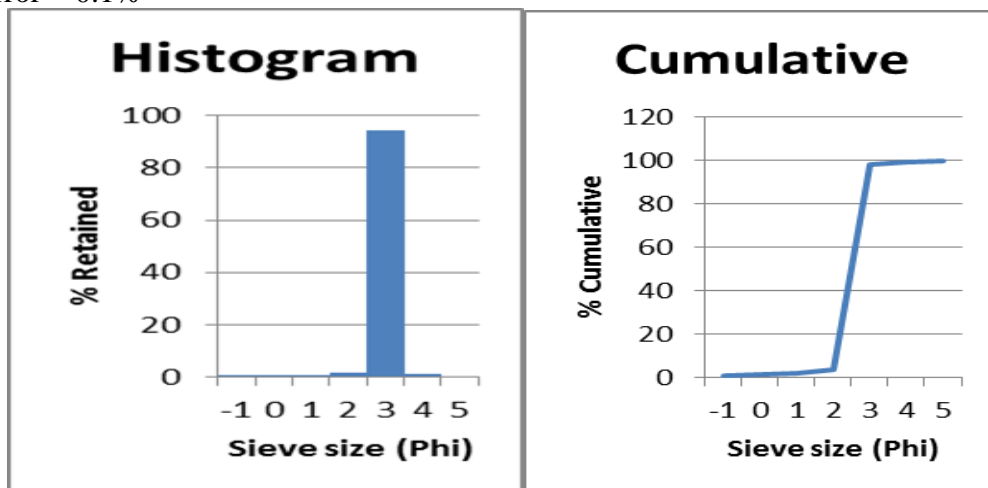


Fig. A.17: Histogram (left) and cumulative frequency curve (right) of sample 20, showing grain size distribution size varied from 1.5 to 4.5 phi, and well sorted nature, with dominant size at 3 Phi (0.125 mm) and minor sizes at 2 Phi (0.25 mm) and 4 Phi (0.0625 mm).

A.18 Sample 21 (Estuarine sand)

Table A.18 Retained and cumulative percentage of grain size for sample 21.

Aliquot mass = 288.64 g.

Sieve size (ϕ)	Mass retained (g)	% retained	Cumulative %
-1	0.48	0.15	0.15
0	0.28	0.09	0.24
1	0.49	0.17	0.41
2	1.52	0.52	0.93
3	281.81	97.95	98.88
4	2.69	0.93	99.86
5	0.44	0.14	99.95
Retained total mass	287.69g		

Error = 0.3%

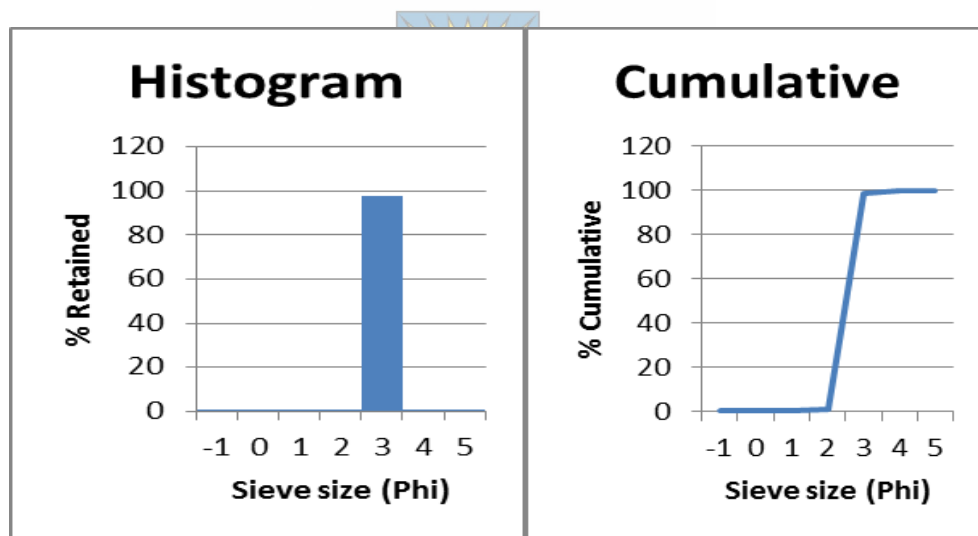


Fig. A.18: Histogram (left) and cumulative frequency curve (right) showing grain size distribution of sample 21. The grain size distribution is dominant at 3 Phi (0.125 mm) and it is well sorted in nature.

A.19 Sample 22 (Estuarine sand)

Table A.19 Retained and cumulative percentage of grain size for sample 22.

Aliquot mass = 279.26 g.

Sieve size (ϕ)	Mass retained (g)	% retained	Cumulative %
-1	0.60	0.21	0.21
0	1.23	0.44	0.65
1	1.87	0.67	1.32
2	3.99	1.42	2.74
3	267.82	95.96	98.7
4	2.88	1.03	99.73
5	0.69	0.24	99.97
Retained total mass	279.08g		

Error = 0.06 %

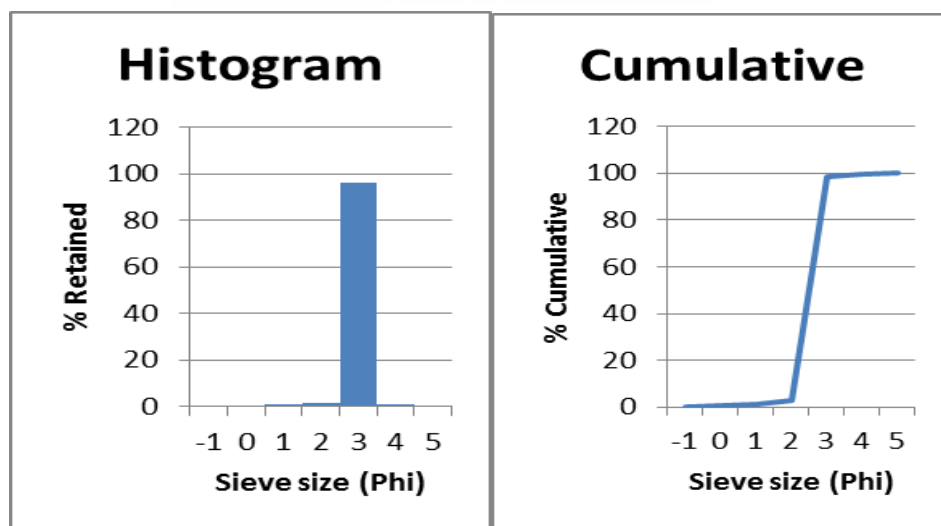


Fig. A.19: Histogram (left) and cumulative frequency curve (right) showing grain size distribution of sample 22. The grain size distribution is dominant at 3 Phi (0.125 mm) and it is well sorted in nature.

A.20 Sample 23 (Estuarine sand)

Table A.20 Retained and cumulative percentage of grain size for sample 23. Aliquot mass = 304.46 g.

Sieve size (ϕ)	Mass retained (g)	% retained	Cumulative %
-1	0.10	0.03	0.03
0	1.48	0.48	0.51
1	1.74	0.57	1.08
2	5.51	1.81	2.89
3	291.00	95.64	98.53
4	3.63	1.19	99.72
5	0.80	0.26	99.98
Retained total mass	304.26g		

Error = 0.06%

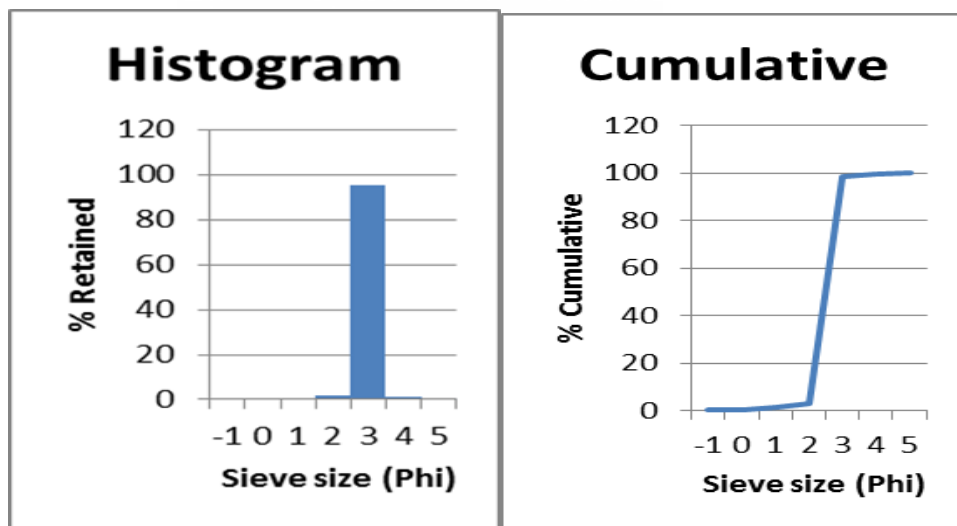


Fig. A.20: Histogram (left) and cumulative frequency curve (right) showing grain size distribution of sample 23. The grain size distribution is dominant at 3 Phi (0.125 mm) and it is well sorted in nature.

A.21 Sample 24 (Estuarine sand)

Table A.21 Retained and cumulative percentage of grain size for sample 24. Aliquot mass = 307.88g.

Sieve size (ϕ)	Mass retained (g)	% retained	Cumulative %
-1	0.30	0.09	0.09
0	1.43	0.46	0.55
1	2.61	0.84	1.39
2	10.15	3.29	4.68
3	289.13	93.94	98.62
4	3.40	1.10	99.72
5	0.76	0.24	99.96
Retained total mass	307.78g		

Error = 0.03 %

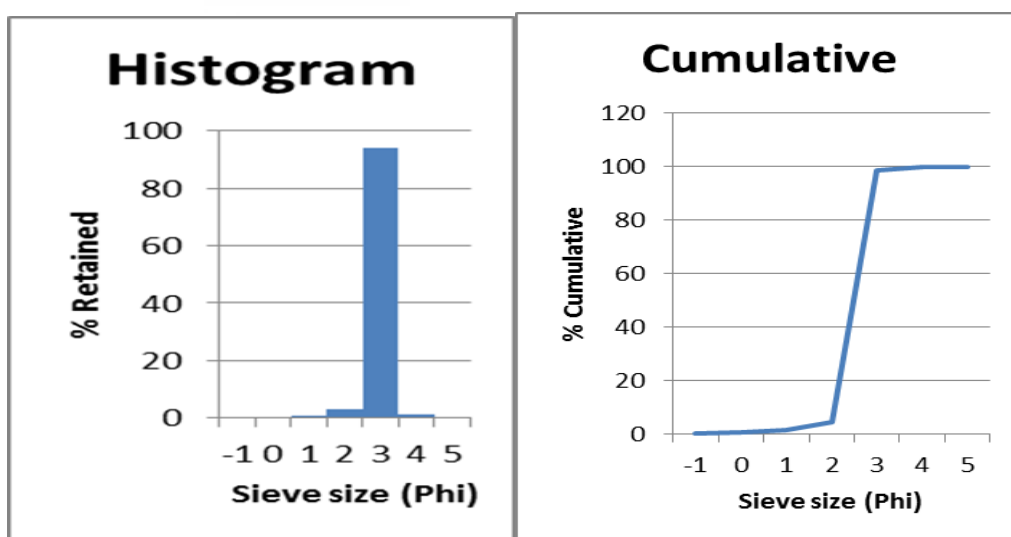


Fig. A.21: Histogram (left) and cumulative frequency curve (right) showing grain size distribution of the Sample 24. The grain size is dominant at 3 Phi (0.125 mm) followed by small percentage of grain size of 2 Phi (0.25 mm).

A.22 Sample 25 (Estuarine sand)

Table A.22 Retained and cumulative percentage of grain size for sample 25. Aliquot mass = 354.36 g.

Sieve size (ϕ)	Mass retained (g)	% retained	Cumulative %
-1	0.34	0.09	0.09
0	2.72	0.76	0.85
1	3.49	0.98	1.83
2	8.59	2.42	4.25
3	336.07	94.96	99.21
4	2.21	0.62	99.83
5	0.47	0.13	99.96
Retained total mass	353.89g		

Error = 0.1 %

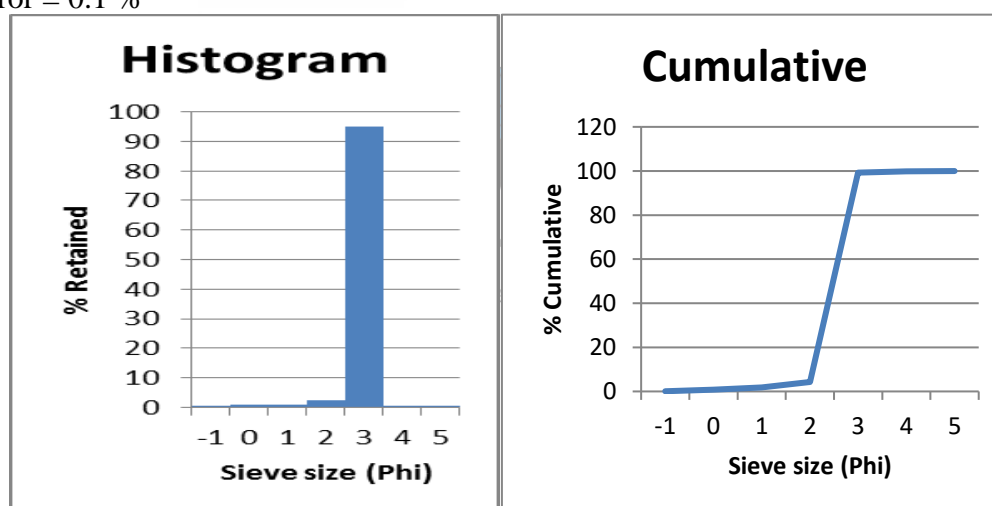


Fig. A.22: Histogram (left) and cumulative frequency curve (right) showing grain size distribution of the Sample 25. The grain size is dominant at 3 Phi (0.125 mm) followed by small percentage of grain size of 2 Phi (0.25 mm).

A.23 Sample 27 (Estuarine sand)

Table A.23 Retained and cumulative percentage of grain size for sample 27. Aliquot mass = 351.01 g.

Sieve size (ϕ)	Mass retained (g)	% retained	Cumulative %
-1	9.29	2.64	2.64
0	7.69	2.19	4.83
1	6.75	1.92	6.75
2	15.35	4.37	11.12
3	305.37	87.04	98.16
4	2.64	0.75	98.91
5	3.74	1.06	99.97
Retained total mass	350.83g		

Error = 0.05 %

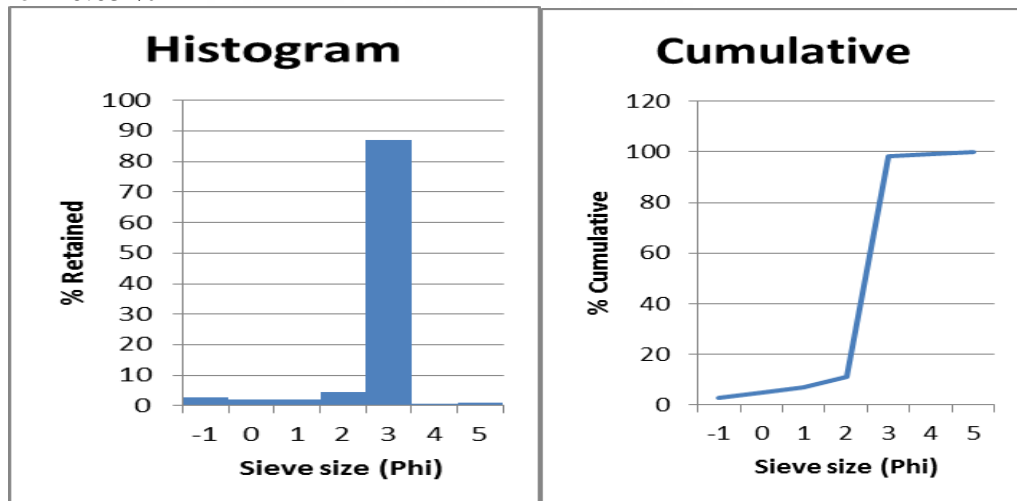


Fig. A.23: Histogram (left) and cumulative frequency curve (right) showing grain size distribution of the Sample 27. The grain size is dominant at 3 Phi (0.125 mm) followed by small percentage of grain size of 2 Phi (0.25 mm) and other smaller percentages of grain size.

A.24 Sample 29 (Estuarine sand)

Table A.24 Retained and cumulative percentage of grain size for sample 29. Aliquot mass = 365.56 g.

Sieve size (ϕ)	Mass retained (g)	% retained	Cumulative %
-1	11.90	3.25	3.25
0	11.67	3.19	6.44
1	7.22	1.97	8.41
2	16.46	4.50	12.91
3	307.50	84.22	97.91
4	4.14	1.13	98.26
5	6.20	1.69	99.95
Retained total mass	365.09g		

Error = 0.12 %

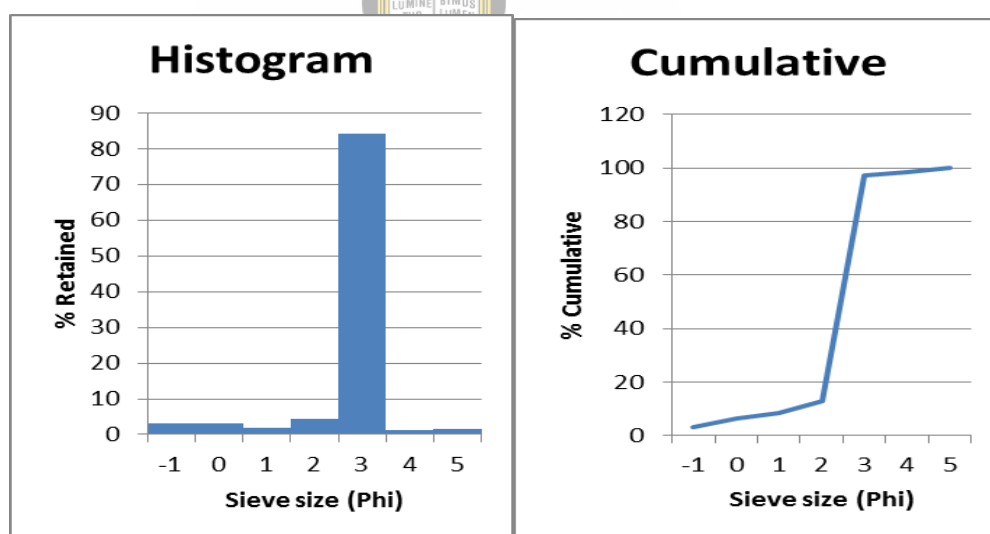


Fig. A.24: Histogram (left) and cumulative frequency curve (right) showing grain size distribution of the Sample 29. The grain size is dominant at 3 Phi (0.125 mm) followed by small percentage of grain size of 2 Phi (0.25 mm) and other smaller grain size percentages.

A.25 Sample 31 (Estuarine sand)

Table A.25 Retained and cumulative percentage of grain size for sample 31. Aliquot mass = 316.05 g.

Sieve size (ϕ)	Mass retained (g)	% retained	Cumulative %
-1	1.49	0.47	0.47
0	0.85	0.26	0.73
1	0.84	0.27	1.00
2	4.58	1.45	2.45
3	301.20	95.60	98.05
4	3.96	1.25	99.30
5	2.12	0.67	99.97
Retained total mass	315.04g		

Error = 0.3%

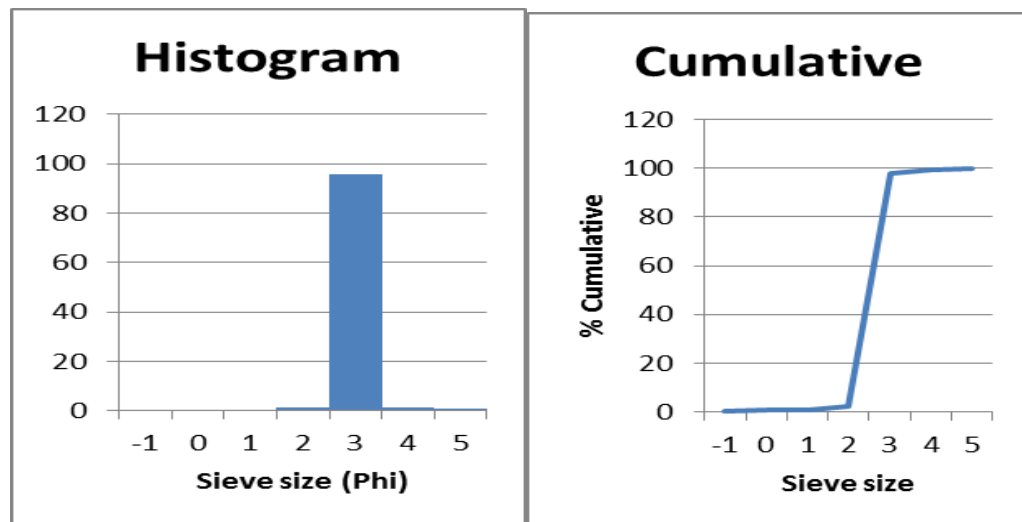


Fig. A.25: Histogram (left) and cumulative frequency curve (right) showing grain size distribution of sample 31. The grain size distribution is dominant at 3 Phi (0.125 mm) and it is well sorted in nature.

A.26 Sample 32 (Estuarine sand)

Table A.26 Retained and cumulative percentage of grain size for sample 32. Aliquot mass = 332.99 g.

Sieve size (ϕ)	Mass retained (g)	% retained	Cumulative %
-1	5.98	1.79	1.79
0	4.98	1.49	3.28
1	6.00	1.80	5.08
2	8.01	2.40	7.48
3	289.89	87.13	94.61
4	6.24	1.87	96.48
5	11.59	3.48	99.96
Retained total mass	332.69g		

Error = 0.09%

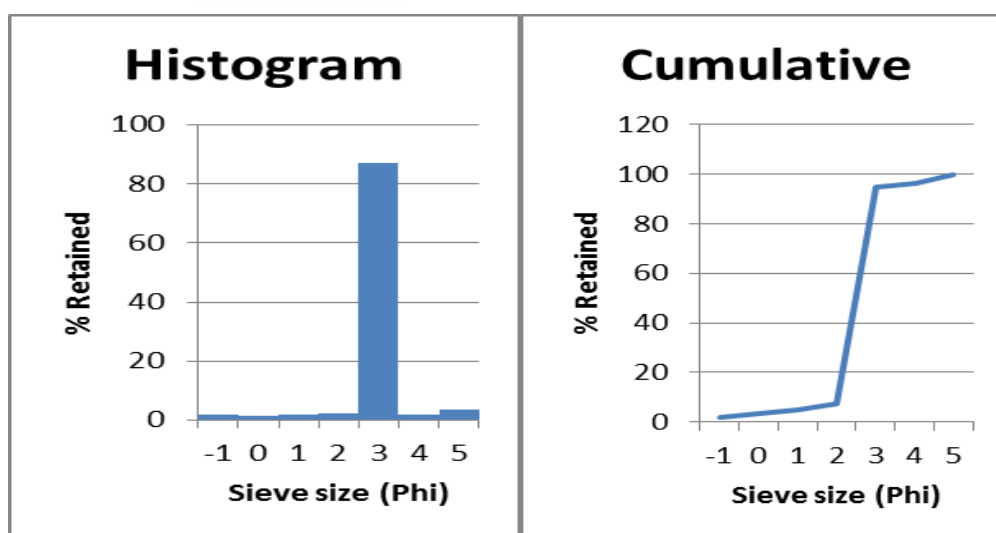


Fig. A.26: Histogram (left) and cumulative frequency curve (right) showing grain size distribution of the Sample 32. The grain size is dominant at 3 Phi (0.125 mm) followed by small percentage of grain size of 5 Phi (0.031 mm) and other smaller grain size percentages.

A.27 Sample 34 (Estuarine sand)

Table A.27 Retained and cumulative percentage of grain size for sample 34. Aliquot mass = 270.01 g.

Sieve size (ϕ)	Mass retained (g)	% retained	Cumulative %
-1	8.08	2.99	2.99
0	4.55	1.68	4.67
1	4.64	1.72	6.39
2	17.98	6.66	13.05
3	229.12	84.98	98.03
4	3.14	1.16	99.19
5	2.09	0.77	99.96
Retained total mass	269.6g		

Error = 0.1 %

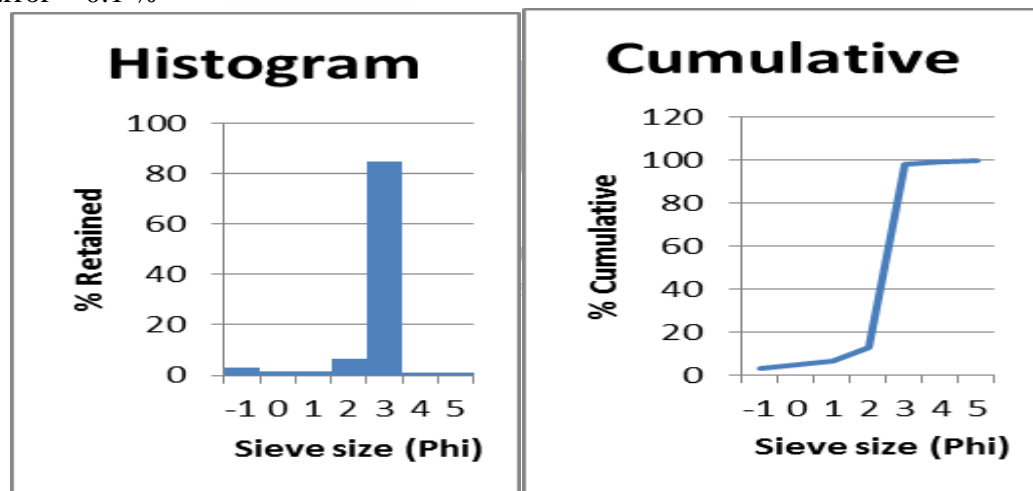


Fig. A.27: Histogram (left) and cumulative frequency curve (right) showing grain size distribution of the Sample 34. The grain size is dominant at 3 Phi (0.125 mm) followed by small percentage of grain size of 2 Phi (0.25 mm).

A.28 Sample 35 (Estuarine sand)

Table A.28 Retained and cumulative percentage of grain size for sample 35. Aliquot mass = 346.26 g.

Sieve size (ϕ)	Mass retained (g)	% retained	Cumulative %
-1	2.53	0.73	0.73
0	1.64	0.47	1.20
1	2.69	0.77	1.97
2	11.09	3.20	5.17
3	323.41	93.43	98.6
4	3.79	1.09	99.69
5	0.99	0.28	99.97
Retained total mass	346.14g		

Error = 0.03 %

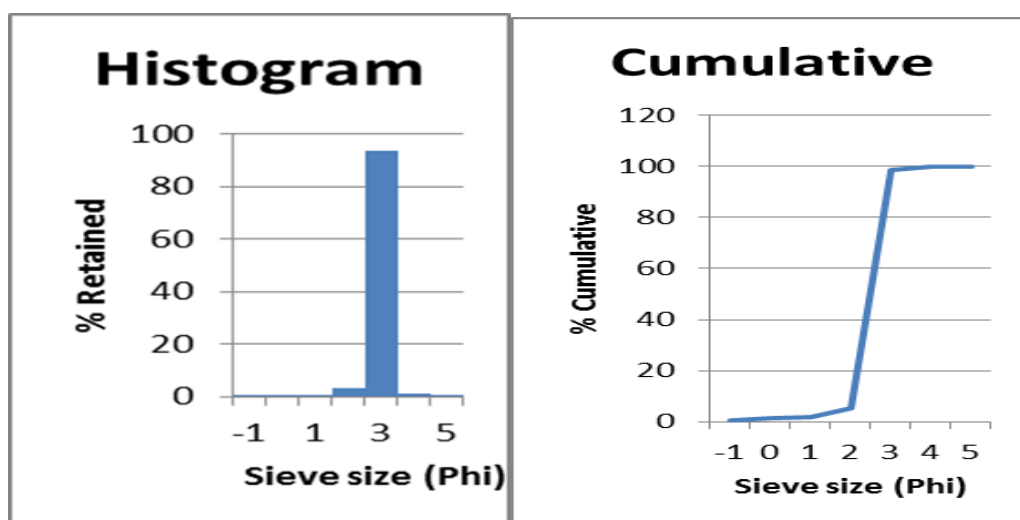


Fig. A.28: Histogram (left) and cumulative frequency curve (right) showing grain size distribution of the Sample 35. The grain size is dominant at 3 Phi (0.125 mm) followed by small percentage of grain size of 2 Phi (0.25 mm).

A.29 Sample 38 (Estuarine sand)

Table 4.38 Retained and cumulative percentage of grain size for sample 38. Aliquot mass = 324.03 g.

Sieve size (ϕ)	Mass retained (g)	% retained	Cumulative %
-1	13.14	4.06	4.06
0	5.32	1.64	5.70
1	3.62	1.11	6.81
2	8.37	2.58	9.39
3	286.80	88.63	98.02
4	3.63	1.12	99.14
5	2.71	0.83	99.97
Retained total mass	323.59g		

Error = 0.1%

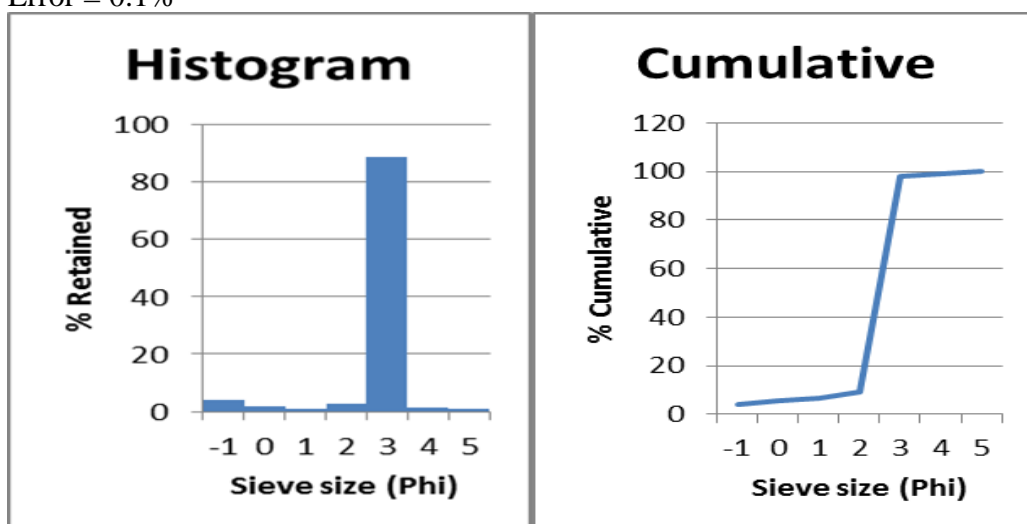


Fig. A.29: Histogram (left) and cumulative frequency curve (right) showing grain size distribution of the Sample 38. The grain size is dominant at 3 Phi (0.125 mm) followed by small percentage of grain size of -1 Phi (2.00 mm) and 2 Phi (0.25 mm), and other smaller percentages of grain size.

A.30 Sample 40 (Estuarine sand)

Table A.30 Retained and cumulative percentage of grain size for sample 40. Aliquot mass = 265.19g.

Sieve size (ϕ)	Mass retained (g)	% retained	Cumulative %
-1	7.34	2.77	2.77
0	1.40	0.52	3.29
1	1.94	0.73	4.02
2	6.09	2.30	6.32
3	241.08	91.09	97.41
4	4.70	1.77	99.18
5	2.09	0.78	99.96
Retained total mass	264.64g		

Error = 0.2%

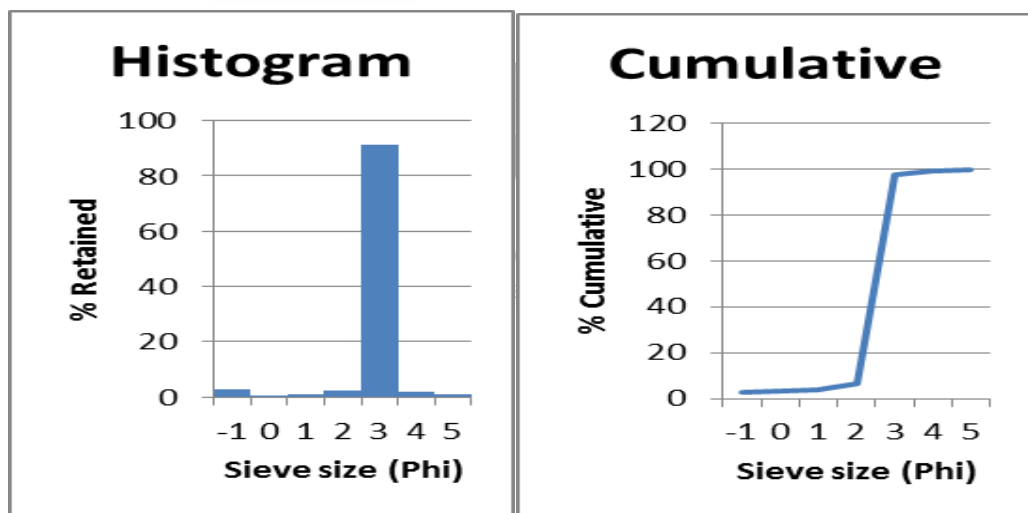


Fig. A.30: Histogram (left) and cumulative frequency curve (right) showing grain size distribution of the Sample 40. The grain size is dominant at 3 Phi (0.125 mm) followed by small percentage of grain size of -1 Phi (2.00 mm) and 2 Phi (0.25 mm), and other smaller percentages of grain size.

A.31 Sample 41 (Estuarine sand)

Table A.31 Retained and cumulative percentage of grain size for sample 41. Aliquot mass = 307.26 g.

Sieve size (ϕ)	Mass retained (g)	% retained	Cumulative %
-1	1.83	0.59	0.59
0	0.77	0.25	0.84
1	0.75	0.24	1.08
2	1.78	0.57	1.65
3	296.19	96.47	98.12
4	4.69	1.52	99.64
5	1.00	0.32	99.96
Retained total mass	307.01g		

Error = 0.08 %

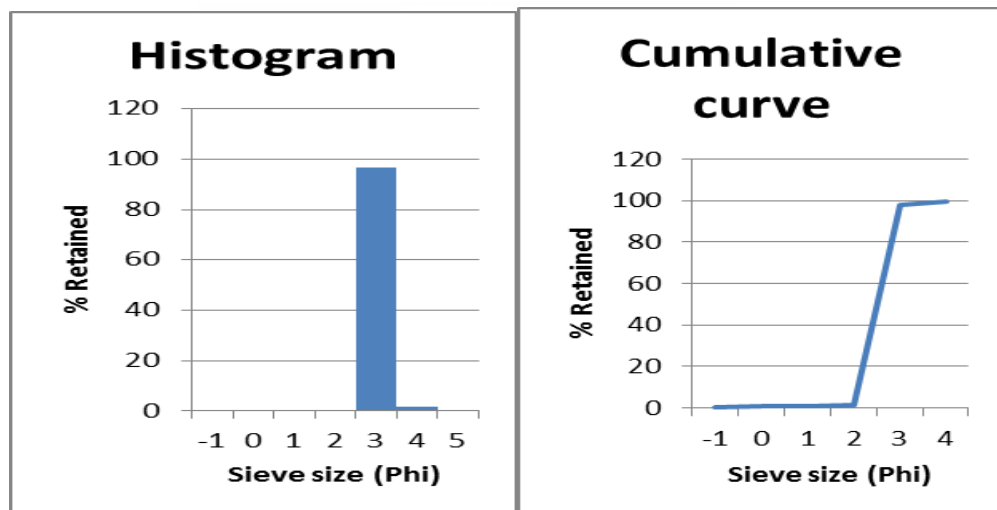


Fig. A.31: Histogram (left) and cumulative frequency curve (right) of sample 41, showing grain size distribution size varied from 3.5 to 4.5 phi, with dominant size at 3 Phi (0.125 mm) and minor sizes at 4 Phi (0.0625 mm).

A.32 Sample 42 (Estuarine sand)

Table 4.42 Retained and cumulative percentage of grain size for sample 42. Aliquot mass = 306.31g.

Sieve size (ϕ)	Mass retained (g)	% retained	Cumulative %
-1	0.51	0.16	0.16
0	0.46	0.15	0.31
1	0.42	0.13	0.44
2	1.31	0.42	0.86
3	296.33	96.85	97.71
4	5.73	1.87	99.58
5	1.18	0.38	99.96
Retained total mass	305.94g		

Error = 0.1 %

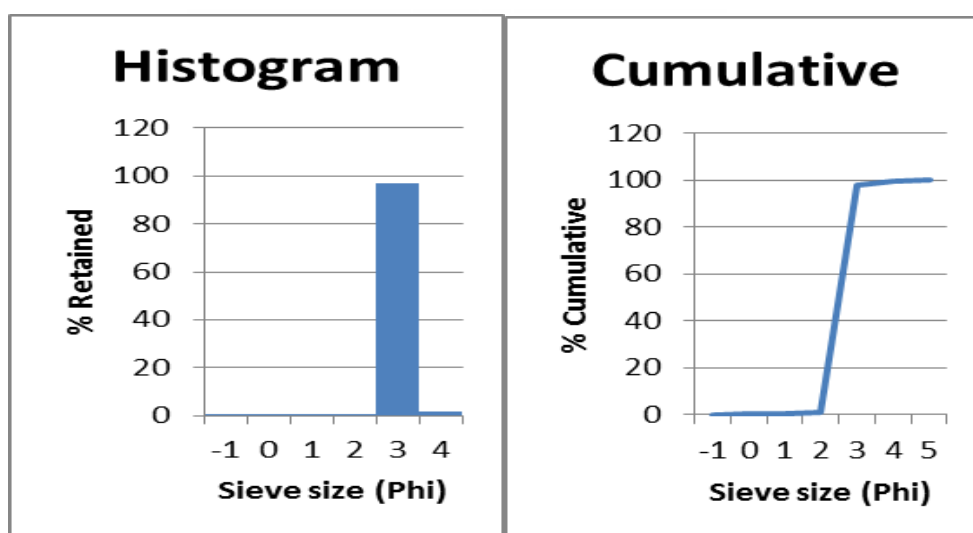


Fig. A.32: Histogram (left) and cumulative frequency curve (right) of sample 42, showing grain size distribution size varied from 3.5 to 4.5 phi, with dominant size at 3 Phi (0.125 mm) and minor sizes at 4 Phi (0.0625 mm).

A.33 Sample 43

Table A.33 Retained and cumulative percentage of grain size for sample 43. Aliquot mass = 286.66 g.

Sieve size (ϕ)	Mass retained (g)	% retained	Cumulative %
-1	18.91	6.60	6.60
0	15.69	5.47	12.07
1	10.10	3.52	15.59
2	16.68	5.82	21.41
3	215.16	75.10	96.51
4	2.68	0.93	97.44
5	7.27	2.53	99.97
Retained total mass	286.49g		

Error = 0.05%

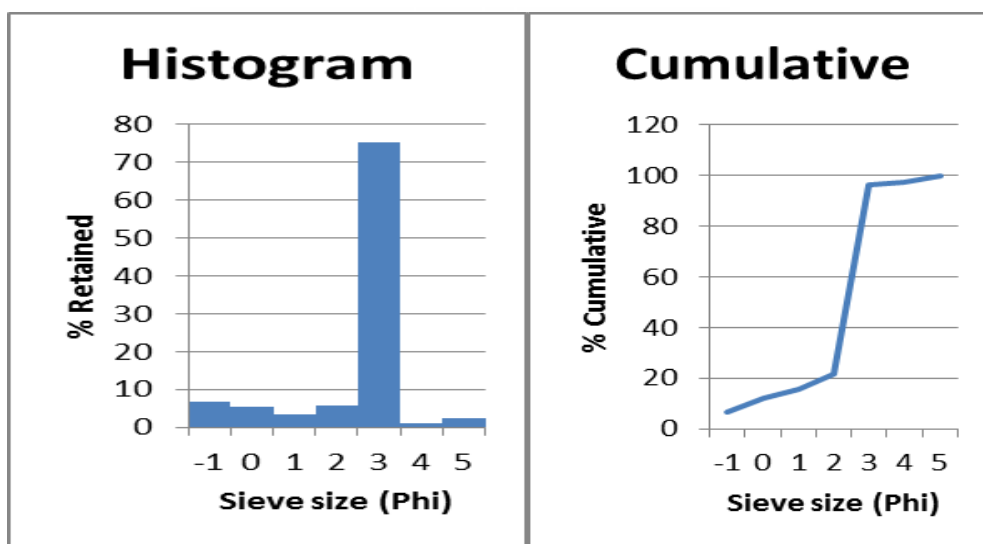


Fig. A. 33: Histogram (left) and cumulative frequency curve (right) showing grain size distribution of the Sample 43. The grain size is dominant at 3 Phi (0.125 mm) followed by small percentage of grain size of -1 Phi (2.00 mm) and 2 Phi (0.25 mm), and other smaller percentages of grain size.

A.34 Sample 48 (Estuarine sand)

Table A.34 Retained and cumulative percentage of grain size for sample 48. Aliquot mass 230 g.

Sieve size (ϕ)	Mass retained (g)	% retained	Cumulative %
-1	52.14	22.71	22.71
0	11.74	5.11	27.82
1	10.74	4.67	32.49
2	20.0	8.71	41.20
3	117.73	51.27	92.47
4	10.36	4.51	96.98
5	6.85	2.98	99.96
Retained total mass	229.59g		

Error = 0.2 %

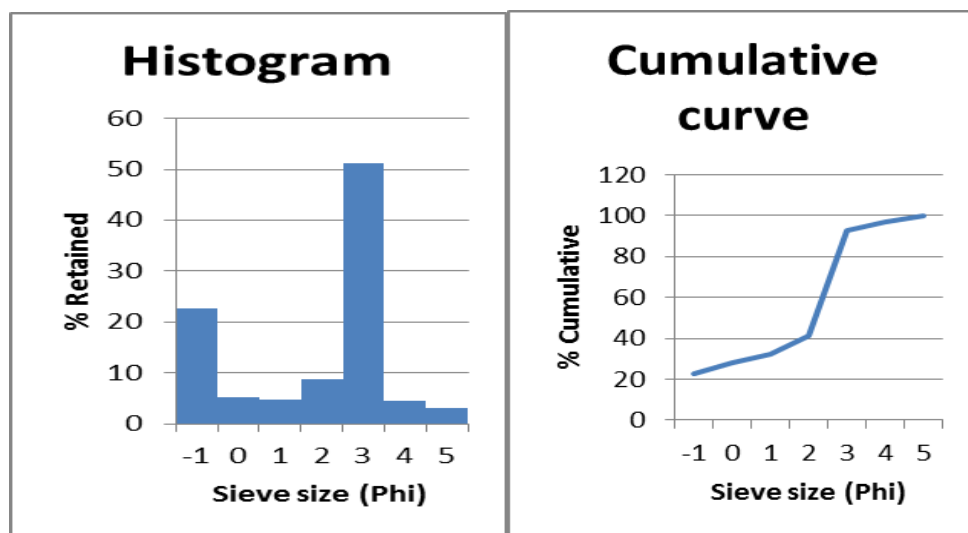


Fig. A.34: Histogram (left) and cumulative frequency curve (right) showing grain size distribution of the Sample 48. The grain size is dominant at 3 Phi (0.125 mm) followed by percentage of grain size of -1 Phi (2.00 mm) and 2 Phi (0.25 mm), and other smaller percentages of grain size.

A.35 Sample 49 (Estuarine sand)

Table A. Retained and cumulative percentage of grain size for sample 49. Aliquot mass = 307.92 g.

Sieve size (ϕ)	Mass retained (g)	% retained	Cumulative %
-1	41.27	13.44	13.44
0	20.30	6.61	20.05
1	11.38	3.70	23.75
2	13.12	4.27	28.02
3	161.72	52.69	80.71
4	31.02	10.10	90.81
5	28.07	9.14	99.95
Total mass	306.88g		

Error = 0.3%

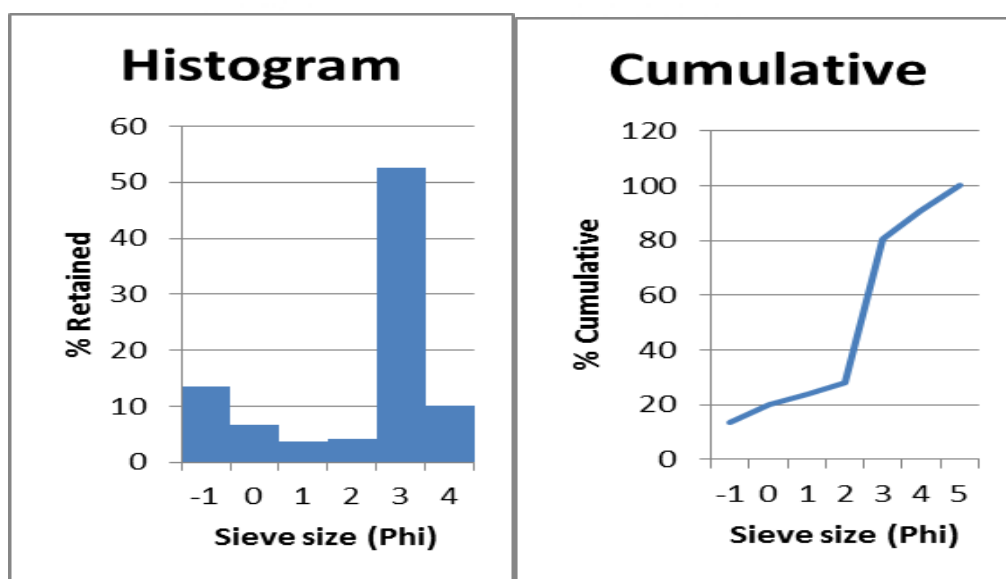


Fig. A.35: Histogram (left) and cumulative frequency curve (right) showing grain size distribution of the Sample 49. The grain size is dominant at 3 Phi (0.125 mm) followed by percentage of grain size of 4 Phi (0.0625 mm) and 0 Phi (1.00 mm), and other smaller percentages of grain size.

A.36 Sample 51 (Estuarine sand)

Table A.36 Retained and cumulative percentage of grain size for sample 51. Aliquot mass = 180.75g.

Sieve size (ϕ)	Mass retained (g)	% retained	Cumulative %
-1	17.84	9.88	9.88
0	4.75	2.63	12.51
1	6.97	3.86	16.37
2	13.57	7.51	23.88
3	110.87	61.41	85.29
4	19.07	10.56	95.85
5	7.46	4.13	99.98
Retained total mass	180.53g		

Error = 0.1%

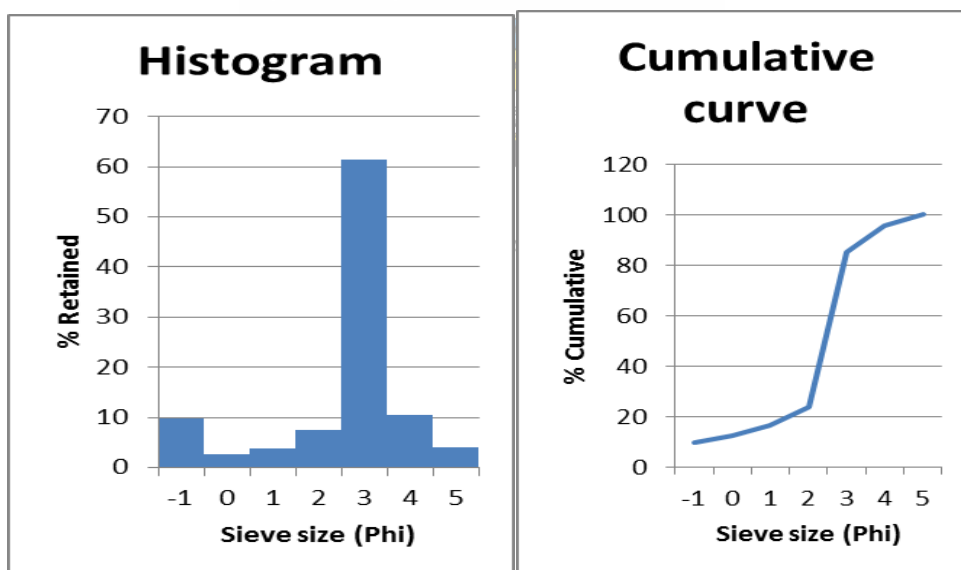


Fig. A.36: Histogram (left) and cumulative frequency curve (right) showing grain size distribution of the Sample 51. The grain size is dominant at 3 Phi (0.125 mm) followed by percentage of grain size of 4 Phi (0.0625 mm) and 1 Phi (0.50 mm) respectively, and other smaller percentages of grain size.

A.37 Sample 52 (Estuarine sand)

Table 4.52 Retained and cumulative percentage of grain size for sample 52. Aliquot mass = 310.72 g.

Sieve size (ϕ)	Mass retained (g)	% retained	Cumulative %
-1	54.37	17.52	17.52
0	12.52	4.03	21.55
1	8.57	2.76	24.31
2	22.76	7.33	31.64
3	197.49	63.64	95.28
4	12.22	3.93	99.21
5	2.36	0.76	99.97
Retained total mass	310.29g		

Error = 0.1 %

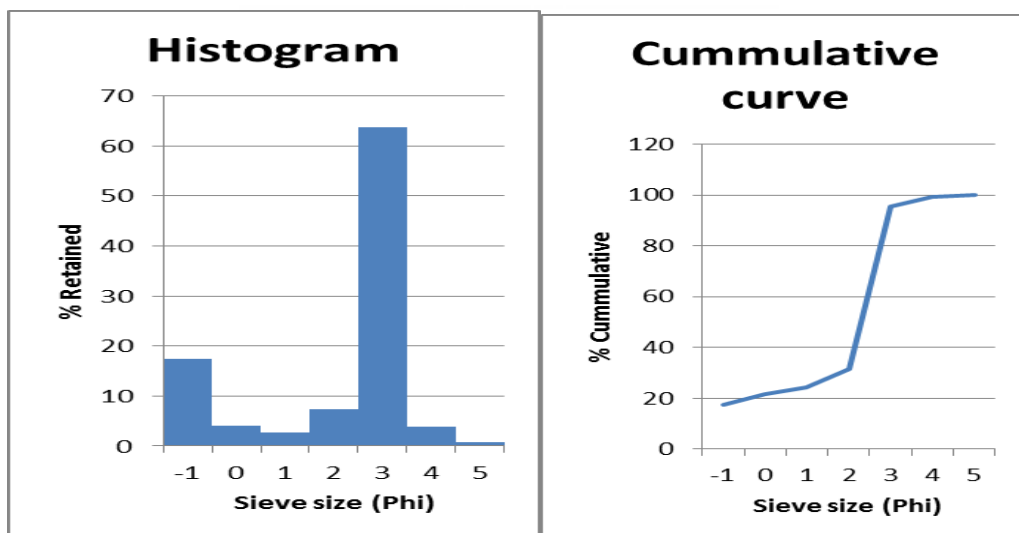


Fig. 4.52: Histogram (left) and cumulative frequency curve (right) showing grain size distribution of the Sample 52. The grain size is dominant at 3 Phi (0.125 mm) followed by percentage of grain size of -1 Phi (2.00 mm) and 2 Phi (0.25 mm), and other smaller percentages of grain size.

A.38 Sample 56 (Estuarine sand)

Table A.38 Retained and cumulative percentage of grain size for sample 56. Aliquot mass =374.53 g.

Sieve size (ϕ)	Mass retained (g)	% retained	Cumulative %
-1	3.06	0.81	0.81
0	3.12	0.83	1.64
1	10.34	2.76	4.4
2	118.66	31.75	36.15
3	236.56	63.31	99.46
4	1.76	0.47	99.93
5	0.12	0.03	99.96
Retained total mass	373.62g		

Error = 0.2 %

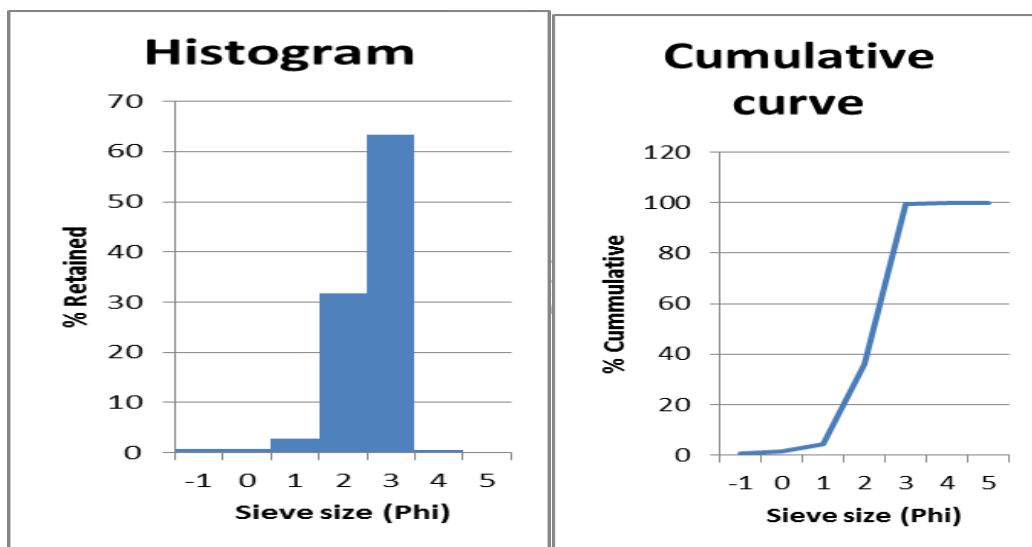


Fig. A.38: Histogram (left) and cumulative frequency curve (right) of the Sample 56, showing the grain size distribution varied from 1.5 to 3.5 phi which is dominant at 3 Phi (0.125 mm) and a part of at 2 phi (0.25 mm).

A.39 Sample 57 (Estuarine sand)

Table 4.57 Retained and cumulative percentage of grain size for sample 57. Aliquot mass = 285.71g.

Sieve size (ϕ)	Mass retained (g)	% retained	Cumulative %
-1	1.82	0.63	0.63
0	2.24	0.78	1.41
1	5.95	2.09	3.5
2	61.55	21.62	25.12
3	211.83	74.42	99.54
4	1.21	0.42	99.96
5	0.04	0.01	99.97
Retained total mass	284.64g		

Error = 0.1 %

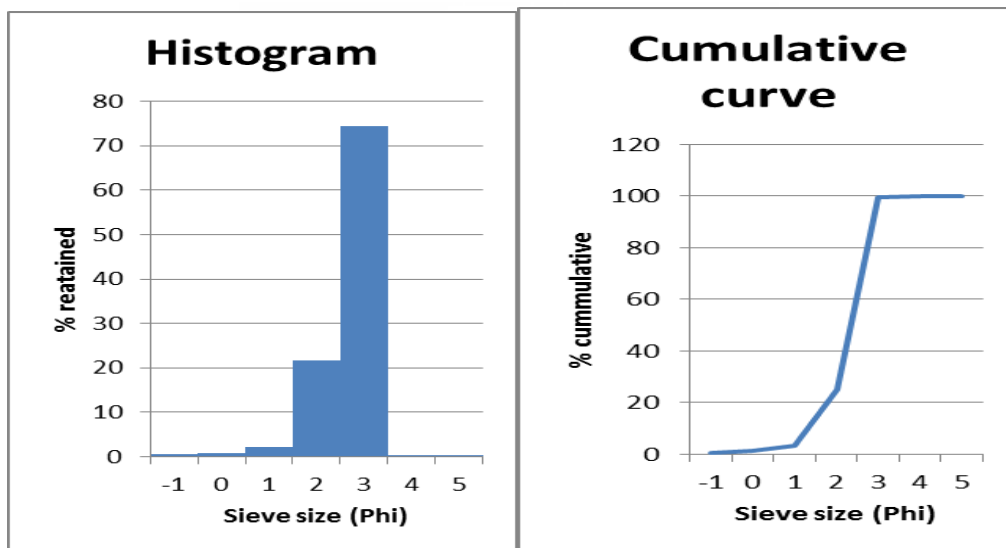
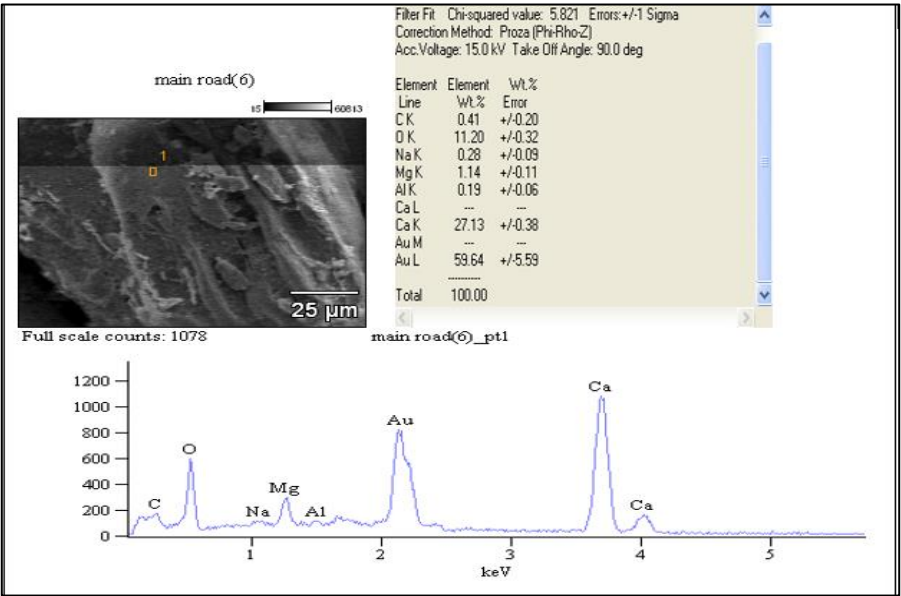


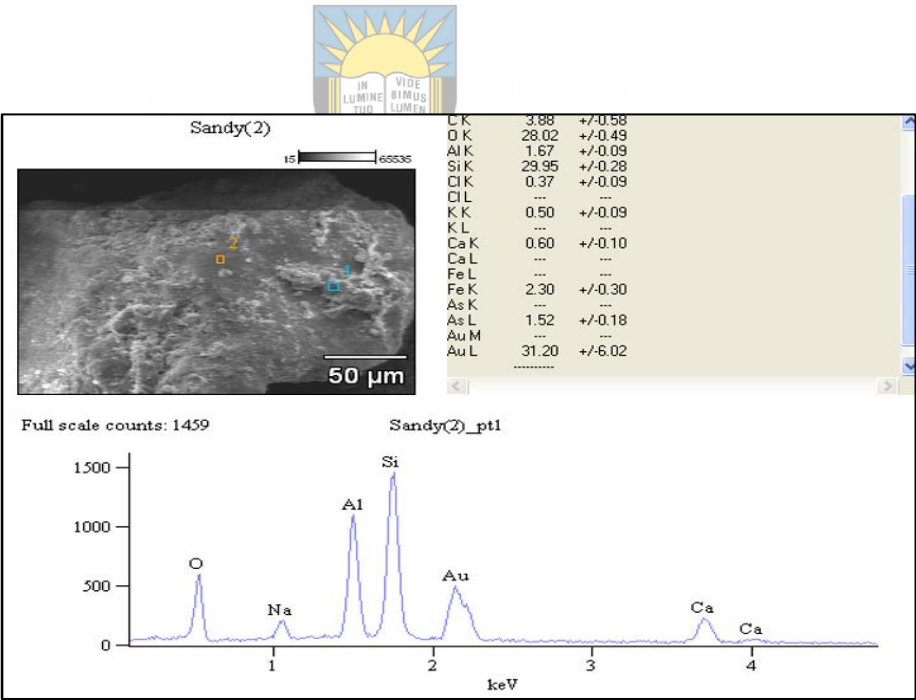
Fig. A.38: Histogram (left) and cumulative frequency curve (right) of the Sample 57, showing the grain size distribution varied from 1.5 to 3.5 phi which is dominant at 3 Phi (0.125 mm) and a part of at 2 phi (0.25 mm).

APPENDIX B: SEM and EDX

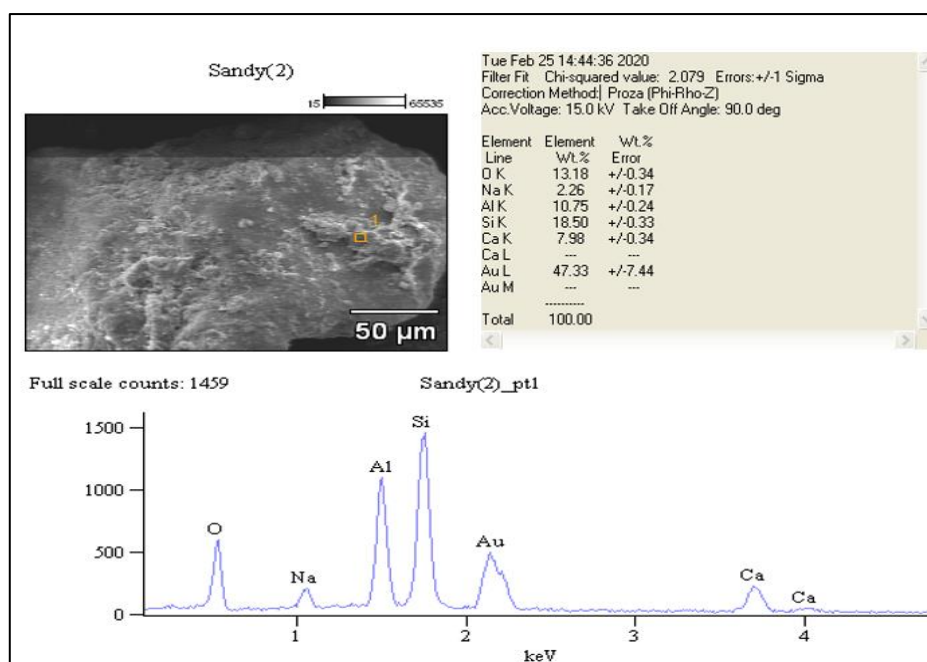
B.1



B.2



B.3



B.4

